Applications of Regression Enhanced Self-Organizing Incremental Neural Networks (RE-SOINN)in an Embedded Intelligent Energy Control System for Off-grid Systems

PUAH BOON KEAT

Thesis submitted to the University of Nottingham
for the degree of Doctor of Philosophy

FEBRUARY 2023

ABSTRACT

Battery Energy Storage System (ESS) is a very important component in most of the off-grid standalone photovoltaic (PV) system as battery ESS can store excess unused solar energy harvested via solar panels for later use. However, normal household electronic appliances often cause irregular load demand, pushing the battery ESS to experience deep power discharge cycles. The intermittent nature of solar irradiance has also contributed to irregular charging patterns of battery ESS. Therefore, battery-supercapacitor Hybrid Energy Storage System (HESS) is introduced as the most promising solution to reduce the harms to the battery. Most of the control strategies in the literature focus on the optimisation of the system operations. For instance, the control strategy is usually implemented to optimally manage HESS based on real-time operating conditions. Though there are applications of intelligent energy control system in the past literature, there are still limited studies on how solar irradiance prediction is being embedded into the energy management system (EMS). Furthermore, many solar irradiance forecasting solutions provided in the literature are based upon deep learning algorithms which require a lot of computational resources, impeding these forecasting solutions to be implemented in off-grid applications. Also, the EMS implemented in the literature are based upon Artificial Intelligence-based optimization algorithms which use iterative computations to reach to optimal decisions making. As a result, an incremental unsupervised learning-based EMS is developed to perform solar irradiance forecasting as well as to manage and control the system operations in an off-grid standalone PV Renewable Energy Power System (REPS). The objectives of this research study are to develop a computational efficient hourly incremental unsupervised learning solar irradiance forecasting model using basic features as well as to develop and to implement an incremental unsupervised learning EMS in an actual standalone PV system with battery-supercapacitor HESS.

The novelties of the incremental unsupervised learning solar irradiance forecasting model includes less computational demanding compared to deep learning models. Moreover, the proposed model takes historical solar irradiance measurements and

timestamps as its sole input. As a mean to improve the forecasting performance of the proposed model, the data is decomposed into low frequency and high frequency components to reduce the influence of noisy variation of solar irradiance on the learning of the model. The incremental nature of the model also allows the proposed model to learn from new data once a gradual change in the data trend is found. The proposed model outperforms Artificial Neural Networks (ANN) by 19% in terms of Root Mean Squared Errors (RMSE) and 34% in Mean Absolute Scaled Error (MASE).

On the other hand, the proposed EMS model implemented does not require any predefined mathematical representation of the entire REPS due to its incremental feature. Then, its lightweight advantage outperforms many controllers in the past literature in terms of computational time, training time and specifications requirement on embedded computational platform. The proposed model introduces significant less battery power oscillations in the REPS, especially at higher battery power amplitudes that are very damaging to the battery while assists the REPS with HESS to harvest extra 26.6% of solar energy compared to a battery only REPS .

AFFIRMATION

The work presented in this thesis is, to the best of my knowledge, original, and has not been submitted for any other degree. This research is carried out in the Department of Electrical and Electronics Engineering, University of Nottingham, Malaysia Campus from October 2017 to October 2022. This thesis does not exceed 100,000 words. The following publication ha been partially based on the research work reported in the thesis:

Journal Papers (Published):

1.	**B. K. Puah**, L. W. Chong, Y. W. Wong, K. M. Begam, Nafizah Khan, M. A. Juman and R. K. Rajkumar, "A regression unsupervised incremental learning algorithm for solar irradiance prediction," *Renew Energy*, vol. 164, pp. 908–925, 2021, doi: 10.1016/j.renene.2020.09.080. (Q1, Impact Factor: 8.634)

ACKNOWLEDGEMENT

Firstly, I would like to express my sincere gratitude to my supervisors, Dr Mumtaj Begam Kasim Rawthar, Dr Wong Yee Wan, Dr Nafizah Khan for their continuous and generous support to my entire PhD study and related research. If it was not for their kind patience, motivations, and immense knowledge to clear my doubts I had during the journey, this PhD study is not possible. I would also like to show my gratitude towards Mr Anandan Shanmugam who acts as the internal moderator of my PhD study. His opinions, constructive suggestions as well as advice have helped to expose me to different research angles, allowing me to explore multiple possible routes to make this research topic a success.

Subsequently, I would like to thank Collaborative Research in Engineering, Science and Technology (CREST) for their generous funding (P20C2-16) to support my research works. Furthermore, my heartfelt gratitude to the University of Nottingham Malaysia for the opportunity and scholarship received towards my PhD study. Last but not the least, I would like to thank my family and friends who have been there for me throughout my PhD research journey.

TABLE OF CONTENT

LIST OF FIGURES

LIST OF TABLES

ABBREVIATIONS

a_1	Nearest or winning node
a_2	Second nearest node
ABC	Artificial Bee Colony
ACO	Ant Colony Optimisation
ADC	Analog-to-Digital Converter
age_{max}	Maximum nodal age
AI	Artificial intelligence
ANFIS	Adaptive neuro-fuzzy inference systems
ANN	Artificial neural network
A-P	Angstrom-Prescott
AP	Air pressure
ARIMA	Autoregressive integrated moving average
ARMA	Auto-regressive moving average
BFOA	Bacterial Foraging Optimisation Algorithm
BMS	Battery management scheme
BNN	Bayesian Neural Networks
C	Nodal connection set
c_1	Personal learning factor
c_2	Global learning factor
CNN	Convolutional Neural Networks
CPU	Computing Processing Unit
CS	Cuckoo Search
D	Duty cycles signal
d	Distance between input vector to a neighbour
DAC	Digital-to-Analog Converter
DC	Direct current
DEA	Differential Evolution Algorithm
DF	Ambient temperature multiplier
dP	Power surplus between power generation, P_{PV}' and load demand, P_{load} (W)
dP_{HF}	High frequency component of dP (W)
dP_{LF}	Low frequency component of dP (W)
$dP_{LF\_prediction}$	Predicted profile of dP_{LF} (W)
$dP_{LF\_prediction}^{max}$	Maximum points of the $dP_{LF\_prediction}$ (W)
$dP_{LF\_prediction}^{min}$	Minimum points of the $dP_{LF\_prediction}$ (W)
E-SOINN	Enhanced Self-Organising Incremental Neural Networks
EA	Evolutionary algorithm
EANN	Evolutionary Artificial Neural Networks
EC	Evolutionary Computation
EE	Excess Energy
ELM	Extreme Learning Machines
EMS	Energy Management Strategy

ENN	Elman Neural Network
ERM	Empirical Risk Minimization
ESS	Energy storage system
ESS-E	High-energy storage
ESS-P	High-power storage
ESVM	Ensemble Support Vector Machine
FBC	Filtration-based controller
FL	Fuzzy Logic
FLC	Fuzzy Logic controller
GA	Genetic algorithm
gbest	Global best
GBR	Gradient Boosted Regression
GMDH	Group Method of Data Handling Neural Networks
GPU	Graphic Processing Unit
GTSOM	Game Theoretic Self-Organizing Map
GWA	Gray Wolf Algorithm
h	Density of a node
H	High
HF RE-SOINN	High Frequency component-Regression Enhanced Self Organising Incremental Neural Networks
HGA	Hierarchical GA
HESS	Hybrid energy storage system
HPF	High-pass filter
HS	Harmony Search
HVAC	Heating, Ventilating and Air-Conditioning
$I_{b,ref}$	Battery reference current setpoint (A)
I_{buck}	Output current of the buck converter (A)
IBSS	Independent Basic Service
ICA	Imperialist Competitive Algorithm
IoT	Internet of Things
I_{out}	Output current (A)
Irr	Solar irradiance (Wm^{-2})
I_{SC}	Supercapacitor current at the input side of DC-DC converter (A)
I_{SC_ref}	Reference supercapacitor current (A)
It_{max}	Maximum number of iterations to obtain the optimal solution
It_{total}	Number of iterations
j	Index number
kNN	K-Nearest Neighbours
LCC	Life Cycle Cost
LEC	Levelized Energy Cost
LF	Low Frequency
LF RE-SOINN	Low Frequency component-Regression Enhanced Self Organising Incremental Neural Networks
li-ion	Lithium-ion
locs_max	Location of *pks_max*

locs_min	The location of *pks_min*
LPF	Low pass filter
LPSP	Loss of power supply probability
LS-SVM	Least-Square Support Vector Machine
m	Number of neighbours
MACO	Multilayer Ant Colony Optimisation
MAE	Mean Absolute Error
MAF	Moving average filter
MAFSA	Modified Artificial Fish School Algorithm
MASE	Mean Absolute Scaled Error
MFs	Membership functions
MLFNN	Multilayer Feedforward Neural Networks
MLP	Multilayer Perceptron
MLR	Multiple Linear Regression
MOPSO	Multi-Objectives Particle Swarm Optimisation
MPPT	Maximum power point tracking
MVO	Mean-Variance Optimisation
N	Number of training data set
n	Number of past steps
NaN	Not a Number
NFC	Neuro-Fuzzy controller
NH	Negative high
NL	Negative low
NMAE	Normalised Mean Absolute Error
NOCT	Nominal operating cell temperature (°C)
N_{PVp}	Number of modules in parallel
N_{PVs}	Number of modules in series
nRMSE	Normalised Root Mean Square Error
NWP	Numeric weather prediction
O&M	Operation and Management
p	Power to raise *d* to (significance of influence of neighbouring data on one point)
P_{batt}	Power flow of the battery (W)
P_{batt_max}	Maximum point of the battery power (W)
P_{batt_peak}	Battery peak discharge power (W)
pbest	Personal best
PH	Positive high
P_H	High power demand to be shared by the supercapacitor (W)
PID	Proportional-Integral-Derivative
p_i	Positions of the particles
P_{load}	Load power before power conversion loss (W)
$P_{load\_prediction}$	Predicted P_{load} (w)
P_{load}'	The load power demand excluded inverter losses (W)
PM	Positive medium
P_{PV}	PV output power (W)

P_{PV_MPP}	PV output power at the maximum power point (W)
$P_{PV\_prediction}$	Predicted P_{PV} (W)
P_{PV}'	PV-generated power after power conversion by the charge controller (W)
P_{RE}	Power generated by renewable energy sources
P_{SC}	The supercapacitor power at the input side of the DC-DC converter (W)
P_{SC} '	Power flow of supercapacitor at the output side of the DC-DC converter (W)
P_{SC_PDA}	Reference supercapacitor power produced by Power Distribution Algorithm (W)
P_{SC_ref}	Supercapacitor reference power (W)
P_{size}	Population size
PSO	Particle swarm optimization
PV	Photovoltaic
QPSO	Quantu-behaved Particle Swarm Optimisation
RBC	Rule-based controller
RBF	Radial basis function
RBFN	Radial basis function network
RE	Renewable energy
RE-SOINN	Regression Enhanced Self-Organising Incremental Neural Networks
REPS	Renewable energy power system
RFR	Random Forest Regression
RH	Relative humidity
RMSE	Root mean square error
S	Sum of points for a node
SBC	Single-board computers
SC	Supercapacitor
SFL	Shuffled frog leaping
SI	Swarm Intelligence
SLA	Sealed Lead Acid Battery
SLT	Statistical Learning Theory
SMC	Sliding Mode Control
SoC	State-of-charge (%)
SoC_{batt}	SoC of battery (%)
SoC_{SC}	SoC of supercapacitor (%)
SOINN	Self-Organising Incremental Neural Networks
SOM	Self-Organising Map
SRM	Structural Risk Minimization
SSR	Self-Sufficiency Ratio
SVM	Support vector machine
SVR	Support vector regression
T_a	Similarity Threshold
T_{air}	Air temperature (°C)
Tc	Charging threshold (W)
T_d	Discharging threshold (W)
TEDA	Typicality-and-Eccentricity Method for Data Analysis
$T_{optimization}$	Total optimization time (s)

T_S	Moving sampling time window (s)
UAV	Unmanned Aerial Vehicle
V_{batt}	Battery voltage (V)
V_{DC}	Voltage of DC bus (V)
v_i	Velocity of the particles
V_{in}	Input voltage (V)
V_{in}	Input voltage (High Voltage Side)
V_o	Output voltage (Low Voltage Side)
V_{out}	Output voltage (V)
Vsc	Supercapacitor voltage (V)
VRB	Vanadium Redox Battery
VRLA	Valve-regulated lead-acid
W_a	Weight vector for node a
WMIM	Wrapper Mutual Information Methodology
WRNN	Wiener Recurrent Neural Network
WT	Wind turbine
x	Vector of input features
y	Label
y_{HF}	High frequency component of solar irradiance value
y_{ORIG}	Original solar irradiance value
y_{LF}	Low frequency component of solar irradiance value
α	Power sharing ratio
β	Multiplier
γ	Power temperature coefficient at MPP (V/°C)
ΔSOC_{SC}	Variation of SOC_{SC} (%)
ΔV_o	Peak to peak voltage ripple at the output (V)
$\frac{\Delta V_0}{V_o}$	Output voltage ripple (%)
ϵDE	Epsilon Differential Evolution
λ	Denoising Iteration Threshold
η_{DCAC}	Efficiency of inverter (%)
η_{MPPT}	Efficiency of charge controller (%)
σ	Parameter of the kernel function

Chapter 1 Introduction

1.1 Research Overview

Petroleum, after its discovery, its applications have been explored vastly to be crowned as the lifeblood of the global economy after Industry Revolutions. Petroleum is vital to the economical aspect in human civilisation as the main energy source to power any industry, domestic homes as well as transportation. Following the introduction of smart digital age, the demand for energy is increasing exponentially ever since. The non-renewable nature of fossil fuels such as petroleum forms bottleneck to existing technological development progress, limiting the pace of our digital age. As so, many researchers have turned to exploring various renewable energy (RE) sources as possible alternative. Unlike fossil fuels and coals, these renewable energy resources are naturally replenished on human timescale and will never run out. Non-renewable energies are usually associated as major pollutants to the environment whereas renewable energies are generally more environmental-friendly.

However, renewable energies naturally suffer due to intermittent energy production. For instance, solar energy is not available at night and wind energy is only available during windy occasions. The existing renewable energy harvesting technologies are yet to achieve high efficiency, leading to high electricity generation cost. As a result, renewable energy technology largely remains at its infancy phase. Solar energy, due to its wide availability, is usually harvested via photovoltaic (PV) systems and then become the most popular and promising alternative to fossil fuel. Photovoltaic energy generation system is subsequently widely commercialized as the most mature renewable energy technology.

In remote areas that are beyond the reach of main power grid, standalone renewable energy generation is one of the better solutions with the benefit of reduced maintenance and running costs [1]. Commonly, energy generation solely from renewable sources is unable to meet the entire load demand all the time due to the random nature of renewable power sources and load demand. Eventually, renewable energy power systems (REPS) rely heavily on energy storage systems (ESS) to ensure a continuous power supply. Lately, battery storage system is used dominantly in the market due to its large energy capacity for real life large energy density applications. Also, their easy implementation and geographical independence have crowned the battery as the most basic and popular ESS [2]. However, the expensive price tag of batteries has almost offset the benefits of ESS [3].

The conventional ESS in stand-alone REPS suffers in short lifespan due to irregular renewable energy generation as well as unpredictable stress level and intermittent peak power demand. Loads such as air-conditioner and motor require high starting instantaneous current. It is very costly to match the battery size to this high current demand [1]. The frequent deep cycles and irregular charging/discharging patterns also shorten the lifecycle of ESS, incurring high maintenance and replacement costs of REPS. These drawbacks have indeed impeded the adoption of solar-based REPS in household applications, not to mention being less favourable to be developed as reliable alternative to conventional grid power networks.

The advanced battery technology now allows extraordinary energy densities but often insufficient power densities to meet demands for applications where the load draws very large power impulses over a very short interval of time. The general practice is to parallel more batteries to share the dynamic stress but such design always incurs very high cost. Therefore, there are suggestions to add supercapacitor in parallel to the battery. Supercapacitor is an example of high-power storage devices which could be used to deal with the high-power density demands [4]. The benefits of having batteries working in parallel with supercapacitors include extending the operation life of battery, reducing the design and manufacture cost as well as increasing the capability of the hybrid energy storage system in handling varying power demands [5], [6].

Many researchers have employed the model of hybrid energy storage system (HESS) as one of the ways to tackle the erratic nature of the power demand. Such measure could combine the advantages of both technologies to complement one another and therefore being more suitable to serve large-scale renewable energy systems [5], [4]. The

HESS is devised upon the ideal thoughts of having high-energy storage (ESS-E) which deals with average long-term energy demand working alongside a high-power storage (ESS-P) that is able to deliver or absorb peak transient power. HESS is thus used to maintain the constant DC grid voltage due to mismatch between generation and demand [5]. Thus, the power balance equation is

$$P_{RE} + P_{ESS} = P_{LOAD} \tag{1.1}$$

where P_{RE} refers to generated power of renewable energy sources, P_{ESS} is the power flow of ESS with P_{LOAD} is the power demand of load. In other words, HESS simply stores excess energy generated as well as delivers the stored energy to meet the demand of load when the energy generation of RE sources is too low or unavailable. However, the main challenge in the HESS technology lies in the power sharing between different technologies [4] as well as the power flow to and from power sources, HESS and loads [7] for better system efficiency.

Accordingly, an energy management strategy (EMS) or control strategy is formulated as the brain of the system. A control strategy is aimed to optimize the energy utilization and sustainability of REPS. The usage of renewable energy technology requires a comprehensive energy management strategy which could achieve optimal fuel economy while having a minimum impact on life cycle of a hybrid power system [8] or hybrid energy storage system in REPS. Chong *et al* have reviewed many literatures and categorised the control strategies available into two types, namely the classical and intelligent control strategies [9]. Classical control strategies include Rule-based controller (RBC) and Filter-based controller (FBC). These strategies require a pre-defined threshold and an exact mathematical model of the system and are prone to errors when parameters vary significantly. On the other hand, the performance of AI-based controllers is investigated in Ref. [9] and it is pointed out that AI-based controllers promise a good potential in improving the efficiency of HESS. Intelligent control strategies consist of Artificial Intelligence controllers such as Artificial Neural Network (ANN), Fuzzy Logic controller (FLC) and Neuro-Fuzzy controller (NFC). In general, intelligent control strategies can handle more complex design requirements of EMS as REPS are getting more complicated nowadays.

In this research, an AI-based control strategy is proposed to power solar-based REPS. The strategy is given the name of RE-SOINN EMS since it is based upon RE-SOINN model. The RE-SOINN EMS, unlike some of the AI-based EMS in the literature, embeds a traditional control strategy into its operation, the FBC to smoothen the system power. With the ability to produce an hourly prediction of solar energy generation and power demand, then the RE-SOINN EMS manages the system power by calculating appropriate system parameters on one-minute interval basis. There are two instances of RE-SOINN in this EMS:

(i) the first RE-SOINN tackles the hourly prediction of solar irradiance and load demand using historical trends and timestamps

(ii) the second RE-SOINN manages the flow of power within the system between solar panels, HESS and loads.

The RE-SOINN EMS developed in the study is compared to conventional system and other popular EMS adopted in both simulations and experiments.

1.2 Problem Statement

This research is aimed to take on the following issues:

- Solar irradiance forecasting has been a very trending research topic. Many literatures from the past have performed weather and solar irradiance forecasting using different AI models with complicated input features such as cloud cover, air humidity, temperature, wind speed and satellite image for better forecast accuracy. The high number of inputs requires the REPS to be equipped with numerous costly sensing instruments, not to mention increasing the system complexity indirectly. On the other hand, insufficient or low number of inputs to the forecasting model would result in a poorer prediction accuracy, affecting the performance of proposed RE-SOINN EMS.

- Erratic load demand together with random local weather pose complicated energy management problem. Conventional EMSs require exact mathematical representation of the entire system under the influence of the multiple stochastic factors. Consequently, user needs to be able to define the REPS mathematically for optimised performance of the REPS, especially in a standalone setting.
- Most of the EMS developed in the past literature are rigid in the sense that they are incapable of performing as the working condition changes. Operational environment can be inconsistent due to a sudden change in consumer / user behaviour, a slow transitional change of climate or even aging of REPS components. Traditional EMS such as RBC and FBC are not flexible as they are predefined using exact mathematical equations describing the states of the REPS prior to deployment stage. AI-based EMS models also suffer plasticity in the sense that once these models are fully trained, new varying data which are collected after training stage will be discarded from training dataset. As a result, these AI models fail to adapt to gradual change in working environment too.
- AI-based EMS models work better than conventional EMS at the expense of much higher computational complexity. The mismatch between EMS computational complexity and REPS computational hardware capability will lead to long training time of the AI models, rendering the system to fail working in real time applications. Eventually, the REPS would require powerful computational hardware for good performance of AI-based EMS models.

1.3 Research Aim and Objectives

This research work is focused to fulfil the aim of developing an embedded energy management and control system for off-grid applications such as solar powered rural households, electric vehicles and battery powered devices to improve the system lifespan.

This study embarks on the following objectives to fulfil the aim of the research work:

1) To analyse the features and variations in solar irradiance for solar irradiance prediction.

2) Based on the identified features and strategies, to develop an online learning energy management strategy to perform real-time prediction and control.
3) To validate the developed algorithms against a wide range of load profiles for various weather conditions.
4) To develop a prototype embedded system with supercapacitors for the implementation in a solar cabin.

1.4 Significance of Research

Throughout the entire research journey, several significant contributions are introduced via this research work:

1) Up to date, there is lack of research in short-term solar irradiance forecast using Unsupervised Learning Artificial Intelligence algorithm. Most of the recent studies utilise more complicated but powerful Deep Learning AI models of Supervised Learning to perform solar irradiance prediction. Despite good prediction accuracy by these Deep Learning AI models, they are very computational expensive, turning the forecasting model into a power-consuming beast in an off-grid REPS. The impractically long training time due to the complex Deep Learning AI model architecture is another blow to off-grid REPS. Thus, a less computational expensive solar irradiance forecasting model is developed based on Unsupervised Learning AI model, namely Regression Enhanced Self-Organising Incremental Neural Network. This new forecast model can work like a black box without any interference from users, adaptive to gradual change in weather, incurs much lower computational complexity and uses historical solar irradiance trend together with timestamps as forecast model inputs.
2) Many conventional EMS models such as RBC and FBC require predefined mathematical representation of the entire REPS under the influence of regular inputs in normal conditions. Though this could ensure accurate response of the REPS, the conventional EMS begins to fail when the working conditions start to change. The proposed RE-SOINN-based EMS is able to adjust its knowledge base

according to newly learnt data via Incremental Learning. Thus, the proposed EMS can produce relevant outputs in long run even though situational circumstances may no longer remain the same.

3) Compared to PSO-optimized based EMS such as PSO-optimised FLC [10] and SOM-PSO model [11], the novel proposed EMS using RE-SOINN is able to output optimal responses using much significantly less time in each round of computation upon reaching maturity after training. The training of SOM takes much longer time than RE-SOINN for the same training data. Thus, the proposed EMS model outperforms controllers in [13-14] in computational time as well as training time.

4) The proposed EMS model is lightweight that it can be implemented in simple embedded system such as Raspberry Pi without significant compromise to EMS performance. As a result, the EMS can run on low-powered devices owing to its low power consumption requirement.

1.5 Scope of Research

This research work places emphasis on prolonging the lifetime of battery in HESS of standalone PV system with battery-supercapacitor HESS with implementation of Artificial Intelligence-based EMS in rural household applications where grid power is inaccessible. The scope of this research work includes improving battery operation lifespan, prediction model to forecast hourly solar irradiance as well as implementation of Unsupervised Learning AI model as prediction and EMS models.

1.6 Thesis Outline

This thesis consists of 7 chapters. In Chapter 1, the overview, problem statements, research aims and objectives, significance as well as scope of the research are presented.

Chapter 2 discusses the background study of the research, including conventional REPS with ESS, present REPS architecture with HESS and the problems arising from erratic power supply and demand. Novel control strategies or EMS from the past literature as well as solar harvesting improvement techniques, short term forecasting of solar irradiance and load demand are critically reviewed in this chapter too.

Chapter 3 depicts the algorithmic structure of E-SOINN as well as the modification from E-SOINN to RE-SOINN. The rationales of the modification and the advantages of RE-SOINN over E-SOINN are also discussed. The tuning operation of hyperparameters in RE-SOINN are briefly studied.

Chapter 4 illustrates the AI model developed for short-term forecasting of solar irradiance and user load demand using AI model with Unsupervised Learning, the Regression Enhanced Self-Organising Incremental Neural Network (RE-SOINN). This novel forecast model is compared with conventional forecast models.

Chapter 5 describes the novel AI-based EMS developed in this study to manage the power flow within the REPS – HESS system. The backbone of the novel EMS is derived from RE-SOINN as well. The ideal and the practical performance of the novel RE-SOINN based EMS are presented.

Chapter 6 concludes the research work. Recommendation of future works to enhance the research is laid out here too. Chapter 7 contains the appendices depicting the integration of the subsystems in the Solar Cabin for the implementation of proposed novel forecasting model as well as proposed novel EMS.

Chapter 2 Literature Review

The literature review chapter details the background information of conventional REPS with ESS as well as HESS. Subsequently, the conventional as well as state-of-the-art energy management strategies (EMS) for REPS with HESS are discussed. EMS that are critically reviewed include traditional control strategies as well as intelligent control strategies consisting of Artificial Intelligence (AI) of different learning topology and structure. Reviews of AI-based Optimisation Control Strategies or EMS in relation to solution quality and satisfying multiple constraints are also presented. The advantages of Incremental Learning in further improving EMS of REPS are also studied. In addition, this chapter also presents the short-term solar irradiance forecasting studies from the past literature, with a focus on basic input features. Embedded systems commonly adopted in AI-based REPS are briefly discussed to provide an understanding on common embedded system in powering the AI-based EMS.

2.1 Standalone Renewable Energy Power System (REPS) with Energy Storage System (ESS) and Hybrid Energy Storage System (HESS)

In remote areas that are out of reach of by main electric grid, standalone renewable energy generation can offer the benefit of reduced maintenance and running costs [12], [13]. Commonly, a renewable energy generation is unable to supply the entire load demand the entire time due to the variable nature of renewable power sources and load demand. Tariq *et al.* propose the use of hybrid REPS by combining two or more renewable energy sources together for more reliable energy productions [14]. Despite the benefits of hybrid REPS, the cost to integrate multiple renewable energies increases due to:

- Increased requirement for ancillary service
- Increased curtailment costs for both renewable and traditional power plant
- Higher operating and maintenance costs for traditional power plant due to increased cycling and ramping due to intermittent nature of REPS

Therefore, REPS alternatively rely heavily on ESS to ensure a continuous power supply to the load. Lately, Battery Storage System is used dominantly in the market as it could handle issues of load demand and power generation fluctuations in real life applications. Also, their easy implementation and geographical independence make them the most basic and popular ESS [15].

Battery, though it is an example of high-energy storage, suffers in high power demand applications. The advanced battery technology now allows extraordinary energy densities but often insufficient power densities for applications where the load draws large power impulses. The general practice is to parallel more batteries to share the dynamic stress but such design always incurs very high cost. Therefore, a supercapacitor is added in parallel to the battery to improve the situation. Supercapacitor is an example of high-power storage devices which is capable of matching high-power density demands [16]. The benefits of battery-supercapacitor design include extending the operation life of battery, reducing the design and manufacture cost as well as increasing the capability of the hybrid energy storage system in handling varying power demands [13], [17]. Dougal *et al.* have investigated the performance of battery-supercapacitor HESS with respect to energy efficiency, power capabilities as well as cost effectiveness [18]. The peak stresses on the battery could be relieved in the presence of supercapacitor. Many research focus on the use of lead acid and lithium-ion batteries whereas some researchers do look into the usage of other chemical batteries such as Vanadium Redox Battery (VRB) [16].

An ideal power source should have high energy storage, capable of delivering high power over a short duration of time [13] (short burst of power), high charge and discharge efficiency, long duration of working life as well as low in cost [19]. However, in real application, due to cost constraints, a battery is generally used as the primary source at the expense of shorter lifespan. Researchers from Illinois Institute of Technology introduce an energy source model where a battery and a supercapacitor work in parallel [20] in electric vehicle. Supercapacitor can supply a huge burst of current but suffers in storage issue. Therefore, the storage and peak current characteristic can be achieved. The implementation of battery and ultracapacitor in parallel has reduced the number of spikes in the current from the battery as seen from Figure 2-1. Table 2-1 also shows the performance comparison between battery and supercapacitor.

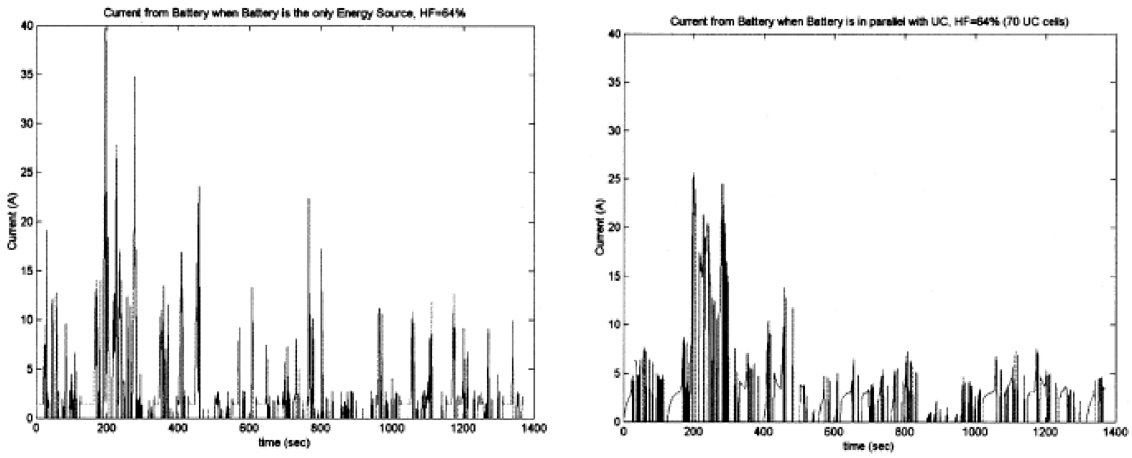

Figure 2-1 - Comparison of Current Profiles of Battery only and Battery in parallel with Ultracapacitor [13]

Table 2-1 - Battery vs Ultracapacitor Performance [13]

Performance	Battery	Supercapacitor
Specific Energy (storage)	10 – 100 Wh/kg	5 – 10 Wh/kg
Specific Power (delivery)	< 1000 W/kg	< 10000 W/kg
Charge/discharge efficiency	50 – 85%	85 – 98%
Life expectancy	3 years	10 years

Gee *et al.* have performed an analysis of battery lifetime extension in a small-scale wind energy system using supercapacitors [21]. The potential improvement in the battery lifetime could be achieved by allowing the supercapacitor to handle the short-term charge and discharge cycles of power. In many cases, battery itself constitutes a huge part of the total cost of REPS but fails easily in high-current cycling events. Therefore, the main goal is always to extend the lifetime of battery. The simulation results have shown that the HESS undergoes significantly fewer polarity reversals and thus fewer charge and discharge cycles. The battery lifetime could be improved by 19%. Also, the low-pass filter used in the system further reduces the battery cyclic wear and current maxima. All these benefits could be reaped at the expense of slightly lower efficiency compared to battery-only system after taking efficiency of the supercapacitor into the consideration.

While most of the research focus on battery-supercapacitor HESS to meet the power demand of the load to prevent unnecessary deep-discharge cycles, Sioe *et al.* seek how this HESS could improve the charging efficiency of photovoltaic battery [22]. The PV source delivers erratic recharge current and sometimes this current is less than the recommended C/2 value. As a result, a longer recharging time is expected and recharging sequence is often interrupted. Also, quick recharging events elevate system temperature which decreases battery capacity and battery life. Therefore, the supercapacitor acts as buffer to reduce battery charge current to control the battery temperature during recharging phase.

A research team from Sweden has sought the possibility of using PV or hybrid PV battery systems to provide self-sufficient energy to meet the user demand in a residential building in Sweden [23]. Three different kinds of batteries, lead acid, NaNiCl (Sodium-Nickel-Chloride) and Lithium ion are studied, and it is found that Lithium-ion battery performs the best since it achieves the highest Self-Sufficiency Ratio (SSR) with the same Life Cycle Cost (LCC) among the three batteries. However, to achieve efficient long term energy storage (storing energy surplus from summer for usage in winter), high capacity of battery required incurs high LCC. Hydrogen fuel cells are thus recommended instead.

German researchers utilise the idea of smart integration and control of short and long-term storage technologies to improve self-consumption rate, conversion efficiency and storage lifetime in PV systems [24]. The hybrid PV system consists of lithium-ion battery, hydrogen and heat storage path. The uncommon heat storage intrigues the researchers due to its low specific investment costs. Researchers from Morocco have explored the usage of supercapacitor to reduce the stresses on batteries to improve the life cycle [25]. Ma, Yang *et al.* have proposed a new type of HESS to perform fast dynamic power regulation for remote areas [26]. An inductor is added into the passive HESS system in series to the battery branch as an upgraded connection. The battery output is stabilised and smoothened by the filtering effect of inductor.

As a summary to Subsection 2.1, HESS is proven to be able to improve performance of REPS by combining the high specific power and high energy devices. The benefits include peak power demand shaving, reduction of battery power oscillation as well as extension of battery lifespan.

2.2 Control Strategy

While the battery technologies are getting more advanced and complex, power circuits are more efficient, there exists a huge room of improvement for EMS. EMS is the brain of the entire REPS-HESS system as it coordinates the power distribution between the sources, ESS and loads to optimize the energy utilization and system sustainability. The usage of renewable energy technology requires a comprehensive energy management strategy to achieve optimal fuel economy while having a minimum impact on life cycle of a hybrid power system [27] or hybrid energy storage system in REPS. In short, successful EMS ensures REPS system stability and protects the components from overloading damage [18]. Its main responsibility is to [29]

- Prevent deep discharge of battery
- Reduce dynamic stress level of ESS-E, peak power demand, charge-discharge cycle
- Reduce the operational cost of the system
- Maintain stable DC voltage
- Improve overall system efficiency

While both off-grid and grid-connected renewable energy power systems share common goals of optimizing energy use and minimizing environmental impact, their control strategies are tailored to their specific operational requirements and the surrounding infrastructure. Off-grid systems prioritize autonomy and energy storage, while grid-connected systems focus on grid stability, adherence to regulations, and participation in energy markets [30], [31]. The control strategies in off-grid REPS are to match energy generation to the varying load demand of the off-grid system. In ensuring continuous power supply, off-grid REPS could employ hybrid REPS combining multiple renewable sources. In grid-connected system, however, the control strategies place huge emphasis on maintaining grid stability despite the fluctuations in renewable energy generation, allowing for bidirectional energy flow. Moreover, frequency regulation and demand response are an integral part of control strategies in grid-tied REPS. The economic considerations do not only cover the cost of implementation of a REPS, but also the participation in energy markets, selling excess energy back to the grid depending on the market conditions.

Traditionally, to achieve system control for an off-grid REPS, the first step is to model the entire system mathematically so that a mathematical model of the system can be used to simulate the response for any given inputs in design and verification stage. However, such measure is only recommended if the overall system is not too complicated and the operating conditions do not change significantly over time. Control strategies using mathematical model also lacks the ability to adapt to environment.

Chong *et al.* have reviewed many literatures and categorised the control strategies available into two types, namely the classical and intelligent control strategies [32]. Classical control strategies include RBC and Filter-based controller (FBC). These strategies require a pre-defined threshold and an exact mathematical model of the system. They are prone to errors when parameters vary significantly. RBC concurrently considers the power demand and evaluates reference power based on pre-set rules whereas FBC decomposes the power demand into high-frequency and low-frequency components using low-pass filter (LPF), moving average filter (MAF) and wavelet transformation.

2.3 Intelligent Control Strategy

In the dynamic landscape of Renewable Energy Power Systems (REPS) and Energy Management Systems (EMS) control, Intelligent Control Strategy such as Artificial Intelligence (AI) emerges as a pivotal force driving innovation. This overview of Intelligent Control Strategies explores the transformative impact of AI-based controllers, including technologies such as Artificial Neural Networks (ANN), Fuzzy Logic Controllers (FLC), and Neuro-Fuzzy Controllers (NFC), in optimizing Hybrid Energy Storage Systems (HESS). The applications of these controllers span a spectrum of critical functions within REPS, from predicting solar radiation and wind speed to forecasting load demand and facilitating seamless grid network integration. As the complexities of REPS evolve, AI's adaptability becomes increasingly evident, reducing the dependence on prior system knowledge. This overview sets the stage for an in-depth examination of AI's role in EMS control, categorizing algorithms based on learning schemes and applications, providing a comprehensive understanding of their contributions to the dynamic field of REPS.

Intelligent control strategies consist of Artificial Intelligence controllers like ANN, FLC and NFC. Chong *et al.* point out that AI-based controllers promise a good potential in improving the efficiency of HESS [32] and Ref [21] states AI can create significant electricity value chain. AI models are usually applied in REPS, especially in prediction of solar radiation and wind speed, forecast of load demand, modeling and sizing of a component in REPS [34] as well as predictive maintenance and reduction of REPS and grid network integration [21]. Researchers in [35] propose the use of AI models to forecast the outcome of analyses due to a planned outage in electricity transmission system to identify optimal period for scheduling grid maintenance. Rising trend in renewable energies would inevitably further complicate the scheduled maintenance of national power system.

There are three main functionalities of AI in energy management field, namely system modeling, knowledge learning and reasoning [24]. Learning is the continuous adaptation of AI models using past experience, either historical relationship or statistical trends so that decisions made will get more and more favourable towards users [26]. Ramos *et al.* prove that trained models produce very consistent predictions with relatively high forecasting accuracy [38]. Its design is independent of system parameters but it needs an enormous amount of past historical data (labelled data) for learning and tuning process in order to get accurate.

ANN-based controller is popular as EMS because it could handle nonlinear and adaptive structure [25]. On the other hand, FLC is easy to be designed and is less sensitive to inconsistent parameters. It uses entirely rule basis and membership functions. FLC suffers in defining suitable membership functions due to its trial-and-error nature. The process is time-consuming for an optimized performance. NFC combines the inference ability deriving from fuzzy logic as well as learning and parallel data processing abilities from ANN. It could identify and tune the membership function of the FLC, highly improving the accuracy of a fuzzy model without long development time.

In general, intelligent control strategies can handle more complex design requirements of EMS as REPS are getting more complicated nowadays. As a result, less prior knowledge of the system nor the mathematical model of the system is needed in designing an intelligent control strategy. Classical control strategies always fail in cases where adaptability is deeply required as these classical strategies only work under specific operating conditions that are being taken into design considerations. Also, certain intelligent control strategies are very intuitive to human reasoning, making them to be very suitable as EMS in highly complex REPS systems.

There is a new trend of using predictive model to input predicted information into control strategies to achieve optimal performance. It allows planning of power distribution prior to an actual power deficit based on predicted future value of load and power output of RE sources. Compared to a classical control strategy, it is easier to incorporate the prediction module into AI-based control strategy. Subsequently, AI-based control strategy is able to fully utilize the predicted information in many ways such as planning the system operation ahead of time. There is no doubt that the learning capability of AI allows historical data to be useful as the model can be tuned for better performance by looking for useful information within the historical data.

Looking at past literature, some researchers integrated both predictive control strategy and optimisation-based controller for better performance [38–40]. For recent studies, Artificial Intelligence (AI) is usually implemented as the backbone of these EMS. Thus, at most of the stages of research, past literature on how different AI is applied in EMS is reviewed. Applications of AI in EMS can be discussed thoroughly from algorithms, adaptations and practical implementations. This review has categorized the AI algorithms into a few categories: Machine Learning algorithms such as Supervised Learning, Unsupervised Learning, AI-based Optimisation and Incremental Learning as well as Computational Intelligence such as Fuzzy Logic and ANFIS based on learning schemes of the AI models as well as fields of applications.

2.3.1 Machine Learning

In general, supervised learning can be understood as "learning with a teacher" [40]. In this learning process, the environment is unknown to an AI model. A "teacher" who has the knowledge of the environment serves as a benchmark or a standard by providing the AI model with desired responses for each input in the training phase. The parameters of the AI model are then adjusted based on the combined influence of error signal and training vector [40]. In the context of EMS, a "teacher" is usually desired output such as desired operating voltages. An important way to perform supervised learning is the *error-correction learning* where the entire supervised learning process is equivalent to a closed-loop feedback system. The discrepancy between the reference or the desired output and the actual output is used to correct or update the parameters of the applied AI model. At the end of the training phase, the AI model is expected to produce outputs similar to the desired outputs.

There are two types of supervised learning AI models which are frequently applied as EMS due to their simplicity and good ability to approximate an unknown input-output mapping. The first is the ANN which mimic the way human brains work and the second being Support Vector Machines (SVM), a fast and effective classification algorithm that performs remarkably well with limited amount of data. In general, supervised learning AI are applied in prediction and simple decision-making cases. Some researchers have shown that embedding a prediction module into EMS could improve power dispatch planning [41]. For instance, accurate prediction of solar irradiance values allows the planning of operation of solar power plants to be more accurate as planning can be made beforehand.

Unlike supervised learning which requires the presence of a "teacher" to explicitly specify the desired outputs, in unsupervised learning, there are no labelled examples to be learned by the AI model [40]. Instead, the AI model needs a task-independent measure of the quality of representation of data [40]. Subsequently, the free parameters of the model are optimized based on the measure. The AI model is tuned based on the statistical information of the input data by forming internal representations for encoding features of the input and thereby creating new clusters [40]. In Ref. [36], only 8.3% of the AI techniques applied in the monitoring component of EMS is Unsupervised Learning, less than 1% of Unsupervised Learning AI is commissioned in both analytical and control components [24].

A common practice in unsupervised learning is the implementation of competitive-learning rule. For instance, in Self-Organizing Map (SOM), the competitive-learning rule dictates that the neurons compete among each other for the opportunity to respond to features contained in the input data such as winner-takes-all strategy [40]. In this strategy, the neuron with the biggest total input "wins" the competition and is thus turned on whereas all other neurons are switched off. The application of unsupervised learning in EMS is usually to perform data clustering and classification so that distinctive cases can be differentiated more evidently, leading to more specific responses towards certain triggering events. In certain cases where the EMS is not too complicated, output of EMS can be obtained from clusters by Unsupervised Learning. In Ref. [33], the researchers have compared a number of machine learning classification algorithms such as Random Forest, Decision Trees, Gaussian Naïve Bayes and K-Nearest Neighbours (kNN) in predicting the scheduling of energy sources. These Unsupervised Learning models can produce good forecast according to this study. Decision Trees model performs the best while kNN scores the worst. The subsequent proposed data normalization extra step can improve kNN model to average performance.

2.3.2 Computational Intelligence

Machine Learning reflects the overarching principles of AI models in learning from data. On the other hand, Computational Intelligence is a broader category that emphasizes the use of intelligent algorithms to handle uncertainty and imprecision in data.

2.3.2.1 Fuzzy Logic

Fuzzy Logic, an idea conceived by Lofti Zadeh is aimed at allowing computers to process ambiguous events resembling human reasoning. The nature of human reasoning is fuzzy as human tends to use the vague terms in describing the quality of a feature of an event or an object. These imprecise terms have increased the difficulty of computers to handle subjective data since computers excel at traditional logics which are binary in nature. Thus, Fuzzy Logic is created to work on range of possibilities of inputs to produce definite output.

A Fuzzy Logic system can be defined as the nonlinear mapping of an input data set to a definite and scalar output [43-45]. In general, there are four main components in Fuzzy Logic system, namely the fuzzifier, knowledge base or rules, inference engine and defuzzifier. Thus, FL control process is made up of an input stage, a processing stage and an output stage [42] based on the four main components as shown in Figure 2-2.

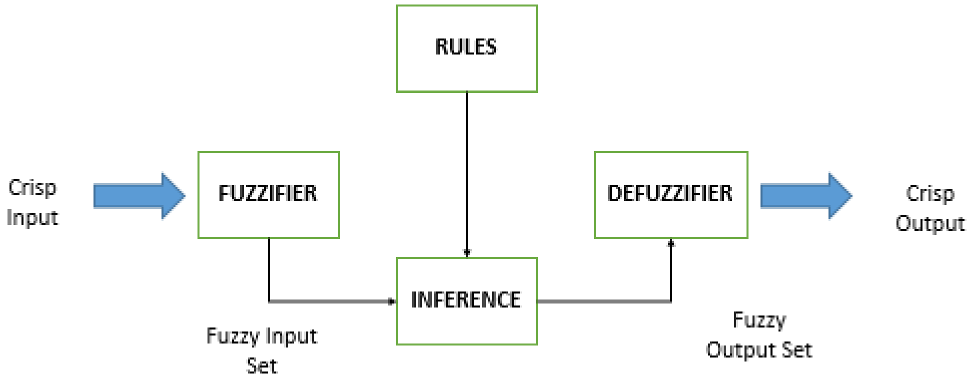

Figure 2-2 - Architecture of a FL system [42]

FL is simple to be implemented in almost all kinds of control problems due to its robustness on non-linear control systems by adopting linguistic descriptions for global behaviour [43] of a controller for a specific application. FL controller does not require any mathematical model of the plant [44]. On fine-tuning, it gives better performance in terms of accuracy compared to traditional controllers. It can also introduce multiple input variables in the controller structure without increasing the complexity [45]. Thus, FL is suitable to be implemented as EMS of REPS provided the Membership Functions (MFs) and the parameters are tuned well. Figure 2-3 shows how FL is applied as EMS controller.

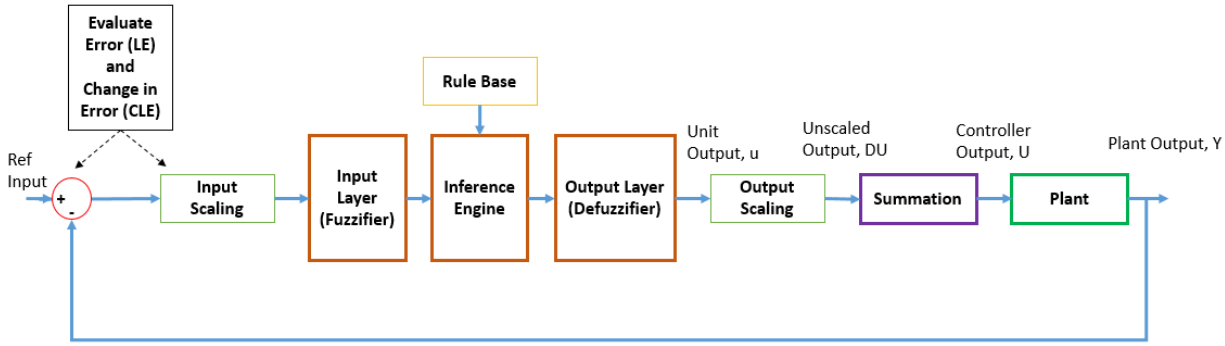

Figure 2-3 - An example block diagrams of a system with FL being implemented as controller

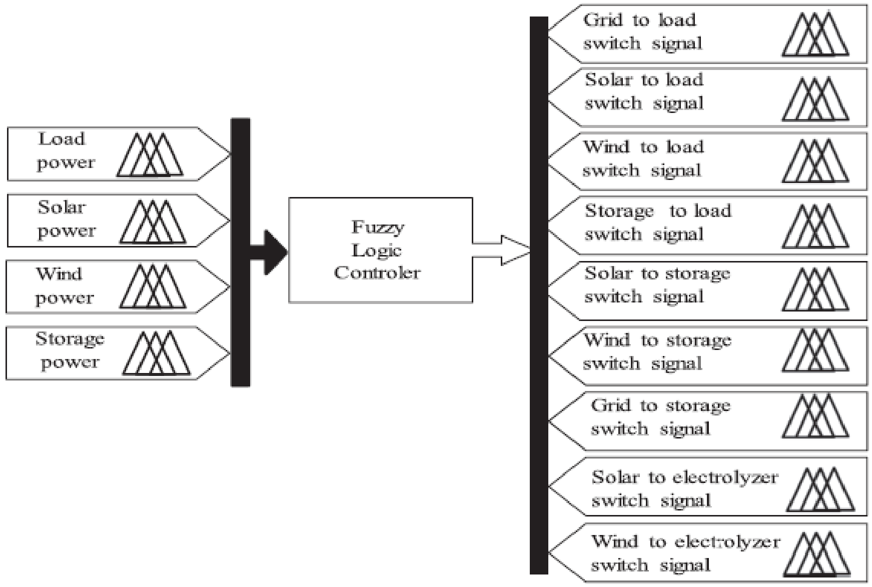

Figure 2-4 - Architecture of multi-input-output FL smart controller [46]

Derrouazin *et al.* have proposed a multi-input-output Fuzzy Logic smart controller to exploit simultaneously the renewable energy produced and to ensure savings of electric grid energy [46]. The controller consists of four inputs, namely the load demand, solar and wind energies, the four energy fluxes of the system and the storage battery system as demonstrated in Figure 2-4. The four inputs are mapped to three levels (High, Medium and Low) using triangular membership function. The nine outputs of the controller are the electronic switch command signals (electronic switches duty cycle levels) to supply the load demand, the batteries and the electrolyser system. The output membership function adopts the Max-Min method and crisp result is obtained by using centre of gravity defuzzification. The MATLAB simulation results have shown that control signals of the electronic switches produced are able to track successfully, leading to energy saving of

77.87% compared to a house without Hybrid Energy System with Fuzzy Logic smart controller.

In the operation of asynchronous motor powered by PV-battery ESS, a Fuzzy Sliding Mode Control (SMC) is presented by Lekhchine *et al.* to curb the chattering issue introduced by regular SMC due to rapid switching [47]. Kamal *et al.* design a two-level centralized FL supervisor controller to produce power references for each decentralized robust FL controller as EMS in standalone Hybrid Power System consisting of a PV panel and Wind Turbine (WT) [48]. The centralized controller is designed based on Mamdani method to manage power production by generating the reference power for PV and WT. Decentralized controller, on the other hand, takes Sugeno method to stabilise each PV panel and WT under disturbances and parametric uncertainties and to ensure the reference provided by centralized controller is reached. Figure 2-5 shows the block diagrams of the system.

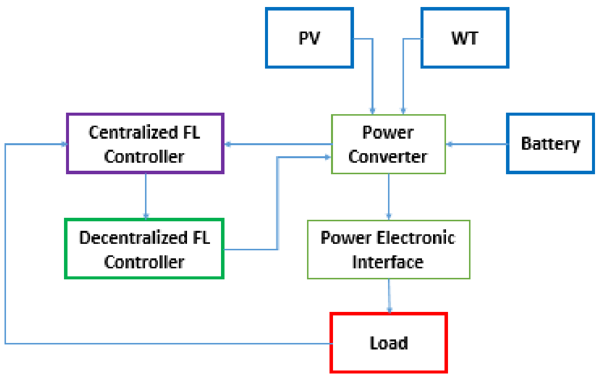

Figure 2-5 – Block diagrams of FLC as EMS in standalone HREPS [48]

In Ref. [44], FL is applied in autonomous control of PV-Solid Oxide-Fuel Cell-Battery micro grid to control the grid voltage and frequency effectively and to smoothen power flow between generation and consumption. Abadlia *et al.* devise a FL-based controller to achieve energy continuity and maximise the production of hydrogen in REPS consisting of PV, hydrogen fuel cell and battery [49]. Application of FL controller has made the design process relatively easier as no prior mathematical model is required for the system to function smoothly. Garcia *et al.* have combined an optimisation strategy together with FL strategy as EMS in hybrid REPS [50] as a supervisor system that only takes charge of the EMS when the SoC and hydrogen level are out of the range for higher control flexibility.

Zhang *et al.* propose a FL energy management supervision strategy to reduce electricity bill, emission of carbon dioxide as well as to ensure energy availability can be met [51]. The objectives of the supervision strategy are subjected to different electricity pricing periods and thus, the controller must adapt to each pricing period. This is easily done in FL where rules are defined accordingly. FL EMS is also applied in cases where smooth transition between two operating modes in PV-fuel cell hybrid system is vital [52]. For a study in [53], FL EMS which consists of various operating processes of the Hybrid REPS is implemented based on weather conditions to switch between PV, WT and diesel generator. A traditional PI controller is added alongside of FL EMS in Ref. [54] to control continuous power supply to the load by maintaining the SoC of supercapacitors and batteries at safe levels to prevent damage on these storage devices.

Cano *et al.* have included a single-level prediction of the DC net power and its uncertainty from Hybrid REPS into the design of FL EMS and thus allowing a suitable decision that improves the lifetime of the fuel cell-electrolyser [55]. The robustness of this EMS can survive through a stochastic Monte Carlo analysis. To study the difference in performance of ANN and FL as EMS in Hybrid REPS, Tabanjat *et al.* design two EMS based on ANN and FL respectively with the objective of minimizing the energy production cost and increase the role of hydrogen storage system as buffer [56]. Over a 24h load variation, FL shows a more superior performance than ANN as ANN would require more training samples to achieve the same performance. In output tracking, ANN EMS needs more sensors than FL EMS.

Some researchers resort to optimisation algorithms to fine-tune the MFs so that the performance of the FL controller can be improved significantly. In Ref. [57], Mean-Variance Optimisation (MVO) is implemented to produce an optimal FL controller. MVO is suitable for real-time optimisation as it only computes one fitness evaluation per iteration. This adaptive controller is proven experimentally to work much better than naïve FL controller. Particle Swarm Optimisation (PSO) is also utilised to tune the membership functions of FL controller. In Ref. [58], the optimisation of FLC results in reduced fluctuations in SoC of batteries as well as less working hours for fuel cell. Chong *et al.* have also approached the control issue of a standalone PV system with battery and supercapacitor HESS the similar manner [59]. The FL controller constantly minimizes the battery peak current demand while monitoring the SoC of the supercapacitor. To further improve the optimality of battery peak current reduction, the MFs are optimized by PSO. In comparison to traditional approaches such as RBC and FBC, FL-PSO controller reduces the battery peak current by further 16% and the average absolute of change of power is even lowered by 96%. Supercapacitor utilization has also reached 80% under the proposed controller.

Santis *et al.* have proposed a hybrid technique consisting of Genetic Algorithm (GA) to work alongside of Fuzzy Logic controller [60] to maximise the accounting profit in energy trading with the main grid. The role of the GA is to tune the knowledge base of the Fuzzy Logic controller so that minimal fuzzy rules can be set as the core inference engine of the controller. In experimental validation, it is shown that the Fuzzy-GA outperforms the classic FL by using only 47% of rules within the knowledge base. Berrazouane *et al.* have adopted the Cuckoo Search (CS) optimisation algorithm in tuning the membership functions of the FL controller [43]. It is found that the CS-optimised FL controller could minimise LPSP, excess energy and levelized energy cost (LEC) better than PSO-optimized FL controller could. Shuffled Frog Leap (SFL) optimisation algorithm is applied to tune a FL controller in [45] for minimizing the operational cost of Hybrid REPS based on weekly and daily prediction of data for grid electricity price, electrical load and environmental parameters. The weekly and daily optimized FL controller is proven to reduce the working hours for fuel cell and electrolyser as well as less fluctuations in SoC of battery slack.

Abedi *et al.* have incorporated EMS with sizing procedure of a Hybrid REPS to determine optimal EMS for entire system including various generators and energy storage devices [61]. In the study, Differential Evolution Algorithm (DEA) together with FL is used to deal with mixed-integer nonlinear multi-objective optimisation problem. The EMS is trained to adapt to climate changes by determine the parameters for EMS monthly as well as to calculate the optimum monthly tilt angles of PV panels and the optimal tower height for wind turbines for efficient power exploitation from REPS.

2.3.2.2 Adaptive Network-based Fuzzy Inference System (ANFIS)

A neuro-fuzzy system is a fuzzy system which employs learning algorithm from Neural Network to determine its parameters [62] by adopting framework of adaptive networks [63]. ANFIS adopts the Sugeno type Fuzzy Inference Method where the premise part is fuzzified and the consequence is a crisp function such as a polynomial function. ANFIS can automatically determine suitable parameters for the MFs using stipulated input-output data pairs. It maps

- Input characteristics to input MFs
- Input MFs to rules
- Rules to output characteristics
- Output characteristics to output MFs
- Output MFs to a single-valued output or a decision associated with the output.

Mahmud *et al.* propose a cooperative performance of a new Proportional-Integral Derivative (PID) control scheme based on ANFIS for PV interfacing inverter and an ANFIS-based supervisory storage EMS to regulate the voltage of three-phase grid-connected solar PV system under any nonlinear and fluctuating operating conditions [64]. ANFIS-PID can adapt the nonlinear states of distribution system voltage profile to tune the PID gain parameters automatically to inject or absorb appropriate reactive power to regulate the voltage at common coupling point. On the other hand, ANFIS-based EMS charges and discharges the ESS whenever there is voltage deviation to cooperate with ANFIS-PID in voltage regulation. The cooperation of the two control schemes can minimize the voltage deviations at common coupling point and reduces reactive power injection/absorption load on the PV inverter.

Garcia *et al.* design an ANFIS-based EMS for a grid-connected hybrid REPS comprising of WT and PV as primary energy sources with hydrogen-based ESS and battery as the HESS [65]. Similar to Ref. [64], ANFIS is preferred in this study because ANFIS performs faster in terms of convergence. In the performance evaluation stage, this control scheme works better than the combined action of state-based supervisory control and PI inverter controller. In Ref. [66], an ANFIS-based EMS is presented to control HREPS connected with AC load. ANFIS works better in this application to improve the power transfer capability between the source side and the load side and to lower system complexity. The said EMS produces appropriate control signals at the testing time to match the source power and load power according to the load variation.

2.4 Supervised Learning-based AI Control Strategy

2.4.1 Artificial Neural Networks (ANN)

Inspired by the operation as well as the architecture of a human brain, ANN consists of a group of neurons. An artificial neuron is an information processing unit that is fundamental to the operation of a neural network [40]. It consists of three basic elements as depicted in Figure 2-6:

- Synapses are represented by weights vectors, *w* to specify the strength of a signal to a neuron.
- An adder (linear combiner) to sum up the input signals weighted by respective synapse strengths [40]
- An activation function to limit the amplitude of the output of a neuron to a finite range of values. A typical activation function is threshold function or sigmoid function.

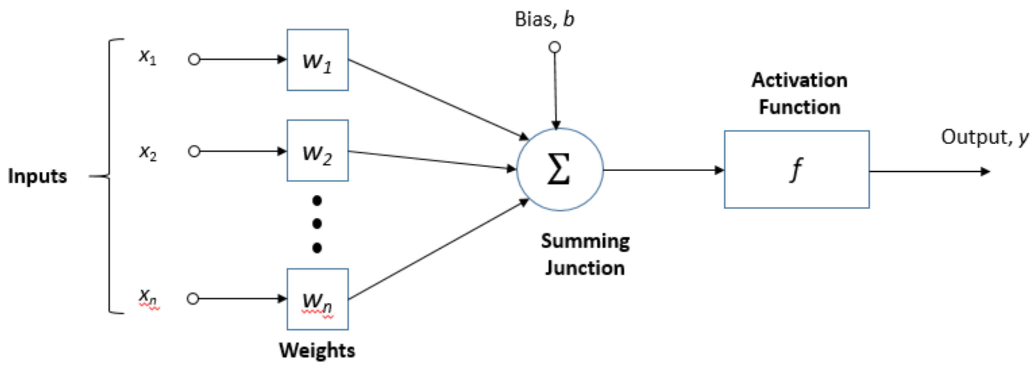

Figure 2-6 - Nonlinear model of a neuron [40]

A neuron, said with a label *k,* can be represented with two mathematical terms

$$u_k = \sum_{j=1}^{m} w_{kj} x_j \tag{2-1}$$

$$v_k = u_k + b_k \qquad (2\text{-}2)$$

$$y_k = \varphi(u_k + b_k) \qquad (2\text{-}3)$$

when a group of neurons are organized in layers where an input layer of source nodes projects directly onto an output layer of neurons [40], this is known as a *feedforward* ANN of single layer. In the presence of additional layers between the input layer and output layer, a multilayer feedforward network is thus formed. These internal layers are known as *hidden layers*. The role of hidden layer is to extract higher-order statistics from its input [40]. A multilayer perceptron (MLP) is a feedforward neural network with one or more hidden layers as shown in Figure 2-7.

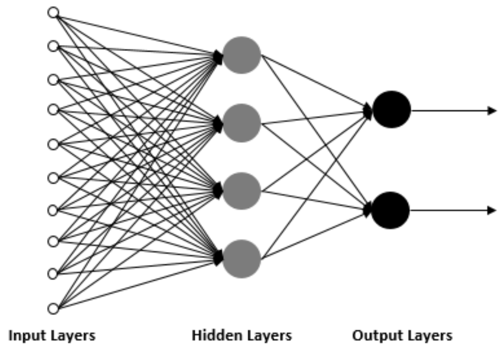

Figure 2-7 - A fully connected feedforward network with one hidden layer and one output layer [40]

ANN, being modelled as a black box regularly, can simplify complicated systems into simpler systems consisting of inputs, outputs and functions defining the relationships without the need to understand the operations in between. As the load demands and power requirements are getting more complicated, the design of REPS would be getting more complex as a response to fulfilling such requirements. As a result, the design of EMS will be a complicated task. ANN, as a universal mapping solution, is therefore a popular solution among the researchers. ANN is also applied as prediction engine to assist in the working of EMS to improve the performance. The learning algorithm of ANN is generally able to construct the relationship between inputs and outputs given inputs are historical data and outputs are data in future time span.

In Ref. [67], an ANN controller approach is chosen due to ANN's faster response compared to optimisation-based methods. Its ability to learn from examples and to produce rapid responses to new data has allowed ANN to be applied widely in this field.

Piazza at al present a novel two-stage EMS for small scale grid-connected electrical systems consisting of REPS and ESS [68]. In the proposed EMS, solar irradiance and load demand are forecasted using historical data and two ANNs respectively. The proposed EMS shows its robustness towards prediction errors with lower normalised Root Mean Squared Error (nRMSE) and normalised Mean Absolute Error (NMAE) scores compared to the reference EMS focusing on improving the user's cash flow.

In a study to determine an optimized smart appliance schedule, Yuce *et al.* combine ANN with Genetic Algorithm (ANN-GA) to reduce energy demand in busy periods, maximizing the exploitation of renewable sources while relying the least on grid energy [69]. The role of the ANN is to learn the complex pattern in EMS based on environmental occupancy factors and to forecast energy consumption and renewable energy generation. The total grid energy usage for a month was 816kWh before implementation of proposed model and after the implementation, the total energy consumption is 734kWh, 612kWh and 490kWh depending on the level of reduction intended. In Ref [70], an EMS is designed to address the intermittent solar energy generation by including an operation to predict solar energy and power generated from the hybrid REPS. The solar energy forecasting model consists of ANN and wavelet transform. The average percentage Mean Absolute Error (MAE) for the prediction is 3.5%.

Taiwanese researcher Huang modifies neural network for dynamic control and operation of a HREPS consisting of PV and wind power with a backup diesel generator [71]. The controller consists of a Radial Basis Function Network (RBFN) which in turns to control the MPPT. A modified Elman Neural Network (ENN) is used to govern the pitch angle of WT. Feedback is added to ENN for better learning efficiency so that the neurons are sensitive to the historical data. The context layer serves as the temporary memory of the hidden layer outputs where the signal recurrence is recognized as a one-step time delay [72]. Usage of ENN increases average output power of WT by 6.2% whereas RBFN increases the output of PV by 14.89%.

Capizzi *et al.* have acknowledged that fluctuations in the energy production of REPS have urged the need of an EMS capable of dealing with possibility of inadequate energy production without jeopardizing user demands [73]. The behavioural profiles of each production plant and consumption devices are first modelled by several ANNs so that energy allocation can be determined thereafter. The predictions of ANN are performed ahead of 48 hours. The ANN model applied is Wiener Recurrent Neural Network (WRNN) to include new data and adapt to the changes over time. The proposed model excels in needing less training data, adapting to temporary phenomena and being able to model the small and large-scale characteristics of the signal, compared to traditional approaches. In another research by the same team [74], they propose the use of cloud technology to enable fast and distributed computation of WRNN while making the data sources and authorised clients to be independent of each other while accessing to the results.

In a microgrid consisting of PV, WT and microturbine, the hybrid control technique consists of a Bacterial Foraging Optimisation Algorithm (BFOA) and ANN to properly control the power flows between the energy sources and the grid [75]. The role of ANN (Feedforward Backpropagation) is to predict the PV, WT, microturbine and battery demands for 24 hours. These predicted values are then given as the input of BFOA so that the optimal outputs for the microgrid can be determined. A reduction of 25% in total generation cost is achieved in a real-time experimentation.

2.4.2 Support Vector Machine (SVM) in EMS

In 1995, Vapnik *et al.* have developed Support Vector Machines (SVM) by employing Structural Risk Minimization (SRM) principle which is considered as more superior to traditional Empirical Risk Minimization (ERM) adopted in ANN [76]. SRM sets an upper limit on the expected risk whereas ERM tries to reduce the error on the training data. Generally, SVM is applied on classification problems where a function (a hyperplane) is produced to separate the two classes without a loss of generality. This is achieved by maximizing the margin or the distance between this hyperplane and the nearest data points of each class. This hyperplane is thus coined as optimal separating hyperplane [76].

The goal of SVM is to produce a model based on training data which predicts the target values of the test data given only the test data attributes [77]. SVM is also known as "kernel" method where the complicated computations within SVM can be simplified using a kernel function. Figure 2-8 shows a dotted red line acting as an optimal separating hyperplane where the distance between this hyperplane and the nearest data point of each class is maximized.

Founded on the concepts of SRM and Statistical Learning Theory (SLT), SVM so far has been widely used in numerous of applications ranging from classification, regression and non-linear function approximation. SVM is used in many REPS applications as a mean to forecast energy consumption with high accuracy due to its ability to solve non-linear problems [78]. One important advantage of SVM is that it is easy to be scaled to deal with high-dimensional data. However, choosing the right kernel function largely depends on designer's experience. Also, the size of ANN can be fixed via number of features but size of SVM is hard to be fixed as each support vector corresponds to a unique feature where the number of unique features can't be known beforehand. In cases of multiple outputs, ANN is usually preferred if the outputs may be interrelated.

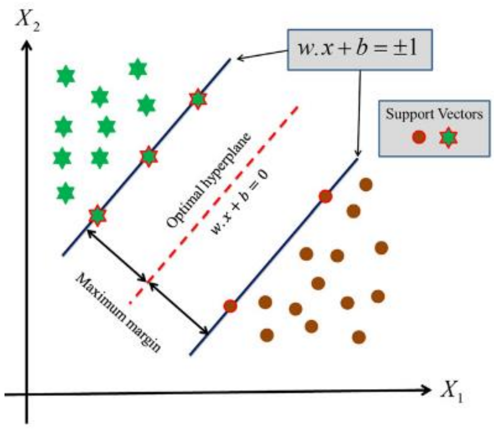

Figure 2-8 - Optimal Separating Hyperplane [77]

Prasanna Vadana *et al.* develop a dynamic EMS controller to make decisions based on status of grid-connected smart microgrid with REPS with SVM and ANN respectively to balance power generation and load demand [79]. The experimental results have indicated that SVM performs better than ANN in this application as training of ANN is tedious as the system becomes more complex. Rambabu *et al.* have designed an EMS of which the goal is to meet the load demand totally while complying to scheme constraints [80]. The proposed model is based on SVM calculation where the output is predicted based on training set produced from projected scheme constraints. Firstly, SVR predicts the load profile and then SVM is trained to classify the actual load profile and to output the control signal to converter for monitoring the power flow. It is reported that SVM outperforms FLC and ANN in this application.

Chia *et al.* propose a load predictive EMS based on SVM to manage the energy flow between a solar energy source, a supercapacitor-battery HESS and load [81]. In the first stage of EMS, a RBF kernel - SVR model is implemented in K-step ahead prediction for load profiles. Subsequently, another SVM performs load profile identification to decide the switching of energy sources such as supercapacitors by using classification method. The experimental results have shown that under the SVM EMS, supercapacitor is able to be turned on much faster to meet the peak load demand whereas the conventional method is 200ms slower, indicating that the battery meets the load first, causing a deep discharge which harms the batteries.

Huang *et al.* use Least-Square SVM (LS-SVM) to predict the output of PV power influenced in designing an EMS for a grid-connected PV microgrid [82]. Then, Modified Artificial Fish School algorithm (MAFSA) is applied to improve the global optimisation ability and the convergence accuracy using cost of electricity as objective function. The LS-SVM model can predict the output PV power very closely to the actual ones. Paudel *et al.* emphasize the importance of prediction of energy consumption in a residential building in formulating an optimal operating strategy [83]. The prediction model is based on SVM-SVR and the relevant days of training data are selected based on Dynamic Time Warping (DTW). Based on the study, usage of DTW with SVR can improve the accuracy of the prediction significantly and reduces the training time significantly from 115 hours to 8 mins on weekdays and from 30h to 7 mins on weekends.

2.5 Unsupervised Learning-based AI Control Strategy

2.5.1 Self-Organizing Map (SOM)

Self-organizing map, as proposed by Teuvo Kohonen, is a mapping tool of a high-dimensional distribution data onto a regular low-dimensional grid in orderly manner [84]. SOM can classify complex and nonlinear statistical relationships found in higher dimensional data items into simpler geometric relationships on lower dimensional display in an unsupervised way. This preserves the topological properties of the patterns in the input space [85]. These neurons are usually arranged over a plane or a line in either rectangular or hexagonal shape with a defined neighbourhood function. The important features, patterns, correlations within the input data are extracted and are incorporated in the internal structure of links and connections of SOM. Thus, the neurons are self-organized based on the inputs.

A three-stage AI-based short term load forecasting is proposed by Hernandez *et al.* as a mean to allow energy production of a microgrid to adapt to the load demand [86]. Firstly, SOM is applied to classify electricity consumption based on days and similarities found in different load patterns and thus forming different classes or clusters. Each cluster is represented by one prototype pattern in the feature space. Then, MLP is used to generate prediction values. This model has reduced the errors generated by prediction compared to a general MLP.

On the other hand, Llanos *et al.* have implemented SOM as a household classifier to study the load patterns by using the socio-economic characteristics of the community [85]. This SOM is essential to improve the efficiency of energy supply for uninterrupted load for 24 hours. A heuristic method is used as a search module to find the closest class for real-time inputs based on similarity. In Ref. [87], SOM is applied in a similar way as [85] and is compared to k-mean clustering method. SOM is easier to be applied because the cluster number does not have to be defined beforehand while achieving similar performance.

2.5.2 *k*-Means Clustering

Clustering is a technique to divide data objects into groups based on information or feature values found in data that differentiates one group from another without labels. Stuart Lloyd first introduced the k-means algorithm in 1957 but it was until 1967 that James MacQueen coined the term "k-means". This algorithm is a partition-based clustering method where all clusters are determined at once and data are being classified into each non-overlapping cluster based on certain feature information. The idea of k-means clustering begins with initializing k objects as initial cluster centres [88]. Then, each object is clustered into the nearest cluster based on shortest Euclidean distance. Subsequently, the averages of all clusters are updated. The entire process is repeated in a loop until the stopping criterion is met.

A three-stage AI-based short term load forecasting is proposed by Hernandez *et al.* as a mean to allow energy production of a microgrid to adapt to the load demand [86]. In the first stage, SOM is applied to cluster the patterns of different days. Then, k-mean clustering is applied in cascade. The classification in cascade could perform better than either individual SOM or k-mean clustering. Since SOM does not provide information on similarity of these clusters to one another, the proposed method relies on k-mean clustering to identify the similarities in different clusters and then group the proximal clusters together. In experimental verification, k-mean clustering can reduce the number of clusters from SOM into three optimal clusters.

2.6 Optimisation in Control Strategy

In some cases of EMS, the goal of the EMS is not to make operation decisions based on triggering events but to make a balanced decision in the presence of two or more conflicting criteria. The supervised and unsupervised learnings-based AI perform well in outputting a reasonable decision based on inputs which usually represent changes in the environment. The goal is usually to supply enough of power to satisfy load demands and to store excess power. In such cases, the operation decisions are usually deduced based on solar irradiance, SoC of each component in HESS and load demands. On the other hand, operation decisions of an EMS could be made to achieve certain goals such as meeting load demands at low solar irradiance while trying to prolong the lifetime of each component in HESS. These goals-driven problems are usually solved using optimisation methods.

In the branch of AI-based optimisation, there are two main categories, namely the Swarm Intelligence (SI) and evolutionary computations (EC). SI builds and studies efficient computational problem-solving methods based on social behaviour of real swarms and insect colonies to find optimal solutions to complex optimisation problem. Coordination using decentralized control and self-organisation is the key to SI [89]. Examples to SI are PSO and CS. On the other hand, based on the idea of survival of the fittest, EC model some natural phenomena such as genetic inheritance as well as Darwinian strife for survival [90]. Evolutionary computation in solving optimisation problems uses loop iterative progress where growth and development of a population is emphasized. The growth and development in evolutionary computations is done via mutation and crossover phases, similar to that of an organism. DE and GA are popular instances of evolutionary computations.

2.6.1 Genetic Algorithm (GA) In EMS

Being one of the most popular algorithms, GA is mainly used to find optimal solutions for a computational problem that involves maximizing or minimizing a particular function (or cost function) [91]. It is classified as an evolutionary algorithm as GA is built upon the biological processes of reproduction and natural selection to determine the best solution. Originally motivated by Darwinian principle of evolution through genetic (or selection) [92], the popularity of GA can be mainly accredited to its ability to allow the user to control the level of randomization without any prior knowledge of given problem [91].

In GA, each **chromosome** refers to a possible solution to a problem. Most of the applications employ haploid individuals [93], in contrast to diploid individuals in an actual organism. The solution is often being encoded in a bit string. Each of the parameter forms a **gene** on the chromosomes. Due to the use of bit string, an **allele** can only be either 0 or 1. If other encoding method is used instead, an allele may have more possible options. **Crossover** is an operation of exchanging information between two parental chromosomes. **Mutation** is done by flipping a bit at a random position on the chromosome. The goal of GA is to optimize the fitness function where this function is mainly used to test and describe quantitatively how good each solution is. The simplest form of GA should consist of three operators, namely **selection**, **crossover** and **mutation** [93].

In applications as EMS, GA is usually one of the top choices in solving contradicting design objectives when traditional optimisation techniques breakdown due to irregularity in search space (lack of gradient information) or the search has become computationally intractable. Another huge advantage of GA is that it allows multi-objective optimisation which is a complicated procedure for traditional optimisation methods. The downside of GA as EMS is that GA only performs well when the parameters are well-tuned and the tuning process can be very lengthy occasionally.

Gholami *et al.* present a modified GA to provide an efficient switching schedule of the capacitors [94] to reduce energy and losses due to peak power, while maintaining the voltage level of the system. The EMS does not only achieve its objectives but also reduction in investment cost of the capacitors. British researchers apply GA to improve ESS schedules initially generated by simple combinatorial optimisation heuristics [95]. The role of GA is to evolve a brand-new schedule not presented in the first heuristic stage. The combinatorial optimisation heuristics are the next-fit, first-fit, best-fit and worst fit which are the efficient solutions to bin-packing problems. It is shown that peak demand reduction is up to 7.7% before GA and it is further cut by another 8% after GA.

Hong *et al.* adopt and modify GA to deal with short-term (24h) energy management and load demand in a factory power system consisting of uncertain photovoltaic power generation [96]. In the novel method, instead of recording down the hourly on-off state using 24 bits, chromosome records the consecutive periods of on or off. Thus, less bits are required. This novelty has allowed the impact of different parameters on optimal solutions to be studied. Elsied *et al.* design a real-time EMS for microgrid systems using GA to lower energy cost and carbon dioxide emission while trying to maximize renewable power generation [97].

Safdar *et al.* implement an EMS for dealing with occupants' comfort index of a residential building, energy saving and energy prediction using GA [98]. The fitness function consists of indoor occupants' comfort index and corresponding energy consumption to reach the least energy consumption. The difference between optimal and real environmental parameters serves as input to the fuzzy controller which in turns adjusts the input power of the building based on available power, required power and user comfort index. The study indicates that this approach improves the comfort index as well as consumes less power compared to PSO-based model. Yuce *et al.* combine ANN and GA in scheduling for an optimized domestic EMS to cut energy demand during peak periods and reliance on grid power while maximizing the use of renewable sources such as PV power [69]. ANN learns the pattern of appliance operation and estimates its energy consumption as well as renewable energy generation. GA is tasked to schedule for desired level of energy reduction whereas ANN acts as the prediction engine to GA so that GA can evaluate the fitness of the solution. The simulation result shows that this model reduces energy demand during peak periods and reliance on grid energy.

Iranian researchers propose a hybrid optimisation algorithm to find an optimal operating point to minimize the fuel consumption cost, voltage stability index and total voltage variation of an autonomous microgrid [99]. The hybrid optimisation algorithm consists of Harmony Search (HS) and GA. The mutation and crossover components of GA are added into HS to improve the exploration and exploitation performance of HS. The combination of HS and GA works better than either HS or GA in finding global minimum as the hybrid method can explore different solutions effectively. Santis *et al.* adopt Hierarchical GA to tune the Rule Base of a FLC to achieve minimal fuzzy rules [60]. HGA emphasizes on an encoding scheme based on control genes and parametric genes. The control genes govern the activation of parametric genes by simply activating or deactivating MFs composing a given fuzzy Rule Base via control genes. HGA manages to reduce the size of rules in the Rule Base by 53%.

2.6.2 Particle Swarm Optimisation (PSO) In EMS

Birds in flocks and fish in schools prove that coordinated behaviour requires no central control [100]. The idea of mimicking social behaviour of birds was conceived to produce computational intelligence by employing social interaction rather than individual cognitive abilities [101]. PSO studies how several simple entities interact and influence each other to move to region of interest such as food in an actual phenomenon. These simple entities are known as particles in the algorithm [101]. They are placed in the search space of problems and each computes its optimality based on objective function at its current location. Each particle then determines its movement via the search space by combining historical information on its current and best (best-fitness) positions with those of the members of the swarm with random perturbations.

In comparison with GA as EMS, PSO tends to more computationally efficient than GA [89] because in evolutionary algorithms, population size is required to be bigger for better performance. PSO also converges to the best solution much faster than GA [89] because PSO shares global best values with all particles in the swarm whereas chromosomes in GA only share information with each other during crossover stage. However, PSO could be trapped in local minimum whereas the mutation feature in GA has reduced the possibility of GA being trapped in local minimum.

Garcia-Trivino *et al.* design an optimized EMS to solve multi-objective problem for a grid-tied HREPS [102]. There are three objective functions, namely operating costs, efficiency and devices lifetime. Weight aggregation method is applied where the set of weights are selected corresponding to minimum value of the multi-objective function. Comparing to EMS based on individually optimized objective function and EMS based on optimisation of multi-objective function with equal weights, the proposed EMS achieves the best performance among the three. In Ref. [103], Multi-Objectives PSO (MOPSO) is applied to simultaneously optimize sizing as well as operation strategies of a HREPS with minimal Net Present Cost Energy Not Served. Binary PSO is applied in Ref. [104] to minimize the energy cost and carbon emission while maximizing the power of the available renewable energy resources. The optimal energy mixing rate between grid power and renewable power is determined by PSO to minimize the daily energy cost of a renewable microgrid in Ref. [105]. In these papers, PSO is proven to have the capability to solve multi-objective problems.

Taiwanese researchers have proposed a PSO-based EMS of a HREPS consisting of PV arrays, wind turbine, microturbine, battery banks and utility grid [106]. Unbalanced power is redistributed to more superior element via roulette wheel redistribution mechanism to preserve the searching diversity of PSO. The proportion of an element in the roulette wheel is decided by its cost as lower cost is more competitive and more preferred. A penalty mechanism is also introduced to reduce deep discharges of battery bank. Simulation results have shown that the proposed PSO method improves the performance by 0.82% and 1.76% respectively compared to PSO based Grid-Priority method and PSO based random method. In Ref. [107], Ju *et al*. design a three-stage hybrid algorithm based on PSO, entropy weight method and fuzzy satisfaction theory to perform multi-objective stochastic scheduling of a virtual power plant. Entropy weight method is used to determine the weight of output of each objective function. Fuzzy satisfaction theory is used to construct model decision-making method for calculation of combined optimisation results. As a result, system operation cost and abandoned energy cost could be minimized while virtual power plant operation income reaches maximum.

Guaranteed Convergence PSO with Gaussian Mutation is developed by Abedini *et al.* as an optimal EMS for PV-WT-Diesel independent hybrid REPS microgrids [108]. The objective is to minimize the capital investment and fuel costs of the system. The position of each swarm is mutated after the update of velocity and positional values randomly if $rand(0,1) < P_n$ where P_n is the mutation probability. Both mutation as well as guaranteed convergence help to find more accurate results with less computational time.

In Ref. [109], Baziar *et al.* propose a self-adaptive optimisation algorithm based on θ-PSO to explore the search space globally as the EMS of microgrids. θ-PSO takes advantage on the phase angle vectors to update the velocity and position of each particle to facilitate faster and more stable convergence. The proposed self-adaptive modification method consists of three sub-modifications which allow the particles to choose their updating operations depending on their current situation. Bigdeli *et al.* compare several different optimisation algorithms, including PSO and its variant, Quantum-behaved PSO (QPSO) in managing load sharing of a hybrid REPS to achieve optimal performance [110]. The optimisation takes the forecasting of solar power and air temperature together with required load as the inputs and the power supplied from each source and the storage of battery in each hour as the outputs. It is found that QPSO can outperform Imperialist Competitive Algorithm (ICA), Ant Colony Optimisation (ACO), PSO and CS with faster convergence rate. In Ref. [111], three EMS responsible of deciding the energy dispatch among the ESS devices are constructed based on PSO and are compared. The study is determined to find the suitable goal which will benefit the entire REPS in long run. The first is aimed to reduce the ESS utilization costs, the second EMS to improve the ESS efficiency with the third to optimize the lifetime of ESS. The study reveals that the third EMS performs the best as it needs smaller ESS with lowest acquisition cost of entire system over a span of 25 years.

As an optimisation algorithm, PSO is also used to tune MFs of FLC, the main controller in EMS of many REPS. For instance, in Ref. [58] where the FLC inputs are net power flow and batteries SoC while scheduling of hydrogen production and consumption being the output of the controller, the role of PSO is to tune the MFs. The optimisation procedure considers the weekly operation and management (O&M) costs and LPSP. As a result, the optimisation improves the system performance by reducing fluctuation in batteries SoC (longer lifetime), increasing average SoC by 6.18% and less working hours for fuel cell. In comparison to an unoptimized FLC, the optimized FLC could reduce the O&M costs and LPSP by 57% and 33% respectively. Chong *et al.* have shown that optimisation of MFs in FLC using PSO allows the REPS to operate the supercapacitor within the recommended SoC range and utilize the limited energy of supercapacitor effectively [10].

2.6.3 Ant Colony Optimisation (ACO)

Ant Colony Optimisation (ACO) is a metaheuristic method for solving combinatorial optimisation problems. ACO is inspired by how ants find the shortest paths from their nest to food sources [100]. The aim is to let the artificial ants find paths through a decision graph which corresponds to good solutions. In common practice, an ant constructs a solution via a sequence of probabilistic decisions where each decision extends a partial solution by adding a new solution component until a complete solution is reached.

Artificial pheromone is left to mark the edge of the corresponding graph in the decision graph if the temporary solution is good. This artificial pheromone will then act as a guide to the ants from following iteration to search near the path for good solutions. The amount of pheromone deposited relies on the quality of the solution found [112]. Some percentage of pheromone from older iterations will be evaporated to reduce the influence on newer iterations [112]. In summary, ACO is an iterative process where these pheromones are transferred from one iteration to the next.

ACO seeks applications in discrete optimisation problems (combinational optimisation) where the variables are usually not continuous in nature. This is similar to the paths selected by ants in searching for food where these paths are discrete: they are either chosen or not chosen. Thus, ACO is very useful as a tool to solve scheduling problems in EMS. This is done via probabilistic calculations such as binomial distribution. Comparing to GA, it is less affected by poor initial solution as its calculation involves random combination of random path selection and colony memory. However, it is slightly more computational expensive as it must retain memory of entire colony, unlike GA which requires to remember the previous generation only. One major disadvantage of ACO is that the probability calculation is complicated as its distribution may change by iterations.

Compared to PSO, due to randomness of probability involved in ACO, it is less prone to getting stuck at local minimum.

Collaboration research among British, Iranian and Spanish researchers have led to an EMS based on multilayer ACO (MACO) which is aimed to determine an optimized energy schedule for operation of a microgrid [113]. The number of layers is equal to the number of design variables and the number of nodes in each layer is equal to the number of allowable values corresponding to each variable. The ants will randomly choose the allowable values and in each time interval this process will be repeated from 00:00 to 23:30. The probability of choosing each path in the first iteration is equalised by placing same amount of pheromone over them. At time 23:30, cost function is calculated for each ant and the least cost is chosen by increasing the pheromone of least expense route. Comparison against conventional EMS and PSO-based EMS has indicated that MACO-based EMS further improves system performance by 20% and further reduces energy cost by 5%. Bigdeli has compared 5 optimisation algorithms, namely PSO, QPSO, ACO, ICA and CS in the context of optimal energy management of HREPS [110]. In the study, the goal of EMS is to minimize the fuel consumption by maximizing the renewable energy use and to improve performance of the battery. It is found that ACO performs better than CS and PSO in terms of ratio of hydrogen production to hydrogen consumption by more than 0.4%.

2.6.4 Bacterial Foraging Optimisation Algorithm (BFOA)

Bacterial Foraging Optimisation (BFOA) is a global optimisation algorithm well-suited for optimisation and control problems. The logic behind the idea is that animals are more likely to survive longer if they are able to obtain enough of food to sustain themselves, allowing them to reproduce easily with higher success rate [114]. Therefore, this has led to an evolutionary principle which seems fit to be applied into optimisation problems.

It is assumed that bacteria obtain nutrients in a way that maximizes their energy intake E per unit time T spent foraging. In computational intelligence sense, the goal is to maximize a function like E/T or to optimize an objective function of E/T. Individual bacterium also communicate with others by sending signals [115]. These two factors affect how a bacterium makes a foraging decision. Passino has developed the BFOA to mimic the chemotactic movement of virtual bacteria in problem search place [115].

Ref. [116] has shown an interesting result that BFOA performs better than PSO and GA when the problem gets higher dimensional. The adjustable run length has allowed BFOA to move towards the minimum easily. Also, PSO relies on a single particle with global best value where the entire process of decision-making bases on. The second-best particle is however ignored. In the reproduction stage of BFOA, half of the population influences the following generation, increasing the accuracy of the result. As a result, BFOA is applied in EMS module when the operating condition is constrained by several contradicting variables where PSO fails to produce satisfying results. BFOA, however, suffers in higher number of parameters involved, making it less simple to be adopted compared to PSO.

Roy *et al.* have designed a hybrid BFOA and Artificial Neural Networks (ANN) based EMS which is aimed at energy production cost reduction and better usage of renewable energy resources by hourly ahead for a microgrid [75]. Firstly, the PV, WT, micro turbines and battery demands are predicted using ANN. Then, the predicted values are given as the input of BFOA so that the optimal outputs for the microgrid system are produced. Comparison with GA and Artificial Bee Colony (ABC) has clearly shown that generation cost reduction by 25% is achieved by hybrid BFOA and ANN EMS with an additional benefit of less computational time.

2.6.5 Cuckoo Search Algorithm (CS)

Cuckoo birds are brood parasites as they do not build their own nests but rather lay their eggs in the nest of another species of birds. The care for the young is left to the host. In the optimisation context, each egg in the nest represents a solution while a cuckoo's egg represents a new solution [117]. The goal of the algorithm is to serve the new and potentially better solutions to replace the less fit solutions in the nest. The algorithm also combines with *Lévy Flight* to describe the random-walk of animals because the next move is based on both current state (location) and the transition probability to the next location [118]. A *Lévy Flight* is a random-walk in which the step-lengths are calculated based on heavy-tailed probability distribution.

CS has fewer control parameters compared to other search techniques [117]. CS starts with an initial population of *n* host nests. These initial host nests will be randomly attracted by the cuckoos with eggs via random *Lévy Flight*. Then, the nest quality will be measured and compared with another random host nest. If the host nest is better, then it will replace the old host nest. This new solution now has the egg laid by a cuckoo. Under the probability P_a, if the host discovers the egg, it will either throw out the egg or abandon the existing nest and build a new one. In computational intelligence wise, this is done by replacing the abundant solutions with the new random solutions [117].

[119] has shown that CS is superior to many metaheuristic algorithms in solving for multimodal objective functions. Simulation results have indicated that the convergence rate is insensitive to the probability P_a and thus tuning is not needed for a specific problem. In short, CS efficiently strikes a balance between the local nearby exploitation and global-wide exploration in the search space of the problem [117]. In the context of EMS, CS has great potential to be a popular option given the fact that it has less control parameters to be tuned. CS, however, loses the flexibility to be tweaked to achieve higher accuracy and shorter convergence time, causing CS to be trapped in local optimal value rather easily.

Berrazouane *et al.* develop an optimized fuzzy logic controller (FLC) for operation of a standalone hybrid power system via cuckoo search algorithm [43]. CS is fed with weekly solar irradiation data, ambient temperature data and load profile to tune the MFs of the FLC within the underlying capacity and operational constraints. As a result, the optimized FLC can minimize the LPSP, excess energy (EE) and LEC. In comparison with FLC-PSO, FLC-CS manages to keep LPSP under 10% and to keep SoC at higher level. In [110], PSO, QPSO, ACO, ICA and CS are compared in the context of optimal energy management of HREPS. In the study, the goal of EMS is to minimize the fuel consumption by maximizing the renewable energy use and increasing performance of the battery. In the study, it is found that CS could perform slightly better than PSO in terms of ratio of hydrogen production to hydrogen consumption by 0.6%.

2.6.6 Differential Evolution (DE)

Evolutionary computation uses iterative progress where growth and development of a population are emphasized. DE emerges as a very competitive form of evolutionary computation. Unlike other evolutionary algorithms, DE uses difference of the parameter vectors to explore the objective function landscape [120]. Also, there are fewer control parameters in DE, making the implementation of DE to be relatively easier compared to many evolutionary algorithms.

The general problem formulation for a Differential Evolution is to find $x^* \in X \text{ such } that\ f(x^*) \leq f(x), \forall\, x \in X$. A typical evolutionary algorithm consists of two main steps: initialization and an iterative transformation of a population of candidate solutions belonging to the search space $D \subset \mathbb{R}^n$ [121]. The elements in each iteration are constructed by mutation and crossover to be included in the next generation. Each element x_i from the current population is created by a mutant element denoted by y_i and a trial element denoted as z_i is produced via crossover from x_i as well as y_i. In almost all DE variants, the selection operators work by comparing the trial element to current element and transferring the best of them in the new population.

Crossover aims to improve the potential diversity by allowing the donor vector to exchange its components with the target vector to form trial vector [120]. Selection is carried out next to determine whether the target or trial vector survives to the next generation to maintain the population size over subsequent generations. DE is a favourable option as core of EMS since it has fewer control parameters compared to GA. In certain cases, if the number of populations is reduced significantly, DE suffers in lower convergence rate compared to GA [122].

Abedi *et al.* propose the use of DE to determine the optimal EMS of hybrid energy systems including various generators and storage units (battery, electrolyser and hydrogen tanks) [61]. The aim is to minimize the overall cost of the system, unmet load and fuel emission simultaneously by taking uncertainties associated with REPS into considerations. Compared to GA and PSO, DE performs the best by scoring lowest cost and minimal fuel consumption.

A hybrid HS with DE algorithm is developed by Zhang *et al.* [123] to solve a day-ahead scheduling problem of a microgrid consisting of PV cells, WT, diesel generators and battery storage system. HS is not efficient in generating new elements and thus the hybrid takes advantage on ability of DE to produce new individual through difference between any two individuals in the population. Spanish researchers have resorted to the use of a novel two-step EA to tackle the joint-optimisation of microgrid structure and operation [124]. The first EA operates to obtain the optimal values for parameters of components in the microgrid while the second EA plans the operational part of the microgrid. The operational part of the microgrid consists of peak-shaving, switching of ESS and main grid to supply power to the load.

Another team of Spanish researchers use nested EA to approach similar issue [125]. The process starts with an initial solution for ESS scheduling using deterministic approach where its initial structure part is taken from first evolution. When this part is set, a different EA is applied in turn to find an optimized ESS scheduling. Subsequently, a different EA is used for structure part. The entire scheme is applied over a sequential pattern until a stopping criterion is met. The nested EA is proven to work better than traditional EA with a similar number of function evaluation.

In dealing with realistic cases where predicted values deviate away from actual values significantly, Ikeda *et al.* have proposed a framework using Epsilon differential evolution (ϵDE) [126]. The goal of the EMS is to minimize the cost while maximizing the energy production. Therefore, a two-time steps recalculation strategy with ϵDE is designed to obtain a quasi-optimal solution under lower computational time. Mallol-Poyato *et al.* devise an optimal discharge scheduling of ESS in microgrids using an evolutionary algorithm (EA) so that consumption from utility grid can be minimized [127]. A total of 26 low-level heuristics to represent different percentage of discharge are defined and encoded before undergoing optimisation by EA. It is found that a reduction of 5% of energy consumption from utility can be achieved.

2.7 Incremental Learning in Control Strategy

In law of nature, a species which fails to adapt to the changing environment will not survive long but go extinct. This survival skill has since then added into the learning scheme of AI models. In AI context, incremental learning is the ability of a model to adjust itself in a flexible manner to new environmental conditions through self-correction over time as new events or operational conditions happen or new input data is available [128].

A learning system is said to possess incremental learning ability [128] when it has:

- Ability to perform on-line and lifelong learning
- No need to remember individual historical data points in subsequent stages
- No prior knowledge about the topological structure of the neural network
- Ability to tune network's structure incrementally
- No requirement on prototype initialization.

Both supervised and unsupervised learnings can be incorporated with incremental learning feature once these learnings have attained said features. In many real-world applications, it is impossible to obtain all relevant data during the training stages. With incremental learning, a useful mechanism to learn new knowledge without having to go through 'catastrophic forgetting' can be devised to refine existing knowledge, to accommodate new data in an incremental way while keeping system under use [128].

In this research, incremental learning is very important to the EMS because the EMS needs adaptability to handle unseen data. For instance, the EMS could be benefitted if it can predict the load demand which in turn is resulted by a change of user's behaviour. As living habits change progressively in nature, incremental learning allows the prediction module in the EMS to learn and adjust itself over time. Considering the global climate change and intermittent nature of renewable energy production, REPS power profile may not be stabilized and settled down to similar level every day, limiting the relevance of training datasets as time passes. Thus, a solution that can adapt to varying conditions swiftly as well as to detect these variations is becoming vital [37]. Trainings of AI models are usually pre-optimized and not entirely continuous due to a fixed training dataset. Thus, model training must be performed regularly or on demand basis to remain context relevance [26]. Without incremental learning, many AI models could lead to a dilemma known as Stability-Plasticity which describes the failure of a network to learn while retaining the previously learned knowledge. This dilemma could lead to a serious issue in real world applications where new classes of data could rise anytime. Also, learning process could be made more efficient when training data can be inputted in batches under incremental learning. Models are thus able to learn anytime while working to produce a decision as EMS. As a result, incremental-learning-enabled EMS can learn anytime, allowing the system to be able to operate from zero initial knowledge.

In real life, data either come in labelled or unlabelled. Labelled data are usually useful for performance improvement but difficult to be prepared. Thus, labelled data are scarce and expensive in terms of resources. On the other hand, unlabelled data are abundant but disorganised. Efforts are therefore required to be put in to prepare and process the unlabelled data. As described in Subsection 2.5, Unsupervised Learning enables the networks to learn using unlabelled data. Thus, no prior knowledge is required on the data [40], [129]. The learning strategy required in this research could be either self-organizing learning or statistical learning. Since the data available in this research is incomplete at initial stage, it is nearly computational impossible to analyse the topological structure for labelling, unless labels could be produced for every known class beforehand. Thus, unsupervised learning can be adopted in this project to approximate and learn the topology of the data distribution.

A suitable AI model for this research is hence Unsupervised Incremental type. An example of such model is the Self-Organizing Incremental Neural Network (SOINN). Following the introduction of SOINN by Hasegawa Laboratory, SOINN which is built and developed based on SOM possesses the capability of associating, reasoning, knowledge-transferring and forecasting except learning [130]. In view of the common Neural Network architecture, most of the ANN require certain information regarding the input data space to be known beforehand [130]. This information could be the statistical distribution of data such as covariance or simply the learning environment of the networks which in turn affects the parameters of creation of the said networks. Despite the shortcomings of other networks, SOINN, resembling SOM, does not need any information on the input data space for efficient performance.

The major advantages of using SOINN are [130]:

- There is no need to pre-define the mathematical model required for learning, unlike Multilayers Perceptron Neurons which require mathematical model for each layer of neurons present (hyperbolic tangent, radial basis function and other suitable models).
- Noise – eliminating capabilities for better pattern recognition.
- SOINN works with any existing programming language and any hardware available.

As far as the review process goes, there is no reported research which uses Incremental Learning AI models as EMS in any power system. Thus, usage of Incremental Unsupervised Learning is a major novelty in the research. Also, there is only a handful of research which use Unsupervised Learning models as EMS as depicted in Section 2.5. In Ref. [11], SOM is first used to cluster the data into classes to reduce the number of labels required to be calculated based on assumption that similar data should share similar labels. Then PSO is used to find optimal label for each data. Sections 2.3 and 2.5 have indicated that Unsupervised Learning could improve the prediction accuracy where prediction module is a significant part of proposed EMS in this research for better system performance.

2.8 Short-term Solar Irradiation Forecasting

Among the RE sources, solar-based RE garners majority of the attention due to its region-wide availability and more matured technology. The intermittent nature of solar energy, however, disfavours its eligibility as primary energy source for many applications. Therefore, EMS is essential to solar-based renewable energy management [132]. Having a predictive control to plan ahead before disruption occurs helps EMS to achieve better management of solar-based energy [133] and to plan, run and preserve the stability of national power grid in cases of grid-tied REPS [134] and [131]. Thus, accurate prediction of solar irradiance trend could be decisive in successful deployment of solar-powered systems [139-140]. As RE is highly dependent on occurrence of natural phenomena such as climate and weather, combining the fact of highly fluctuating user demand, forecasting techniques such as AI models help to make predictive control strategy possible to achieve better performance and robustness [134]. Good performance solar forecasting improves the integration of solar power generation into the grid when solar intermittencies could be expected in time [135]. It will also reduce the usage of storage battery, helping to prolong the battery lifespan [137].

Solar irradiance forecasting also helps in predicting output of solar power generated since the intensity of solar irradiance contributes to the amount of solar power generated by solar panels. Most of the literatures show that solar irradiance forecasting requires atmospheric information as well as satellite data [138], depending on the time horizon of forecast [144-145]. Prediction of solar irradiance can be classified based on prediction horizon, the long-term (more than a day) and short-term (less than one day). The selection of solar irradiance forecasting model depends on forecast time horizon, time resolution and climate type specific to the region under studied [146-147]. In general, the common models applied include clear sky model, clear sky and clearness indices model, persistence model, regressive methods, Artificial Intelligence model, Remote Sensing model and Numerical Weather Prediction model [139]. Image recognition techniques are also applied in [140] for prediction time horizon from 30 minutes to 2 hours. Researchers in [141] combined the use of sky-imaging techniques together with real-time irradiance measurements to produce a hybrid method to tackle highly variable solar irradiance cases.

Empirical models can be considered as mathematical equations combining the input variables with numerical coefficients [131]. Accuracy of empirical models such as Angtröm-Prescott (A-P) model depends on the coefficients and mathematical functions describing the solar irradiance conditions. In Ref. [142], an AI model, ABC is applied to calculate the optimal coefficient of empirical regression model of solar irradiance forecasting. The statistical errors are then improved by 40%.

In short-term solar irradiance forecasting, Blaga *et al.* conclude that Machine Learning models and hybrid models (Machine Learning models with classical statistics) perform very well regardless of climate type [143]. The most common AI models applied in solar irradiance forecasting are none other than ANN and SVM [131], [134], [144]. Paulescu *et al.* study 5 different statistical models and compare their novel model to Random Walk, Moving Average, Exponential Smoothing, Autoregressive Integrated Moving Average for performance evaluation of short-term forecasting of solar irradiance [145]. The developed model consists of an experimental clear-sky solar irradiance estimator and a statistical estimator determining whether the sun shines or not. It is worthy to point that there is no best model in the study. In daily horizon, Khosravi *et al.* study how AI models such as Group Method of Data Handling (GMDH) Neural Network, Multilayer Feedforward Neural Network (MLFNN), ANFIS, ANFIS with PSO, ANFIS with GA and ANFIS with ACO perform in forecasting [146]. With inputs such as month, day, average air temperature, air pressure and other variables recorded in different locations in Iran, GMDH Neural Network model outperforms the rest with RMSE of 0.2466 kWh/m^2/day. A wide variety of inputs helps to uncover the hidden patterns and relationship in complicated solar irradiance trend, further improving the forecasting performance of these AI models [146].

Indian researchers compare a few weather forecasting models built upon Data Mining techniques, Regression approaches such as Multiple Linear Regression (MLR), Autoregressive Integrated Moving Average (ARIMA) and ANN [147]. It is noted that weather prediction is accurate with large training dataset consisting of years of data. It is also acknowledged that combining the outputs of the models would improve the forecasting results. Since each model learns differently, knowledge from one model could complement and supplement one another. Combining multiple AI models simultaneously or sequentially can benefit from individual predictive power and complement one another

[151], [149]. Ref. [144] describes these methods as Ensemble Methods. It works on the idea that by combining the knowledge bases together, Ensemble Method is able to produce better overall generalizability. Ref. [150] use regression and clustering models to model REPS components and forecast of active power. In Ref. [151], ensemble forecasting methods are shown to outperform non-ensemble methods. Several researches have proven that hybrid approach consisting of clustering model as well as a predictor model could perform better than ANN and SVR individually [135], [34], [39]. Combination of several predictor models such as SVR, Gradient Boosted Regression (GBR) and Random Forest Regression (RFR) could perform better than single AI model, as proven in Ref. [152]. Jiang *et al.* propose a SVR with Gray Wolf Algorithm (GWA) EMS model to accurately estimate the total load demand of hybrid electrical vehicles so that the operating cost can be optimized in 24-hour time frame [153].

French researchers investigate 11 statistical and machine learning algorithms for solar irradiance forecasting with 1 to 6 hours of time horizon [154]. It is interesting to find that MLP and Autoregressive Moving Average (ARMA) work very well in poor variability cases, ARMA and Bagged-Regression Trees dominate in the medium variability cases whereas RFR and Bagged-Regression Trees ace in complex variability situations. Benali *et al.* decompose the solar irradiance into three components, namely normal beam, horizontal diffuse and global components [155]. Then, three methods, Smart Persistence, ANN and RFR are applied for prediction for time horizons from next hour to next 6 hours. RFR is found to be the best predictor with increasing forecasting horizon due to its ensemble feature.

Akarslan *et al.* propose a prediction strategy for short-term application using historical data [156]. The strategy is based data similarity. Prediction of future solar irradiance (next hour) data is made using data of a day statistically similar to the prediction day. Advanced AI models fail to produce good forecasting performance using only hourly solar irradiance values as sole input. Akarslan and his team also improve A-P method by including empirically parameters [157]. These empirical parameters could be historical solar irradiance, extra-terrestrial irradiance and clearness index. These studies prove that data similarity could improve the forecasting performance.

Grantham *et al.* suggest the use of interpolation to produce five-minute solar irradiance values (global horizontal and direct normal irradiance) from the hourly mean values recorded [158]. Extreme Learning Machine (ELM) is used in [159] together with mutual information to form WMIM for short-term forecast horizon between 5-minute and 3-hour ahead. The research concludes that ELM is more computationally efficient than ANN. Khosravi *et al.*, on the other hand, develop two forecasting models using machine learning algorithms based on types of input data [160]. The first type of input data consists of atmospheric parameters whereas the second type includes additional historical solar irradiance data. With the second type of input, ANFIS, SVR and MLFNN could produce correlation coefficient score higher than 0.95. Some researchers also try *k*-mean together with SVR to cluster the data depending on the seasonality, greatly improving the forecast results [161]. In Ref. [162], SVR with RBF scores nRMSE of 12.41% with combination of temperature, humidity and sunshine duration. Marzouq *et al.* explore the usage of AI model in automatic selection of suitable inputs to General ANN to save computational resources while estimating daily global solar irradiance [163]. Evolutionary ANN (EANN) is proven to be able to carry out these two tasks simultaneously.

Bright *et al.* use a chain of Markov chains to determine future weather conditions such as pressure, wind speed and cloud height for calculation of atmospheric transmission of solar irradiance. Then, the one-minute interval irradiance could be forecasted accurately [164]. Alfadda *et al.* consider the measurement of aerosol into forecasting MLP model to explain fluctuating solar irradiance trends in desert areas [165]. In Ref. [166], ground measurements of meteorological variables and Global Horizontal Irradiance are proven to be essential for Moroccan weather forecasting.

Lotfi *et al.* forecast solar power using historical input data available publicly with a novel ensemble algorithm based on kernel density estimation [167]. In this study, the most similar cases from historical dataset to the input are used to calculate ensemble prediction. In Ref. [168], the team uses Symbolic Aggregate Approximation method to explore time-series data in other feature dimensions to increase calculation speed as well as dimension reduction. Reikard *et al.* approach short-term solar irradiance prediction problem using frequency domain models in [133]. When the forecast horizon is between 1-3 hours, frequency domain model has comparable results compared to ARIMA. Researchers in [169] present a work to estimate photovoltaic generation using historical data such as generated power and past temperature forecasts without solar irradiance data. With the aid of theoretical clear-sky irradiance model, the work could produce good forecast despite lacking irradiance data. Mpfumali *et al.* prove that statistical-based forecasting method could outperform general machine learning algorithms (Stochastic Gradient Boosting and SVR) in day-ahead hourly global horizontal solar irradiance forecasting [170]. Methods which emphasize on solar irradiance trend such as Triple Exponential Smoothing [171] is applied in a study in Singapore for forecast horizon of 15 minutes. Huang *et al.* demonstrate that Boosted Regression Trees could achieve good forecasting performance with nRMSE of 24.3% for forecasting horizon of one hour [172].

Many AI algorithms adopted in the literature such as Deep Learning (in Refs [173], [174] and [175]), ANN, SVR and their variants are Supervised Learning models. This is because labelled data are very important in the learning stage of these AI models before they are readily deployed to perform real-time weather forecasting. Labelled data serve as the teacher in the learning phase so that feedbacks can be fed immediately to the model itself to correct its parameters. Weather forecasting such as solar irradiance forecasting is a regression problem with continuous data in nature. As a result, it is very instinctive to approach the problem via Supervised Learning AI models. However, it is irrefutable that the trends of the weather conditions do play a very important role in forecasting future weather conditions. Wang *et al.* find that Unsupervised Learning AI models greatly improves general AI forecasting performance by reducing the possibility of irrelevant data interfering [176]. Chinese researchers such as Wang *et al.* use Unsupervised Learning model (SOM) to label clustered high-resolution solar irradiance data with prediction label prior to application of Deep Learning networks to establish classified forecasting model [177]. Rego *et al.* have also developed k-Nearest Neighbours algorithm to forecast solar irradiance conditions in Lisbon for performance comparison with ANN [178]. It is noted in the research, K-Nearest Neighbours method outperforms ANN. Ghayekhloo *et al.* propose a short-term hybrid solar radiation forecasting using clustering approach, game theoretic self-organizing map (GTSOM). The role of GTSOM is to determine the appropriate cluster of the input data such that the cluster information serves as the input to the predictor model, the Bayesian Neural Networks (BNN) [135].

Zhou *et al.* review 232 research papers related to solar radiation prediction by comparing three main input parameters as well as feature selection methods [39] as shown in Figure 2-9. AI models reviewed are categorized based on model structure and model destinations.

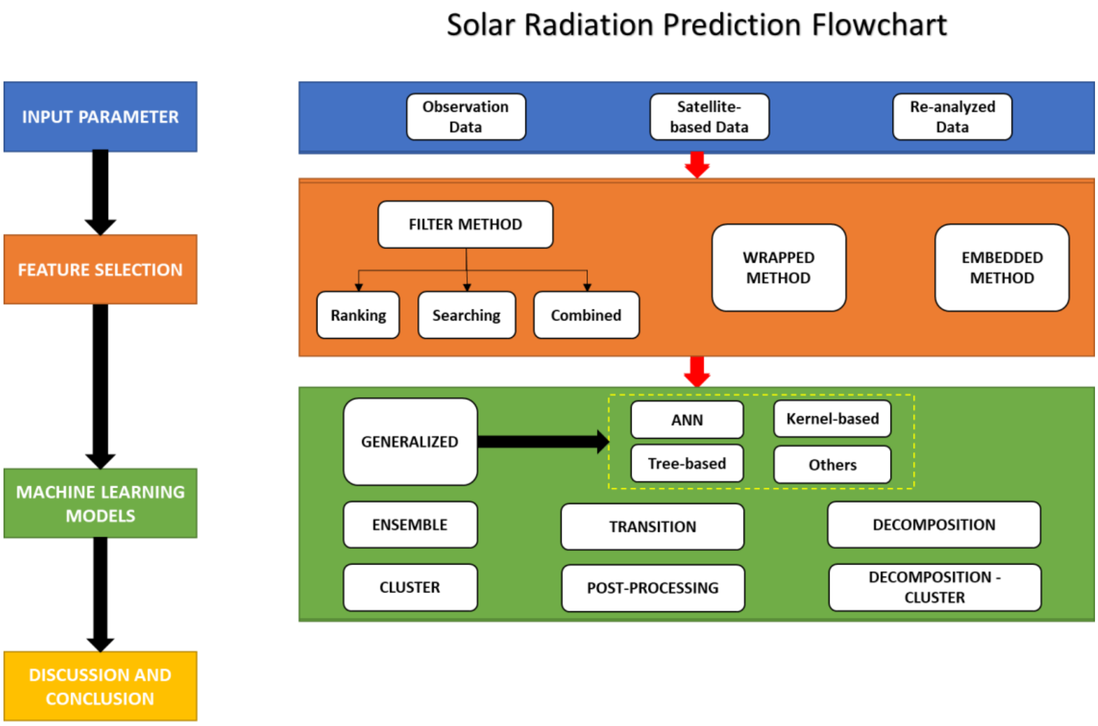

Figure 2-9 – Flowchart of Solar Irradiance Forecast summarised by [39]

Even though some Supervised Learning models do consider statistical trends of the input data, models such as Deep Learning require complicated networks and huge number of neurons to achieve this. Models such as SVR and ANN fit the input data with complex polynomials equations to achieve generalization.

Other than the Supervised Learning, Incremental Learning, which enables adaptation to new data through real-time learning is extensively studied [128]. In many real-world applications, it is impossible to collect all relevant data during the training stages. With Incremental Learning, a useful mechanism to learn new knowledge without having to go through 'catastrophic forgetting' can be devised to refine existing knowledge, to learn new data in an incremental way while keeping system running as usual [128].

In solar irradiance prediction, Incremental Learning improves AI models by learning new weather data which are unseen previously. Brazilian researchers proposed an ensemble of models of Typicality-and-Eccentricity Method for Data Analysis (TEDA) as well as fuzzy model to forecast mean monthly temperature using historical values of monthly temperature data, cloudiness and humidity [179]. TEDA is a supervised incremental model that operates on data density and data cloud scattering without any prior knowledge. TEDA helped improving the forecast model significantly. In short, Incremental Learning allows a system to learn and work from zero knowledge simultaneously.

2.9 Embedded Systems

Artificial Intelligence models, though are adaptive and much smarter than classical EMS, are generally more computationally complex than classical EMS. Despite the adaptive and intelligent nature of AI models, their inherent computational complexity poses a significant obstacle, particularly when considering real-time applications. As a result, most of the EMS implemented using AI in past research are either simulated in MATLAB (via a PC) or using PC as an interface between systems using Python, C or Java environments. Such situation has heavily reduced the popularity of AI-based REPS due to bulky and costly system physical size.

Addressing these limitations, the current trend suggests the exploration of cloud technology as an alternative to PCs for implementing AI-based REPS. Cloud platforms offer substantial computing power and data storage at a reduced cost. The drawbacks are lack of agility, responsiveness, privacy and personalization [180]. Cloud technology also relies heavily on internet connection. Since this REPS system is a standalone system which seeks applications in rural areas, internet connection is not a guarantee but also a luxury.

Amidst these considerations, embedded systems emerge as a pragmatic solution. An embedded system is an electronic system which is tasked to perform a specific function within a larger system [181]. Embedded system is usually used in a real-time system where there exists a guaranteed worst-case response time to any critical event as well as acceptable response time to general events. Embedded systems are generally smaller in size and boot faster. They are usually cheaper because they use less computational resources.

Although embedded systems could be the alternative to PCs, come with computational limitations compared to PCs. In regular PCs, cooperation of both Computing Processing Units (CPU) and Graphic Processing Units (GPU) could accelerate the training of AI models. The compute-intensive portions of the application can be loaded onto GPU whereas CPU runs the remaining codes [182]. CPUs, in fact, are designed to have a few cores optimized for sequential serial processing whereas GPU has massive parallel processors consisting of thousands of smaller cores which are best at handling multiple tasks simultaneously [182]. On the other hand, for AI to be able to run in embedded systems, the AI models must be simplified so that they do not need many resources. Therefore, in Ref. [183], optimisation techniques are introduced so that machine learning operations can be run freely on embedded platforms. So, the AI model chosen in this research should involve minimal computational expensive steps as possible so that it can be successfully implemented in embedded systems for real-time applications.

An example of embedded platform is Raspberry Pi. Given the specification of Raspberry Pi 3 B+, many machine learning algorithms need to be optimized so that the complex mathematical operations in these algorithms can be performed within the computational capabilities of Raspberry Pi. Based on the reviews that follow, microcontroller such as Raspberry Pi does possess the minimal capability of running Artificial Intelligence models. A group of British researchers uses Convolutional Neural

Networks (CNN) to enable angular readjustment of a projector within a fringe projection system in real-time without having to recalibrate the system [184]. The CNN is implemented on Movidius USB stick so that common hardware such as Raspberry Pi can be used in real time. Thus, reliance on computational resources is greatly reduced.

Oniga *et al.* have designed a highly-developed assistive system for elderly and sick persons using ANN [185]. Health data such as heart rate, temperature and arm posture recognition as well as daily routines recognition are training data to the ANN. To reduce the complexity of the recognition system without compromising the recognition rate significantly, a simpler neural network with 20 neurons in hidden layer is adopted. The recognition system is also implemented in Raspberry Pi in real time successfully.

In collaborative research that develops a face recognition framework to assist law-enforcement services, the research team has proposed a Raspberry Pi and cloud assisted face recognition framework using a small-sized portable camera and Raspberry Pi [186]. Due to limited resources in Raspberry Pi, the face recognition model, Ensemble SVM (ESVM) is trained in the cloud before being migrated to the Pi. Murad proposes a cost-effective and real-time autonomous pavement condition assessment using deep learning, Unmanned Aerial Vehicle (UAV) with Raspberry Pi [187]. Similar effort to that of [186], the object detection module SSD with MobileNet feature extractor is trained externally before being deployed in Pi. Preliminary results show that accuracy of 60% is achieved.

An Artificial Intelligence based Smart Building Automation Controller is designed by a group of Sri Lankan researchers to allow building services to adapt to user preferences based on user comfort, safety and energy performance [188]. The controller is implemented in Raspberry Pi to take advantage on its ultra-low power consumption and extensive communication capabilities. The AI model implemented in the controller is Fuzzy Logics. In the experiment, the controller can set an optimal temperature setting for Heating, Ventilating and Air-Conditioning (HVAC) system, smart switching on and off of artificial lighting source to acquire additional illumination. These instances showcase the adaptability of AI in real-time scenarios, even within the resource constraints of embedded systems.

The choice of Raspberry Pi as the embedded system for this project is justified by its compact size, cost-effectiveness, and versatility. Raspberry Pi aligns well with the project's requirements, offering a balance between computational capabilities and power efficiency. Its affordability makes it accessible for a diverse range of applications, while its small form factor enables seamless integration into space-constrained projects. Additionally, the extensive community support, accessibility, and a broad ecosystem of peripherals contribute to its suitability for implementing AI models in real-time applications. In conclusion, Raspberry Pi emerges as a robust and practical choice, allowing for the efficient integration of AI into the envisaged REPS without compromising on computational efficiency.

2.10 Summary

This chapter presents literature review about standalone REPS with HESS, control strategies including both traditional methods as well as modern methods associated with Artificial Intelligence, common AI and optimisation models in EMS, Incremental Learning in AI models in REPS field, short-term solar irradiance forecasting as well as suitable embedded system for standalone REPS. A review on past literature has commended on the REPS-HESS configuration to extend battery operation lifetime and to reduce system maintenance and service costs. AI-based EMS or control strategy performs better than traditional methods in many researches with faster response time, more adaptive as well as higher flexibility in handling cases with contradicting working conditions. To date, there is a lack of research using Unsupervised Learning AI models in EMS compared to Supervised Learning AI models although it is proven in a few research that Unsupervised Learning AI models could readily improve the overall system performance. With the aid of AI-based optimisation models, Unsupervised Learning models can then work as a black box with zero initial knowledge on the system without data labels. Similar conclusion can also be drawn on short-term solar irradiance forecasting where Unsupervised Learning models can produce results on par with Supervised Learning models using only basic input data such as historical solar irradiance trend. Thus, in both EMS and short-term forecasting cases, E-SOINN emerges as the potential Unsupervised Learning model.

The E-SOINN distinguishes itself from other AI models implemented in the discussed context through its unique learning approach. E-SOINN is specifically designed for unsupervised learning, allowing it to adapt and evolve iteratively based on incoming data without the need for labelled information. This characteristic makes E-SOINN particularly well-suited for scenarios where the system's structure and patterns may change over time, as it can continuously learn and update its knowledge without explicit supervision.

Unlike some AI models that may require extensive preprocessing or labelled datasets, E-SOINN minimizes the need for data cleaning and pre-processing, making it more efficient in handling raw sensor data. Its ability to dynamically adjust the number of nodes in response to the complexity of the input data contributes to its adaptability in capturing intricate patterns, especially in the context of solar irradiance forecasting.

Moreover, E-SOINN's application in the discussed framework, particularly in the clustering and forecasting of solar irradiance trends, showcases its capability to provide meaningful insights without relying on predefined network architectures. Its incremental learning feature ensures that the model can adapt to new datasets without forgetting prior knowledge, facilitating continuous improvement in forecasting performance.

In summary, E-SOINN stands out by offering an unsupervised learning approach, adaptability to changing patterns, efficiency in handling raw data, and the ability to dynamically adjust its structure, making it a valuable addition to the suite of AI models employed in the discussed energy management and solar irradiance forecasting context.

Lastly, this review discusses the common embedded platform adopted for small-powered energy harvesting or management system in different fields.

Chapter 3 Regression Enhanced Self-Organizing Incremental Neural Network (RE-SOINN)

In view of this research, Artificial Intelligence is applied in two parts of the projects, namely the solar irradiance forecasting module as well as energy management strategy in the REPS. Implementing AI in solar irradiance forecasting is crucial for enhancing the efficiency and reliability of REPS. Solar irradiance, a key factor in solar power generation, is inherently variable and influenced by dynamic environmental conditions. AI models offer the ability to learn and adapt to these intricate patterns, providing more accurate and timely predictions. AI can be implemented through sophisticated algorithms that analyze historical solar data, weather patterns, and other relevant factors. These AI models consider various parameters, including time of day, seasonal changes, and local weather conditions, to forecast solar energy production. The implementation involves training the AI models with historical data, fine-tuning their parameters, and continuously updating them with new information. This precision is essential for optimal energy management in REPS, allowing for better anticipation of fluctuations in solar energy production. AI-driven forecasting enables utilities, systems and grid operators to make informed decisions, optimize energy distribution and mitigate the impact of intermittency in solar power generation. As the civilization progresses towards a more sustainable energy future, the integration of AI in solar irradiance forecasting serves as a fundamental strategy to maximize the effectiveness of renewable energy sources and contribute to a reliable and resilient power infrastructure.

3.1 Self-Organizing Incremental Neural Network (SOINN) and Enhanced Self-Organising Incremental Neural Network (E-SOINN)

A Self-Organizing Incremental Neural Network (SOINN) is an example of Unsupervised Incremental Learning Artificial Intelligence models. Similar to SOM, SOINN possesses the capability of associating, reasoning, knowledge-transferring and forecasting except learning [130]. In contrast to the popular AI models such as Neural Networks of Supervised Learning, SOINN does not need any prior information regarding the input data space to be known beforehand [130] for efficient performance. To these Supervised

Learning models, information such as statistical distribution of data such as covariance or simply the learning environment of the networks affects the hyperparameters of creation of these AI models.

The major advantages of using SOINN are [130]:

- There is no need to pre-define the mathematical model required for learning, unlike Multilayers Perceptron Neurons which require mathematical model for each layer of neurons present (hyperbolic tangent, radial basis function and other suitable models).
- Noise – eliminating capabilities for better pattern recognition.
- SOINN works with any existing programming language and any hardware available.

The principal SOINN variant adopted for this research is the Enhanced SOINN (E-SOINN). Compared to the original SOINN, E-SOINN is capable to perform all functions of SOINN as well as to separate high-density overlapped classes in the input data space [131]. Overlapped classes have always been a shortcoming in SOINN as separation of overlapped data requires supervised learning for better accuracy. E-SOINN uses fewer parameters compared to SOINN as it uses between class-insertion to realise incremental training.

The algorithm of E-SOINN of SOINN variant is given as follow [131]:

1. Initialise two nodes randomly with weight vectors, W_a using data from input pattern, X, as A. Connection set, C is initialised as empty set. Similarity threshold, T_a is also initialised as the distance between the two nodes.
2. New pattern $x \in R^n$ is sent to the network.
3. The nearest node, a_1 and the second nearest node, a_2 are computed as follow:

$$a_1 = arg\, min_{a \in A} \left|\left| x - W_a \right|\right| \tag{3-1}$$

$$a_2 = arg\, min_{a \in A[a_1]} \left|\left| x - W_a \right|\right| \tag{3-2}$$

   The input data becomes a new node when similarity threshold, T_a is smaller than the distance. Add this new node to A and process subsequent data using Step 2.

4. The age of all edges of winning node, a_1 is increased by 1.
5. Connect the two nodes with an edge
   I. If the winner or the second winner is a new node, or
   II. If the winner and second winner are both belonged to the same subclass, or
   III. If two different subclasses are involved, combine the two nodes instead if $\min(h_{winner}, h_{second\ winner}) > \alpha_K K_{max}$ or $\alpha_L L_{max}$ where h is the density of node and α as a parameter determined by a threshold function.
6. The density of the winner is updated using

$$h_i = \frac{1}{N} S_i = \frac{1}{N} \sum_{j=1}^{n} \left(\sum_{m=1}^{\lambda} P_i \right), \tag{3-3}$$

   where S is the sum of points for node i and P being "point" of the node.

7. Adapt the winner weight vectors and its direct topological neighbours using a fraction $\in_1(t)$ and $\in_2(t)$ of the total distance to the input signal,

$$\Delta W_{a1} = \in_1 (M_{a1})(\xi - W_{a1}) \tag{3-4}$$

$$\Delta W_i = \in_2 (M_{a1})(\xi - W_i) \tag{3-5}$$

8. Find the edge whose ages are greater than a predefined parameter age_{max}, then remove such edges.
9. If the number of input signals generated so far is an integer multiple of parameter λ,
   I. Update the subclass label of every node.
   II. Delete noisy nodes as follow:
      i. For all nodes in A, if node a has two neighbours, and $h_a < c_1 \sum_{j=1}^{N_A} \frac{h_j}{N_A}$, then remove the node a. N_A is the number of nodes in node set A.
      ii. For all nodes in A, if node a has one neighbour and $h_a < c_2 \sum_{j=1}^{N_A} \frac{h_j}{N_A}$, then remove the node a.
      iii. For all nodes in A, if node a has no neighbour, then remove node a.
10. Go to Step (2) to continue unsupervised online learning if the learning is not finished.

There are three main hyperparameters in E-SOINN as compared to SOINN, making E-SOINN to be more superior than SOINN in noise elimination. These hyperparameters are lambda (denoising iteration control), denoising threshold and maximum age. The optimal performance of E-SOINN depends on how these three hyperparameters work together. The nature of the case application also plays an important role in determining the aggressiveness of E-SOINN in identifying and eliminating the noises.

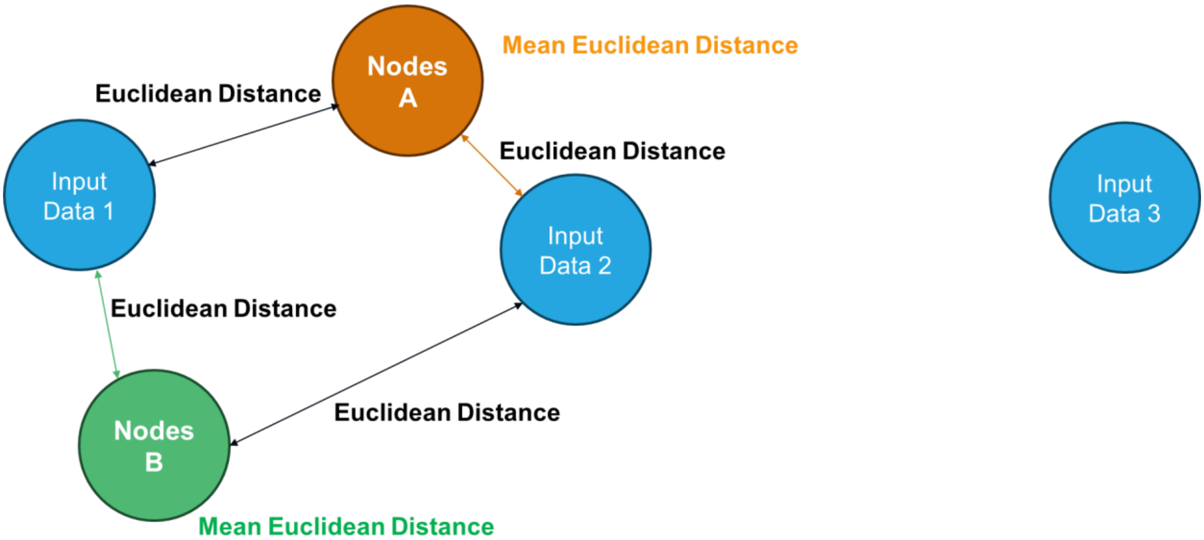

Figure 3-1 – Illustration of nodes, input data in the E-SOINN knowledge space

With reference to the step 8 in the outlined algorithm and Figure 3-1, when an input instance is classified into a particular node due to closest proximity, a connection is formed between this node and the neighbouring node of second closest proximity. This connection is defined as connection age. Every time a connection is formed between these two specific nodes, the age of the connection gets refreshed to 1. So, when the age of a connection gets too old (or large), this means that there is no new input instance supporting the connection between these two nodes since its establishment. The hyperparameter of maximum age limit, age_{max} defines the maximum age a connection can grow into to ensure the specific nodes remain relevant after a long period of time. A noise or noisy node can be loosely interpreted as a singular instance which is unable to form any meaningful relationship or connection with its neighbouring nodes or data over a long period of time.

Denoising threshold, c, defines the density threshold where a node would be recognised as a noisy node. When a node is significantly less dense, it means that the node only consists of a small number of instances. In the presence of large data instances, a very less dense node can be recognised as a noise. Lambda, λ, refers to denoising iteration control. For every λ new input instance being clustered successfully, denoising operation is conducted to check every single node formed in the knowledge base for nodal density. Any node with nodal density less than denoising control, c, at each λ interval is to be labelled as noise and to be erased.

3.2 Challenges of Implementation of E-SOINN in Forecasting and Optimisation Problems

E-SOINN excels in clustering problems where the nature of the problem is in discrete form. This is because Unsupervised Learning-based AI models are developed for clustering and pattern recognition problems. E-SOINN adapts and learns the structure of data without the need for explicit labels. For applications requiring outputs in continuous form such as measurements from sensor networks, then the accuracy of the E-SOINN or any other Unsupervised Learning AI models suffer. This is because the output of the Unsupervised Learning AI models is limited to the number of predefined discrete nodes, thus the accuracy can be defined as a function of granularity of the clusters. It requires mapping operation of continuous values to discrete clusters. It appears that the only way to improve the accuracy significantly would be increasing the number of discrete nodes significantly so that the number of nodes covers the entire range of the possible output values. However, a major drawback of this mitigation is the accuracy is achieved at the expense of unnecessarily high computational requirements.

Forecasting a continuous variable in a time-series problem is a challenging task to Unsupervised Learning models like E-SOINN. The Incremental Learning nature of E-SOINN is also a valuable prerequisite to many real-world problems. One key advantage lies in its adaptability to gradual changes in the environment. In numerous applications, such as weather forecasting, financial analysis, or industrial processes, data patterns may evolve over time. Moreover, in situations where data arrives incrementally or in streaming fashion, E-SOINN's Incremental Learning becomes indispensable. E-SOINN's Incremental Learning feature allows the model to seamlessly integrate new information while retaining insights gained from historical data. This adaptability ensures that the model remains relevant and effective in capturing shifting trends, a critical aspect for real-world applications.

Intuitively, a time-series input is clustered into a node depending on its Euclidean distance to the nearest node. Subsequently, the output to the said input is returned using the information stored in the nearest node. For E-SOINN to produce a more accurate forecast output, it is intuitive that a higher number of E-SOINN nodes will lead to better forecast as the resolution of data learnt by E-SOINN is higher. Ideally, if E-SOINN could cluster all possible variants of data into a complete distinctive number of nodes, E-SOINN model would be able to produce a forecast output that is possibly very close to the actual value. In practice, it is impossible to train E-SOINN model with all possible variants of knowledge base.

In optimisation applications, the challenges of E-SOINN can be associated with striking a balance between solution accuracy and computational efficiency. When applying E-SOINN for optimization tasks, especially in those involving discrete decision spaces, E-SOINN’s ability to adapt and self-organize can facilitate the exploration of complex solution spaces. E-SOINN's ability to incrementally learn and adapt reduces the need for frequent retraining on the entire dataset. This not only conserves computational resources but also facilitates real-time decision-making. However, in continuous problems, due to the necessary mapping of continuous parameters to discrete nodes, the granularity of such discretization can directly impact the precision of the optimisation process, not to mention the computational resources required.

Essentially, it is evident that balancing precision with computational efficiency is a critical consideration, especially for an off-grid application where the electrical power available is limited. In the domain of forecasting, the choice between employing complex models that capture intricate patterns and simplifying models to reduce computational costs hinges on the specific application and available resources. Similarly, for optimization problems, the pursuit of optimal solutions necessitates a judicious trade-off between the level of accuracy and the computational demands, guiding the selection of suitable methodologies. Ultimately, the success of both forecasting and optimization endeavours depends on an astute understanding of the problem's characteristics, an adept choice of algorithms and techniques, and a pragmatic assessment of the computational constraints, ensuring that the solutions obtained are both practical and effective.

3.3 Regression Enhanced Self-Organizing Incremental Neural Network (RE-SOINN)

The two areas where Artificial Intelligence are applied in include solar irradiance forecasting and optimisation in the energy management system. The expert model used in this research is the proposed RE-SOINN. The RE-SOINN is based on the E-SOINN [131]. It is chosen because of its Incremental Learning ability and unlike other incremental supervised learning models, it requires very minimum model customization. The E-SOINN has been used in classification and produces discrete outputs via clustering of data, data with similar trends could be grouped together. As weather conditions fluctuate significantly from one moment to the next, it is almost impossible to produce forecast with little to no error. However, the forecasting error can be reduced by using the average of all data trends that are clustered into the same group (or node). The RE-SOINN incorporates the regression method into the E-SOINN to produce continuous output which yields better approximation to time-series solar irradiance data.

The most important contribution of E-SOINN in this forecasting operation is the clustering of data trends into nodes. Despite the advantages, there exists a drawback of using Unsupervised Learning in forecasting cases. Solar irradiance values are continuous in nature whereas the output of E-SOINN is discrete in nature. Ideally, if E-SOINN could cluster all possible variants of solar irradiance profiles into a complete distinctive number of nodes, E-SOINN model would be able to produce a highly accurate forecast output that is possibly very close to the actual value. In practice, it is impossible to train E-SOINN model with all possible variants of solar irradiance profiles and thus, some modifications are made to improve E-SOINN without the need of being trained by a complete training dataset.

To produce continuous outputs, E-SOINN is modified and further extended so that discrete outputs can be interpolated into continuous values. Together with the interpolation, Regression Enhanced Self-Organising Incremental Neural Networks (RE-SOINN) is proposed. Say there are *n* features in every input training data where the *n*th feature is the solar irradiance value after 60 minutes. Hence, the Euclidean distances between these input data and nodes are computed based on the first (*n*-1) features. The actual value of *n*th feature of the input data, based on statistical assumptions, is within the neighbourhood of the *n*th features of the nearest nodes to the input data. To estimate the value of the *n*th feature of the input data, a conclusion is to be drawn from *m* closest nodes to the input data. Then, the *n*th feature of the input data is interpolated using the relation as follow:

$$f(t+\epsilon) = \frac{\sum_{i=1}^{m}\left(\frac{y_i}{{d_i}^p}\right)}{\sum_{i=1}^{m}\left(\frac{1}{{d_i}^p}\right)} \tag{3-6}$$

where ϵ refers to forecasting horizon (60 minutes in this research), p is the power, d is the distance between input vector to a neighbouring node and y is nth feature of all neighbouring nodes.

The output can then be understood as the weighted average of neighbouring data based on Euclidean distances. Two hyperparameters in Equation (3-6) are required to be tuned to produce the estimate. *p* determines the strength of the influence of neighbouring distance information and *m* is the number of closest nodes to be considered in the interpolation. Figure 3-2 depicts the simulated operations on how close neighbours are being considered to produce a weighted average output for any input.

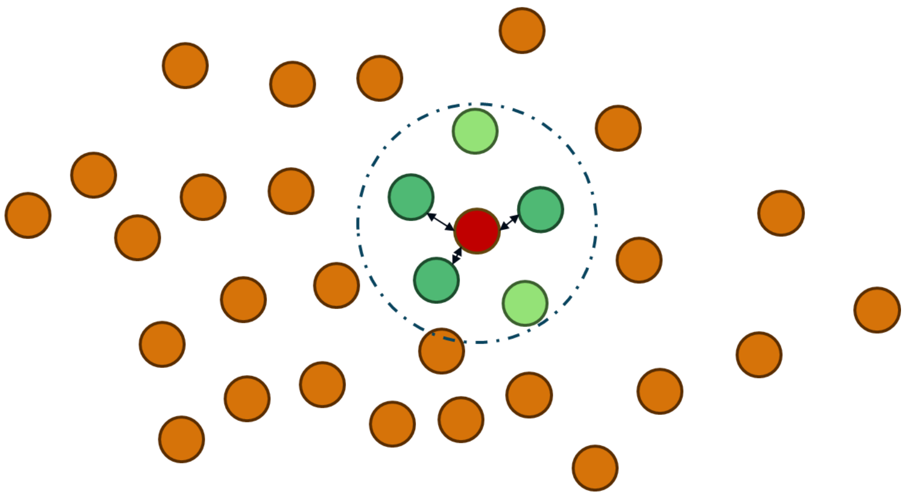

Figure 3-2 - Visualisation of Input (red circle) surrounded by neighbours (green circles)

3.4 The Advantages of RE-SOINN

RE-SOINN has several notable features which demonstrate its versatility and suitability for various applications despite being an Unsupervised Learning model.

1. **Statistical Information Translation**: RE-SOINN excels in uncovering meaningful trends by translating statistical information within data into Euclidean distances, allowing for effective pattern recognition and clustering. Such operation also allows RE-SOINN to summarise multi-dimensional data into lower dimensional nodes, easing the computational procedures in the later stage.

2. **k-Nearest Neighbour Inverse Distance Weighting (kNN-IDW)**: The kNN-IDW technique employed by RE-SOINN enhances its ability to make informed decisions about data points, contributing to robust clustering and data analysis. By combining information from neighbouring nodes, the output of RE-SOINN can be estimated rather than requiring full range and variants of data in the input space.

3. **Data Density-Based Denoising**: RE-SOINN incorporates data density-based denoising techniques to effectively eliminate noise, ensuring that the model can focus on relevant and significant data patterns. Any node with density less than a predefined threshold is regarded as a noise if the node is an isolated from any neighbourhood.

4. **Adaptive Network Architecture**: Unlike many other AI models, RE-SOINN does not require a predefined network architecture, which simplifies model development and makes it adaptable to varying data structures and complexities.
5. **Minimal Data Cleaning and Pre-processing**: One of the strengths of RE-SOINN is its ability to work with raw sensor data, reducing the need for extensive data cleaning and preprocessing. This feature streamlines the data analysis pipeline and saves time and effort.
6. **No Labelling Required**: A standout advantage of RE-SOINN is its capacity for unsupervised learning. It does not rely on labelled data, making it readily deployable for applications where obtaining labelled training data may be challenging or costly.

3.5 Tuning Hyperparameters of RE-SOINN

Prior to the application of RE-SOINN, it is of vital importance to ensure the RE-SOINN is working under the influence of optimised hyperparameters so that any computational procedure in RE-SOINN can be operated in a more efficient manner, yielding superior performance without compromising the entire system of application. There are a total of six parameters, namely:

- Denoising Density Threshold
- Denoising Iteration Control
- Maximum Age Limit
- Number of Neighbours
- Radius of Neighbourhood
- Influence Strength of neighbouring information

In this research, a Grid Search methodology is employed to determine the optimal hyperparameters for RE-SOINN. Based on the experience, certain hyperparameters can be limited to a rather narrow range of suitable values. The key of optimising the hyperparameters is to ensure the RE-SOINN can have an extensive knowledge base, to include as many patterns or trends as possible. The reasonable ranges of hyperparameters are established differently, depending on problem characteristics as follows in Table 3-1:

Table 3-1 - RE-SOINN Hyperparameters and the Ranges of Hyperparameter Values

Hyperparameters	**Ranges of Values**
Denoising Density Threshold	[0.0001, 1]
Denoising Iteration Control	[100, 10000]
Maximum Age Limit	[10, 10000]
Number of Neighbours	[1, 10]
Radius of Neighbourhood	[10, 1000]
Influence Strength	[1, 3]

Grid Search works by generating a grid of hyperparameter combinations by taking all possible combinations within the specified ranges. Once a set of hyperparameter combination is generated, RE-SOINN model is trained using this generated set of hyperparameters. Metrics to evaluate the quality of the RE-SOINN model trained is designed to reward the set of hyperparameters producing the highest number of nodes in RE-SOINN knowledge base. The hyperparameter set which produces the highest number of nodes in RE-SOINN knowledge base is then recorded to serve as the optimal hyperparameter sets of subsequent training of RE-SOINN.

It is to be acknowledged that Grid Search is limited by the size of the hyperparameters set as well as the range of values to be tested on the hyperparameters, resulting in a very computationally expensive method. Alternative methods such as Random Search or Bayesian Optimisation can be applied on this problem as well. However, hyperparameters in RE-SOINN possess a relatively narrow range of suitable hyperparameter values not to mention that RE-SOINN has relatively short computational time. The nature of the problem makes Grid Search feasible and efficient without incurring excessive computational costs. The choice of applying Grid Search to pre-determine the hyperparameters of the RE-SOINN model is rooted in its systematic and thorough exploration of the hyperparameter space. Grid Search ensures a comprehensive examination of all possible hyperparameter combinations, providing a thorough understanding of the model's behaviour and performance.

Consequently, the meticulous exploration in the parameter space via Grid Search can greatly assist to identify the hyperparameter configuration that optimises RE-SOINN's performance in terms of denoising and clustering accuracy.

Chapter 4 Solar Irradiance Forecasting with RE-SOINN

This chapter presents the implementation of a new artificial intelligent algorithm namely the Regression Enhanced Incremental Self-Organizing Neural Network (RE-SOINN) for accurate (even for highly fluctuating profile) and adaptive solar irradiance forecasting. The general outline of the proposed solar irradiance forecasting method is described and its performance in solar irradiance forecasting is critically evaluated. On a brief note, a summary consisting of key points of the chapter is presented.

EMS is important in managing solar-based renewable energy source [132] and having the ability to plan ahead of time before any disruptions could achieve better management of solar-based energy [133], [139-140]. Solar irradiance forecasting also helps in predicting output of solar power generated since intensity of solar irradiance is directly related to the generation of solar power in such a way that the higher the intensity of solar irradiance, the higher the amount of solar power generated by solar panels.

Many AI algorithms adopted in the literature such as Deep Learning [181-182], ANN, SVR and their variants are Supervised Learning models. This is because labelled data are very important in the learning stage to serve as the teacher in the learning phase so that feedback can be fed immediately to the model itself to correct its parameters. Other than the Supervised Learning, Incremental Learning, which enables adaptation to new data through real-time learning is extensively studied [128]. In many real-world applications, it is impossible to collect all relevant data during the training stages. With Incremental Learning, a useful mechanism to learn new knowledge without having to go through 'catastrophic forgetting' can be devised to refine existing knowledge, to learn new data in an incremental way while keeping system running as usual [128].

In solar irradiance prediction, Incremental Learning improves AI models by learning new weather data which are unseen previously. Instead of using supervised learning model, this research proposes usage of Unsupervised Incremental Learning AI model in solar irradiance forecasting with historical solar irradiance data and timestamp as sole input.

The advantage of using Unsupervised Learning is that no pre-defined network architecture is needed as in the Supervised Learning. The model to be based upon is E-SOINN.

4.1 Solar Irradiance Profiles in Malaysia

The data used in this research is actual solar irradiance recorded from April 2018 to June 2018. The solar irradiance values were recorded by Texas Electronics SP-LITE Solar Radiation Sensor installed in a solar cabin located at The University of Nottingham Malaysia in Semenyih, Malaysia (2.9474° N, 101.8451° E). The dataset is made up of two measured variables, namely the timestamp (dd-mm-yyyy hh:mm) and solar irradiance (W/m^2).

Figure 4-1 - Location of Semenyih in Malaysia (research site of this section)

Being a tropical country, solar irradiance in Malaysia is erratic due its humid and hot climate as depicted in Figure 4-1. Such climate is mainly resulted by its proximity to the Equator line. Cloud formation is very common during the day and as a result, these clouds could block the sunlight occasionally at any time, causing unpredicted variations in solar irradiance measurements, as seen in Figure 4-2.

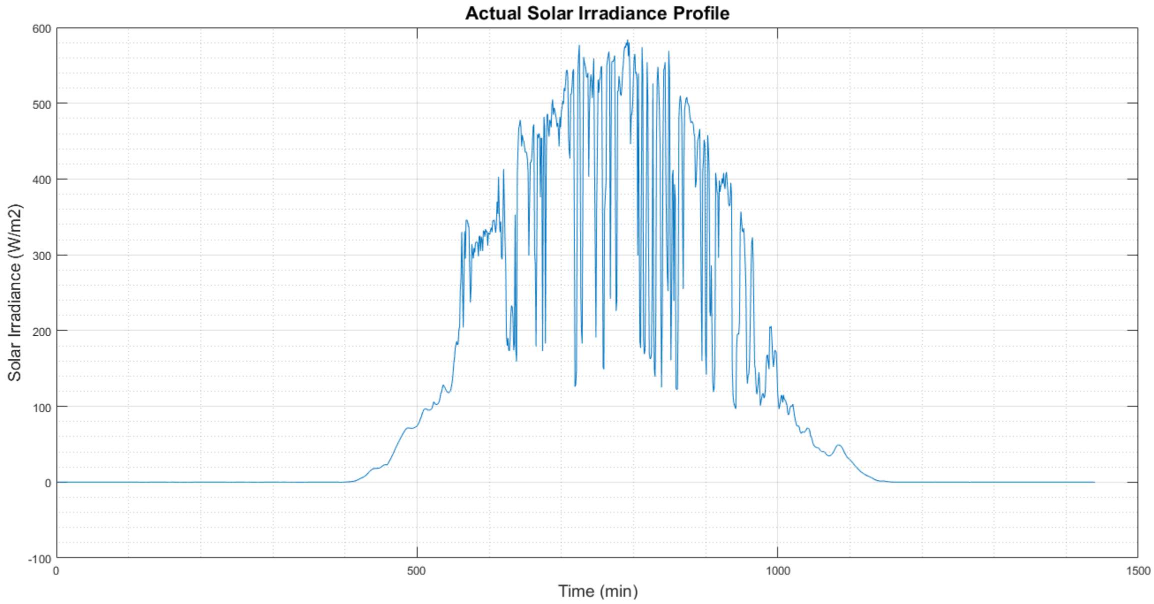

Figure 4-2 - Actual Solar Irradiance Profile in Section Site

From literature review there is no standard on size requirement of the dataset required in forecasting of solar irradiance. Also, the resolution of the dataset is not uniform across the literature. The three month-worth of data is divided into training, validation and testing datasets in ratio of 14:3:3 or 70%:15%:15%.

The dataset consists of 21476 hourly solar irradiance trends of 1-minute interval coupled with a timestamp. The solar irradiance value is sampled every minute, producing 60 data points in each hour. The formats of the data are illustrated in Table 4-1 and Table 4-2:

Table 4-1 - Format of Training and Validation Dataset

Feature 1	**Feature 2**	**Feature 3**	**...**	**Feature 61**	**Feature 62**
Timestamp	$f(t-59)$	$f(t-58)$	$\ldots$	$f(t)$	$f(t+60)$

Table 4-2 - Format of Test Dataset

Feature 1	**Feature 2**	**Feature 3**	**...**	**Feature 61**
Timestamp	$f(t-59)$	$f(t-58)$	$\ldots$	$f(t)$

Feature 61 refers to the solar irradiance value recorded for timestamp stated as Feature 1. Features 2 to 60 are the historical one-minute interval solar irradiance values with respect to Feature 61. Feature 62 is the solar irradiance value recorded 60 minutes after Feature 61. Feature 62 is only present in both training and validation datasets but it is omitted from the test dataset because this feature is to be forecasted. Thus, the length of each instance in the test dataset is one unit less compared to those in training and validation dataset.

4.2 Solar Irradiance Data Decomposition

In general, any trend could be categorised into two trending components, namely the hard trend and the soft trend. The process of decomposing data into low and high frequency components is often associated with time series and signal processing techniques. A trend is 'hard' when its occurrence could be determined easily due to highly probable nature. Such event is usually the consequence of a well-known fact such as estimating the peak traffic hour solely based on the general working hours. A soft trend is those events of which their probabilities cannot be easily defined such as traffic accidents. Forecasting works very well with hard trend and performs poorly in soft trend.

From Figure 4-2, the general trend of daily solar irradiance in tropical regions such as Malaysia loosely resembles to the shape of a normal distribution probability density function where the mid of the day (location of where peak solar irradiance occurs) is the mean of a normal distribution probability density function. In tropical regions, solar irradiance readings are usually at the peak during the middle of the days and close to zero during the nights because these regions receive intense sunlight throughout the year, keeping the climate temperature relatively constant. Such repetitive hard trend, as shown in Figure 4-3, can be assumed as the low frequency component of solar irradiance trend and works as the backbone of hourly predicted solar irradiance profile.

From Figure 4-4, the main variation in daily or hourly solar irradiance measurement is significantly resulted by cloud movements which block the sunlight momentarily, causing varying solar irradiance readings between one moment and the subsequent moment. For instance, it is highly probable that the solar irradiance values between 12.00pm and 12.05pm do not remain the same at all. The range of variation within these 5 minutes could be as large as 75% of the peak solar irradiance recorded on that day. This main variation can be approximated as the high frequency component of solar irradiance trend. Such soft trend is no less than a noise as the pattern is not apparent (softer) or totally erratic as clearly seen in Figure 4-5 which depicts the noisy high soft trend between 11.30am and 1.30pm.

It is intuitive to have the solar irradiance values be decomposed into two components (long-term and short-term) because the forecasting model applied here is Unsupervised Learning. Unlike Supervised Learning, there is no apparent way of altering the architecture of an Unsupervised Learning model such as adding additional layers to extract useful information from training data like Artificial Neural Networks. Also, the main information which Unsupervised Learning models extract is usually statistical and geometrical ones. Combination of both low frequency and high frequency components in training data will result in noisy complex statistical information. It is also worth mentioning that both soft and hard trend components are statistically different from one another. As a result, Unsupervised Learning models are unable to perform well with noisy data as the presence of high frequency and low frequency components together may have disrupted the learning process.

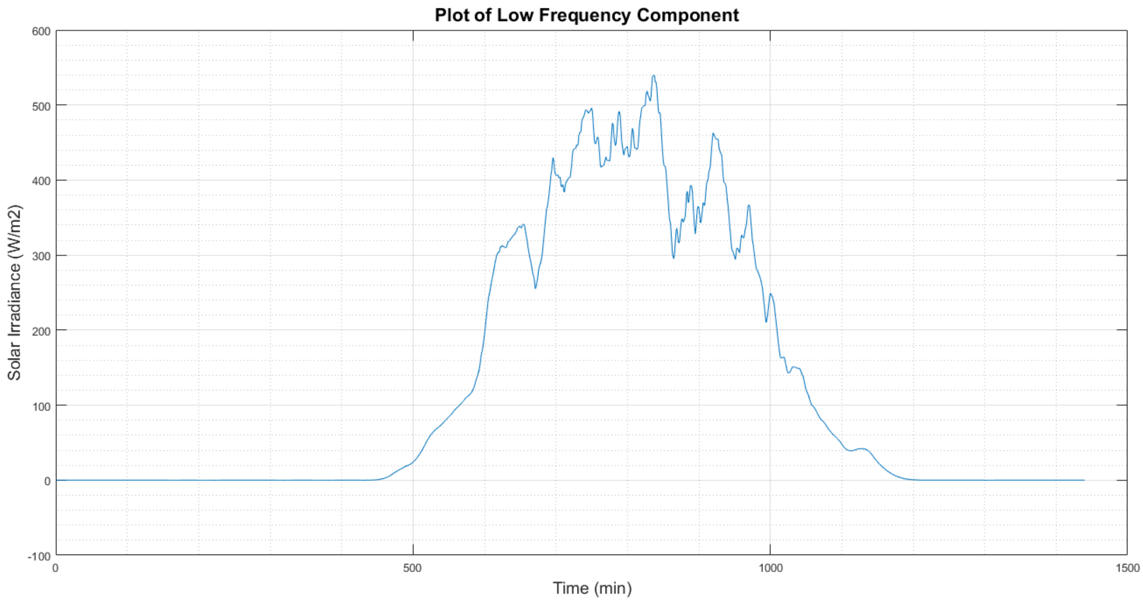

Figure 4-3 - Low frequency component of solar irradiance

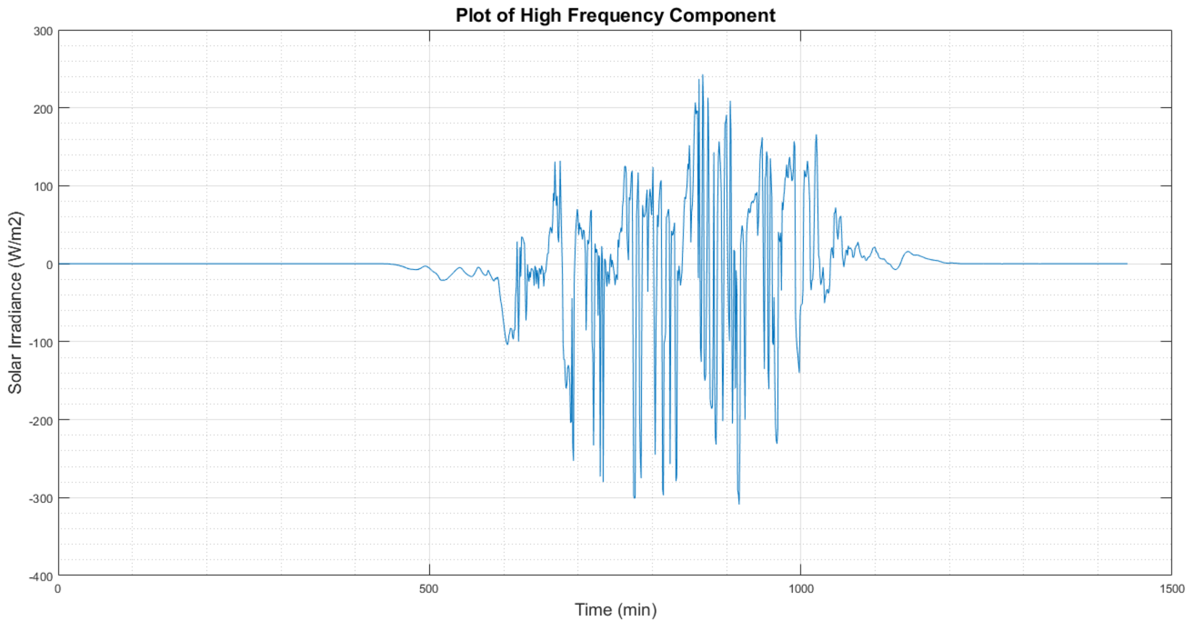

Figure 4-4 - High frequency component of solar irradiance

It is to be noted that the weather sensor used in this research could record the data at an interval of 0.1s or 10Hz. For every minute of solar irradiance values, the values belonging to the same minute frame are averaged and the output mean value represents the solar irradiance value for the minute. Missing values and Not-a-Number (NaN) values found in the dataset are removed.

Since the solar irradiance forecasting model is derived from Unsupervised Learning AI model, the important features to be studied include the timestamp as well as the hourly

1-minute solar irradiance trends as shown in Table 4-1. To search for 'hard trend' in the trends, the hourly 1-minute solar irradiance trends undergo the operation of a MAF. This MAF considers 24 historical points together with current point to evaluate the average. The arbitrary period of 24 is set using iterative method, starting with the assumption of dominating seasonality of hourly weather to be around 15 minutes to 30 minutes. This smoothened trend now shows the 'hard trend' or the low frequency component of the pattern. The 'soft trend' or the high frequency component, on the other hand, can be determined from the following $y_{HF} = y_{orig} - y_{LF}$ Equation 4-1:

$$y_{HF} = y_{orig} - y_{LF} \quad \text{Equation 4-1}$$

Where y_{LF} is the filtered solar irradiance value (low frequency component, as shown in Figure 4-3), y_{HF} is high frequency component of solar irradiance (as depicted in Figure 4-4) and y_{orig} is the original solar irradiance value recorded by sensor.

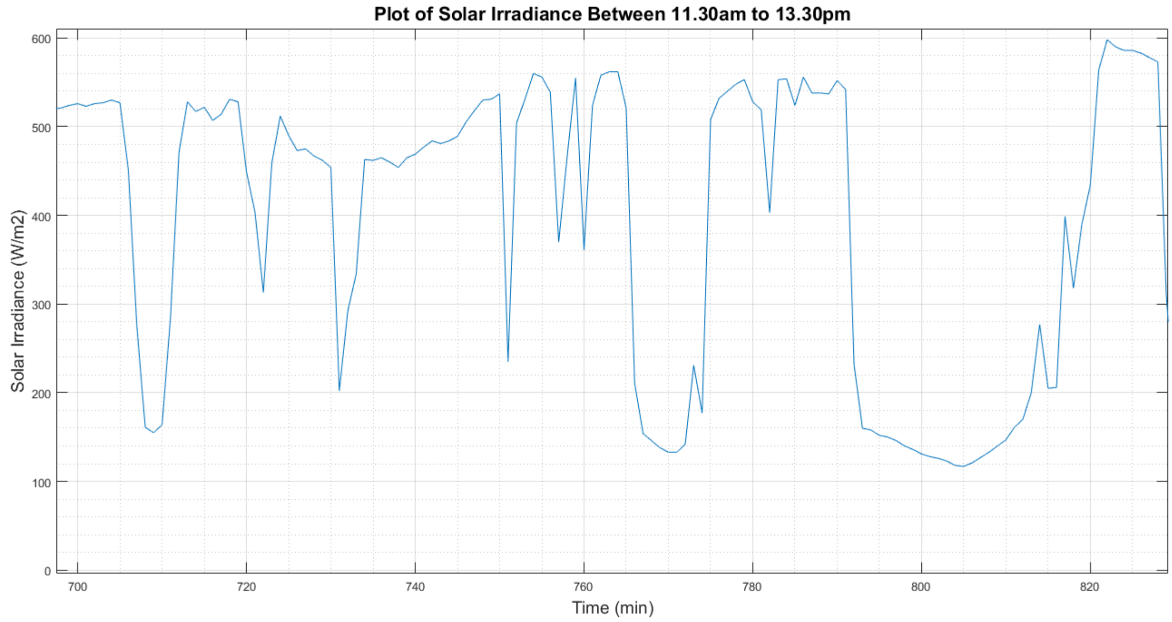

Figure 4-5 - Short-term variations during mid of the day

Thus, the proposed solar irradiance forecasting framework would need to consist of two smaller models, one model is responsible for forecasting low frequency component of solar irradiance trend whereas another is tasked to predict the high frequency component of the trend. The input to the low frequency forecasting model is straightforward in the sense that there are 62 points in each input (timestamp, 60 points of historical solar irradiance values from f(t-59) to f(t) and solar irradiance value in the next 60 minutes or f(t+60)). The 'hard trend' of low frequency component of solar irradiance trends depicts the long-term shape of solar irradiance values, making sense of using the entire input trends in the dataset.

Since the soft trend affects the readings in a short-term duration, the soft trend component of solar irradiance profiles does not possess significant long-term statistical properties, rendering the longer horizon of historical high frequency data less significant. Thus, the historical input can be greatly shortened from one hour to 5 minutes based on a series of grid search analyses. The forecasting performance on high frequency data does not differ much as the data horizon is reduced from 60 minutes to 5 minutes. Table 4-3 illustrates the format of the training data for high frequency components of solar irradiance profiles.

Table 4-3 - Format of Training Data for high frequency components

Feature 1	**Feature 2**	**Feature 3**	**...**	**Feature 6**	**Feature 7**
Timestamp	$f(t-4)$	$f(t-3)$	...	$f(t)$	$f(t+60)$

4.3 Outline of Proposed Model

The proposed hourly solar irradiance trend forecasting framework is depicted in Figure 4-6. The process starts with reading solar irradiance values from Texas Electronics SP-LITE Solar Radiation Sensor. Solar irradiance data are very noisy in nature (Figure 4-2). To forecast hourly solar irradiance values using historical profiles, these noisy profiles will be inevitably used as the inputs to the prediction model. The complex statistical information present within the noisy solar irradiance profile would prove to be a difficult challenge for Unsupervised AI model to learn. This is because AI models are trained to approximate the trend of the input and disregard randomness such as the noise in the solar irradiance data. Thus, in this subsection, solar irradiance profiles will be first decomposed into average daily solar irradiance trend (low frequency component) and noisy component (high frequency component). Then two Unsupervised Learning models will be trained with each component of solar irradiance profiles respectively. By doing so, an expert model is dedicated to approximate not only the low frequency data but also the noisy high frequency data which is valuable for solar irradiance fluctuation prediction.

Each RE-SOINN model extracts valuable statistical information from respective component and make predictions based on these pieces of information. From Figure 4-2, Figure 4-4 and Figure 4-7, it can be observed that the variations mainly occur at the mid of a day (between 11am to 4pm). The variations observed in each day is different from one another. As noise is erratic in nature, this means that the high frequency component of solar irradiance values could be high in this instant and low in the next. While the low frequency component of solar irradiance values could be similar at similar timestamp on different days, this case is not valid for high frequency component. Thus, the high frequency component could be further improved in the following way,

1. Find the mean of last elements of training vectors clustered in the same nodes of HF RE-SOINN model based on timestamps.
2. Add the mean value to the forecast output from HF RE-SOINN model based on the forecasting timestamp.

By adding the average value of high-frequency component into the high frequency solar irradiance forecast based on the same timestamp, it could help to ensure the forecast of the high-frequency components is well-kept close to the mean amplitude of high-frequency component of historical readings. As more and more data are added to train RE-SOINN, the mean amplitudes are more significant, keeping the forecast in an acceptable range in long run without scoring huge errors. A benefit is that the variation added to the prediction is the average of all historical variations, although the forecast output could not be exact value, it is still within the 'vicinity' range of the noise. Thus, it could be applied regardless of randomness of noise.

Forecast outputs from both models are then combined to produce actual forecast. Figure 4-6 shows the system block diagrams of the proposed framework using RE-SOINN model.

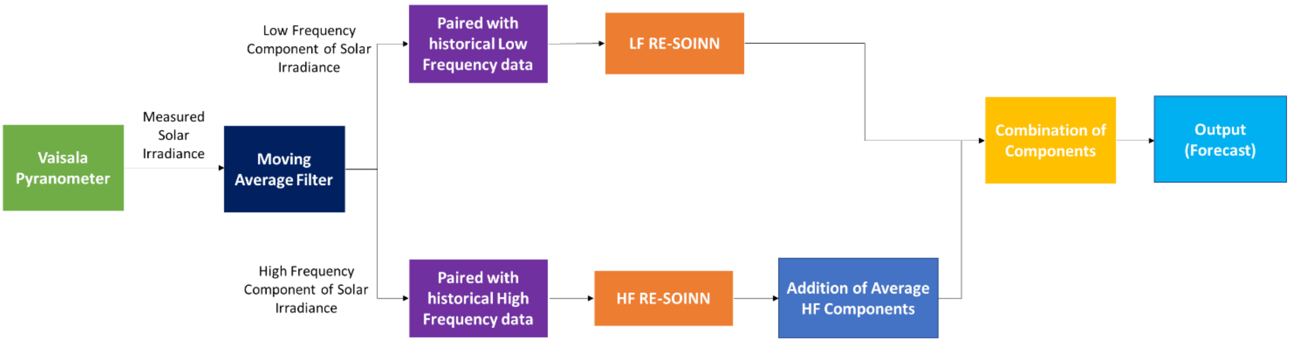

Figure 4-6 - Block diagrams of proposed hourly solar irradiance forecast framework.

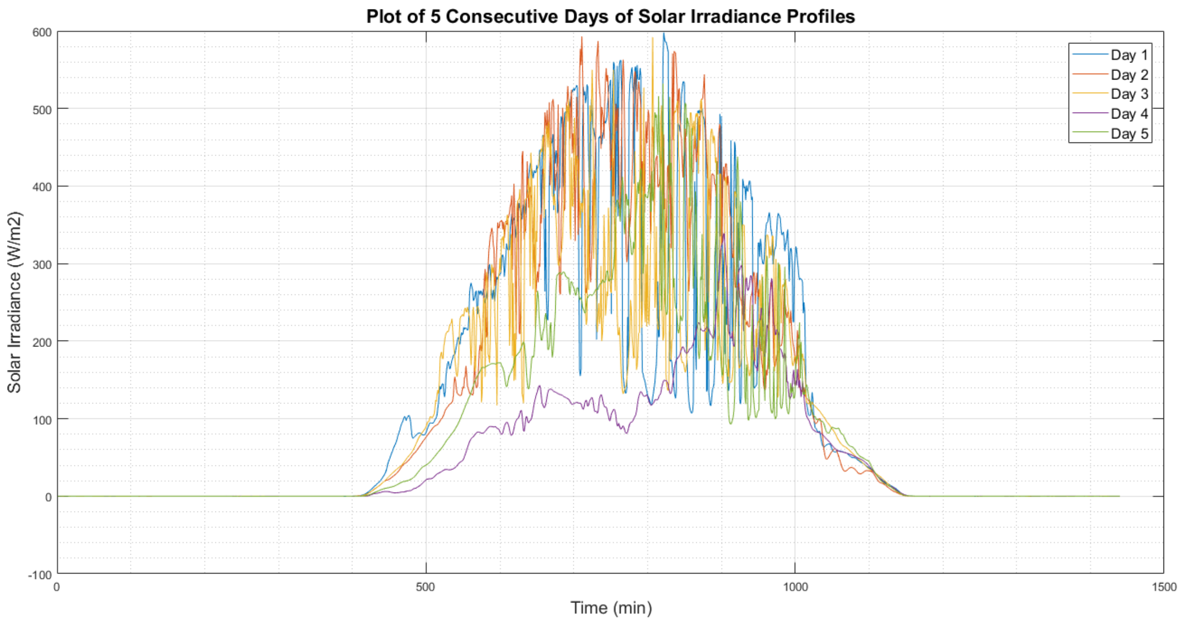

Figure 4-7 - Plot of 5 consecutive days of solar irradiance profiles, showing the varying noises present.

4.4 Forecast Evaluation and Benchmark Models

Performance metrics are deployed to evaluate the performance of RE-SOINN model in forecasting hourly solar irradiance trend. The performance metrics consist of Mean Absolute Scaled Error (MASE) and RMSE. The following equations define the performance metrics:

$$MASE = mean\left(\left|\frac{y_t - y_t'}{\frac{1}{T-m}\sum_{t=m+1}^{T}|y_t - y_{t-m}|}\right|\right) \quad \text{Equation 4-2}$$

$$RMSE = \sqrt{\frac{1}{n}\sum_{i=1}^{n}\left(y_i' - y_i\right)^2} \quad \text{Equation 4-3}$$

MASE is proposed by Hyndman and Koehler [189] to compare two series with different units. MASE is scale-free, making it very suitable to compare forecast accuracy. MASE can be loosely defined as the ratio of MAE of chosen model over the MAE of naïve model. In case of seasonality, a Naïve Model assumes that the trend or pattern is repeated for every periodic cycle. Thus, the value is assumed to be the same to those of the previous cycles.

The performance of model according to MASE is explained as follows: When MASE is equal to 1, MAE of the chosen model is only as good as the Naïve Model. If MASE score is 0.5, MAE of the chosen model is twice as good compared to the Naïve Model.

4.4.1 Persistence Model

In many literatures, persistence model is the standard of comparison by being a trivial reference to determine if a forecasting model could perform better than it. This trivial reference model assumes that the solar irradiance at current instant is the same as previous instant assuming that there is no significant change in weather conditions and the time horizon is not too long. Equation 4-4 shows the assumption made by Persistent Model.

$$f(t+1) = f(t) \quad \text{Equation 4-4}$$

4.4.2 Exponential Smoothing

Exponential Smoothing uses weighted averages of past values with weights decaying exponentially as the values get older. The more recent an observation, the more significant influence it has on the forecast. The equation is as follow:

$$y_{t+60} = \alpha y_t + \alpha(1-\alpha)y_{t-1} + \alpha(1-\alpha)^2 y_{t-2} + \cdots \quad \text{Equation 4-5}$$

Where y_t is current value, y_{t-n} is historical value after n intervals, y_{t+60} is forecast value after an hour and α is a constant. When α is equal to 1, Exponential Smoothing becomes Persistence Model.

After a series of experimentation, a fifth order Exponential Smoothing model is found to produce better forecasting performance [190]. Thus, a fifth order model is developed as comparison model.

4.4.3 Artificial Neural Networks

Artificial Neural Network(s) (ANN) is considered the most versatile AI model as it works similarly to those in a mammal's brain. In ANN, the neurons are usually arranged in the input layer, hidden layer and output layer. The neurons in the layers are connected to each other via synaptic weights. Given the desired output, the synaptic weights of the neurons are adjusted based on the errors so that the ANN could output a value close to the desired output.

A feedforward neural network with backpropagation method is adopted to forecast the hourly solar irradiance values. The input is the 1-minute interval of hourly solar irradiance trend. The optimal number of the neurons in the hidden layer is taken as 55 after several trials and errors using validation dataset.

4.5 Performance of Forecast Model

4.5.1 Effect of Incremental Learning

From Grid Search, SOM produces better performance when SOM consists of 25 neurons whereas denoising control of 0.1, lambda of 50 and maximum age of 2000 lead to an optimised ESOINN model. After the suitable hyperparameters are set for each SOM and E-SOINN, the training dataset is split into 5 equal-size groups to determine the effect of Incremental Learning on solar irradiance forecasting. The data used in this subsection is the original undecomposed dataset. Both SOM and E-SOINN models are trained with the first group of data and their performances are evaluated against actual solar irradiance values. As SOM does not possess incremental learning capability, it is retrained with previous training data with addition of new data. E-SOINN which possesses incremental learning capability, does not need old data to be added into new training data, allowing batch training to be performed for each new dataset. Table 4-4 and Table 4-5 summarise the results obtained.

Table 4-4 - Performance of SOM with new batches of training data

Batch Training	MASE	RMSE (Wm^{-2})	Training Time (s)
1	6.261886	413.5812	63.677
2	5.046964	333.3111	159.75
3	7.824766	509.2435	373.57154
4	4.724261	315.4872	594.31714
5	7.824766	509.2435	1019.1958

Table 4-5 - Performance of E-SOINN with new batches of training data

Batch Training	MASE	RMSE (Wm^{-2})	Training Time (s)
1	0.88992	110.966	14.36598
2	0.83061	106.1829	71.53866
3	0.846988	107.5342	167.6246
4	0.839077	105.9463	272.6899
5	0.835421	104.8017	427.8516

From both error measures, performance of SOM in solar irradiance forecasting is not consistent. While the error measures may improve with the addition of more training data, they also deteriorate as more data accumulates within the neurons. This inconsistency suggests that, despite optimizing the number of neurons, the presence of noisy solar irradiance data may disrupt the effective learning of SOM in extracting both statistical and geometrical information essential for understanding the solar irradiance trend.

On the other hand, the E-SOINN is showing an overall improvement in forecasting 60-minute ahead solar irradiance value on both MASE and RMSE measures. The inherent noise-removal capability of E-SOINN minimizes disruptions during the learning stage. The increasing training time of E-SOINN also indicates that, as more data populate the nodal space of E-SOINN, a greater number of constraints, connections, and comparisons are made throughout the incremental learning stage. This adaptability and noise-filtering attribute contribute to the E-SOINN's effectiveness in solar irradiance forecasting, particularly when faced with varying levels of data noise.

4.5.2 Performance Comparison of RE-SOINN and E-SOINN

In this subsection, the solar irradiance forecasting performance of RE-SOINN and E-SOINN is investigated. Both models are fed with the same training data using hyperparameters found via Grid Search previously and their performances in producing an accurate hourly ahead solar irradiance value are recorded in Table 4-6. The hyperparameters set are the same set used by E-SOINN model in Subchapter 4.5.1. RE-SOINN has additional hyperparameters of power (p=2.5) and number of neighbours of 5.

Table 4-6 - Performance of E-SOINN vs RE-SOINN in solar irradiance forecasting

Models	**MASE**	**RMSE (Wm^{-2})**
E-SOINN	0.8162	102.3504
RE-SOINN	0.6782	82.7869

The effectiveness of E-SOINN in forecasting hourly solar irradiance values becomes apparent, particularly when equipped with the capability to generate continuous outputs. As MASE approaches 0.5, RE-SOINN almost outperforms Naïve model by a factor of two. The improvement in the Root Mean Squared Error (RMSE) measure by 20% further solidifies the conclusion that RE-SOINN excels over E-SOINN in forecasting applications involving continuous data. Notably, the results suggest that RE-SOINN can achieve a more accurate forecast even in scenarios where the resolution of training data is not particularly high. Comparing to Nearest Neighbour mechanism adopted by E-SOINN, weighted average of neighbours allows the model to consider the trends of neighbouring nodes. This approach is grounded in the rationale that similar trends should yield similar solar irradiance values in the next hour. As the resolution of nodes increases, accuracy of E-SOINN as well as RE-SOINN will get improved as both models produce the forecast results based on the nodal information. This insight underscores the significance of considering neighbouring trends for accurate solar irradiance forecasting, and it positions RE-SOINN as a robust model for such applications.

The performance of RE-SOINN after being trained incrementally is demonstrated in Table 4-7.

Table 4-7 - Performance Comparison of E-SOINN and RE-SOINN in Incremental Learning

Batch Training	RE-SOINN	
	MASE	RMSE (Wm^{-2})
1	0.7690	92.9153
2	0.7131	86.9235
3	0.7231	87.2185
4	0.6919	83.9259
5	0.6831	82.6209

In general, the performance of models improves as they are trained incrementally and the forecasting performance of RE-SOINN is better than E-SOINN. RE-SOINN has successfully transformed discrete outputs into continuous forecasts, allowing the forecast outputs to be any value in between discrete clusters. As a result, unlike E-SOINN, RE-SOINN does not heavily rely on the number of nodes in the model to produce forecast outputs of better accuracy.

4.5.3 Performance with Decomposed Data

After solar irradiance data are decomposed into low and high frequency components, two RE-SOINN models are created where each model is dedicated for low and high frequency components respectively. With the optimal values found via Grid Search method previously, both Low Frequency and High Frequency models are trained with the respective training sets and their performances against entire test dataset are obtained and recorded in Table 4-8. It is noted that the training vector of low frequency RE-SOINN model (LF RE-SOINN) consists of 62 elements (historical trend with time horizon of 60 minutes) whereas the training vector of high frequency RE-SOINN model (HF RE-SOINN) is made up of 7 elements (historical trend with time horizon of 5 minutes).

Table 4-8 - Suitable Hyperparameters for both LF RE-SOINN and HF RE-SOINN

Models	Denoising Control	Lambda	Maximum Age	Power	Number of Neighbours
LF RE-SOINN	0.001	1000	1000	1	3
HF RE-SOINN	0.001	1000	1000	1	3

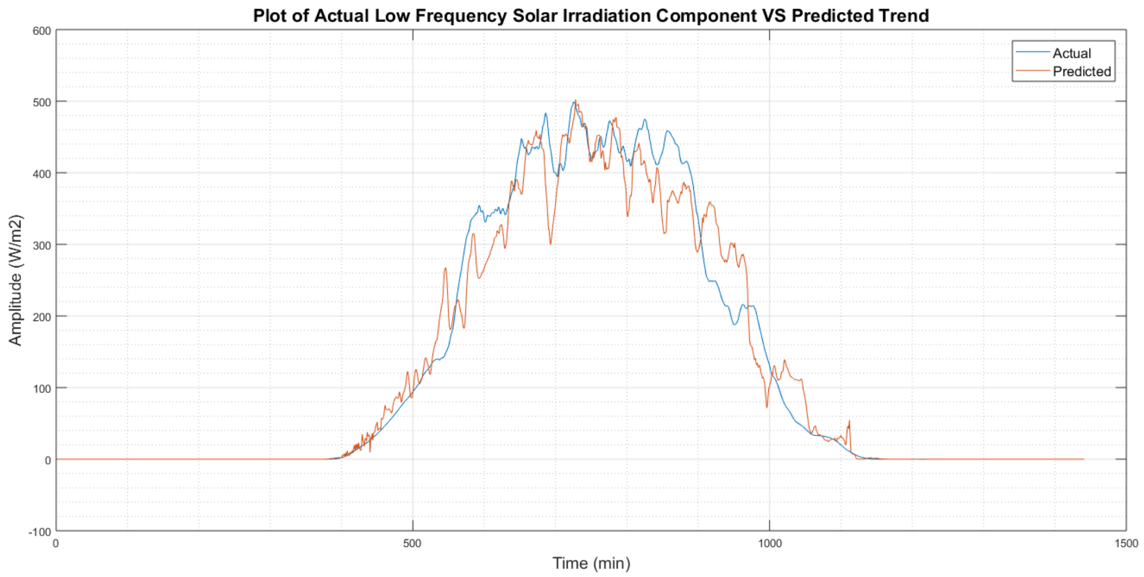

Figure 4-8 - Plot of actual low frequency solar irradiation component vs predicted trend

The plot in Figure 4-8 above shows the visual performance of LF RE-SOINN model in forecasting the low frequency component of one-day solar irradiation trend. It can be clearly seen that the predicted trend is able to follow the general trend of the actual solar irradiation. The proposed model could forecast majority of the peaks and produce similar amplitudes. Our proposed model has in fact shown that Unsupervised Learning model can produce satisfactory results in forecasting applications. The proposed model has produced 6678 nodes of distinctive trends. These nodes are important factor in governing the performance of the proposed model as there are more references to act as closest neighbours.

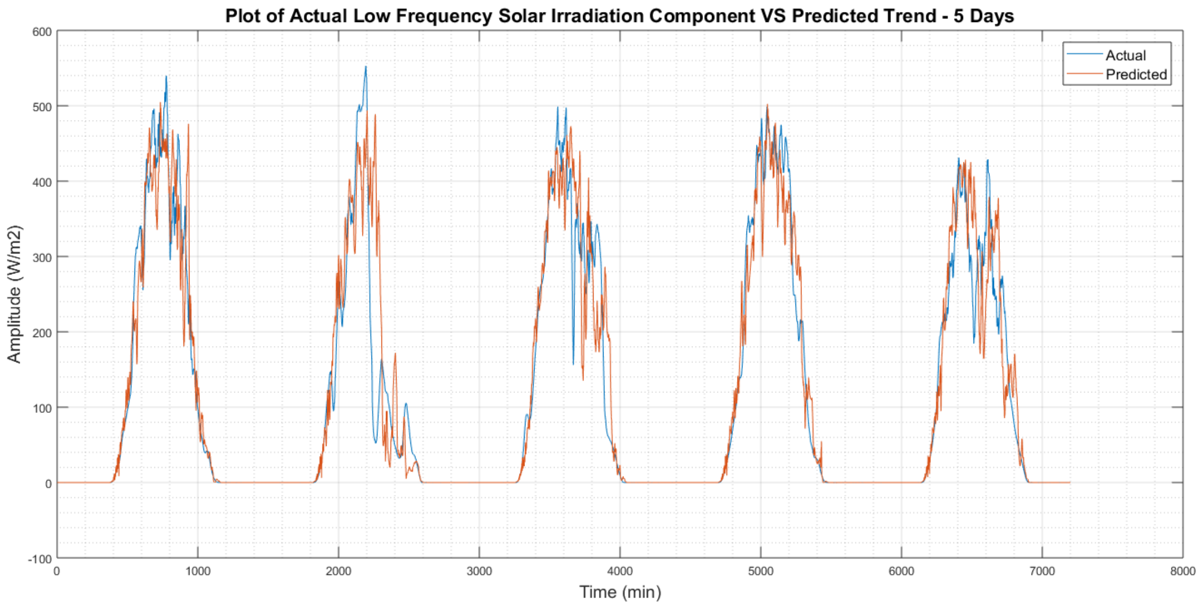

Figure 4-9 - Plot of actual low frequency solar irradiation component vs predicted trend across 5 days

Figure 4-9 shows how the proposed model performs in forecasting low frequency component of solar irradiation for 5 consecutive days. This plot further depicts the ability of the proposed model in tracking the actual trend. On a macroscopic view, the deviation between actual trend and predictive trend mainly occurs at highly oscillating part found in the solar irradiation. This performance is showing good outlook that RE-SOINN could also produce good forecasting results purely with historical solar irradiation trend.

Even though the improvement in MASE is small compared to E-SOINN in Table 4-6, there is a significant improvement in RMSE by 42.3% based on Table 4-9. Both measures suggest that decomposition method has allowed Unsupervised Learning models to produce good performance in forecasting solar irradiance with less and small number of variations.

Table 4-9 - Performance metrics of LF RE-SOINN and HF RE-SOINN models

Components	**MASE**	**RMSE (Wm^{-2})**
Low Frequency	0.7969	60.6870
High Frequency	0.70975	47.992

Figure 4-10 shows how RE-SOINN performs in forecasting the 1-day worth of high-frequency component of solar irradiation values. Forecast from RE-SOINN manages to capture the trend of the high-frequency component although it encounters challenges in accurately replicating the magnitudes of the amplitudes. From the actual high-frequency component of solar irradiation in Figure 4-5, it is observed that the noisy trend significantly varies no matter in terms of frequency and amplitude. RE-SOINN being one of the Unsupervised Learning models, places more emphasis on the statistical information within the dataset. As a result, the forecast output of RE-SOINN is aligned with the general trend.

On the other hand, the amplitudes of the dataset are averaged in the nodes. Unless the amplitudes of each trend occurring at similar timestamp are very similar, in the view of Unsupervised Learning, the differing amplitudes will be either averaged to produce a mean amplitude representing a particular cluster or be removed if the dispersion is too large (may be regarded as noise). Due to the noisy nature of high-frequency component of solar irradiation, the amplitudes vary significantly even though it happens at the same hour and minute daily. As a result, the model struggles to accurately forecast these amplitudes. One potential avenue for improving prediction accuracy is to increase the number of nodes in the RE-SOINN model. This approach allows for the creation of more distinctive nodes, potentially enhancing the model's ability to capture and forecast the varied amplitudes of the noisy high-frequency components.

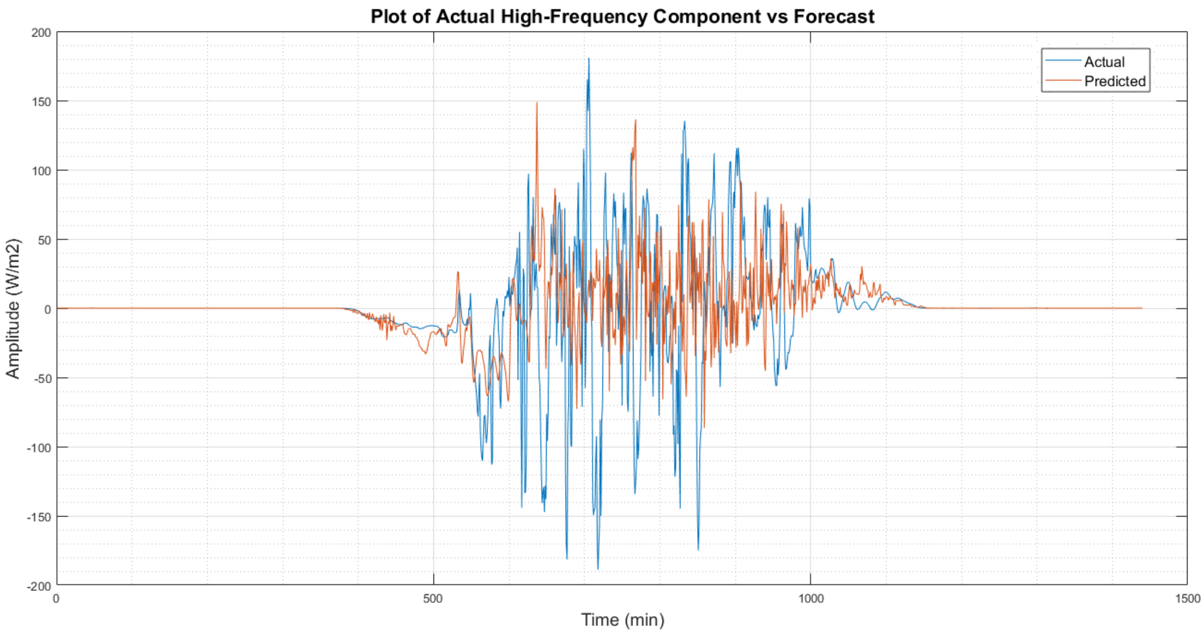

Figure 4-10 - Plot of actual high frequency solar irradiation component vs predicted trend

Both measures show that RE-SOINN performs better in high frequency data compared to low frequency data regardless the fact that LF RE-SOINN model produces better performance in the plot. This contradicting result can be explained when the amplitudes of low frequency and high frequency data components are considered. The mean of low frequency component of the data is 114.03Wm^{-2} whereas the mean of high frequency component of the data is 0.05Wm^{-2}. The normalised RMSE (nRMSE) for low frequency component is approximately 0.53 and the nRMSE for high frequency component is 959.84. nRMSE has shown that the high frequency component of solar irradiance data is highly random and unpredictable. There is hardly any solid geometrical pattern found in the high frequency components of the data.

Table 4-10 - Comparison of overall results of forecasting with decomposed data and original data by RE-SOINN

Models	**MASE**	**RMSE (Wm^{-2})**
Combined Model (LF + HF)	0.6675	79.785
RE-SOINN with Original data	0.6782	82.7869

As outputs from both LF RE-SOINN and HF RE-SOINN models are combined together, the combined outputs from both models are slightly more accurate than RE-SOINN running on original data, as shown in Table 4-10. The decomposition of data has allowed each model to learn slightly more on the statistical and geometrical information available in the training data it is fed with, producing a more accurate forecast eventually when they are combined.

4.5.4 Further Accuracy Improvement

As concluded in Subsection 4.5.3, RE-SOINN model exhibits superior performance when the training data are decomposed into low and high frequency components. As noisy high frequency components data becomes the limiting factor, any improvement made to this aspect could improve the overall forecasting accuracy. Using the proposed improvement method detailed in Subsection 4.3, Table 4-11 shows the improvement in performance by addition of averaged high frequency component based on timestamp. This improvement reinforces the significance of addressing and refining the high-frequency components to elevate the forecasting accuracy of the RE-SOINN model.

Table 4-11 - Performance comparison between models developed in Subsection 4.3 and combined models based on proposed framework

Models	**MASE**	**RMSE (Wm^{-2})**
Previous Model (LF + HF)	0.6675	79.785
Combined New Model (LF + HF + Mean of HF)	0.65755	73.945

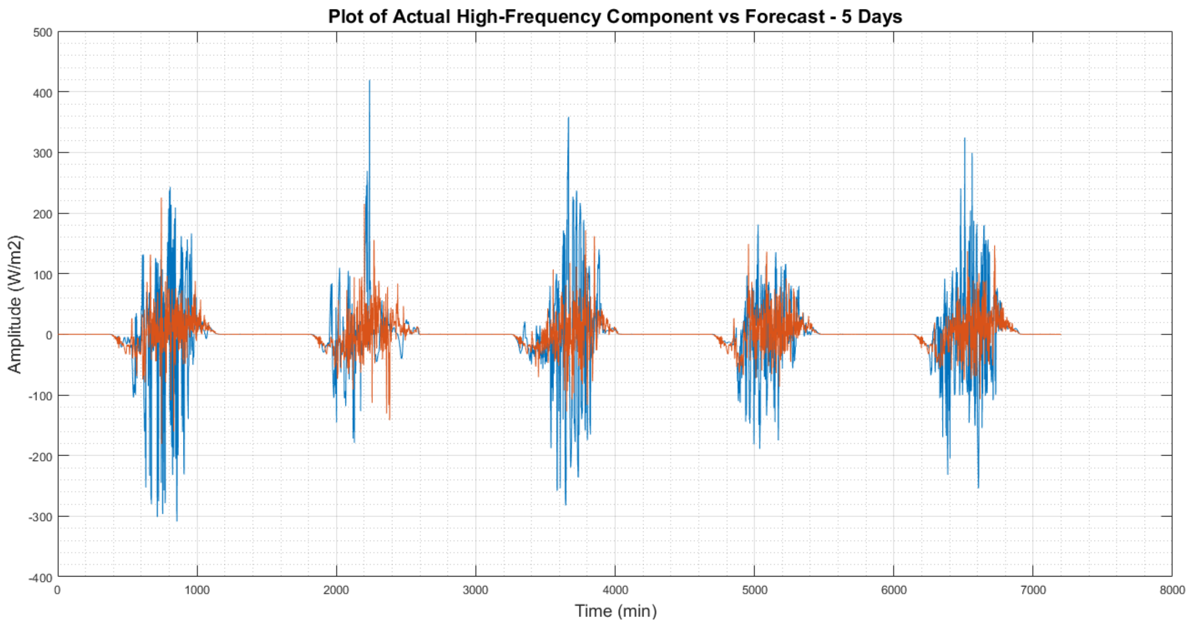

Figure 4-11 - Plot of actual high frequency solar irradiation component vs predicted trend across 5 days

Both MASE and RMSE measure have indicated that inclusion of mean high frequency component to the high frequency forecast output of RE-SOINN has produced better performance. Over the course of the 5 days depicting actual soft trend in solar irradiation trend (shown in Figure 4-11), it is evident that the high-frequency component of solar irradiation differs significantly. The performance of the RE-SOINN forecast aligns with previous descriptions; although exact amplitude replication may not be achieved, the forecast successfully captures the overall shape of the trend and generates means of the noisy amplitudes based on historical data. Table 4-11 further confirms the improvement in forecasting accuracy based on reduction in both MASE and RMSE measures. This corroborates the effectiveness of incorporating the mean high-frequency component to refine the RE-SOINN forecast output.

4.5.5 Comparison with Other Models

Figure 4-12 and Figure 4-13 show the one-day solar irradiation profiles of test data. Notably, both figures illustrate that the solar irradiation in the test data is significantly influenced by short-term variations, particularly during peak daylight hours. The difference between the profiles in Figure 4-11 and Figure 4-12 is that the profile in Figure 4-11 is less noisy. Persistence Model, Exponential Smoothing and Artificial Neural Networks (ANN) are trained with the same batch of train data. Subsequently, the test data is fed into each of these models and their performances are reported in Table 4-12. It is noted that the single-day RMSE and MASE are calculated based on test data from Figure 4-13 given its higher noise levels in comparison to other profiles. This distinction allows for a more focused evaluation of the models' performance under conditions of increased noise in the solar irradiation profile.

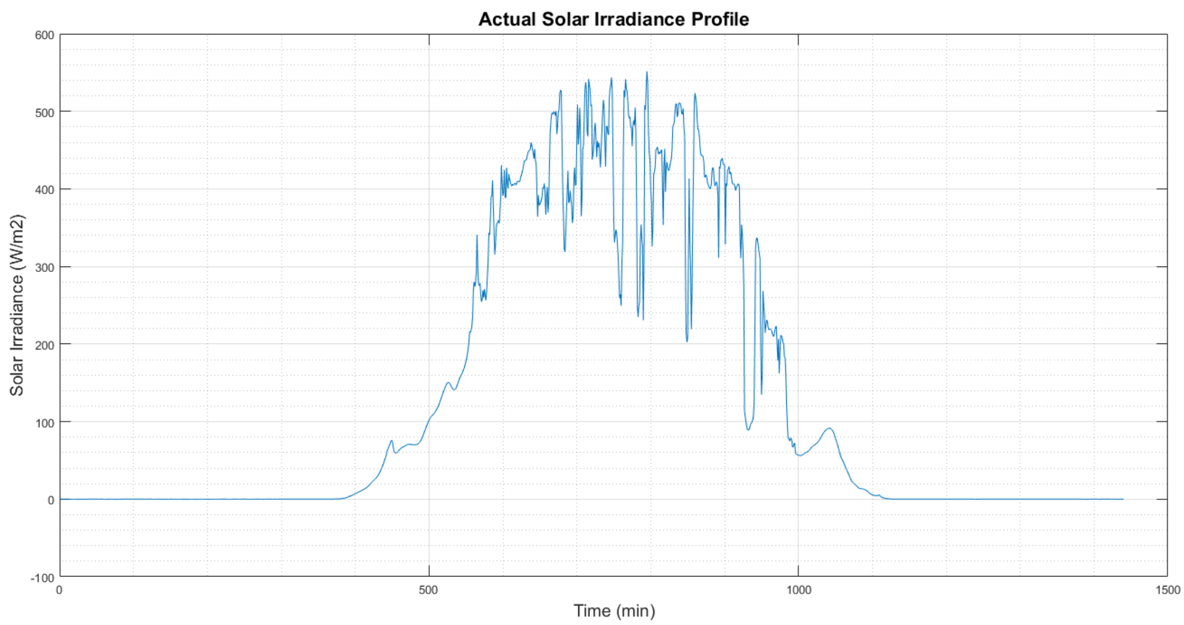

Figure 4-12 - Plot of actual solar irradiation #1 – Less Noisy Profile

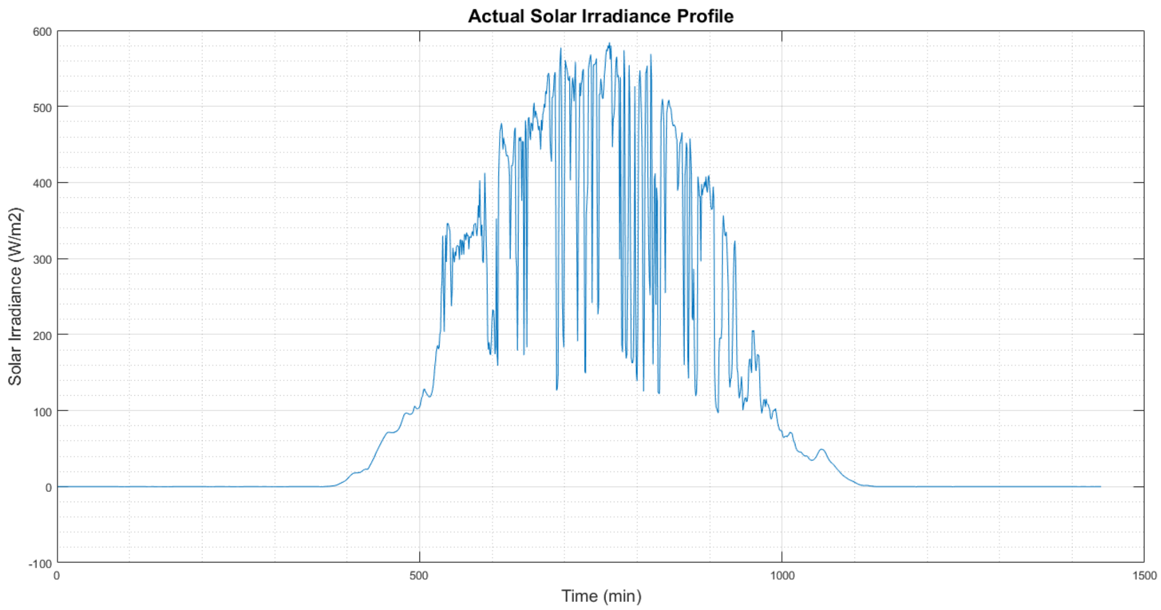

Figure 4-13 - Plot of actual solar irradiation #2 – Noisy Profile

Table 4-12 - Performance metrics of other models vs proposed framework and models

Model	**MASE**	**RMSE (Wm^{-2})**
Proposed Model	0.65755	73.945
Persistence Model	1.2074	103.9485
Exponential Smoothing	0.86862	91.465
ANN	1.0045	90.559

Figure 4-14 to Figure 4-17 show the performance of each model on forecasting the solar irradiation profile recorded in Figure 4-12 whereas Figure 4-18 to Figure 4-21 plot the forecast of each model based on test day from Figure 4-13.

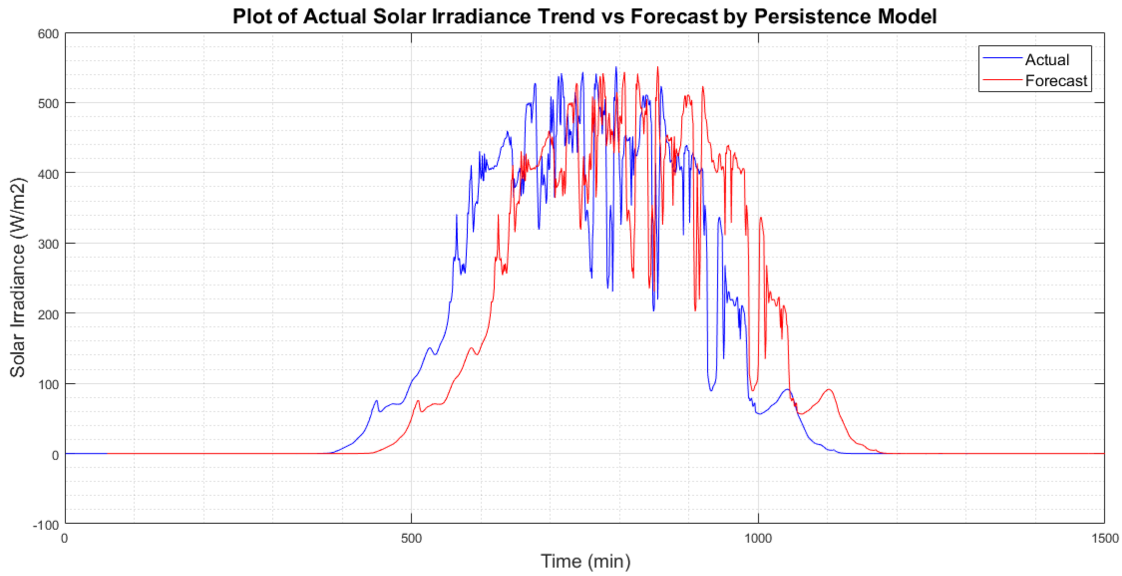

Figure 4-14 - Plot of actual solar irradiation vs predicted trend by Persistence Model on less noisy profile (shown in Figure 4-12)

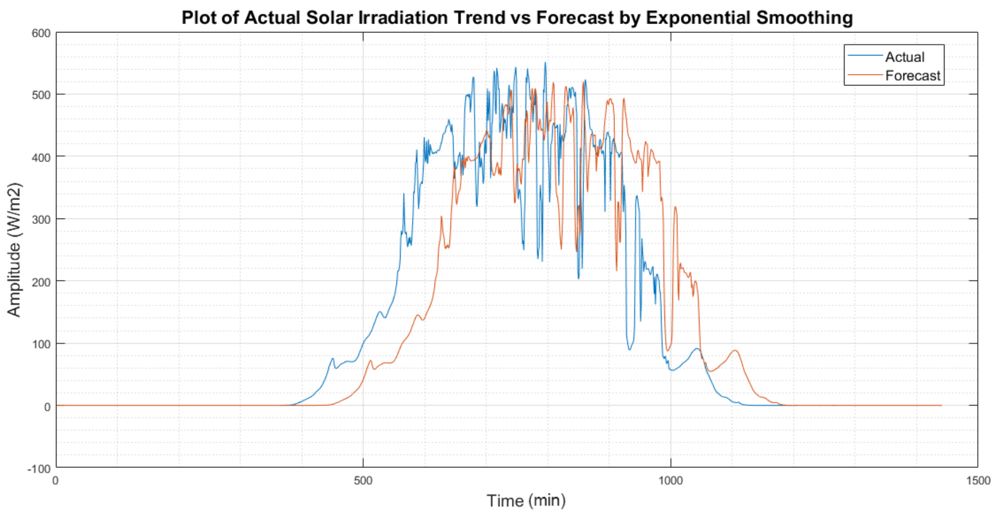

Figure 4-15 - Plot of actual solar irradiation vs predicted trend by Exponential Smoothing on less noisy profile (shown in Figure 4-12)

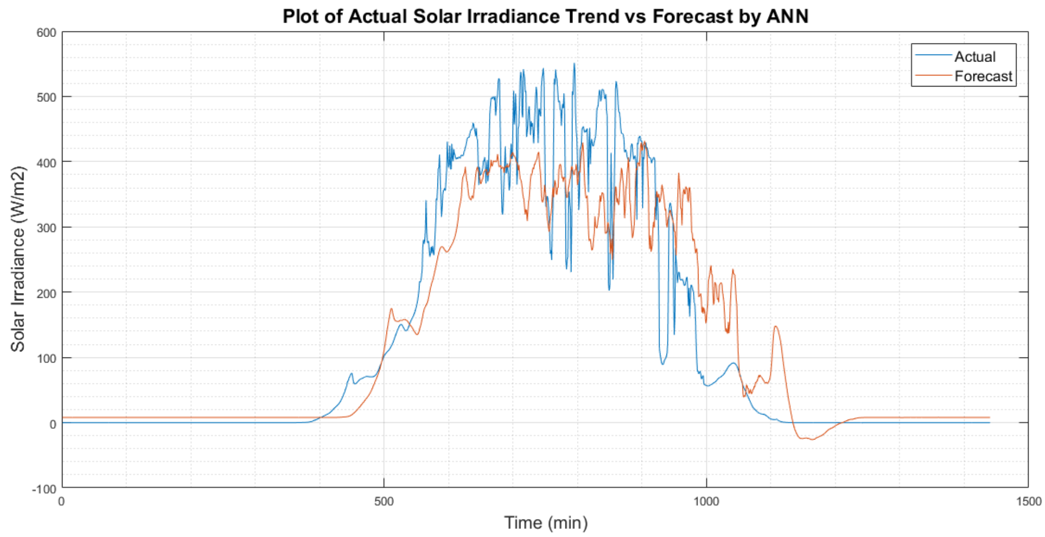

Figure 4-16 - Plot of actual solar irradiation vs predicted trend by ANN on less noisy profile (shown in Figure 4-12)

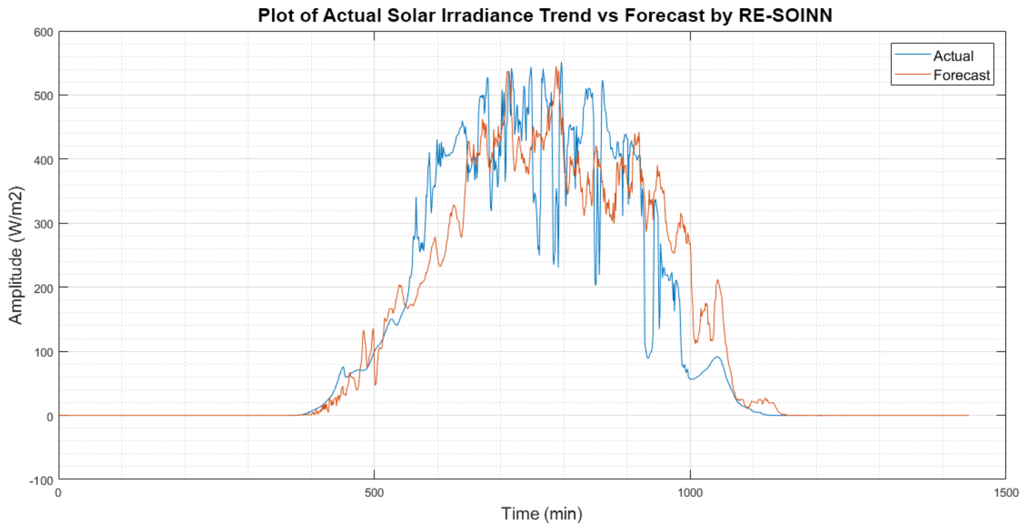

Figure 4-17 - Plot of actual solar irradiation vs predicted trend by Proposed Framework with RE-SOINN on less noisy profile (shown in Figure 4-12)

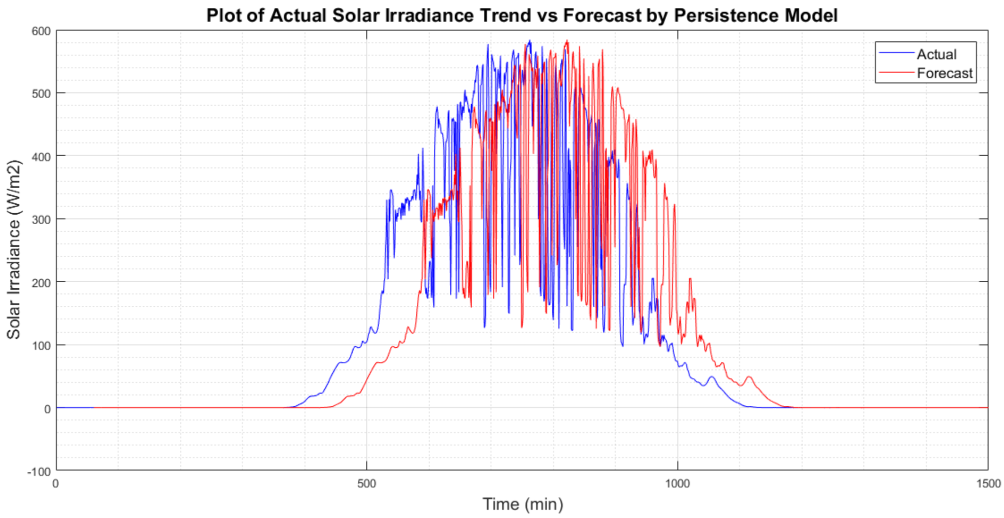

Figure 4-18 - Plot of actual solar irradiation vs predicted trend by Persistence Model on noisier profile (shown in Figure 4-13)

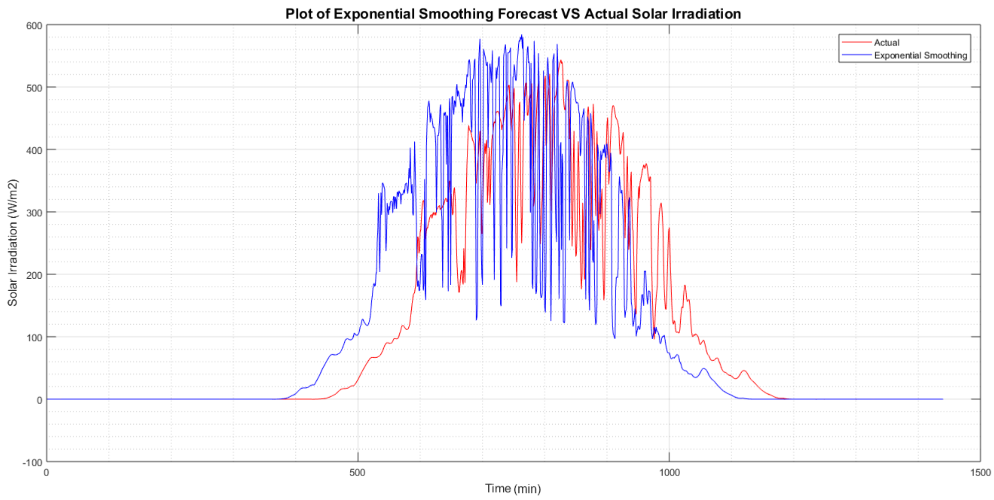

Figure 4-19 - Plot of actual solar irradiation vs predicted trend by Exponential Smoothing on noisier profile (shown in Figure 4-13)

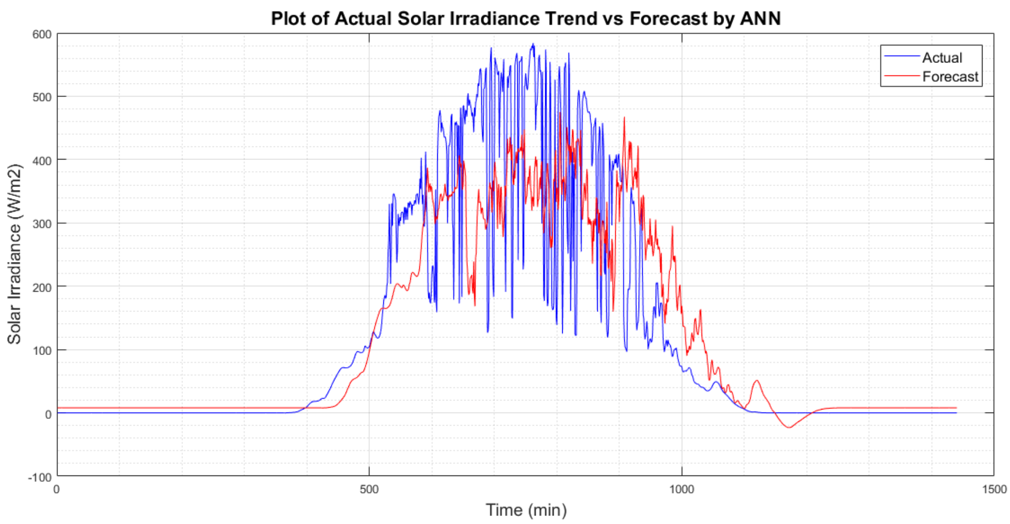

Figure 4-20 - Plot of actual solar irradiation vs predicted trend by ANN on noisier profile (shown in Figure 4-13)

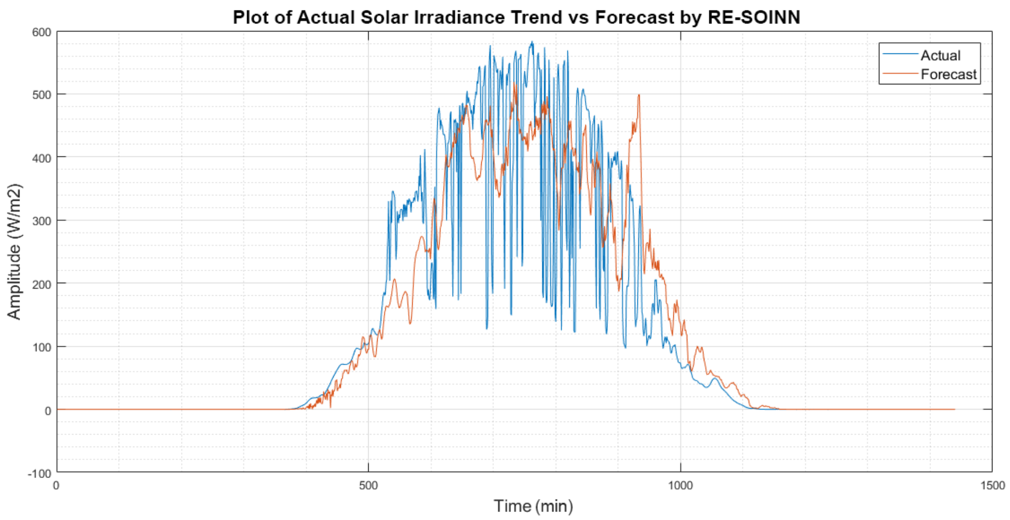

Figure 4-21 - Plot of actual solar irradiation vs predicted trend by Proposed Framework with RE-SOINN on noisier profile (shown in Figure 4-13)

The visual analysis of the plots reveals that both the Persistence Model and Exponential Smoothing models exhibit trends that closely resemble the actual trend, albeit with a lag equal to the forecast horizon. This lag, indicative of the delay in predicting future values, is a characteristic shared by both models. These methods prove particularly effective in regions with less irregular and cloudy solar irradiation profiles, where the likelihood of the next instant's solar irradiation value resembling the most recent observation is higher. However, challenges arise in tropical regions near the Equator, where cloud formations and frequent rainfall are common. The dynamic movement of clouds in the sky intermittently obstructs sunlight, resulting in sudden drops in solar irradiation readings. In such instances, the Persistence and Exponential Smoothing models face limitations in accurately forecasting solar irradiation values, making them less suitable for these regions influenced by tropical climate conditions.

ANN as well as our proposed framework featuring RE-SOINN model show superior performance comparing to Persistence Model and Exponential Smoothing models. According to Table 4-12, RE-SOINN model exhibits a better average performance than the ANN, as evidenced by lower values of both RMSE and MASE. Notably, MASE is a measure of comparison between Naïve model and a specific forecasting model. In this measure, our RE-SOINN model excels in tracking the profile of the actual data in forecasting, producing fewer anomalous amplitudes. In terms of RMSE, the RE-SOINN model demonstrates fewer oscillating amplitudes as compared to ANN. The ability of any forecasting method to follow and produce similar oscillating amplitudes for one set of test data is important because short-term variation is random in nature. Thus, instead of learning the randomness of training data and force RE-SOINN model to find any correlation within, the mean of the short-term variation for each timestamp is used as the baseline of randomness in our forecast. This strategy contributes to the RE-SOINN model's effectiveness in capturing and reproducing similar oscillating amplitudes in the forecasted data.

By adopting to this approach, the forecast values outputted by RE-SOINN model will be consistently in the ballpark range of actual values, allowing our RE-SOINN model to produce a generalised estimation on the randomness found in the solar irradiation profile. Therefore, our RE-SOINN model can produce more superior performance than ANN in the long run since the mean of variation is applicable for any other day as long as there is no significant change in climate over the said region. Also, by leveraging the Incremental Learning feature of ESOINN, our model can learn over time and adapt to the evolving weather patterns, improving the overall forecasting performance that surpasses the plasticity limitations of ANN. With more nodes being created by the RE-SOINN, the higher the forecast resolution since it has seen more distinctive solar irradiation trends, allowing it to produce forecast which can account for higher degree of randomness. This adaptability and increased forecast resolution make our RE-SOINN model well-suited for dynamic weather conditions and contribute to its efficacy in long-term forecasting scenarios.

To further explore the viability of this proposed method across different periods of the year, a random day from December is taken. Figure 4-22 shows the performance of the proposed model on solar irradiance profile taken from a particular day in December 2018. Upon close examination of Figure 4-22 and Figure 4-2, a notable similarity emerges in the short-term trend of the solar irradiance profiles. Both exhibit a common distribution shape, resembling a normal distribution, with peaks occurring around midday. The MASE score is 0.81089 and the RMSE is 72.658 Wm^{-2}. These results affirm the effectiveness of the proposed method in capturing and forecasting solar irradiance profiles for other periods of the year beyond the original dataset. The commonality in short-term trends indicates that the proposed method holds promise for broader applications, demonstrating its adaptability and robustness across various temporal contexts.

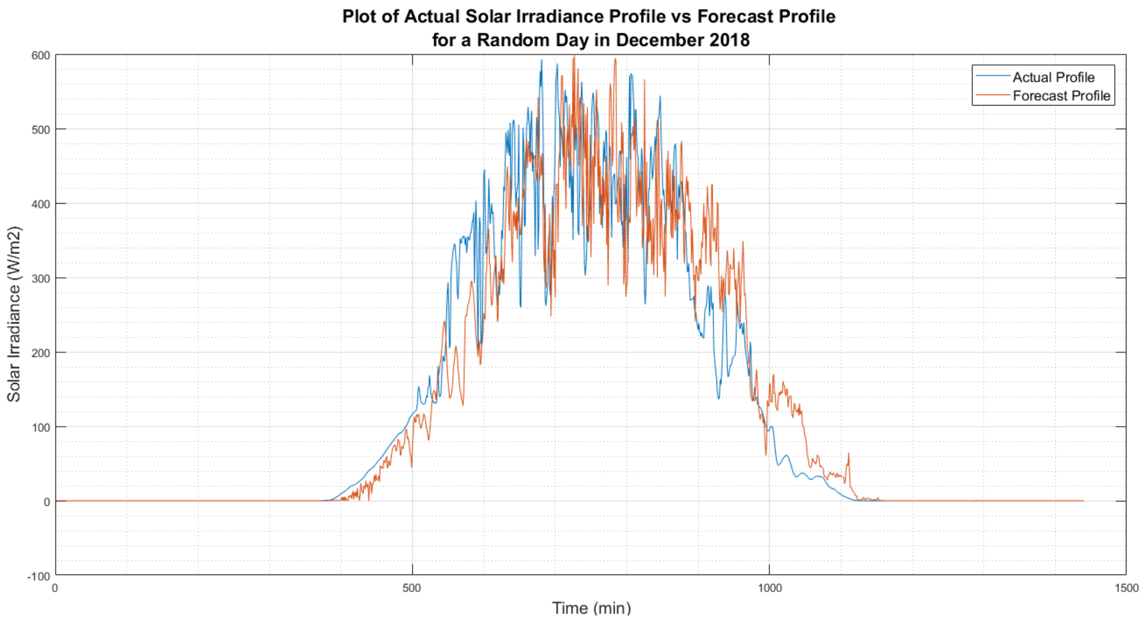

Figure 4-22 - Plot of Actual Solar Irradiance Profile vs Forecast Profile for a Random Day in December 2018

4.6 Summary

An Unsupervised Learning algorithm, RE-SOINN is introduced and complemented by a framework to produce a comparable forecast performance compared to Supervised Learning such as ANN, presents a promising avenue for applications reliant on historical solar irradiance trends. This framework enables RE-SOINN to generate continuous forecasts based on learned solar irradiance patterns, positioning it as a viable alternative in scenarios where Supervised Learning models are conventionally employed. The framework designed can ensure the model to operate within allowable range of forecast accuracy, promising a good forecast performance in long run. Together with its Incremental Learning feature, the model could adapt and learn from new datasets without forgetting previously acquired knowledge, allowing it to adapt to gradual change in the environment.

However, a primary limitation lies in the challenge of optimizing hyperparameters specific to the climate trends observed in solar irradiance profiles. Given the unsupervised learning nature of RE-SOINN, the identification of an optimized set of hyperparameters becomes crucial for its forecasting performance. In this section, Grid Search method is applied to deal with this optimisation issue. It is noted that Grid Search procedure could take a lot more time and computational resources compared to actual application of optimised RE-SOINN model to predict hourly solar irradiance. In future work, AI-based optimisation algorithms such as Particle Swarm Optimisation (PSO) can be applied to make the proposed model to start running with the least human interference possible. PSO is recognized for its efficiency in reducing unnecessary computational steps, offering a potential avenue for enhancing the optimization process beyond the resource-intensive Grid Search method.

Chapter 5 RE-SOINN Model Energy Management Strategy

This chapter proposes a novel optimization and control strategy method for any standalone PV-based REPS with battery-supercapacitor HESS. The proposed EMS adopted in this project is optimised every minute based on solar irradiance and load demand profiles. The originalities are as follow:

Unsupervised Learning Artificial Intelligence model is adopted in the EMS controller. This model, together with T_c and T_d (charging and discharging thresholds) [11] as data labels offer a flexible operation to the REPS with battery-supercapacitor HESS. The model behaves smartly by studying hourly historical data trend and makes deduction using its knowledge base.

The incremental feature of RE-SOINN allows the AI model to learn new data to adapt to new changes gradually. By having PSO as a teacher at its early learning stage, EMS could work as a black box and learn on its own with the least interference from human.

5.1 System Structure and Modelling

The overall structure of the proposed system is demonstrated in Figure 5-1 as shown below. The proposed system consists of four main components, namely the PV system, supercapacitor, battery and bidirectional DC-DC converter, forming standalone PV system in the study. The proposed system adopts semi-active Supercapacitor-Battery HESS architecture where only supercapacitor is controlled directly by EMS whereas battery responds passively to the system demand. Therefore, the dynamic power equation representing the proposed system can be summarised as Equation (5-1):

$$P_{PV} - P_{batt} - P_{sc} - P_{load} = 0 \quad [10] \qquad (5\text{-}1)$$

where P_{PV}, P_{batt}, P_{sc} and P_{load} are the PV output power, battery power, supercapacitor power and load power demand respectively.

A small note to be taken is that since semi-active HESS topography is used in this study, supercapacitor power must go through additional route via DC-DC converter before it reaches DC bus. Assuming the DC-DC converter has an efficiency of η, P_{sc_actual} reaching the DC bus is now ηP_{sc}. In this segment, DC-DC converter is assumed to be ideal with its efficiency η = 100%, making P_{sc_actual} = P_{sc}.

Taking inspiration from [10], the dynamic power equation of the proposed system is rearranged to simplify the power distribution problem. A term, dP is created to consider the generated PV power and load demand, denoting the power surplus between power generation side and load demand side, producing Equation (5-2).

$$dP = P_{PV} - P_{load} = P_{batt} + P_{sc} \tag{5-2}$$

If dP is positive, it indicates a power surplus and the extra power can be stored in both battery and supercapacitor. If dP is negative, power deficit occurs and stored power in battery and supercapacitor should be used to satisfy the power mismatch.

Table 5-1 lists down the component specification of the proposed system.

Table 5-1 - Specifications of components present in the system under study

Components	**Specification**	
PV	Power	2kW
Battery	Voltage	48V
	Capacity	250Ah
Supercapacitor	Voltage	60V
	Capacitance	200F

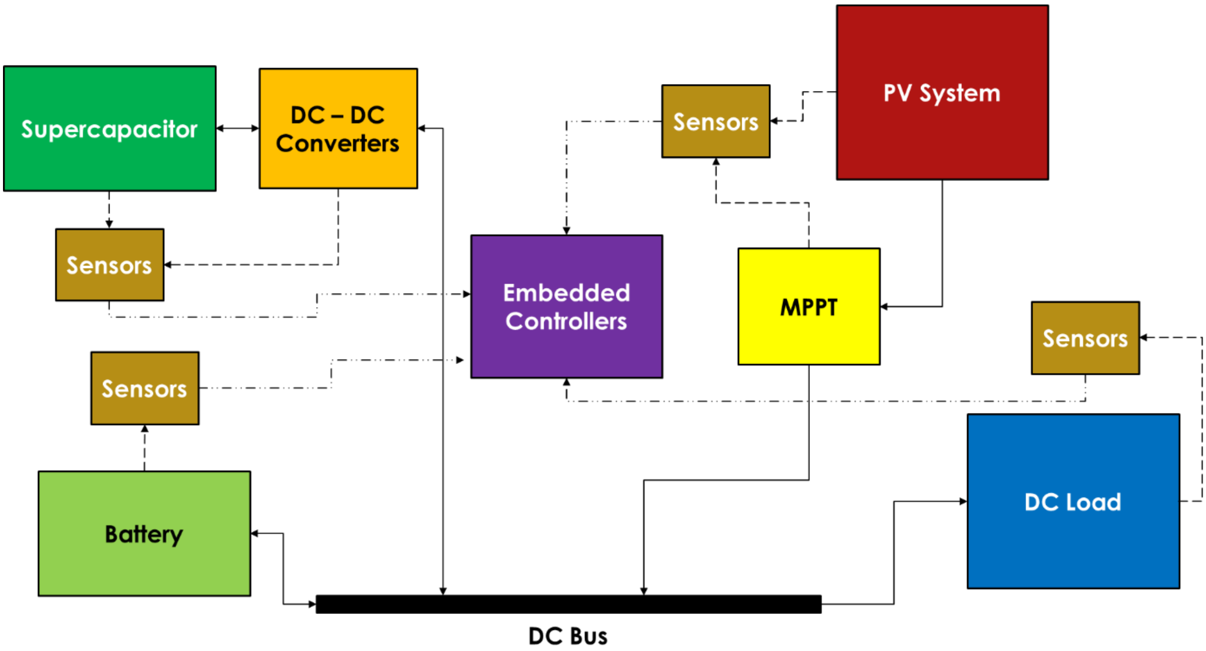

Figure 5-1 - System block diagram for system developed in this study

5.2 Proposed Control Strategy

REPS with HESS usually operates with higher energy density storage device (SLA battery) as the primary ESS and higher power density storage device (supercapacitor) as the secondary ESS. Primary ESS is responsible to meet a significant part of load demands or to store larger amount of harvested solar energy whereas the role of secondary ESS is to supply any energy deficit or to absorb energy surplus leftover by primary HESS. Batteries, especially sealed lead-acid based batteries (SLA), are commonly used as primary ESS. The cheaper price tag of SLA batteries, however, comes with a few drawbacks that could cause REPS a low return and less favourable investment [132]. The common issues that could damage SLA batteries are

- Peak battery power demand
- Oscillations of battery power between charging and discharging operations, or excessive battery charge-discharge cycles
- Huge battery charge/discharge rate

The goals of the EMS applied in this research are therefore

- to extend the battery lifetime which in turn prolongs the system service life and reduces system maintenance cost, as well as
- to assist the REPS to improve solar energy harvesting

Table 5-2 shows how these issues are addressed by the proposed EMS.

Table 5-2 - Issues experienced by Lead Acid battery and measures offered by proposed EMS

Factors affecting battery life cycles	**How proposed EMS helps**
Peak battery power demand	Battery is coupled with supercapacitor and EMS should be able to schedule supercapacitor charging and discharging operations more frequently.
Excessive battery charge-discharge cycles	Filtration is added to the EMS so that the oscillating component in the load demand or dP can be filtered out for supercapacitor operations.
Huge battery charge / discharge rate	EMS should be able to schedule longer operation of supercapacitor so that the battery charging or the discharging power amplitudes are reduced by sharing a portions to the supercapacitor.

In common applications, pre-defined rules (Rule-Based Controllers) are used to control the operation of secondary ESS for power distribution between primary and secondary ESS. However, this strategy restricts the efficiency of EMS due to the rigidity of pre-defined rules.

In Ref. [11], a flexible power distribution strategy is proposed so that the secondary HESS in the REPS can be charged and discharged in any condition as the EMS sees fits. There are two thresholds (T_c and T_d) where each of the thresholds can be adjusted freely to control the amount of shared power by supercapacitor. T_c and T_d control the charging as well as discharging operation of the supercapacitor respectively. Therefore, the proposed EMS outputs optimal T_c and T_d for each varying condition of dP and SoC_{sc}.

The proposed EMS consists of 4 modules or components where each of the modules is tasked to respond to each of the issues in Table 5-2 effectively. The system handles the load demand in a sequential manner via these modules, resulting a smoothened load demand power draw for the battery. Thus, the final output of proposed EMS can be viewed as a sequential summation or response of each module output.

Figure 5-2 shows the system block diagram of the proposed EMS applied in this study. There are a total of 4 major components in the EMS of the system, namely:

i. Moving Average Filtration

ii. RE-SOINN Input Data Clustering and Decision Output

iii. Power Distribution Strategy

iv. Circuit Voltage and Current Protection

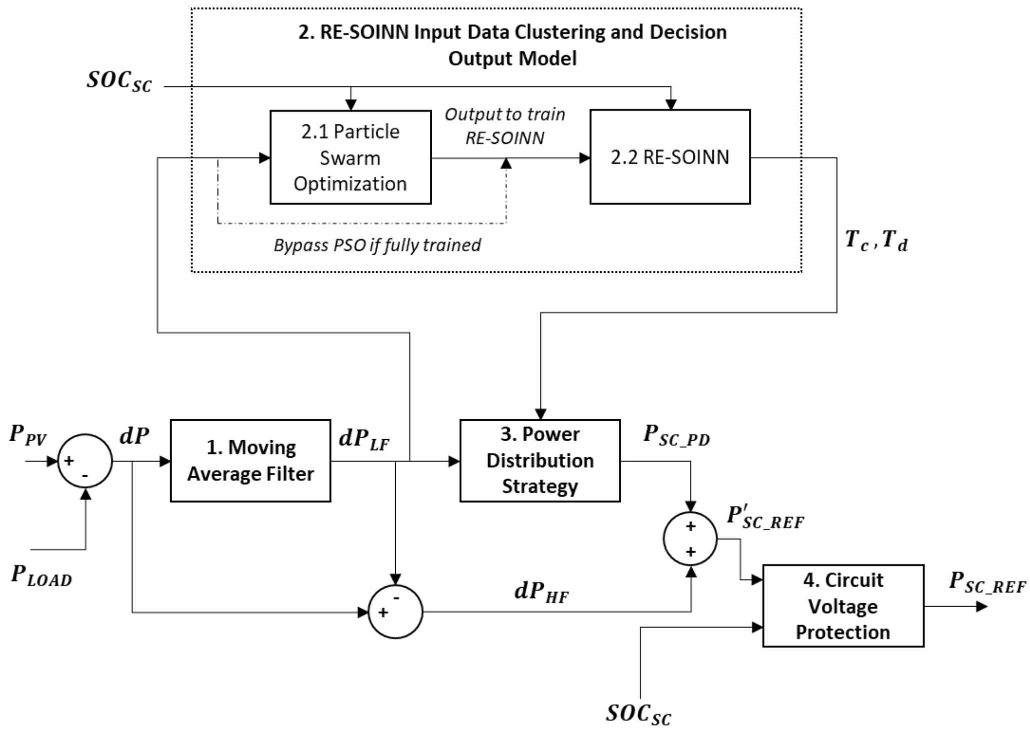

Figure 5-2 - System block diagram of proposed EMS

In Figure 5-2, dP is first evaluated based on power difference between load power demand and renewable power generation. Then, dP is decomposed into its low frequency component (long-term trend) dP_{LF} and high frequency component (short-term trend) dP_{HF}. Subsequently, dP_{LF} is inputted to RE-SOINN Input Data Clustering and Decision Output Model. At initial stage, Particle Swarm Optimisation training model is initiated to train RE-SOINN model with optimal labels to dP_{LF} and SoC_{sc}. Immediately after RE-SOINN model is fully trained, dP_{LF} and SoC_{sc} are inputted to RE-SOINN model directly, bypassing the PSO training model. The RE-SOINN model then produces optimal supercapacitor charging and discharging thresholds, the T_c and T_d. The power distribution strategy module interprets the T_c and T_d to determine the amount of absorbed or supplied power to be shared by supercapacitor. Finally, the circuit voltage and current protection module ensures the supercapacitor works within its operating range without any overcharging and over-discharging event.

5.3 Moving Average Filtration (MAF)

The main purpose of moving average filtration in the EMS is to minimise the dynamic stress of high energy density ESS such as lead-acid battery. Early research such as [29], [59], [132] have shown that filtration method or any Filtration-based Controller (FBC) is able to improve the battery lifespan by lowering battery stress level and oscillation cycles. MAF decomposes the dP into its fast transient (high-frequency) as well as its steady slow (low-frequency) components. It is the fast transient component in the dP that causes ESS to experience oscillating power profiles, resulting in damaging battery current cycles which hurt the battery lifetime. The moving average component of dP is determined using the mathematical equation as follows:

$$dP_{LF} = \frac{1}{T}\int_{t}^{t-T} dP\, dt \qquad (5\text{-}3)$$

where *T* refers to the moving sampling time window and *t* is the sample to be considered at the time of computation. Once dP_{LF} (low frequency component) is determined, the high frequency component of *dP* can be found using the relationship as follows:

$$dP_{HF} = dP - dP_{LF} \qquad (5\text{-}4)$$

Moving average filtration model itself is not particularly useful to work alone as sole component of EMS. It can work well in reducing battery power oscillation by allowing supercapacitor to deal with dP_{HF}. However, filtration-based EMS is unable to alleviate the battery current deep discharge problem effectively, leaving a relatively huge room of improvement for EMS. Thus, other modules are added into the system sequentially to further improve the system performance. In this application, the period is set as 25s.

5.4 RE-SOINN Input Data Clustering and Decision Output Model

T_c and T_d are the two thresholds that are being adjusted continuously so that active control of supercapacitor (charging and discharging) can be possible. Eventually, power distribution between the power generation, load demand as well as HESS can be managed via active control of supercapacitor. In this subsection, the proposed control strategy adopts an Unsupervised Learning Artificial Intelligence model, Regression Enhanced Self-Organizing Incremental Neural Networks (RE-SOINN) to summarise as well as to learn from the input data. The EMS operation is to identify the similarities between input data and historical data stored in the database of RE-SOINN to produce optimal T_c and T_d based on data similarity. The model is run at one-minute interval so that the power in the system can be managed in one-minute interval manner. As a result, data clustering from RE-SOINN could reduce the computational complexity in producing an optimal T_c and T_d values, leading to minimal overall computational time.

As an unsupervised learning model, RE-SOINN is unable to label the data it has not seen. In this application, the labels for the data are the optimised T_c and T_d values which are to be computed separately. Thus, an optimization model is added to compute the optimal T_c and T_d at early stage of untrained RE-SOINN. This optimization model, PSO, serves as the teacher to the RE-SOINN model so that RE-SOINN could start to label the subsequent data with optimal T_c and T_d after learning stage. Thus, RE-SOINN would have to go through a single learning stage to expand its knowledge base.

i. LEARNING STAGE - When RE-SOINN starts operating from scratch or zero knowledge, PSO will serve to assist RE-SOINN in labelling the inputs. Then the inputs together with optimal labels are to be stored in the knowledge base as nodes.

ii. AFTER LEARNING – After RE-SOINN is fully trained with variety of inputs for a said duration, PSO can then be suspended where the labels of new inputs are determined solely using RE-SOINN. At this stage, the computation of optimal T_c and T_d can be done without complexity due to calculation iteration in PSO.

5.4.1 Particle Swarm Optimisation (PSO) Model

Bird flocking and fish schooling are proofs that coordinated behaviour emerges without central control [100]. PSO studies how several simple entities (particles) interact and influence each other to move to region of interest [101]. The particles are placed in the search place of problems and each evaluates the objective function at its current location. Each particle then determines its movement by combining historical information on its current and best-fitness locations with those of one or more members of the swarm with some random perturbations.

Figure 5-3 denotes the flowchart involving PSO in the computation of optimal T_c and T_d as labels to the dP_{LF} trend coupled with SoC of supercapacitor. During initialisation, the particles consist of random T_c and T_d where PSO would determine the best and optimised particle to maximise solar energy harvesting as well as to minimise battery peak demand due to real time dP_{LF} and SoC_{sc}. A fitness function is embedded into the PSO to evaluate the performance of each particle (or each set of T_c and T_d) in each case as described by its input vector.

5.4.2 Fitness Function of PSO

As PSO uses iteration method to find better T_c and T_d to suit conditions described by input vectors, fitness function is the key to determine the suitability of each T_c and T_d represented by particles. Fitness functions are usually in the form of mathematical model of a system to simulate the effects of varying variables represented by the PSO particles onto the system. In this study, the inputs to the PSO are historical T_c, historical T_d, dP_{LF} and SoC_{sc} where battery and supercapacitor power profiles are the outputs. Thus, during each PSO computational iteration, each set of T_c and T_d from the PSO particles is inputted into the fitness function so that the best performing particles can be determined based on the power profiles.

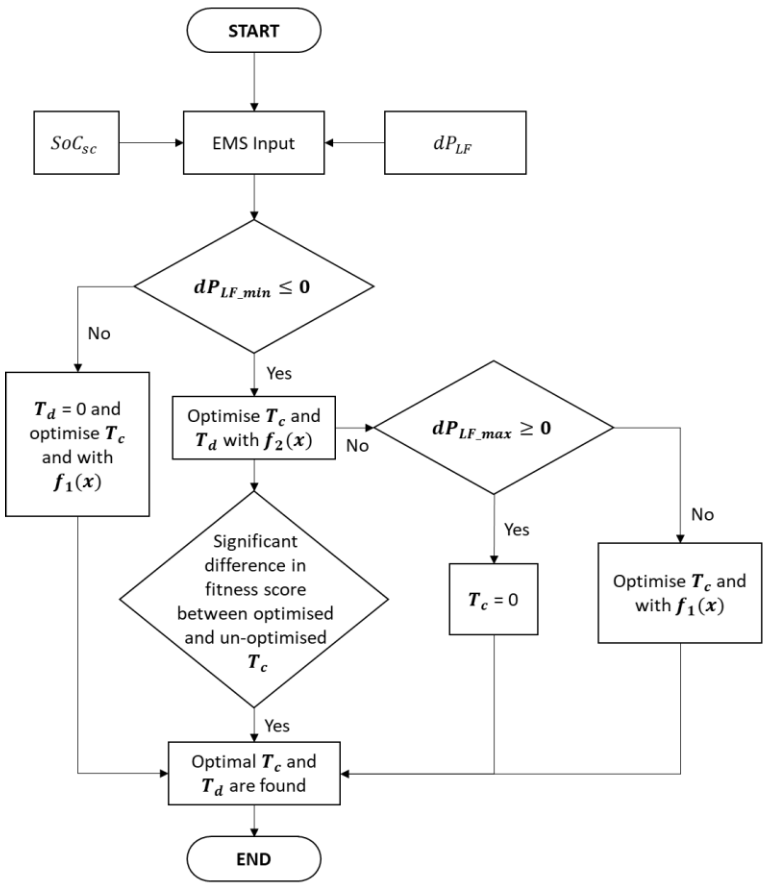

Figure 5-3 - Algorithmic flowchart of PSO application in the EMS

Unlike [11] which aims to reduce the peak battery power (either during charging stage or supplying load demand) by utilising supercapacitor, the EMS in this study also considers maximising the solar energy harvesting by prioritising the usage of supercapacitor to store harvested energy during low solar irradiance conditions. Furthermore, as dP_{LF} could span between positive and negative values, the ideal performance for battery could be very different under differing conditions. Thus, specialised fitness functions are introduced to satisfy the constraints of different cases.

An important aspect for consideration while devising the EMS based on this study is that supercapacitor only operates when the dP_{LF} is higher than T_c or dP_{LF} is lower than T_d as depicted in Figure 5-4. The possible cases based on dP_{LF} are described as follow:

I. When the hourly dP_{LF} trend is entirely positive, battery undergoes charging operation only since load demand is successfully satisfied. To reduce the battery power oscillation between charging and discharging cycles, T_d is set to 0 so that supercapacitor only discharges to meet unexpected load demand. T_c is set based on SoC_{sc}. Lower SoC_{sc} would yield a smaller T_c so that more solar energy harvested can be allocated to supercapacitor. Thus, in this case, the fitness function is to reward T_c and T_d values that maximise solar energy harvesting as well as reduce instantaneous battery peak charging power.

II. When the hourly dP_{LF} trend is entirely in the negative region, the load demand is greater than renewable energy generation. Thus, HESS discharges to match the power deficit. If SoC_{sc} is too high, T_c is set at 0W (or any other positive value) so that supercapacitor will be ready to be activated for charging. As so, battery will be less likely to undergo damaging short charging-discharging cycles. On the other hand, T_d is set to be 0W as well so that supercapacitor can be readily discharged to meet load demand. If the SoC_{sc} is extremely low, T_c will be set lower than 0W so that a small amount of power is drawn from battery to prevent supercapacitor from discharged completely. T_d is also lowered. The fitness function mainly aims to bring battery power profile close to 0W. Activation of T_c can be determined by comparing the simulated system performance in the absence of T_c values since discharging operation dominates.

III. If the hourly dP_{LF} trend consists of positive and negative values, then the EMS will need to go through two optimisation processes. The first optimisation uses the fitness function from case 2 to reduce battery peak discharging power. Then both T_c and T_d will be tested to further evaluate the optimisation performance of T_c. This is because fitness function in case 2 does not place huge emphasis on optimising T_c. T_c will be further optimised with the same T_d if the difference in performance for cases with optimised T_c and absence of T_c is significant. The fitness function of the second stage optimisation is similar to that of case 1 where solar energy harvesting is maximised and instantaneous battery peak charging power is reduced.

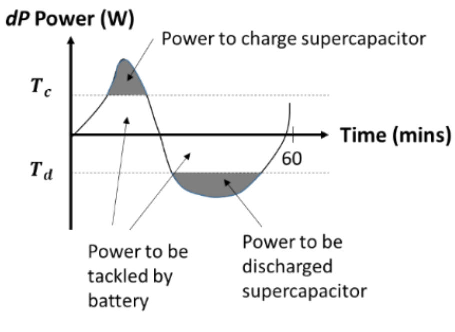

Figure 5-4 - Plot of power distribution based on T_c and T_d values

Table 5-3 – Table of fitness functions in each of the cases described in Subsection 5.4.2.

	dP_{LF_MAX}	dP_{LF_MIN}	**Optimisation Goals**	**Fitness Function**
CASE 1	Positive	Positive	Maximising Energy Harvesting and minimising battery peak charging power	$f_1(x) = \min\left(\frac{P_{batt\_max}}{Area\ under\ Graph}\right)$ (5-5)
			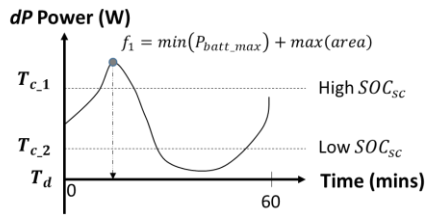 *Figure 5-5 - Plot of power distribution based on T_c and T_d values when dP is entirely positive*	
CASE 2	Negative	Negative	Maximising battery peak discharging power without going through multiple charge-discharge cycles	$f_2(x) = \max(P_{batt\_min})$ (5-6)
			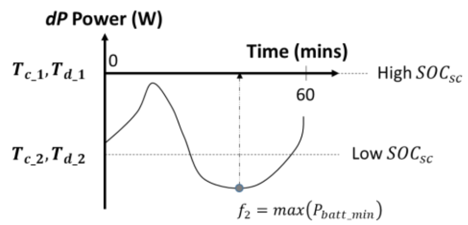 *Figure 5-6 - Plot of power distribution based on T_c and T_d values when dP is entirely negative*	
CASE 3	Positive	Negative	*Step 1*: similar to Case 2 *Step 2*: similar to Case 1	1. $f_2(x) = \max(P_{batt\_min})$ (5-7) 2. $f_1(x) = \min\left(\frac{P_{batt\_max}}{Area\ under\ Graph}\right)$ (5-8)
			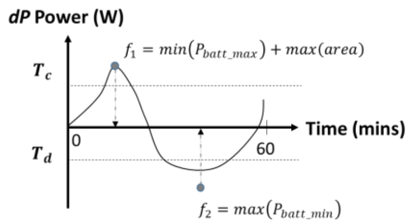 *Figure 5-7 - Plot of power distribution based on T_c and T_d values when dP are both negative and positive.*	

5.4.3 Data Clustering using RE-SOINN

The RE-SOINN [190] adopted is based on the E-SOINN [131]. Its Incremental Learning ability is important for this application so that the model can work from scratch without the need of accurate mathematical framework with minimal model customization. Based on explicit statistical features found in the input data, homogenous and distinctive data can be grouped together or partitioned to form new classes or nodes. Therefore, the clustering feature could store important information from historical data without the expense of oversized database due to increasing accumulated historical data. It also facilitates data comparison between input and stored data via lower dimensional complexity. The E-SOINN has thus been used in classification applications extensively for cases requiring discrete outputs [130].

The RE-SOINN in [190] incorporates the regression method into the E-SOINN to produce continuous output to ensure that the output is adjusted accordingly based on degree of data similarity instead of taking the information from the nearest node as output. Also, it reduces the resolution of nodes required by EMS for an optimised T_c and T_d output. Thus, RE-SOINN could estimate optimal T_c and T_d threshold without needing an exact identical data in the knowledge base of RE-SOINN. The clustering feature of RE-SOINN manages to group all similar data trends into a single class and thus greatly reduces the computational time.

The data stored in the knowledge base of RE-SOINN consist of vectors of 63 elements. The first 60 elements are made of the historical hourly dP_{LF} trends, the 61st element is the SoC of supercapacitor with 62nd and 63rd elements representing the labels or the T_c and T_d pair optimised by PSO for the case. The number of nodes or neurons in RE-SOINN is determined dynamically by the model itself during the stage of clustering. A new node is created when Euclidean distance between input vector and nodes available in RE-SOINN is greater than the similarity threshold. The parameters of RE-SOINN such as denoising control, denoising iteration, maximum nodal age, number of neighbours and power for significance adjustment are determined using Grid Search method.

Upon maturity, the input to RE-SOINN model is an hourly dP_{LF} trend sampled at 1 minute interval coupled with current state-of-charge (SoC_{sc}) of supercapacitor. Thus, the input vector has total elements of 61, corresponding to 60 one-minute interval data points and one SoC value. As input vector is fed into the RE-SOINN model, all 61 elements in the input vector will be compared with first 61 elements of all nodes to determine its closest neighbours. Then, the T_c and T_d values for the input vector are interpolated from the 62nd and 63rd elements from its neighbouring nodes respectively.

As the EMS runs from zero initial knowledge, when the first input arrives, PSO assists RE-SOINN by providing the optimal labels to the input. Then, the input together with its optimal labels is recorded temporarily. This process is repeated for every minute of the day until one day worth of dataset (one-minute interval inputs with their respective labels) is obtained. Subsequently, RE-SOINN is trained with these new data to form its knowledge base. The training is usually conducted in the middle of the night such as 3am during the regular resting hours of human activities where there should be minimal dP variations. The entire procedure is repeated for at least ten days so that RE-SOINN reaches maturity.

5.5 Integration with RE-SOINN Forecast Model

The importance of allowing the EMS to be able to plan ahead of time has been indicated in refs [133], [139-140]. This is an important advantage to the EMS due to the following points as follows:

- The dynamic characteristics of solar energy generation as well as load demands resulting from user's erratic behaviours require dynamic response from HESS.
- In the events where supercapacitor has fully utilised its charges completely, being able to anticipate any incoming power disturbance requiring the operation of supercapacitor will allow EMS to arrange the charging of supercapacitor to regain charges prior to the power disturbances.

- Due to restrictions from computational resources available for the system, the charging and discharging operations of supercapacitor cannot be controlled at a very high time resolution (such as 1 second) but at a one-minute interval manner. This indicates that during the one-minute duration between each computational step, supercapacitor is to be charged and discharged the same regardless of the change in dP trend. Thus, the system performance should perform better if the semi-active control of supercapacitor can consider longer time horizon into the future so that the HESS is ready to tackle the future dP.
- The system can be avoided from operating blindly and it is more intuitive in looking for optimal time for Incremental Learning of the EMS.
- The system can also avoid a huge power mismatch from one computational step to another when there is a sudden huge change in incoming dP trend.

The prediction is carried in time horizon of one hour or 60 minutes since the forecasting model developed in Chapter 4 works well on hourly time horizon. As the input to the EMS are dP_{LF} and current SoC_{sc}, dP_{LF} is replaced with a forecasted 60-minute ahead $dP_{LF\_forecast}$. The $dP_{LF\_forecast}$ can be evaluated from $dP_{forecast}$ using Equation (5-9) via forecasted PV output power, $P_{PV\_forecast}$ and forecasted load demand, $P_{load\_forecast}$.

$$dP_{forecast} = P_{PV\_forecast} - P_{load\_forecast} \tag{5-9}$$

The PV output power forecast can be determined mathematically via output of solar irradiance forecasting model from Chapter 4 [191]. A mathematical equation to formulate PV output power has been suggested as follows [191]:

$$P_{PV} = P_{PV\_STC} \times \frac{G_T}{1000} \times \left[1 - \gamma \times \left(T_j - 25\right)\right] \times N_{PV\_S} \times N_{PV\_P} \tag{5-10}$$

where P_{PV_STC} refers to rated PV power at MPP and standard test conditions (STC), G_T refers to solar irradiance level, γ refers to power temperature coefficient at MPP, T_j is the PV cell temperature with N_{PV_S} , N_{PV_P} being number of modules in series and in parallel respectively. T_j can be further expressed as

$$T_j = T_{amb} + \frac{G_T}{800} \times (NOCT - 20) \tag{5-11}$$

where T_{amb} is ambient temperature, NOCT is the nominal operating cell temperature ($T_{amb\_NOCT} = 20$°C, $G_{T_NOCT} =$1000Wm^{-2}, and wind speed of 1ms^{-1}. Table 5-4 shows the parameters specifications for Equations (5-10) and (5-11) based on solar panels specifications used in this research.

With the aids from Equations (5-10) and (5-11), PV output power forecast of 60-minute ahead can be evaluated by taking the output of solar irradiance prediction model from Chapter 4 into G_T term in Equation (5-10). The same forecast model from Chapter 4 is applied on load power demand prediction. Via Equation (5-9), $dP_{forecast}$ can be computed using forecast values of PV output power and load power demand. The average MASE and RMSE of hourly $dP_{forecast}$ with respect to the actual dP is 0.758 and 82.543Wm^{-2}. MASE of 0.758 indicates that the forecast values are performing 50% better than Naïve Prediction model. The prediction accuracy of $dP_{forecast}$ is slightly lower compared to Table 4-11 because the highly erratic components from both $P_{PV\_forecast}$ and $P_{load\_forecast}$ have contributed to the prediction errors.

Table 5-4 – Table of Parameters specifications for Equations (5-10) and (5-11)

P_{PV_STC}	100W
γ	0.00127
N_{PV_S}	2
N_{PV_P}	10
NOCT	45℃

To allow the EMS to plan ahead of time, the input to the RE-SOINN EMS is now replaced with hourly forecasted $dP_{LF\_forecast}$ instead of dP_{LF}. $dP_{LF\_forecast}$ is obtained from $dP_{forecast}$ undergoing filtration process described in Subsection 5.3. Thus, the new input consists of instantaneous dP_{LF} and 59 one-minute interval forecasted $dP_{LF\_forecast}$ values to form hourly ahead dP_{LF} input data trend together with instantaneous SoC_{sc} of supercapacitor.

5.6 Power Distribution Strategy

Since charging and discharging operations cannot be carried out simultaneously, only either T_c or T_d can be effective at one time. T_c should be numerically larger than T_d as supercapacitor should only be charged at positive surplus due to larger dP_{LF} and only be discharged at negative surplus due to lower dP_{LF}.

From Figure 5-2, power distribution strategy outputs the ideal power P_{SC_PD} according to EMS output of T_c and T_d. As a rule of thumb, HESS operates only when $dP_{LF} >$ 0 or $dP_{LF} <$ 0. In the former case, HESS is charged with the excess energy whereas in the latter, HESS supplies to energy deficit to avoid power disruption. Three working conditions of the power distribution strategy are as follows:

i. $dP_{LF} > T_c$
ii. $dP_{LF} < T_d$
iii. $T_c \geq dP_{LF} \geq T_d$

The first case occurs when the harvested energy is greater than load demand or when supercapacitor is required to be charged. T_c is set to be lower than dP_{LF} so that supercapacitor is allowed to absorb the excess energy as described in Equation (5-12)

$$P_{SC\_PD} = dP_{LF} - T_c \,, \qquad if\ dP_{LF} > T_c \tag{5-12}$$

When dP_{LF} is less than T_d, the supercapacitor is activated to discharge energy to meet the load demand as expressed in Equation (5-13). This case usually occurs when supercapacitor is needed to deal with the fast transient component in the load demand.

$$P_{SC\_PD} = dP_{LF} - T_d \,, \qquad if\ dP_{LF} < T_d \tag{5-13}$$

In cases where supercapacitor can remain idle during the operation and battery is sufficient to solely satisfy dP_{LF}, then both T_c and T_d shall be higher and lower than dP_{LF} respectively. Thus,

$$P_{SC\_PD} = 0 \,, \qquad if\ T_d < dP_{LF} < T_c \tag{5-14}$$

In summary, supercapacitor only operates when the T_c and T_d thresholds are placed within dP_{LF} and the supercapacitor power is constrained by the difference between respective threshold and dP_{LF}. As for dP_{HF}, it is tackled by the supercapacitor as well. Therefore, the distribution of supercapacitor power between dP_{LF} and dP_{HF} is required to be managed well. In this paper, 50% of the supercapacitor capacity is reserved for dP_{LF} operation with T_c and T_d thresholds, 25% of the capacity is meant for tackling dP_{HF} and unforeseen errors that are unaccounted for during EMS computation. The remaining 25% is kept unused to keep the supercapacitor at minimal voltage required to prevent huge voltage mismatch between DC bus, DC – DC converters and supercapacitors since supercapacitor voltage is proportional to its SoC_{sc}.

5.7 Circuit Voltage and Current Protection

After P_{SC_PD} is obtained, P_{SC_ref} is calculated by Power Distribution module with consideration of P_{SC_PD} and dP_{HF} where the polarity of P_{SC_ref} denotes the intended flow of power to and fro of the supercapacitor. P_{SC_ref} refers to the theoretical power to be absorbed or supplied by the supercapacitor as the resultant outputs of the EMS. As mentioned in Subsection 5.6, supercapacitor working range is limited between 25% and 100% of its SoC_{sc}. The remaining 25% of SoC is meant to keep the supercapacitor to be within the ballpark voltage range of DC bus.

A multiplier, μ, is added to implement the SoC regulation of supercapacitor. Thus, the power safety regulation of the supercapacitor can be summarised as follow:

$$\mu = \begin{cases} 0, & if\ P_{SC\_ref} > 0\ and\ SoC_{sc} \geq 100\% \\ 1, & if\ 25\,\% \leq SoC_{sc} \leq 100\% \\ 0, & if\ P_{SC\_ref} < 0\ and\ SoC_{sc} \leq 25\% \end{cases} \tag{5-15}$$

Thus, given that $P'_{SC_{ref}}$ is the actual supercapacitor power after the SoC regulation procedure, $P'_{SC_{ref}}$ can be explained as follow:

$$P'_{SC_{ref}} = \mu \cdot P_{SC\_ref} \tag{5-16}$$

5.8 Performance Metrics and Benchmark Models

The performance of proposed REPS is evaluated based on the criteria listed below:

- Average energy charged by supercapacitor during positive dP, $E_{sc\_charging}$
- Battery peak discharging / charging power, P_{batt_peak}
- Oscillations in battery power profile and amplitudes of the oscillations, ΔP_{batt}

Average energy charged by supercapacitor during positive dP, $E_{sc\_charging}$ helps to determine if more solar energy is harvested successfully. This effect is very significant when small energy harvested falls easy prey to heat loss during battery charging. Subsequently, excessively high battery peak discharging and charging power, P_{batt_peak} could cause a huge power draw or sudden huge charging power in the battery, causing irreversible damage in the batteries. Furthermore, oscillations in battery power profile as well as their respective amplitudes, ΔP_{batt} could help to identify the number of charge-discharge cycle the battery has gone through. The greater the number, the closer the battery to its end of service life.

Several external models are taken from the past literature to compare the performance with the proposed model on existing application. The external models chosen for this experimental comparison are Moving Average Filter (MAF) based Filtration Based Controller (FBC), Fuzzy Logic Controller (FLC) and PSO-based EMS that are widely applied in recent research.

MAF-based FBC filters the low frequency and high frequency components from one another in dP. As mentioned previously in Subsection 5.3, it uses a list of values from a moving window of a period T to calculate for a moving average value. This value thus forms the more significant trending component in dP. The complementing high frequency component is then evaluated using Equation (5-4) [11]. This model can also help to assess the significance of optimization procedure as well as RE-SOINN operation in improving system performance.

Fuzzy Logic control strategy (FLC) is widely applied in the past literature as EMS to REPS, not limited to solar-based REPS only. FLC implemented in this study uses PSO-optimized membership functions to achieve precision control of supercapacitor. PSO-based control strategy is another popular EMS widely adopted in many REPS applications as well as in the past literature. Based on the literature, one of the common goals for PSO-based control strategy is to control the amplitude of battery discharging or charging power to reduce the peak battery power draw or absorption that could lead to permanent change of battery electrolyte. In this study, the PSO EMS developed for comparison purpose uses a fitness function that is aimed to lower battery peak charging and discharging power where $f(x) = \max(P_{batt\_min})\; or \min(P_{batt\_max})$, depending on polarity of dP.

5.9 Experimental Setup

The research experiments are conducted in a facility in the University of Nottingham Malaysia located at Semenyih, state of Selangor, Malaysia. This facility or the laboratory is given the name of Solar Cabin and all mentions of Solar Cabin in the following texts refer to this facility. Figure 5-8 shows the exterior of Solar Cabin whereas Figure 5-9 shows the block diagram of the entire system setup. The Solar Cabin consists of a 2kW-rated standalone PV panels, SLA batteries, supercapacitors, DC-DC converters, programmable loads and inverters. Table 5-5 details the models, technical specifications as well as rating of the equipment in Solar Cabin.

Figure 5-8 - Exterior look of solar cabin. The roof of the solar cabin is the 2kW solar panels.

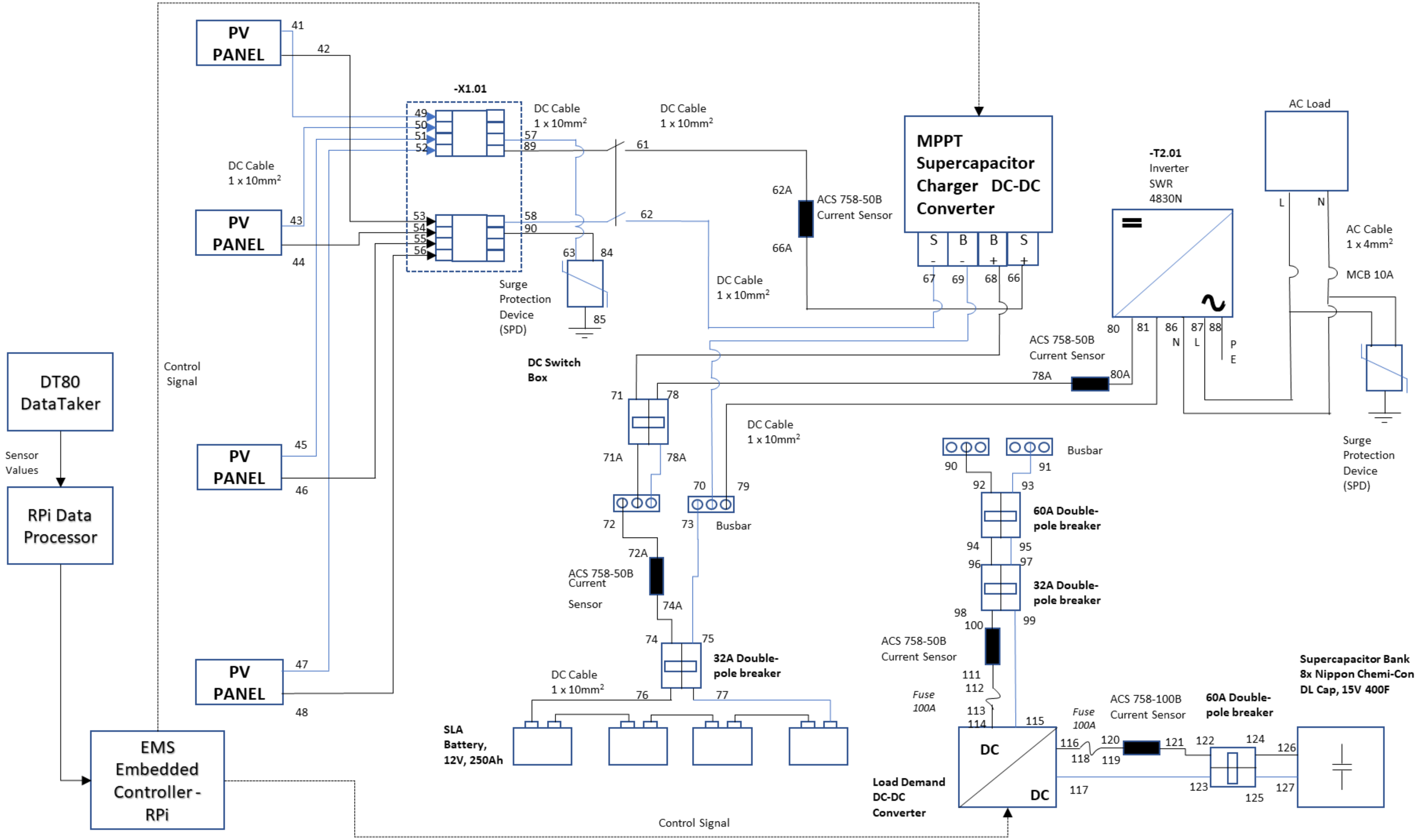

Figure 5-9 – System block diagram of the Standalone PV System with battery-supercapacitor HESS implemented in Solar Cabin

Table 5-5 - List of components in Solar Cabin with their respective models, specifications, quantities and configurations

Components	Model & Technical Specification	Quantity & Configuration	Rating
PV panel	**<u>Kaneka UEA100</u>** • Cell Type: Thin-film • Nominal Power: 100 W • Open Circuit Voltage: 71 V • Short Circuit Current: 2.25 A • Module Efficiency: 8.2%	20 (2s10p: 10 strings of 2 PV panels in series are connected in parallel)	Max. Power: 2000W Max. Voltage: 142V Max. Current: 22.5A
Battery	**<u>Powerbatt AGM Lead Acid Battery</u>** • Nominal Voltage: 12V • Rated Capacity: 250Ah	4 (4 are connected in series)	Voltage: 48V Capacity: 250Ah
Supercapacitor	**<u>Nippon-Chemi-Con DLCAP module</u>** • Rated Voltage: 15 V • Capacitance: 400 F	8 (2s4p: 4 strings of 2 in series are connected in parallel)	Maximum Voltage: 30 V Capacitance: 800 F
MPPT Supercapacitor Charger DC-DC Converter	**<u>Self-made in Laboratory</u>** • Supercapacitor Voltage Working Range: 7-48 Vdc • Rated Power: 2.4kW • PV array Operating Voltage:150V • Maximum Charge Current: 70A • Maximum Output Power: 3.5 kW • Typical operation rating: 60V, 40A • Efficiency, η_{MPPT}: ≈ 92% (low load of 500W), ≈ 86% (high load of 2kW)	1	Maximum Operating Voltage: 0 - 150V Maximum Charge Current: 0 - 60A Maximum Output Power: 3.5kW
Load Demand DC-DC Converter	**<u>Self-made in Laboratory</u>** • Rated Power: 2.4kW • Input & Output Voltage range: 0-100 V	1	Rated Power: 2.4kW Input & Output Voltage range: 0 - 100 V

	• Input & Output Maximum Current: 100A • Typical operation rating: 60V, 40A • Efficiency, η_{DCDC}: ≈ 95% (low load of 500W), ≈ 83% (high load of 2kW)		Input & Output Maximum Current: 100A
Inverter	**Sontime 4830N** • Battery Voltage Range: 12/24/48 V • Output Voltage Range AC: 230 V ± 5 % • Output Frequency: 60 Hz ± 0.5% • Power Rating: 2730W • Efficiency, η_{DCAC}: >91 %	1	Output Voltage Range AC: 230V ± 5% Output Frequency: 60 Hz ± 0.5% Power Rating: 2730W

5.10 Load Profile

Malaysian National Electrical Power Supplier, Tenaga Nasional Berhad Malaysia (TNB) has recorded the maximum power demand of rural household, inclusive of low-cost flats, single-story terrace as well as studio apartment, to an approximate of 1.5kW [192]. The main power consumption from a typical rural household in Malaysia, especially in East Malaysia consisting of Sabah and Sarawak states, is resulted from a series of electrical appliances such as fluorescent lights, TV and fans [193].

Since off-grid rural household which serves the main scope of the research is not within the service coverage of TNB, there is no official record of any off-grid rural household load demand data. As a result, 31 days' worth of load demand data is collected from a grid-tied household from a low-cost flat whose load demand characteristics match the general characteristics of rural household as described in both Refs [192], [193]. It is noted that the load demand data collected is sampled at 100Hz so that these load demand can be reproduced by laboratory equipment such as programmable load during experimentation stages.

The chosen household for load demand collection consists of two occupants where one leaves the house for work at 8am and only returns at 6pm whereas the other occupant stays at the house most of the time and only leaves the house for grocery shopping in the morning. Table 5-6 shows the electrical appliances found in the chosen household. These appliances can be regarded as simple appliances in [193]. The analysis of the 31-day load demand has found that this chosen household records a maximum daily energy consumption of 4.89kWh/day and maximum power demand of 0.762kW. A programmable load (EL 9080-170B) is used to emulate the load profile in the experiments.

Table 5-6 - Electrical appliances found in the chosen household

Appliance	Model	Rated Power	Quantity	Usage
Toaster	MAG 2 slide Toaster MF-008	600W-700W	1	1.5 mins/day
Washing Machine	Media MFW-701S	Spin Power: 160W Wash Power: 340W	1	40mins/week
Fridge	Midea Refrigerator MS-196	130W	1	On time= 24 hours/day, Compressor Running time = 12 hours/day
Ceiling Fan	DEKA Kronos F5P 5-Blade Ceiling Fan	50 W	2	18 hours/day
Table Fan	Sharp 16” Table Fan PJT405	50W	1	10hours/day
Laptop	Asus ZenBook UX330UA	45W	1	16 hours/day
Television	Sony 32-inch LED TV SNY-KDL32R300E	39W (in operation) 0.4W (standby)	1	4 hours/day
Light	Philips E27 cap, Cool daylight LED bulb	18W	6	6 hours/day

5.11 Result and Discussion

This subsection consists of three parts. The general improvement made by the proposed EMS in managing power flow in standalone REPS with battery-supercapacitor HESS is evaluated in the first subsection. The experimental comparison of working performance of different EMS such as FBC, FLC, PSO and proposed EMS on standalone REPS with battery-supercapacitor HESS is discussed in the second part of the subsection. In the final part of the subsection, the performance of proposed EMS in dealing with scenarios of different weather and load demand profiles is evaluated.

5.11.1 RE-SOINN EMS Model

This subsection discusses the performance of RE-SOINN model as EMS of REPS. As instantaneous dP is obtained based on the power mismatch between renewable power generation and load demand, together with hourly ahead forecasted 59 one-minute interval $dP_{forecast}$ values and SoC_{sc}, these $dP_{forecast}$ values form an input to the proposed EMS. The $dP_{forecast}$ input trend first undergoes filtration decomposition as depicted in Subsection 5.3. Figure 5-10 shows the typical dP profile of a day. dP profile can be very noisy due to tropical climate, irregular load demand such as occasional peak power draws and supplies from loads. The Moving Average Filtration operates with a period of 25 samples so that the decomposed dP trends do not lag too far behind of time. Figure 5-11 and Figure 5-12 show the decomposed plots of the dP profile based on low and high frequency components.

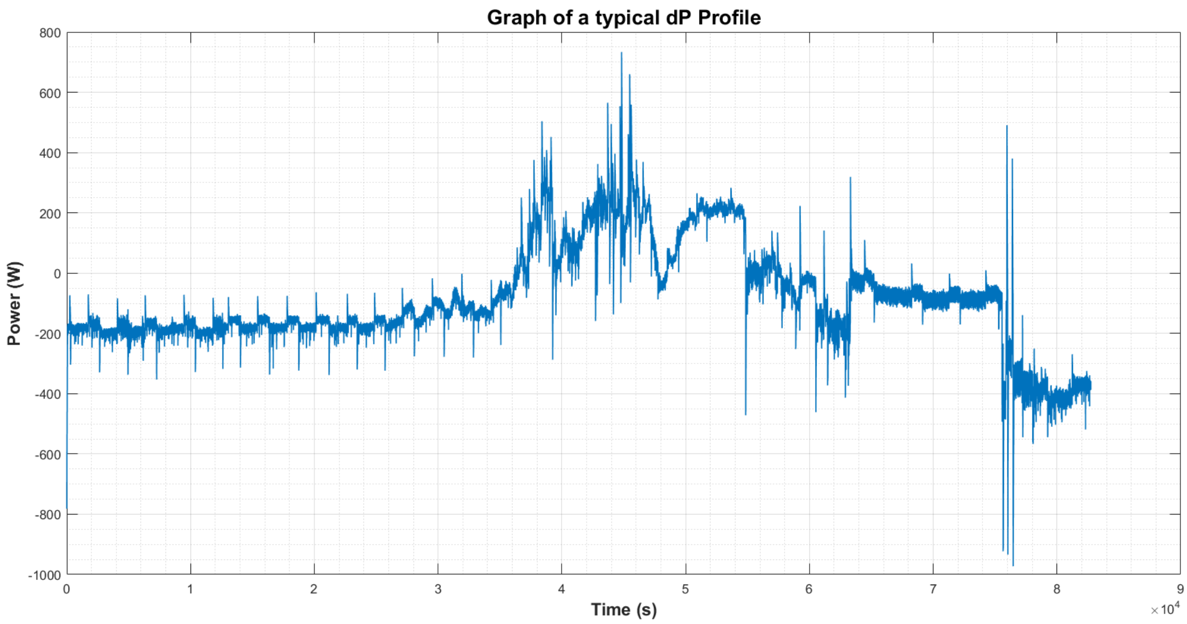

Figure 5-10 – Plot of a typical dP profile where positive peaks are shown in the mid of the day and negative trend spans over the rest of the time due to unavailability of solar irradiance

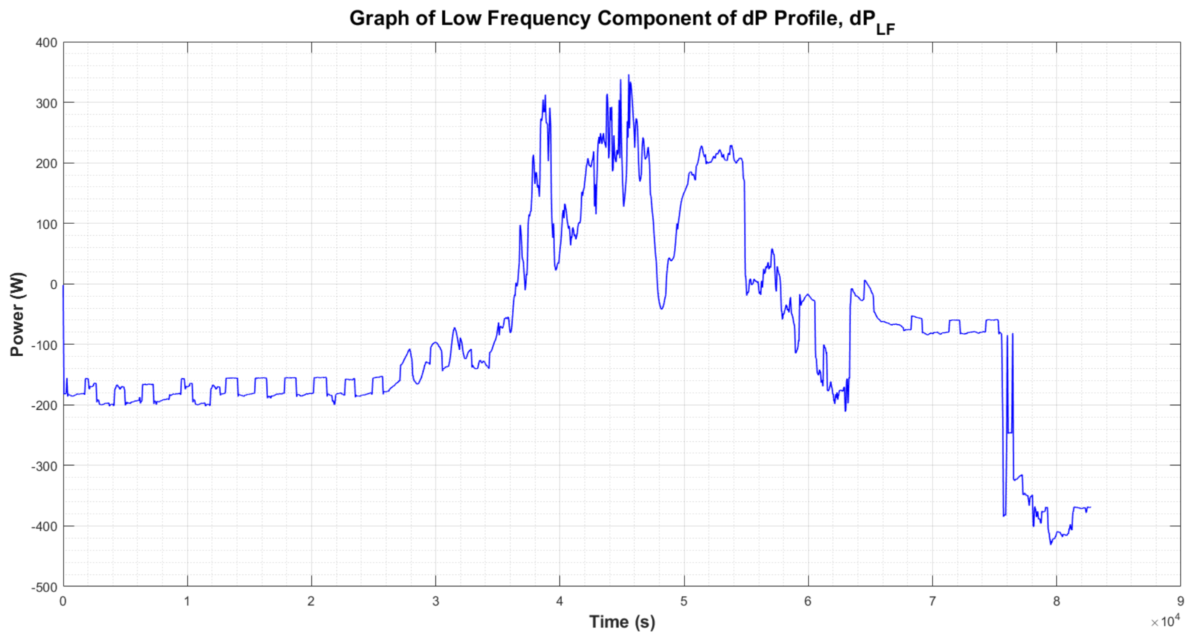

Figure 5-11 - Plot of low frequency component of dP profile shown in Figure 5-10

The low frequency component, dP_{LF} is very much smoothened compared to the original dP profile. With noisy small oscillations being removed, dP_{LF} is now suitable to be operated by SLA batteries. On the other hand, the highly erratic high frequency component, dP_{HF} is reserved for supercapacitor operations. Figure 5-13 shows the dP profile together with its low and high frequency components. The decomposition has successfully reduced the instantaneous peaks in dP_{LF} and thus, lesser harms are done to the battery.

There is a single learning stage for RE-SOINN EMS model. In this learning stage, PSO is the teacher to help RE-SOINN with labelling the dP_{LF} trends with respective T_c and T_d based on SoC_{sc}. RE-SOINN is trained with PSO for the first ten days of the operation. The performance of RE-SOINN model during learning stage is not emphasized because the optimisation carried out does not differ from a conventional PSO EMS model.

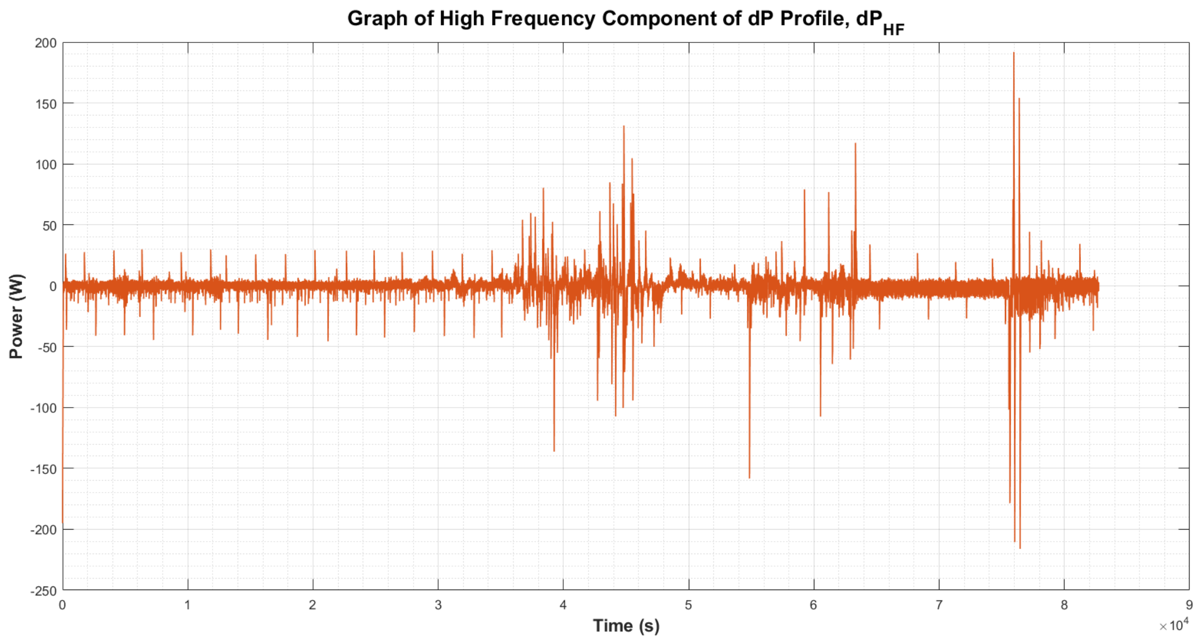

Figure 5-12 - Plot of high frequency component of dP profile shown in Figure 5-10

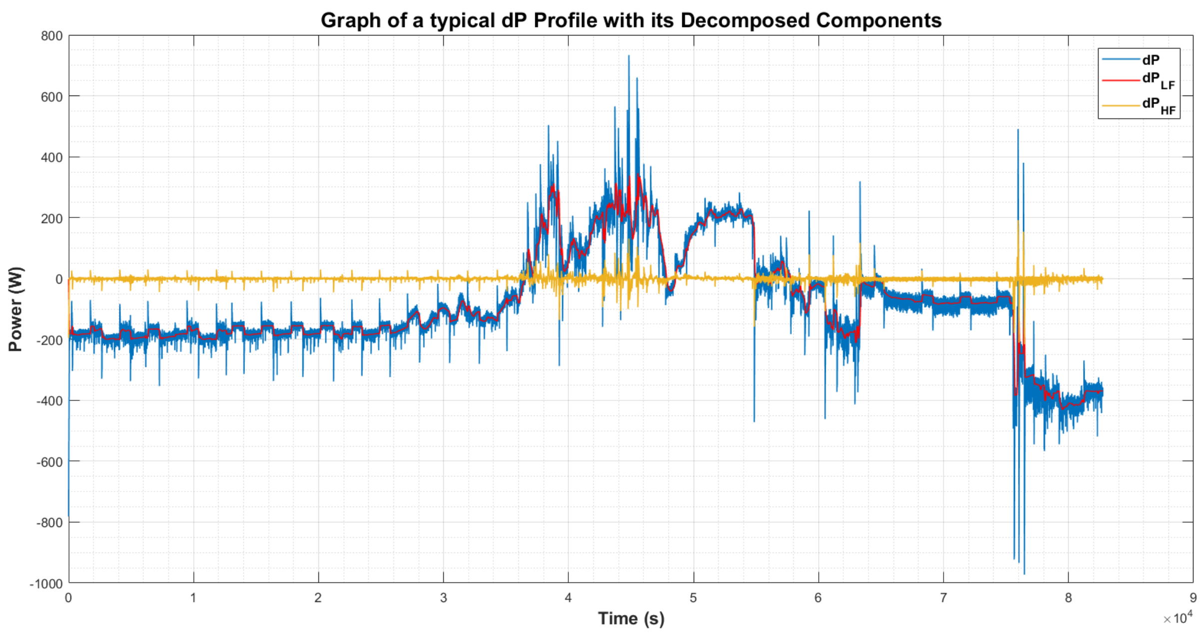

Figure 5-13 - Plot of original dP profile and its low and high frequency components

EMS statistical operational data using RESOINN in the system operating on dP profile shown in Figure 5-10 are recorded in Table 5-7. RE-SOINN based EMS are run for 10 times for benchmarking purposes. It is found that RE-SOINN takes an average computational time of 2.87s for one computation of optimal T_c and T_d. One full day of optimal T_c and T_d computation uses an average of 3957.8s or approximately 65 minutes. Among the 10 runs, the maximum time taken for one computation during a full day operation is recorded to be 19.9s, within the computational interval of one minute.

Table 5-7 – Statistical operational performance of RE-SOINN as proposed EMS on dP profile shown in Figure 5-19

Run	Average One Iteration Computational Time (s)	Total Computational Time for One Day Operation (s)	Maximum Time Taken for One Iteration (s)	RE-SOINN Training Time (s)
1st Run	2.7563	3803.7	15.4631	5.28
2nd Run	2.7549	3801.8	18.2529	4.98
3rd Run	2.8433	3923.7	15.3876	5.05
4th Run	2.9637	4090	19.7637	4.94
5th Run	2.9519	4073.6	18.2052	5.01
6th Run	2.8656	3954.6	18.0384	5.01
7th Run	2.8794	3973.6	19.9497	4.99
8th Run	2.9813	4114.2	18.1788	5.11
9th Run	2.8217	3893.9	18.3898	4.96
10th Run	2.8616	3949	18.1578	5.05

As an Unsupervised Learning AI model, RE-SOINN requires to be trained with data and labels regularly during deployment for better working performance. The adaptive feature of the RE-SOINN is also dependent on training events of RE-SOINN model with new weather and load demand data featuring gradual changes in statistical properties. Thus, it is important to keep the training time of RE-SOINN to be as minimal as possible. In Table 5-7, the average RE-SOINN training time is 5.04s. The short training time of Re-SOINN shows a good prospect of RE-SOINN as adaptive intelligence EMS.

Table 5-8 – Performance Comparison between PSO, SOM-PSO and RE-SOINN

	PSO	SOM-PSO	E-SOINN-PSO	RE-SOINN
Training Time (s)	-	1168.9	2.81	5.04
No. of neurons	-	400	118	10965
Average time for one computational step (s)	7.8	4.5	3.91	2.87

Table 5-8 summarises the operational comparison of PSO, SOM-PSO [11], E-SOINN -PSO and proposed RE-SOINN models. All the PSO models in Table 5-8 have population size of 50, maximum iteration of 100 and stopping criteria tolerance of 1W. Since PSO is the labelling teacher to RE-SOINN, the performance of RE-SOINN EMS is similar to PSO EMS with the same fitness function. SOM–PSO from Ref [11] uses Self Organising Maps to effectively reduce the search space of PSO so that PSO can reach convergence faster. Therefore, SOM-PSO EMS model uses PSO to label each dP_{LF} trend as well. E-SOINN – PSO model is modelled after SOM-PSO model in Ref [11] to compare the clustering effect of SOM and E-SOINN models. Table 5-8 indicates that SOM-PSO method reduces the average optimisation time for one iteration by 43% whereas E-SOINN – PSO reduces the time by 50% compared to conventional PSO method. Proposed RE-SOINN model can further shorten the computational time for each iteration with a total of 64% of reduction compared to PSO model. PSO relatively takes much longer time owing to its iterative mechanism. Both SOM-PSO and E-SOINN - PSO reduce the search space of the PSO and thus less iteration is needed to reach convergence. RE-SOINN, however, evaluates based on neighbouring nodal information without involving iterative steps.

On the other hand, RE-SOINN has much lower training time (5.04s) compared to SOM model (19.5 mins or 1168.9s) in SOM-PSO due to algorithmic simplicity of RE-SOINN. E-SOINN – PSO model has the shortest training time due to smaller nodal size. E-SOINN in E-SOINN PSO model is only responsible of reducing the search space of PSO where PSO handles majority of the computation while RE-SOINN requires bigger nodal size for more precise computational resolution so that the computational result of RE-SOINN leads to better and optimal performance of EMS.

The qualitative performance of RE-SOINN is shown in the subsequent subsection.

5.11.2 Performance Comparison of Control Strategies for standalone PV system with Battery – Supercapacitor HESS

In this subsection, experimental results from several control strategies from the literature implemented in the proposed standalone PV system with Battery and Supercapacitor HESS are presented. One of the inputs to this performance comparison experiment, dP profile used is shown in Figure 5-10. The PV output power is taken from a cloudy day where fluctuating PV output power is recorded between 12pm and 3pm. Due to erratic cloud cover events, PV output power is usually inconsistent. The load profile used in this study is recorded from a simple household with sampling rate of 100Hz. Regular household electronic appliances such as washing machine and refrigerator have introduced spikes and oscillations to the load profile. dP profile is then obtained from these two data using Equation (5-2) and is visualised in Figure 5-10. Smoothened dP profile consisting of low frequency component, dP_{LF} as well as highly oscillating high frequency component, dP_{HF} are obtained after the decomposition of MAF. For all comparison models except the proposed model, dP_{LF} is used in the input. In RE-SOINN EMS, dP_{LF} undergoes prediction module developed in Chapter 4 to produce hourly forecast, $dP_{LF\_forecast}$. Hourly forecast $dP_{LF\_forecast}$ trend subsequently pairs with SoC_{sc} to produce input to the RE-SOINN EMS.

Table 5-9 compares the peak charging and discharging battery currents, daily and average iteratively computational times, daily energy stored by supercapacitor as well as daily total energy harvested by REPS due to different control strategies. The oscillations with respective amplitudes of battery power profiles due to these control strategies are discussed thereafter. Model 1 is a battery-only REPS without supercapacitor and any EMS. This model exists as a benchmark for following control strategies to verify if their performances are better than raw REPS. Model 2 is a MAF-based FBC with sampling period of 25s. Model 3 sees the application of Fuzzy Logic controller, a widely chosen choice of EMS as the backbone of the brain of REPS in this study. Model 4 is the popular PSO-based control strategy with a fitness function of reducing peak battery power. Model 5 is the proposed RE-SOINN EMS.

Table 5-9 - Performance comparison of Proposed EMS RE-SOINN model against other models

Models		Peak Charging Battery Current (A)	Peak Discharging Battery Current (A)	Daily Computations Runtime (s)	Average Computation Time (s)	Daily Energy Stored by SC (J)	Daily Total Energy Harvested (J)
1	Battery only	295.46	-510.21	-	-	-	3.04×10^{6}
2	FBC	290.08	-490.14	106.1	0.07	1.98×10^{5}	3.23×10^{6}
3	FLC	272.11	-533.00	315.0	0.14	2.98×10^{5}	3.31×10^{6}
4	PSO	332.44	-438.79	28155.4	20.37	9.52×10^{5}	3.77×10^{6}
5	RE-SOINN	284.17	-460.01	11152.4	8.05	1.06×10^{6}	3.85×10^{6}

Figure 5-14 shows the number of oscillations in battery current profile by each model with respect to the amplitudes of the oscillations. Since most of the oscillations occur at lower amplitude range, the plot in Figure 5-14 is zoomed at lower amplitude range to produce Figure 5-15. Performance of Model 2 (FBC) is not shown in Figure 5-14 largely owing to being similar to Model 3 (FLC) as well as to reduce the complexity of plots displayed. In Figure 5-16 and Figure 5-17, both Models 2 and 3 produce similar number of the oscillations for a wide range of amplitudes. Thus, Model 2 is omitted to simplify the displayed content of the comparison plot in Figure 5-14 and Figure 5-15.

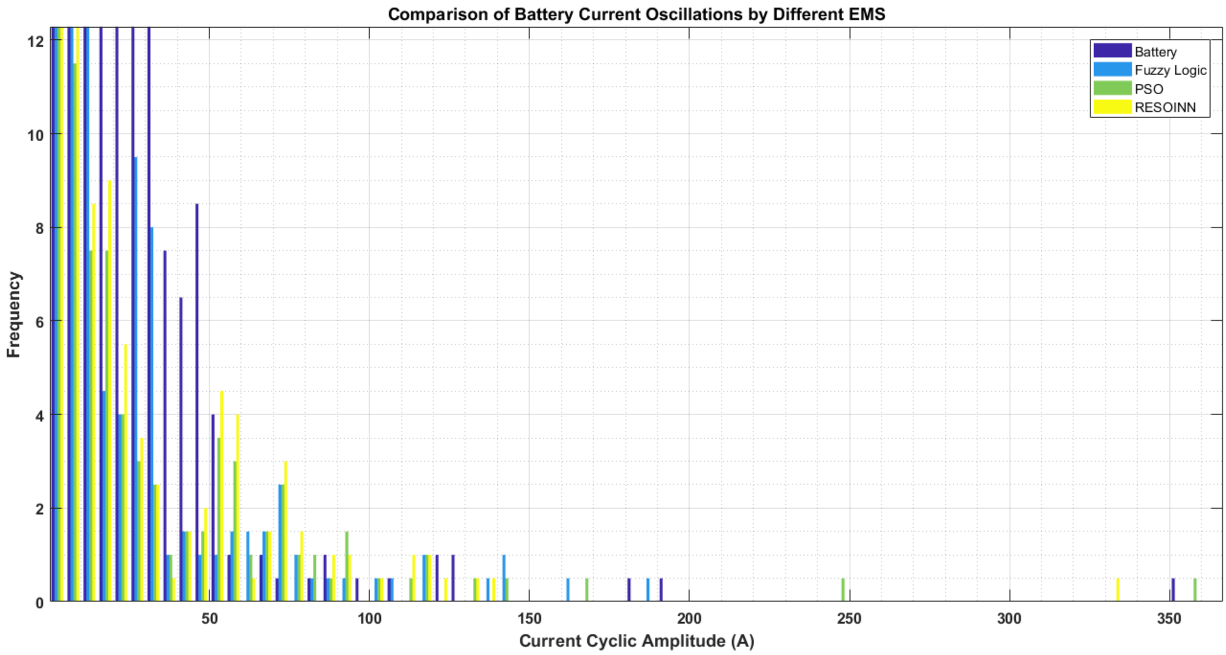

Figure 5-14 – Comparison of battery current oscillations resulted by different EMS

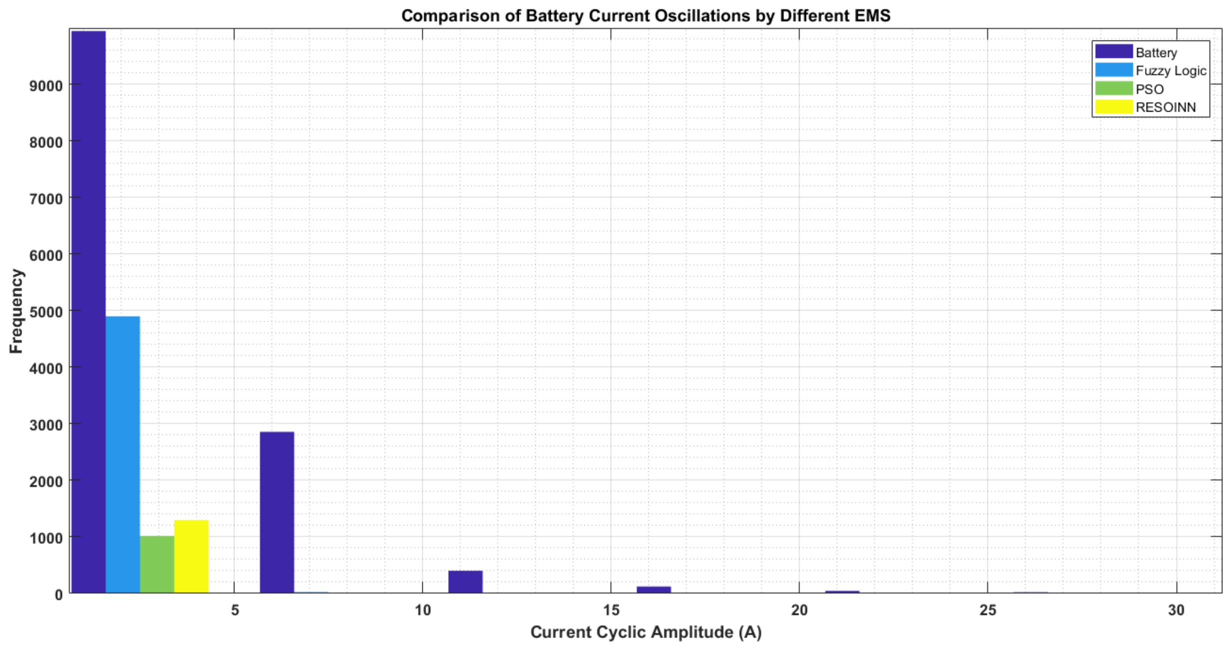

Figure 5-15 - Comparison of battery current oscillations resulted by different EMS (zoomed at lower current amplitude range)

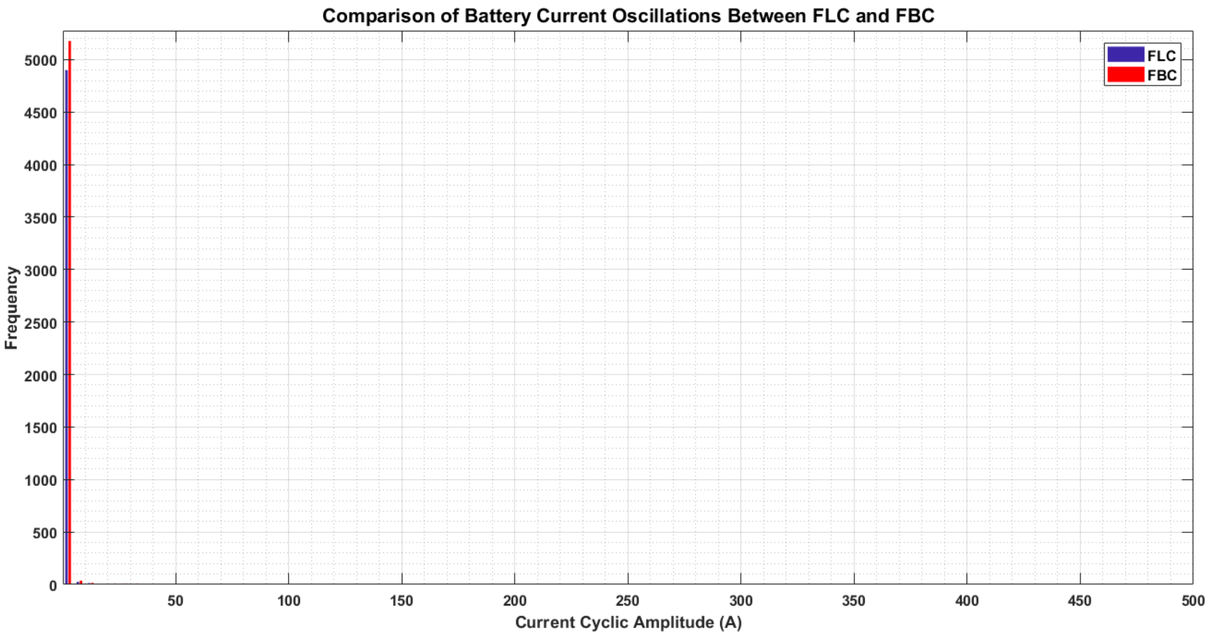

Figure 5-16 – Comparison of battery current oscillations between FLC (Model 3) and FBC (Model 2)

Model 1, being a battery-only REPS without any secondary ESS refers to the most basic REPS system readily available in the market. EMS is not needed in such a system as power harvested by solar panel is transferred to its sole ESS (battery) after meeting load demand. As a result, load demand is mainly satisfied by battery power in absence of solar irradiance. Figure 5-18 shows the performance plot produced by Model 1. The battery power profile of Model 1 is almost identical to dP profile due to prerequisite condition of power balance and absence of other ESS. Battery in Model 1 suffers from experiencing highly fluctuating cyclic dP profile as well as sudden peak dP power surge as shown in Figure 5-14. At low amplitude range (less than 5A), the oscillations made are close to ten times more than the other models in comparison, reaching 10000 oscillations. As battery lifetime significantly depends on the charge-discharge cycle, raw dP input would seriously harm the battery lifespan during the system operation. When the dP is in negative region, the battery power is drawn deeper whereas battery charging power is always less than the positive dP trend. This observation can be explained with the non-ideal efficiency of Lead Acid battery of approximately 85%. The non-ideal efficiency of the battery is also demonstrated in the following experiments.

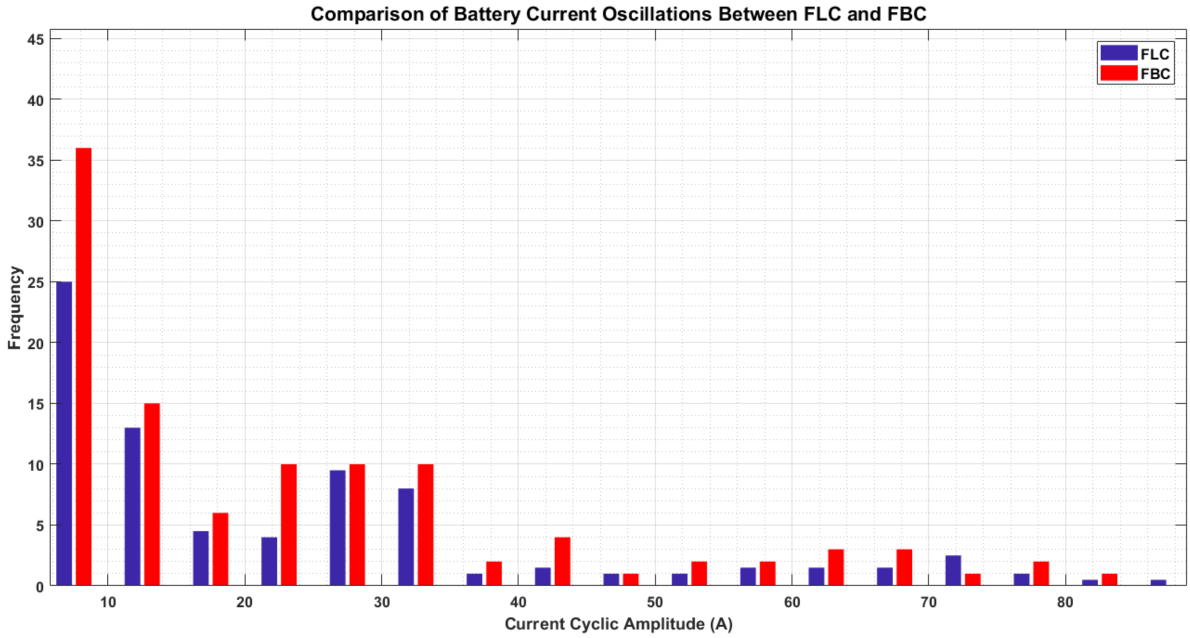

Figure 5-17 – Comparison of battery current oscillations between FLC (Model 3) and FBC (Model 2) (zoomed at lower current amplitude range)

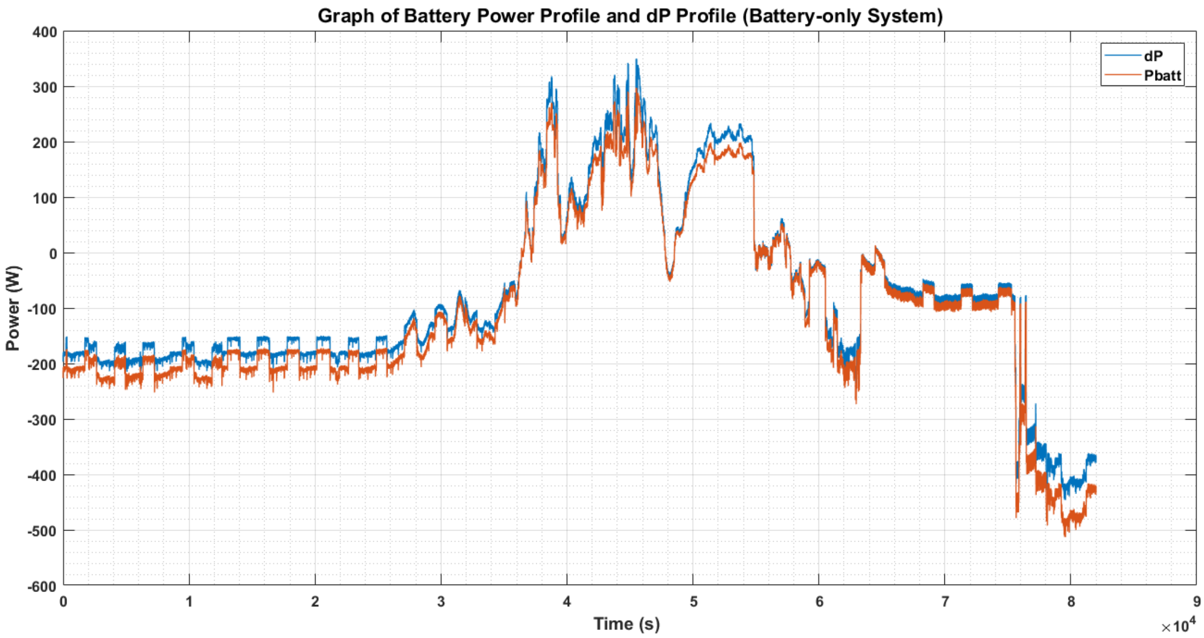

Figure 5-18 – Plot of battery power profile and dP profile in battery-only system

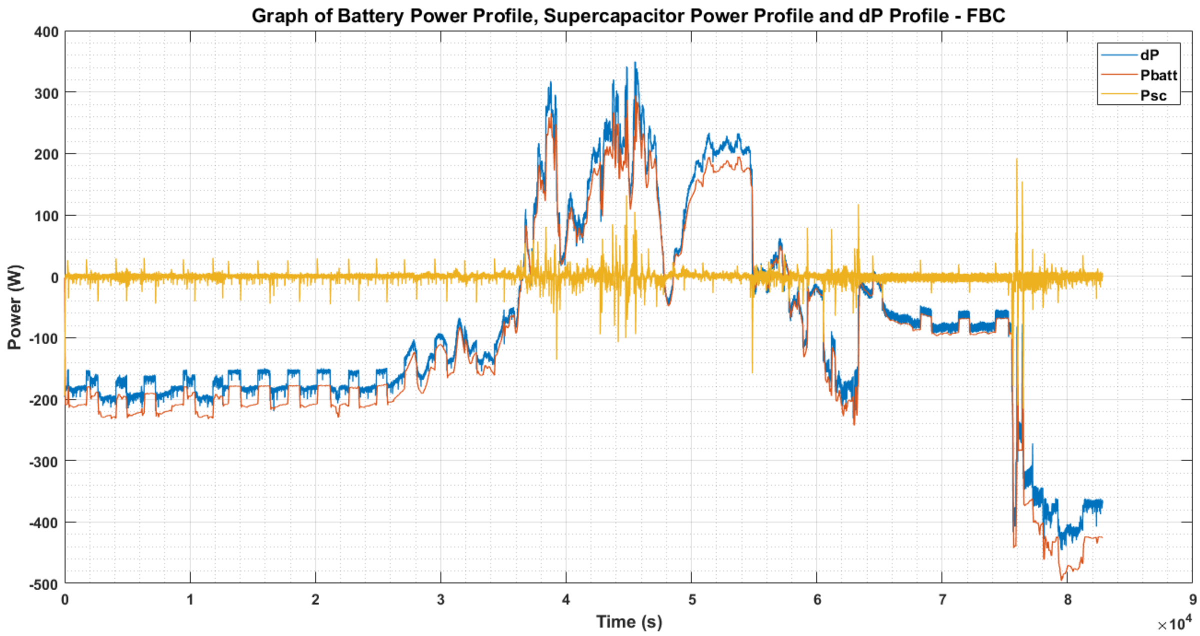

Figure 5-19 - Plot of battery and supercapacitor power profiles vs dP profile resulted by FBC model

Model 2 studies the effect of Filtration-based controller (FBC) as EMS on the REPS developed in the study. As mentioned previously, Model 2 serves as a significant intermediate model since the subsequent models including the proposed EMS model are built upon FBC. FBC decomposes the dP profile into two components, the low frequency component (dP_{LF}) and high frequency component (dP_{HF}). Supercapacitor deals with dP_{HF} whereas dP_{LF} is reserved for battery operations. As a result, from Figure 5-19, battery power profile is similar to dP_{LF} trend whereas supercapacitor power profile is almost identical to dP_{HF} profile. Compared to Model 1, Model 2 has successfully reduced small oscillations in battery power profile which harms battery health, resulting in a smoothened battery power profile. This can clearly be seen in Figure 5-16 and Figure 5-17 where battery power profile in Model 2 produces similar number of oscillations compared to Model 3 where Model 3 shows its oscillations at low amplitude range are successfully reduced by half comparing to Model 1 in Figure 5-14. The peaks in the dP are shaved by 1.8% and 4% respectively by Model 2 for battery charging and discharging current so that battery experiences lower power demand and charging surges than in Model 1 although the reduction is not significant. Between the time range of 7×10^4s to 8×10^4s (between 7.30pm to 10.10pm), FBC EMS fails to alleviate the pressure of peak load demand because

FBC is only effective in handling frequency aspect of power profile. When dP_{LF} is in negative region for too long, supercapacitor discharges completely. Model 2 has no direct control over the recharging of supercapacitor because FBC EMS does not consider SoC of supercapacitor in its operation.

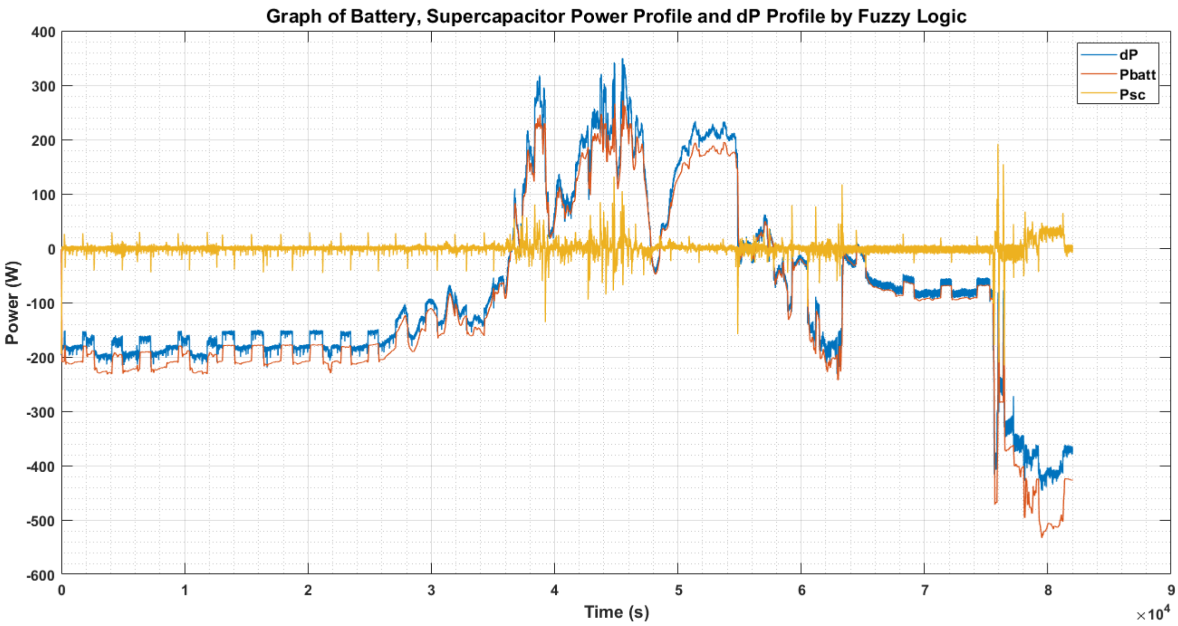

Figure 5-20 - Plot of battery and supercapacitor power profiles vs dP profile resulted by FLC model

Comparing Model 3 and Model 2, the battery power profiles resulted from both profiles are very similar. One main reason is that the Fuzzy Logic Controller model is trained using dP_{LF}. This indicates that input data in Model 3 first undergo filtration decomposition, the same operation conducted in Model 2. Based on the rules of FLC, supercapacitor is generally discharged to deal with a portion of dP_{LF}. Thus, the main difference between Model 2 and 3 is that supercapacitor is allowed to deal with a portion of dP_{LF} in Model 3 whereas supercapacitor in Model 2 tackles dP_{HF} only. Due to low capacity of supercapacitor, the dP_{LF} portion shared by supercapacitor cannot be too high or else supercapacitor would be completely discharged. Model 2 performs better than Model 3 when the dP trend is in negative region for a long period of time followed by a sudden peak power spike. It can be observed from Figure 5-19 and Figure 5-20 around $t = 8 \times 10^4$s (around 10pm) as well as Table 5-9 that battery power profile measures a deeper power spike in Model 3 compared to Model 2 (-533W against −490.14W). This is mainly because in Model 3, supercapacitor does not only deal with dP_{HF} but also a portion of dP_{LF}. As a result, supercapacitor depletes much faster in Model 3 than in Model 2, causing battery discharge more and adding extra 4% peak battery power amplitudes in Model 3 instead of a reduction of 4% in Model 2. During the noon of the day where the solar irradiance profile recorded is the maximum, the peaks on the battery power profile during this period are shaved by 8% compared to 1.8% in Model 2. The shaving effect is resulted by a portion of dP_{LF} is being dealt by supercapacitor. Another weakness of Model 3 is that the output membership function in FLC lacks the flexibilities to adjust the dP_{LF} portion shared by supercapacitor in a timely manner as the membership functions are not adjusted after deployed. Figure 5-19 and Figure 5-20 indicate that the battery power profiles are very similar but Model 3 shows a slightly worse plot to indicate the participation of supercapacitor in dealing with dP_{LF} where battery power is drawn occasionally to charge the supercapacitor.

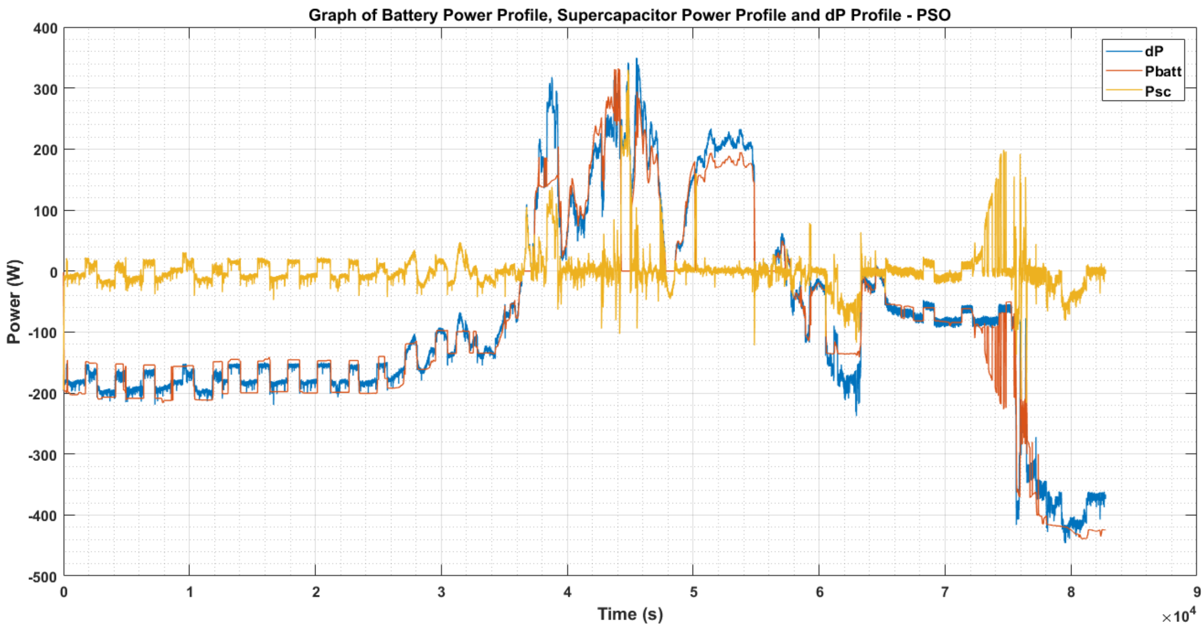

Figure 5-21 - Plot of battery and supercapacitor power profiles vs dP profile resulted by PSO model

In Model 4, the amplitudes of overall battery power profile are lower than those in Model 2 and 3, as observed from Figure 5-21, confirmed quantitatively in Table 5-9. When the dP trend is relatively stable, experiencing less oscillations and lower peaks, Models 2, 3 and 4 perform similarly. The main variation comes from how different models of EMS approach the highly oscillating and higher peak amplitudes of dP trend. Though Model 4 works better in shaving peaks in battery power profile by 14% or 10% improvement to Model 2 peak shaving performance, it also introduces oscillations to battery power profile, especially between the time range of 7×10^4s to 8×10^4s (between 7.30pm and 10.10pm). The rationale behind the finding is that the limited capacity of supercapacitor becomes the limiting factor. In Model 2, supercapacitor power is preserved the best among the other models because supercapacitor in Model 2 only deals with dP_{HF} whereas a portion of dP_{LF} is dealt by supercapacitors in the other models. Thus, supercapacitor power depletes much faster than in Model 3 and 4 compared to Model 2. As supercapacitor is required to discharge to deal with transient part while dP_{LF} has been in negative region for long period of time, battery is forced to discharge to recharge the supercapacitor. Similar observation is seen on the charging state of HESS between $t = 4 \times 10^4$s to 5×10^4s, corresponds to 11am to 2pm. A battery power peak with amplitude 12% larger than that of in Model 1 is detected. Since Model 4 allows supercapacitor to participate in tackling dP_{LF} more actively compared to Model 3 with rigid rules, supercapacitor gets fully charged very fast, leading to occasional discharges to battery, adding extra peaks to battery charging power. Figure 5-14 shows that the battery power oscillations have been reduced significantly compared to Model 1, 2 and 3 with significantly lesser oscillations at lower and mid amplitude range, even minimal oscillations at higher amplitude range.

In Model 5, the amplitudes of battery charging power profile are shaved much lower than those in Model 4 (reduction of 4% against extra 12%). At the same timeframe, the battery power peaks in Model 5 are shaved without the expense of increasing significant power fluctuations. This can be observed from Figure 5-22 because the RE-SOINN model (Model 5) prioritises the usage of supercapacitor in harvesting solar power and the planning is done ahead of time. As a result, the supercapacitor gets replenished faster, being able to shave the battery power peaks without causing unnecessary power oscillations. At $t = 7.6 \times 10^4 s$ (or 9.15pm), comparing both Model 4 and 5, the battery is drawn more power in Model 5 (10% with respect to Model 1, 4% less than Model 4) than in Model 4 but the oscillating condition in Model 5 is greatly improved whereas Model 4 suffers heavy oscillations with significant amplitudes. In Figure 5-22, Model 5 introduces very significantly less oscillations in the mid to high amplitude ranges compared to Model 4. As oscillations are forecasted to happen, supercapacitor is managed to focus more on tackling power oscillation. Thus, RE-SOINN EMS can produce more regulated battery power profile.

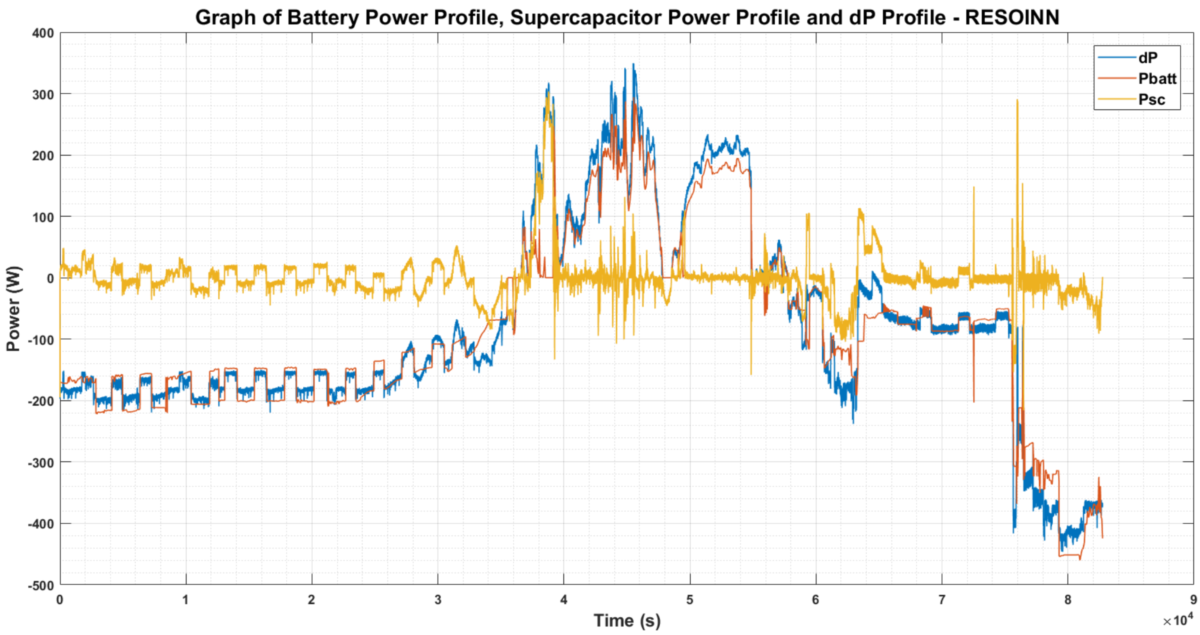

Figure 5-22 - Plot of battery and supercapacitor power profiles vs dP profile resulted by proposed RE-SOINN model

In terms of peak battery current, FLC model shaves charging battery power the most (reduction by 8% as compared to battery-only model, Model 1) whereas PSO model performs the best in reducing peak discharging battery current (improvement by 14% with respect to Model 1). Though FLC model performs the best in charging event but its discharging performance is the poorest (4% deeper than Model 1). Proposed model of RE-SOINN, on the other hand, shaves 4% of peak in Model 1 in charging operation with a 10% peak reduction in discharging operation. PSO, being a close competitor to RE-SOINN model, causes an extra 12.5% surge of peak in Model 1 in charging event as well as 14% of peak reduction in discharging event. Thus, RE-SOINN (Model 5) has overall better and balanced performance.

In terms of computational time, FBC and FLC use the least time due to their simple algorithmic structure. For instance, FBC is a moving average filter where the mathematical operations involved are fundamental to all other models. RE-SOINN being a more complicated artificial intelligence model, takes more computational time due to the extensive number of nodes (approximately 10965 distinctive classes) in RE-SOINN. PSO takes the longest computational time due to the iterative method employed in the computational process. Thus, with the restriction of one-minute interval operation of the EMS, RE-SOINN can produce satisfactory performance with lower computational time compared to the popular PSO.

Since the RE-SOINN is trained to optimise the use of supercapacitor to improve solar energy harvesting via supercapacitor energy storing efficiency, Model 5 records the highest amount of energy harvested by supercapacitor (5.35 times compared to Model 2 of FBC). The daily total harvested energy by Model 5 is thus increased by 27% with reference to Model 1 battery-only system. PSO improves the supercapacitor harvesting by 4.8 times compared to Model 2, resulting a 24% improvement for daily total harvested energy with respect to Model 1. FLC improves supercapacitor harvesting by 50%, leading to an extra 8.9% energy being harvested daily. FBC model is only capable of extract additional 6.3% of solar energy daily compared to Model 1. Consequently, RE-SOINN clearly outperforms the other models in managing the storage of harvested solar energy, improving the overall energy harvesting.

5.11.3 Case Studies with Different dP Scenarios

In this subsection, the proposed RE-SOINN EMS is tested against other weather profiles and load demand profiles to identify the versatility and efficiency of the RE-SOINN EMS in highly erratic profiles. This is important in the sense that Malaysian solar irradiance conditions are irregular in nature. Together with stochastic load demands resulted by random user's behaviours, EMS of REPS developed will be expected to work on different varieties of dP profiles.

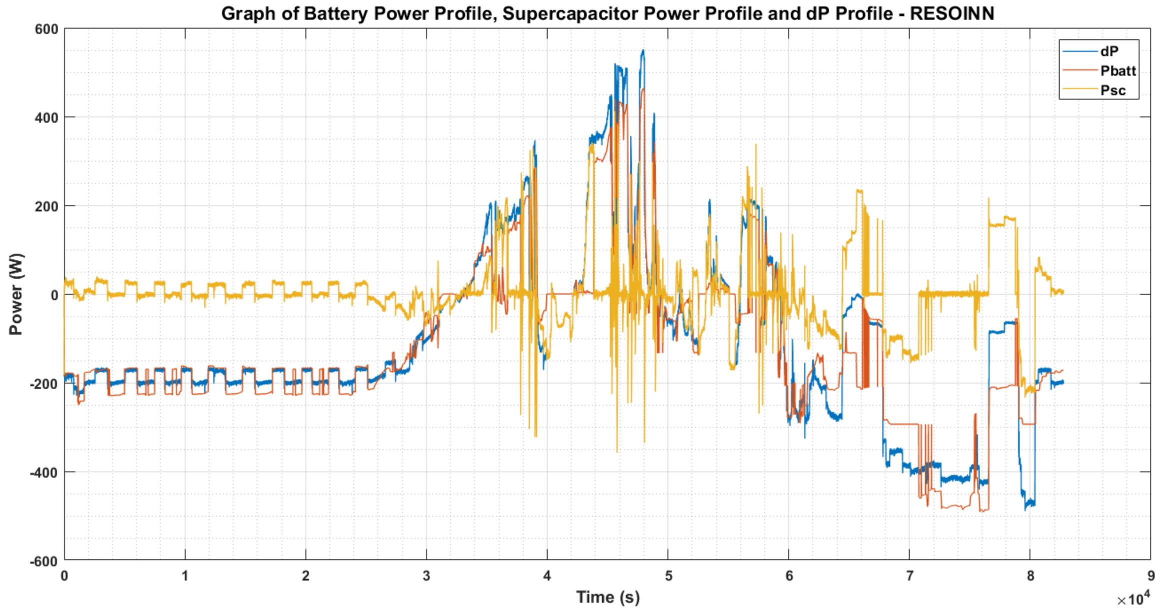

Figure 5-23 - Plot of battery and supercapacitor power profiles vs dP profile resulted by proposed RE-SOINN model on a rainy day

In Figure 5-23, there is a short period of rain in the middle of the day between t = $4 \times 10^4 s$ and t = $4.4 \times 10^4 s$ (11am to 12.10pm). During the day, the solar irradiance profile becomes very noisy due to the rain and cloudy nature. As a result, supercapacitor reacts by dealing with the highly fluctuating dP_{HF} so that battery can be spared from the damaging power oscillations. As the load demand gets huge closing to the end of the day, only HESS supplies energy to the system in the absence of solar irradiance. The limited capacity of supercapacitor is temporarily met using the energy stored by battery. This can be examined in the plot where t = $7 \times 10^4 s$. Supercapacitor can shave the deep power draw from dP until it fully depletes. After the event of supercapacitor energy depletion, battery experiences slightly deeper discharging to recharge the supercapacitor as well as to compensate the loss due to high current discharge. As a result, around t = $8 \times 10^4 s$, supercapacitor has enough stored energy to discharge to reduce another sudden deep power draw in the battery power profile. In overall, with the ability to plan ahead of time, the EMS has managed to deploy supercapacitor to reduce battery power oscillations as well as sudden deep battery power draw resulted by this dP profile.

In Figure 5-24, the solar irradiance profile shows a very sunny condition in the mid of the day, followed by cloudy hours between t = $5 \times 10^4 s$ and t = $6 \times 10^4 s$ (1.52pm to

4.40pm). Disparity is observed during battery recharging period during the mid of the day due to energy loss resulted by 85% efficiency of Lead Acid battery. As the solar irradiance gets erratic around t = $5 \times 10^4 s$, supercapacitor gets into the operation of charging and discharging to shave the sudden power peaks. Compared to Figure 5-23, the load demand in the late evening in Figure 5-24 is slightly lower with less oscillations. Despite the recharging of supercapacitor and loss from the non-ideality of Lead Acid battery have led to slightly deeper battery power draw, the fluctuating conditions on the power demand, however, is improved by supercapacitor operations, especially between t = $7 \times 10^4 s$ and t = $8 \times 10^4 s$ (7.26pm to 10.13pm) where battery power oscillates less than dP. As a summary, supercapacitor takes over the highly fluctuating peak component of the dP profile, allowing the battery to experience smoother operation.

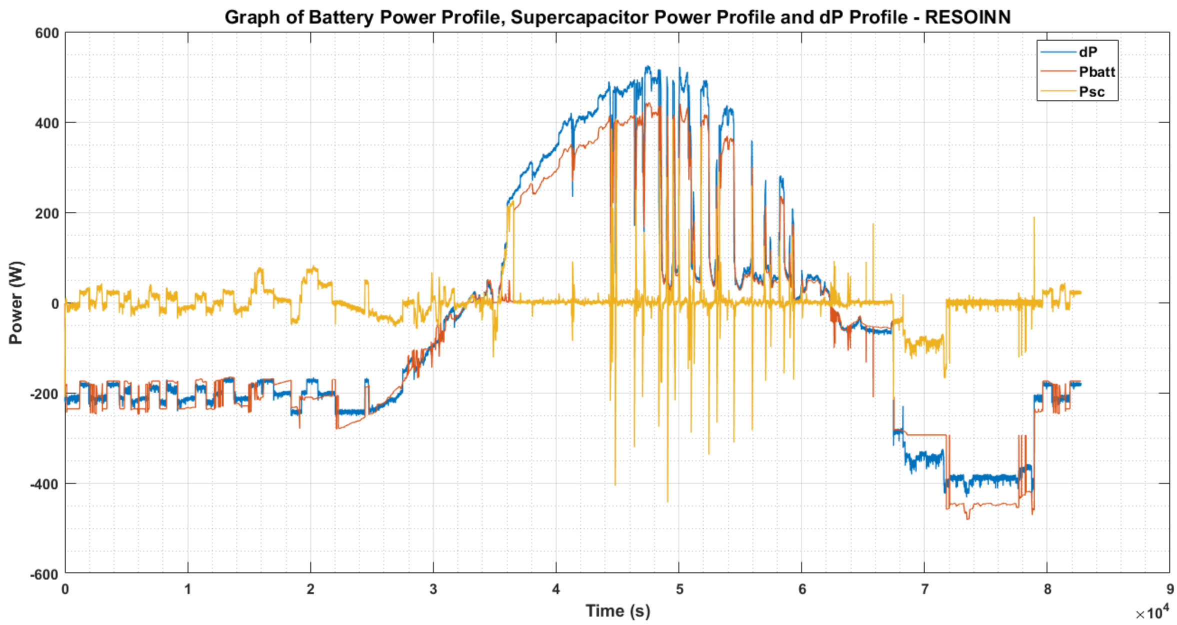

Figure 5-24 - Plot of battery and supercapacitor power profiles vs dP profile resulted by proposed RE-SOINN model on a sunny day

5.12 Conclusion

A novel Unsupervised Learning Artificial Intelligence EMS is introduced to reduce peak power demand as well as dynamic power stress of battery while improve solar energy harvesting especially in low solar irradiance conditions in a standalone PV system with battery-supercapacitor HESS. The EMS operation is run at one-minute interval as a balance between unnecessary power distribution oscillations as well as optimal battery-supercapacitor HESS performance. RE-SOINN based EMS first learns via a PSO teacher for first ten days through its incremental learning nature. Once matured, RE-SOINN based EMS starts working on its own to compute optimal T_c and T_d based on hourly dP trend. Subsequently, RE-SOINN EMS is compared to popular control strategies in the literature. The results have shown that RE-SOINN EMS is able to assist in harvesting more solar energy even in low solar irradiance conditions while reduces peak battery power demand and battery power dynamic stress. The significant reduction in battery power oscillations, especially in higher cyclic amplitude range, can eventually extend battery lifespan. The short computational time as well as training time of RE-SOINN EMS indicates good outlook for this Unsupervised Learning EMS model to be implemented in platforms with lower computational resources, leading to much lower internal system power consumption.

Chapter 6 Conclusion

In remote areas that are far beyond the reach of the national power grid network, a standalone power generation system is needed to provide essential electrical energy to the residents of the said area. An example of sustainable power generation system is Renewable Energy Power System (REPS) that utilises renewable energy sources such as solar energy to generate the much-needed electricity. An advantage of REPS is that renewable energy does not get depleted as time passes, unlike the carbon-based energy sources which does not get replenished in years. However, the main hurdle of popularising REPS lies in the fact that many renewable energy sources are intermittent in nature, generating inconsistent energy output as a reliable alternative to hydrocarbon-based fuels.

Furthermore, in solar energy, much of the generated energy is lost when the solar irradiance is very low during sunset and sunrise, limiting the window of solar energy generation duration. At very low solar irradiance, negligible solar energy is generated and lost due to inefficiency of energy transfer within the system. The widely adopted energy storage system, batteries, especially the SLAs, are potentially the most expensive component in the entire REPS system. However, batteries could easily fall prey into highly erratic solar energy generation as unnecessary high amplitude oscillations and power spikes severely harm the batteries. Consequently, the ROI of a solar-based REPS disappoints many interested parties.

In this research work, two main novelties are proposed to fulfil the research aims. Firstly, an hourly solar irradiance trend forecasting model is introduced so that the system can learn the solar irradiance condition beforehand. The forecasting model is also introduced to perform forecast of other system parameters. Secondly, a novel EMS based upon an Unsupervised Incremental Learning Artificial Intelligence model is devised to control the HESS operation indirectly while prolonging the system lifetime.

In the novel hourly solar irradiance trend forecasting model, an Unsupervised Learning algorithm, RE-SOINN is introduced into a forecasting framework to produce a forecast performance comparable to Supervised Learning such as ANN using solely historical solar irradiance trend. Using only solar irradiance trends learnt, the model shows a good outlook to be deployed in many applications requiring Supervised Learning models. The framework designed can ensure the model to operate within allowable range of forecast accuracy even in cases affected by noise, promising a good forecast performance in long run. Its Incremental Learning feature allows the proposed model to adapt and learn from new datasets continuously, allowing it to adapt to gradual change in the environment. The proposed forecasting model scores 0.658 in MASE and 73.945Wm^{-2} in RMSE whereas competing models such as ANN scores 1 in MASE and 90.56 Wm^{-2} in RMSE.

A novel Unsupervised Learning Artificial Intelligence EMS is introduced to reduce peak power demand as well as dynamic power stress of battery while improve solar energy harvesting in a standalone PV system with battery-supercapacitor HESS. The RE-SOINN model is used as the EMS model in this research due to its capability to reduce computational complexity of operating the system. Upon comparing with other popular control strategies in the literature, RE-SOINN has shown many advantages. The results have shown that RE-SOINN EMS is able to assist in harvesting more solar energy while reduces peak battery power demand and battery power dynamic stress. The significant reduction in battery power oscillations, especially in higher cyclic amplitude range, can eventually extend battery lifespan, prolonging system lifetime. The short computational time as well as training time of RE-SOINN EMS indicates good outlook for this Unsupervised Learning EMS model to be implemented in platforms with lower computational resources, leading to much lower internal system power consumption. The experimental results have shown that the novel EMS model is able to shave the battery peak power draw by 10%, harvests 26.6% more solar energy and lower battery power oscillations in higher cyclic amplitude range comparing to battery-only system. The findings of this thesis also confirm that the research aim and objectives are achieved.

6.1 Future Works

Though the proposed system and its EMS have shown its capability in managing the system operations, improving solar energy harvesting as well as prolonging battery lifetime in a standalone PV system with battery-supercapacitor HESS, there are further enhancements that could be done to improve the system performance or to reduce the overall system complexities.

As the solar panels used in the research are installed many years ago and have a maximum efficiency of less than 10% whereas the average efficiency of solar panels in current market has reached 30%, replacing the old solar panels in the Solar Cabin would improve the system performance, especially in solar energy harvesting.

The forecast performance of Unsupervised Learning RE-SOINN forecasting module can be further improved by increasing the resolution of nodes in RE-SOINN knowledge base. However, extensive size of RE-SOINN knowledge base increases the computational complexity, leading to requiring a powerful computational platform. In this research, Raspberry Pi is chosen due to its low-cost benefit. When performance is given higher priority than system cost, Raspberry Pi can be replaced with commercial grade professional computing boards that can be custom designed.

Grid Search method is applied to pre-determine the hyperparameters of the RE-SOINN EMS model. This has complicated the possibility of the EMS model to be applied from scratch easily. AI-based optimisation algorithms such as Particle Swarm Optimisation (PSO) can be applied to make the proposed EMS model to start running with the least human interference possible. This is because PSO can effectively reduce unnecessary computational steps made by Grid Search.

Chapter 7 Appendices - Standalone PV System and Equipment Setup

This research work sees its application in a rural region with a focused aim on household usage. Thus, this appendix chapter discusses the structural details of proposed standalone PV system with battery-supercapacitor HESS developed for rural household applications. Secondly, the specifications and load demand profiles meeting the general characteristics of a rural household scenario are depicted. Subsequently, the proposed system is constructed in the Solar Cabin of The University of Nottingham Malaysia after the system components are sized accordingly to meet the general load demands in a rural household setting.

7.1 Structure of Standalone PV System

The overall structures of a traditional standalone PV system with Battery as its ESS as well as proposed standalone PV system with battery-supercapacitor HESS are provided in this segment.

7.1.1 Conventional Standalone PV system with Battery Energy Storage System (ESS)

A typical block diagram for conventional standalone PV system with Battery ESS is depicted in Figure 7-1. In general, the four main components in a conventional standalone PV system include the PV solar panel system, battery ESS, load as well as a charge controller. In most of the cases, MPPT serves as the charge controller in these standalone PV systems. In rural applications, an inverter is added in between the DC bus as well as the load as most of the electronic appliances are powered by AC instead of DC. Embedded controller and sensors may or may not be present in a typical standalone PV system depending on the type of control being implemented in the system. Commonly, embedded controller is omitted from the design due to straightforward design of conventional systems.

The conventional standalone PV system can be described mathematically as follow. Assuming the power conversion efficiency of MPPT is η_{MPPT} and η_{IVT} represents the working efficiency of inverter in cases where inverter is required, both the resulting PV power, P'_{PV} as well as the actual load power demand, P'_{load} can be expressed respectively as Equations (7-1) and (7-2) where P_{PV} refers to output power from PV solar panel and P_{load} is the reference load power demand including the power conversion loss due to inverter inefficiency.

$$P'_{PV} = \eta_{MPPT} \times P_{PV} \tag{7-1}$$

$$P'_{load} = \eta_{IVT} \times P_{load} \tag{7-2}$$

Thus, the overall power equation of the entire conventional standalone PV system can be described as follow at Equation (7-3),

$$P'_{PV} - P'_{load} = P_{batt} = dP \tag{7-3}$$

where battery power flow is denoted as P_{batt}. The power mismatch between the generated PV power and the load power demand is simplified by Equation (7-3) as difference in power, dP where it is to be fully compensated by the only storage device present in the system, the battery ESS.

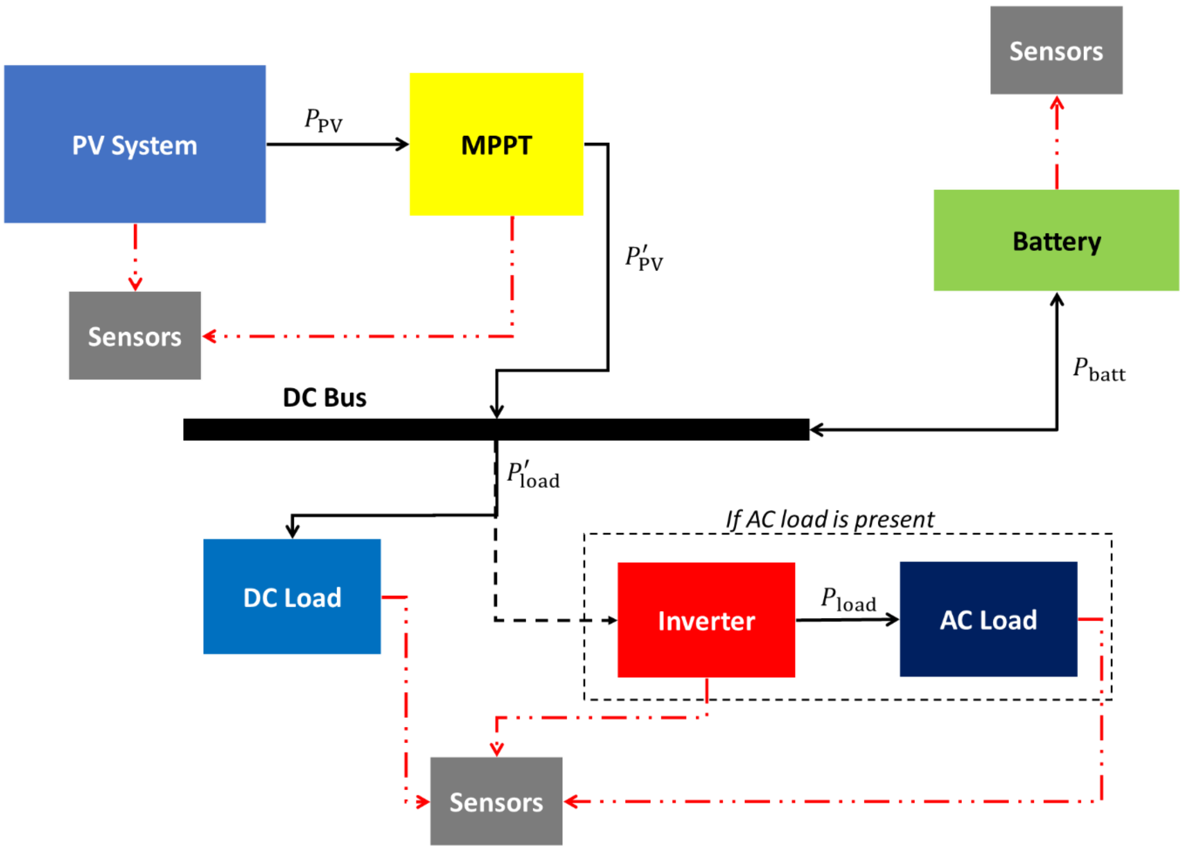

Figure 7-1 – System block diagram of conventional standalone PV system with Battery ESS

7.1.2 Standalone PV System with Battery-Supercapacitor Hybrid Energy Storage System (HESS)

This research work suggests that the system will be more advantageous if supercapacitor is added into the ESS to form HESS for rural household applications. Due to poor recharging rate of battery under low current due to low solar irradiance, these energies are lost instead of being stored accumulatively for future use. Thus, a standalone PV system with battery-supercapacitor HESS is more preferred. The configuration that is adopted in this work is a semi-active one. Figure 7-2 shows the overall structure of a standalone PV system with battery-supercapacitor HESS of semi-active control configuration.

An important component in any HESS design is to include a subsystem which could manage and distribute the power flow between each of the HESS devices. In the absence of such power regulating and managing subsystem, the charging and discharging of both battery as well as supercapacitor will not be controlled actively and directly. The power distribution between the two devices will then be managed by the power mismatch between load demand and power generation as well as natural circuit characteristics of these ESS devices. Thus, in Figure 7-2, a bidirectional DC-DC converter is added as an interface between supercapacitor and the DC bus to decouple the supercapacitor from PV system as well as DC bus. It is noted that such design is designated as semi-active control configuration as only supercapacitor is controlled actively whereas the battery reacts passively to satisfy the power balance of the entire system.

Equation (7-3) can be rewritten to include supercapacitor power to produce Equation (7-4) as follow:

$$P'_{PV} - P'_{load} = P_{batt} + P'_{sc} = dP \quad (7\text{-}4)$$

where P'_{sc} represents supercapacitor power after going through the bidirectional DC-DC converter. Let η_{DCDC} be the efficiency governing the operation of the bidirectional DC-DC converter, Equation (7-5) describing P_{sc} as supercapacitor power before bidirectional DC-DC converter is derived as

$$P'_{sc} = \eta_{DCDC} \times P_{sc} \tag{7-5}$$

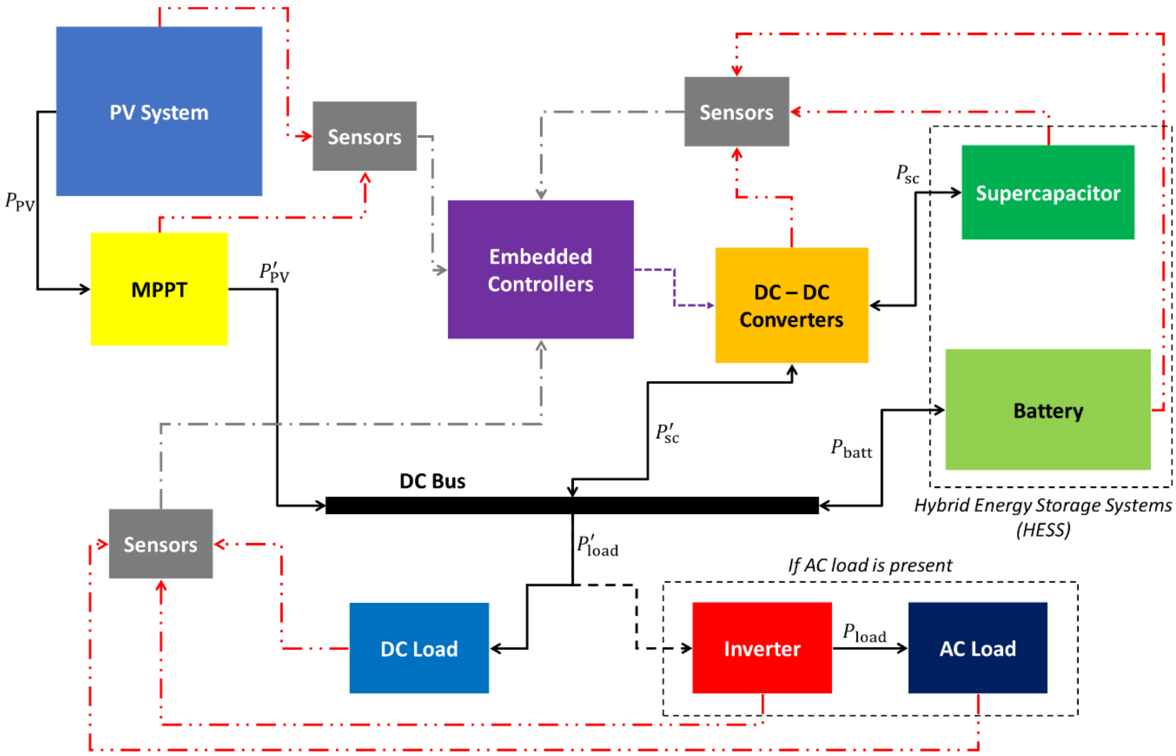

Figure 7-2 – System block diagram of conventional standalone PV system with battery-supercapacitor HESS

Since dP is dealt by both battery and supercapacitor, a system control strategy or EMS is required to distribute dP properly between battery and supercapacitor. EMS produces a reference supercapacitor power, $P_{\mathrm{sc\_ref}}$ to be outputted by supercapacitor based on relevant operating conditions. Since DC-DC converter in the system adopts input current control, $P_{\mathrm{sc\_ref}}$ is further expanded to Equation (7-6).

$$I_{sc\_ref} = \frac{P_{sc\_ref}}{V_{DC}} \tag{7-6}$$

where $\mathrm{V_{DC}}$ is DC bus voltage. As battery is directly coupled to DC bus, $\mathrm{V_{DC}}$ is equal to battery voltage. As a result, the calculated $\mathrm{I_{sc\_ref}}$ is sent to the controller of DC-DC converter so that the actual supercapacitor current can be regulated to $\mathrm{I_{sc\_ref}}$ before any charging or discharging operations occur.

7.2 Solar Cabin Setup

This subsection contains the actual photos for the experimental setup for this project.

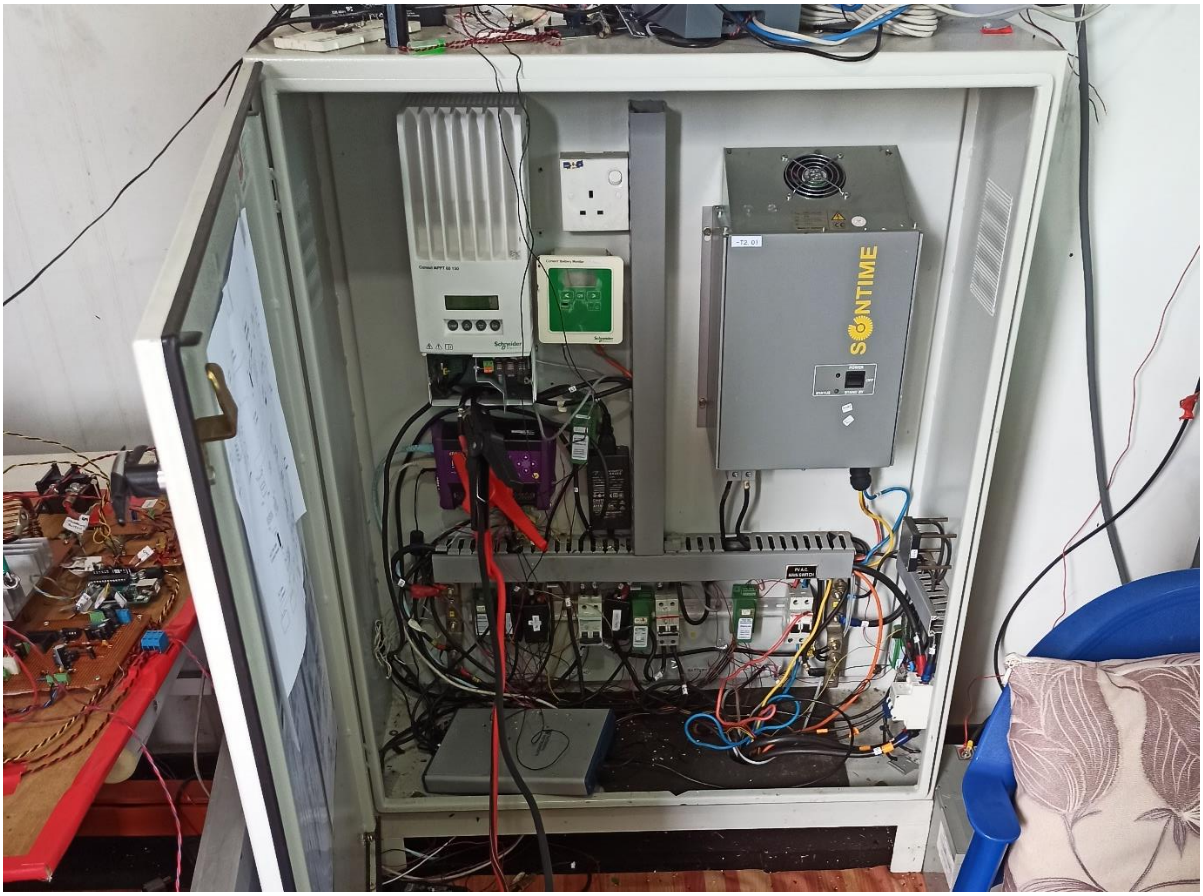

Figure 7-3 - Actual experimental setup showing the DC bus, inverter and MPPT Supercapacitor Charger DC-DC converter

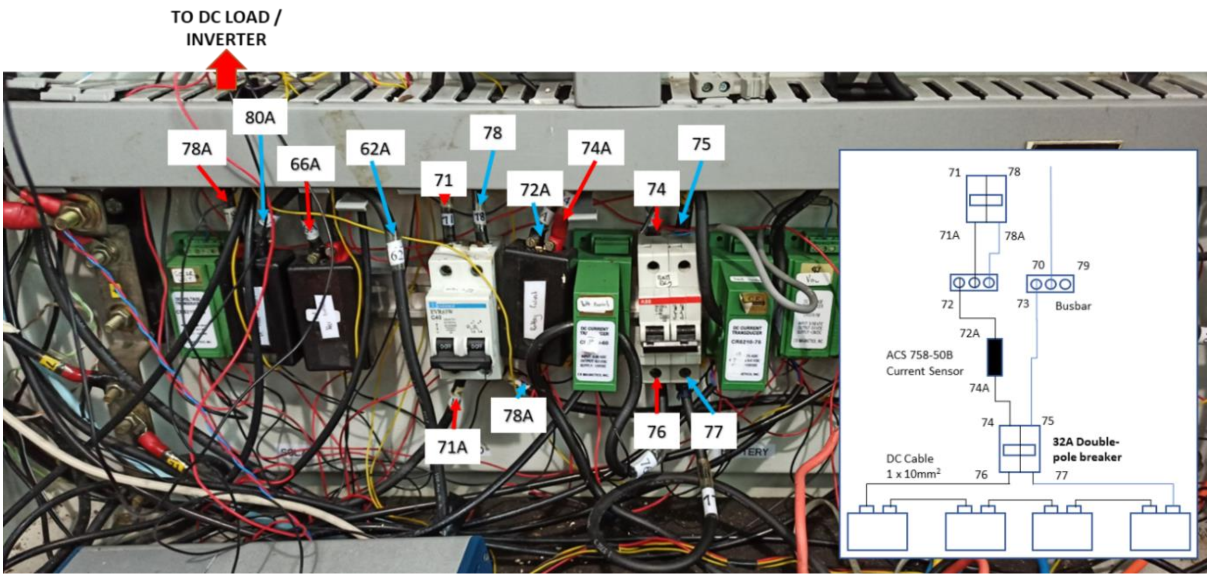

Figure 7-4 – DC Bus

Figure 7-5 – Operation of MPPT Supercapacitor Charger DC-DC Converter

Figure 7-6 – Operation of Load Demand DC-DC Converter

7.3 Sizing of Standalone PV System with Battery-Supercapacitor HESS

The load demand in Subsection 5.10 has presented a need for the standalone PV system implemented in this research to be sized accordingly so that the standalone PV system with battery-supercapacitor HESS is able to operate throughout the entire duration of a day operation without any interruption while being able to achieve system building economy. The Department of Natural Resources (DNR) of State of Louisiana has issued a simple guideline on sizing procedure of any standalone PV system. It is important to point out that the guideline produced considers the working efficiencies of battery and inverter present in the system so that unexpected events such as loss of power supply possibility can be minimized significantly. Table 7-1 shows the design considerations during the sizing procedure of a standalone PV system whereas Table 7-2 illustrates the sizing procedural worksheet prepared by the DNR agency.

Table 7-1 – PV system sizing design consideration factors

Day of energy storage required	2
Maximum battery depth-of-discharged limit	0.8
Battery average round trip efficiency	0.85
Inverter round trip efficiency	0.91
Average peak sun hours per day	4
Ambient temperature multiplier (DF)	0.9

Based on Table 5-6, combining the power specifications as well as the usage time of each electrical appliance on the list produces the total energy demand per day for the household under study. The adjusted power consumption of each appliance in A6 considers the inefficiency of inverter to adjust their respective rated power accordingly. The PV system is set to have its factor B1 of "Days of storage desired" as 2 so that the system stores enough of energy to power the entire household for 2 consecutive days in the absence of generated PV power. Ref. [197] defines any discharge over 80% of rated capacity of a battery as a deep discharge and thus the "Allowable depth of discharge limit" in B2 is taken as 0.8. The “Total battery amp-hour capacity” in B8 is determined to be slightly less than the required battery capacity due to economic decision that 250Ah is about 10% lower than required battery capacity but 500Ah is excessively larger than the requirement. Also, not all electrical appliances in Table 5-6 are turned on on daily basis. The mismatch between required battery capacity and chosen battery capacity can easily be met with an hour of PV system if solar energy is available. Therefore, the determined battery capacity is able to support the household power demand with close to 2 days of operation. The 0.75 factor in “Average daily depth of discharge” in B10 is used to assume that PV system is only able to supply the load for 25% of a day duration.

Table 7-2 - PV system sizing procedural worksheet

A. LOADS					
A1	Inverter Efficiency			91	%
A2	Battery Bus Voltage			48	V
A3	Inverter AC Voltage			240	V
	A4	**A5**	**A6**	**A7**	**A8**
Appliance	Rated Wattage (W)	Adjustment Factor (1.0 for DC system, A1 for AC system)	Adjusted Wattage (W) (A4/A5)	Hours per Day used	Energy per Day (Wh/day)
Ceiling Fan (2 units of 50W)	100.00	0.91	109.89	18.00	1978.02
Table Fan	50.00	0.91	54.95	1.00	54.95
Light (6 units of 18W)	108.00	0.91	118.68	6.00	712.09
Fridge	130.00	0.91	142.86	12.00	1714.29
Washing Machine	300.00	0.91	329.67	0.01	3.30
Laptop	45.00	0.91	49.45	16.00	791.21
TV	39.00	0.91	42.86	4.00	171.43
Toaster	650.00	0.91	714.29	0.01	7.14
A9	Total energy demand per day (Sum of A8)			5432.42	Wh
A10	Total amp-hour demand per day (A9/A2)			113.18	Ah
A11	Maximum AC power requirement (Sum of A4)			1422.00	W
A12	Maximum DC power requirement (Sum of A6)			1562.64	W

B. BATTERY SIZING			
B1	Days of storage desired / required	2.00	days
B2	Allowable depth-of-discharge limit	0.80	
B3	Required battery capacity [(A10 x B1) / B2]	282.94	Ah
B4	Amp-Hour capacity of selected battery	250.00	Ah
B5	Number of batteries in parallel (B3/B4)	1	unit(s)
B6	Number of batteries in series (A2/selected battery voltage)	4	units
B7	Total number of batteries (B5 x B6)	4	units
B8	Total battery amp-hour capacity (B5 x B4)	250.00	Ah
B9	Total battery kilowatt-hour capacity [(B8 x A2) / 1000)	12.00	kWh
B10	Average daily depth of discharge (0.75 x A10/B8)	0.34	

C. PV ARRAY SIZING			
C1	Total energy demand per day (A9)	5432.42	Wh
C2	Battery round trip efficiency (0.70 - 0.85)	0.85	
C3	Required array output per day (C1/C2)	6391.08	Wh
C4	Selected PV module max power voltage at STC (x0.85)	45.48	V
C5	Selected PV module guaranteed power output at STC	100.00	Wh
C6	Peak sun hours at design tilt for design month	4.00	hours
C7	Energy output per module per day (C5 x C6)	400.00	Wh
C8	Module energy output at operating temperature (DF x C7) DF = 0.8 for hot climates and critical applications DF = 0.9 for moderate climates and non-critical applications	360.00	Wh
C9	Number of modules required to meet energy requirements (C3/C8)	20	modules
C10	Number of modules required per string (A2/C4) rounded to the next higher integer	2	modules
C11	Number of strings in parallel (C9/C10) rounded to the next higher integer	10	modules
C12	Number of modules to be purchased (C10 x C11)	20	modules
C13	Nominal rated PV module output	100.00	W
C14	Nominal rated array output (C13 x C12)	2000.00	W

Based on Table 7-2, the optimal design of the proposed standalone PV system with battery-supercapacitor HESS can be partially given as follow:

- PV Array : 2000W (20 modules of Kaneka UEA-100 solar panels of 100W each)
- Battery : 48V, 250Ah (4 units of Powerbatt AGM Lead Acid batteries of 12V, 250Ah)

These design considerations have led to additional design criteria to be met by other components present in the system such as

- The DC-DC converters must be able to handle power up to 2000W from PV arrays
- PV array operating voltage must be higher than 142V so that DC-DC converters are not harmed during the operations
- Able to charge or compatible with 48V Lead-Acid AGM battery bank
- Components connected to the load side should be able to deal with requirement set in A12 "Maximum DC Power Requirement" of 1562W
- The standard AC voltage and frequency adopted in Malaysia is 230V and 50Hz

From these design requirements, the DC-DC converter built to harvest solar power from PV array is designed with criteria listed in Table 5-5 under "MPPT Supercapacitor Charger DC-DC Converter". The MPPT algorithm adopted is InC method so that the array operating voltage can be adjusted continuously to produce maximum power at any instant. As for the DC-DC converter interfacing the HESS to load, it is designed to have rated power at 2.4kW, maximum input and output voltage and current at 100V and 100A respectively so that high power transfer is possible between HESS and the load. Sontime 4830N inverter is chosen as it satisfies the requirements resulted from the design considerations with power rating of 2730W, output frequency of 50-60Hz, output voltage range of 230V.

As supercapacitor does not possess high energy capacity like SLA batteries, it is usually common to size the supercapacitor suitable to the standalone PV system via cost-matching method. Thus, eight units of Nippon-Chemi-Con DLCAP supercapacitors are added into the HESS to produce 30V, 800F supercapacitor bank, matching the cost of 4 units of Powerbatt AGM Lead Acid Batteries of 12V, 250Ah. Consequently, the proposed EMS can be operated efficiently and effectively without oversized supercapacitor of uneconomical building cost as well as without undersized supercapacitor banks that lead to restricted supercapacitor action in the EMS.

7.4 DC-DC Converters

Based on the requirements of proposed Standalone PV System with battery-supercapacitor HESS listed in Table 5-5 and Table 7-2, the DC-DC converters should be designed to be able to handle 2.4kW with an absolute maximum rating at 100V/100A. The typical load operations listed in Table 5-6 have suggested a typical operation rating of DC-DC converter to be set at 60V/40A.

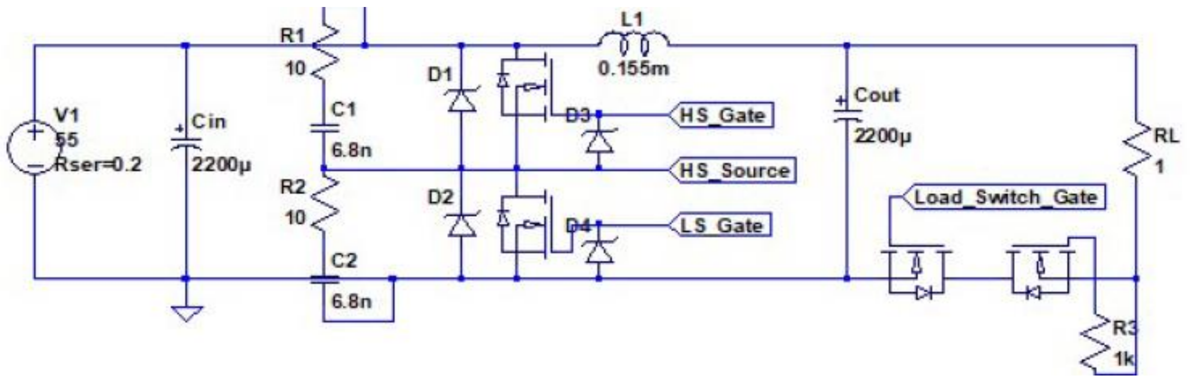

Figure 7-7 – Schematic diagram of MPPT Supercapacitor Charger DC-DC Converter

Figure 7-7 shows the schematic diagram MPPT Supercapacitor Charger DC-DC Converter. Since the PV panels could reach to 142V while the DC bus is set to be 48V, MPPT Supercapacitor Charger DC-DC Converter should adopt the configuration of a buck converter. Synchronous buck converter configuration is chosen for better operating efficiency. A RC snubber circuit is added to the High Side (HS) and Low Side (LS) of MOSFET to minimize voltage spikes resulted from switching operations. A 100V Zener diode is essential to the circuit so that the Drain-Source voltage of MOSFET during the operation does not exceed its maximum rating of 150V whereas a 18V Zener diode prevents the Gate-Source voltage of MOSFET exceeds its maximum rating of 20V. To prevent events of overcurrent, an electronic load switch is inserted to the ground between the DC-DC converter output and load so that the current can be cut off anytime.

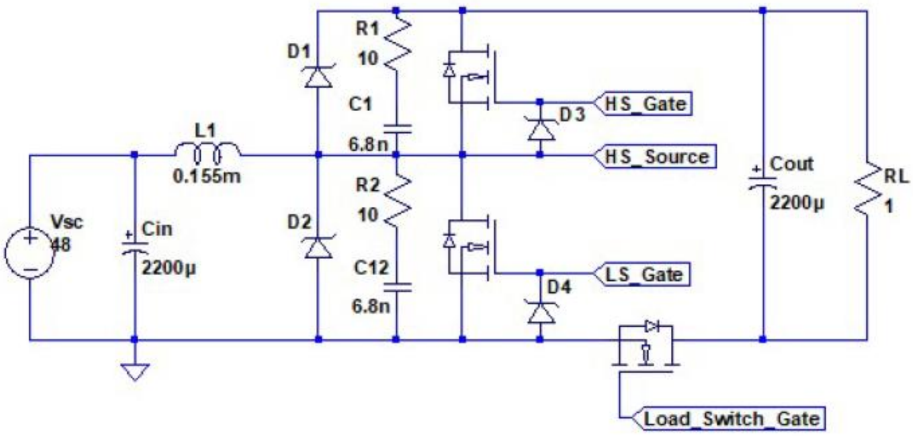

Figure 7-8 – Schematic Diagram of Load Demand DC-DC Converter

Figure 7-8 shows the schematic diagram of Load Demand DC-DC Converter. Based on the operations of supercapacitor in the proposed Standalone PV System with battery-supercapacitor HESS, the voltage of supercapacitor is usually lower than the DC bus of 48V since supercapacitor voltage is proportional to its SoC. Thus, the discharging of supercapacitor requires a boost converter. Subsequently, supercapacitor is required to be charged from the DC bus when supercapacitor SoC gets too low. Therefore, bidirectional current flow is important in Load Demand DC-DC Converter. Comparing to MPPT Supercapacitor DC-DC Converter, current-blocking diode MOSFET is absent in Load Demand DC-DC Converter so that the DC-DC converter can operate in forward boost mode for discharging and in reverse-buck mode during charging. A load MOSFET switch is essential to the boost converter so that the converter can be turned off without interruption from always forward-biased antiparallel diode of HS MOSFET.

The working operation of MPPT Supercapacitor Charger DC-DC Converter is as follows in Figure 7-9. The operation is controlled by Arduino Uno microcontroller. Current regulation is added to prevent overcurrent events especially when supercapacitor is in very low SoC during very high solar irradiance conditions (higher PV generation, resulting in way higher buck ratio to produce high output current). The regulation is done by not allowing the PV energy generation to operate at MPP and the threshold is set at 70A.

Figure 7-9 – Algorithmic flowchart for MPPT Supercapacitor Charger

As for the supercapacitor discharging operation of Load Demand DC-DC Converter, its working operation is shown in Figure 7-10. Average current control is achieved by implementing a proportional controller with a proportional gain of K_P. To prevent excessive oscillating current in the converter, an adaptive setpoint is needed for this proportional controller. Every time the supercapacitor enters discharging mode, the initial duty cycle can be calculated using Equation (7-7) to reduce settling time because long settling time slows down the discharging of supercapacitor.

$$V_{out} = \frac{1}{1-D} V_{in} \tag{7-7}$$

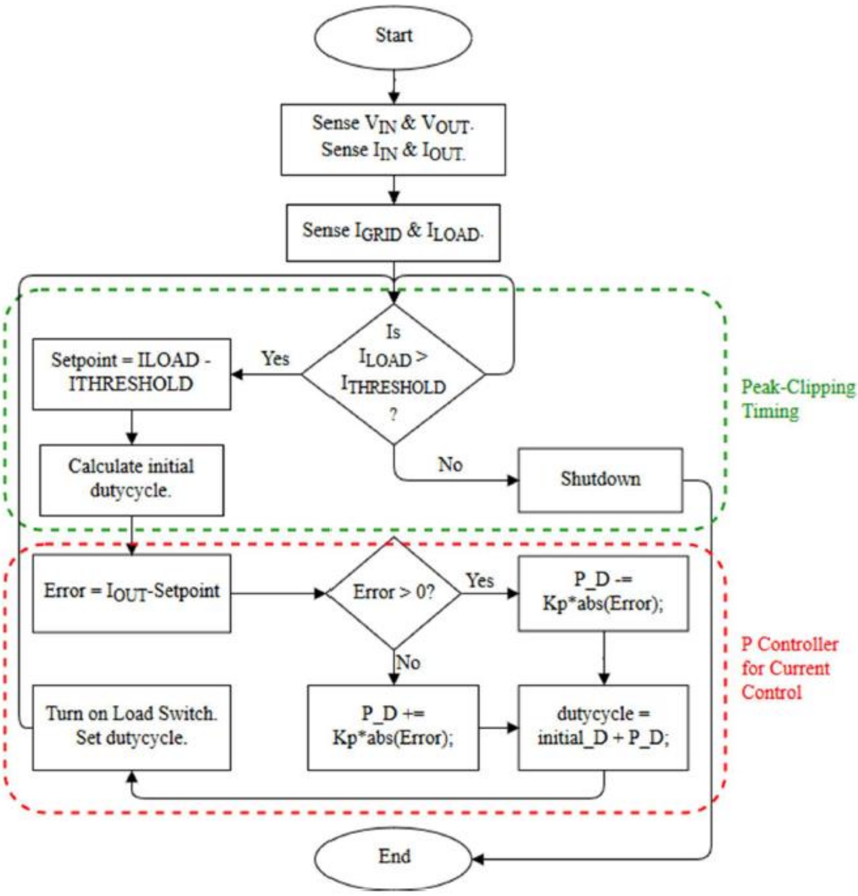

Figure 7-10 – Algorithmic flowchart of supercapacitor discharging operation of Load Demand DC-DC Converter

The supercapacitor charging operation of Load Demand DC-DC Converter works as described in the flowcharts in Figure 7-11. The charging of supercapacitor is done by adjusting the duty cycle with a step size of 0.01 for longer rising and settling time to minimize the overshoot of charging current and to achieve smooth charging operation.

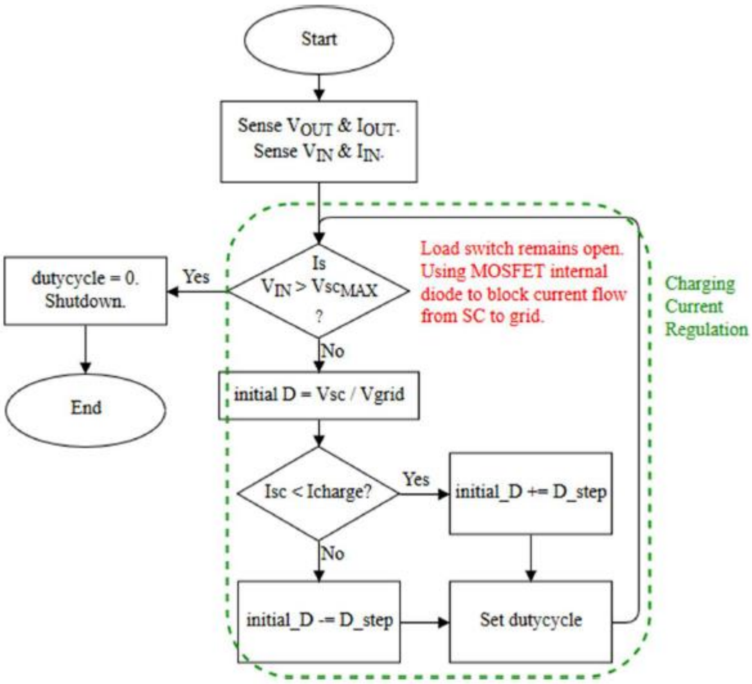

Figure 7-11 – Algorithmic flowchart of supercapacitor charging operation of Load Demand DC-DC Converter

7.5 Sensors and Instruments

An efficient and effective working of EMS is highly dependent on the states of the system, or the feedback of each component during the operation. The feedbacks are usually fed back to EMS via sensors. Table 3-5 lists the types of sensors and instruments installed in the standalone PV system with battery-supercapacitor HESS in Solar Cabin. Their respective interfaces and measurement ranges are recorded in Table 7-3. Table 7-4 shows how system state measurements are calculated or obtained directly from these instruments and sensors.

Table 7-3 - Interface and measurement range of sensors and instruments installed for proposed standalone PV system

Sensors/ Instruments		**Interface**	**Measurement Range**
Sensor	DC Voltage Transducer CR6310-100	Analog	DC Voltage (0V-100V)
	DC Current Transducer CR5210-60	Analog	DC Current (0A-60A)
	True RMS AC voltage Transducer CR4510-250	Analog	RMS Voltage (0V -250V)

	Loop Powered AC current Transducer CR4220-15	Analog	RMSE Current (0A -15A)
	Texas Electronics SP-LITE Solar Radiation Sensor	Analog	Solar Irradiance (0-1400 W/m^2)
	Texas Instrument LM35	Analog	Temperature (−55°C to 150°C)
Instrument	Schneider Electric Battery Monitoring System	RS485	State of Charge of Battery (0 % - 100 %)
	Vaisala Weather Transmitter WXT520	RS485	Wind speed (0 m/s– 60 m/s) Wind Direction (0° - 360°) Precipitation (mm) Atmospheric pressure (600 hPa - 1100 hPa) Air Temperature (-52 °C – 60 °C) Relative humidity (0% RH - 100% RH)

Table 7-4 - Methods of obtaining parameters from instruments and sensors installed

Component	**Parameter**		**Instruments/Sensors/ Calculation**
PV	Voltage	V_{PV}	DC Voltage Transducer CR6310-100
	Current	I_{PV}	DC Current Transducer CR5210-60
	Power	P_{PV}	$V_{PV} \times I_{PV}$
	Temperature	T_{PV}	Texas Instrument LM35
Battery	Voltage	V_{batt}	DC Voltage Transducer CR6310-100
	Current	I_{batt}	DC Current Transducer CR5210-60
	Power	P_{batt}	$V_{batt} \times I_{batt}$
	State-of-charge	SoC_{batt}	Schneider Electric Battery Monitoring System
Supercapacitor	Voltage	V_{SC}	DC Voltage Transducer CR6310-100
	Current	I_{SC}	DC Current Transducer CR5210-60

	Power	P_{SC}	$V_{SC} \times I_{SC}$
	State-of-charge	SoC_{SC}	V_{SC}^2 / (rated supercapacitor voltage)^2 × 100%
DC-DC Converter	Input Voltage	V_{DC}	DC Voltage Transducer CR6310-100
	Input Current	I_{SC}	DC Current Transducer CR5210-60
	Input Power	P_{SC}	$V_{DC} \times I_{SC}$
	Output Voltage	V_{SC}'	DC Voltage Transducer CR6310-100
	Output Current	I_{SC}'	DC Current Transducer CR5210-60
	Output Power	P_{SC}'	$V_{SC}' \times I_{SC}'$
Inverter	Input Voltage	V_{dc}	DC Voltage Transducer CR6310-100
	Input Current	I_{load}	DC Current Transducer CR5210-60
	Input Power	P_{load}	$V_{load} \times I_{load}$
	Output Voltage	V_{load}'	True RMS AC voltage Transducer CR4510-250
	Output Current	I_{load}'	Loop Powered AC current Transducer CR4220-15
	Output Power	P_{load}'	$V_{load}' \times I_{load}'$
Charge controller	Input Voltage	V_{PV}	DC Voltage Transducer CR6310-100
	Input Current	I_{PV}	DC Current Transducer CR5210-60
	Input Power	P_{PV}	$V_{PV} \times I_{PV}$
	Output Voltage	V_{PV}'	DC Voltage Transducer CR6310-100
	Output Current	I_{PV}'	DC Current Transducer CR5210-60
	Output Power	P_{PV}'	$V_{PV}' \times I_{PV}'$
Meteorological Data	Solar Irradiance	Irr	Texas Electronics SP-Lite Solar Radiation Sensor
	Air Temperature	T_{air}	Vaisala Weather Transmitter WXT520

	Relative Humidity	*RH*	Vaisala Weather Transmitter WXT520
	Air Pressure	*AP*	Vaisala Weather Transmitter WXT520
	Wind Speed	*WS*	Vaisala Weather Transmitter WXT520

7.6 Interfacing Sensors and EMS Embedded Platform

Table 7-3 lists down the sensors made available in the proposed standalone PV system with battery-supercapacitor HESS system setup in Solar Cabin. In this subsection, the integration of sensors with embedded platform used to run the system EMS is presented in Figure 7-12.

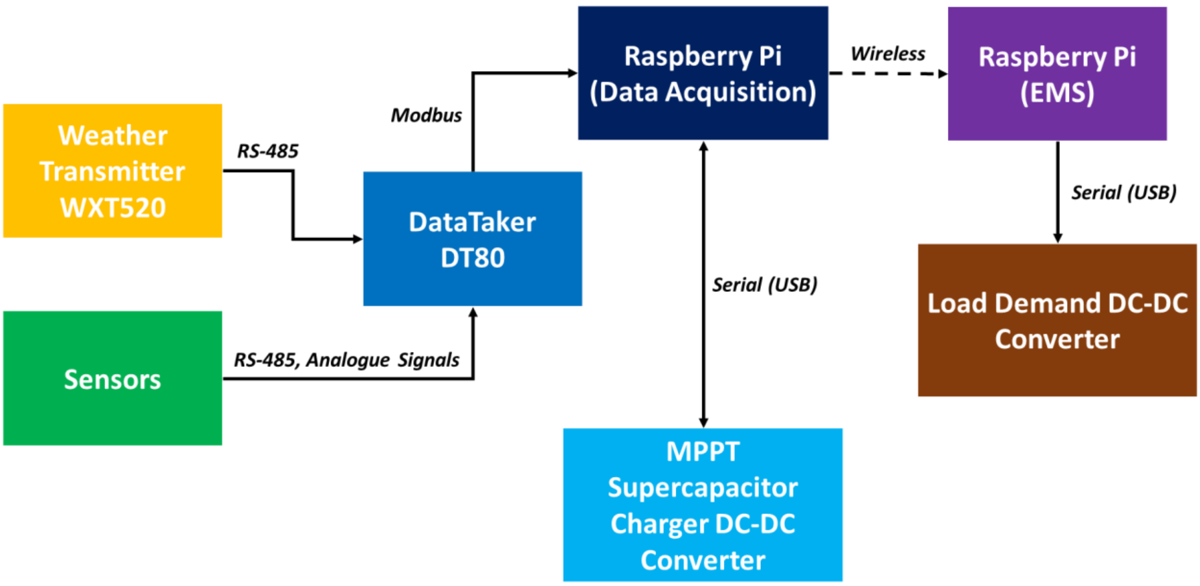

Figure 7-12 – Structure of interface between sensors, EMS embedded controller and DC-DC converters

Based on Figure 7-12, two Raspberry Pis are deployed into the system where one acts as the data acquisition module with the other one being implemented as EMS embedded controller. Raspberry Pi is chosen for this application because Raspberry Pi is a very common electronic device in any IoT project and thus there are plenty of supports, resources as well as hardware accessories compatible with Raspberry Pi. Secondly, Raspberry Pi runs on Linux operating system which is very efficient on single-board computers (SBC) or embedded system, resulting in much lower consumption in computing and storage resources. Its lower power consumption is an added benefit to a standalone system where the energy available in the system is very limited. Subsequently, Raspberry Pi excels in connectivity since it has built-in Wi-Fi and Bluetooth modules in addition to 4 USB ports and an Ethernet port. One of its close competitors, the Arduino-based microcontrollers are less favourable due to lacking non-volatile memory to store certain EMS parameters essential to continuous operation of the entire system.

Before the first Raspberry Pi (data acquisition module), sensors such as Weather Station, Pyranometer, voltage and current sensors placed throughout the system are first connected to the DT80 DateTaker unit via RS-485 and simple analogue signals. The stored data are then transmitted and saved in a server if DT80 unit is connected to the internet via Ethernet cable. The need of passing the sensor measurements to DT80 unit is because Raspberry Pi does not have analogue GPIOs whereas most of the sensor measurements are naturally analogue outputs. Thus, an external ADC circuits or external data logger system becomes essential to complete the data transmission between the sensors and Raspberry Pi. Usage of external ADC circuit is not scalable when Raspberry Pi has only 26 usable GPIOs. This limitation would then restrict the number of working sensors in this research project if external ADC circuit method were to be adopted. Also, not all sensors employ the same communication methods. For instance, some sensors use RS-232 while some go with simple analogue outputs. DT80 DataTaker supports a total of 28 analogue inputs, 8 digital inputs, 8 low speed counters, 4 high speed counters. DT80 DataTaker also supports a wide range of communication channels, ranging from RS-232, RS-485, RS-422, Modbus, FTP, HTTP, XML, SMTP, NTP, SDI-12, USB and Ethernet.

DT80 unit is connected to the Raspberry Pi via USB-Modbus method. Raspberry Pi then stores these data into a csv file. If the internet is present, Pi could be programmed to upload the stored data into online server via services such as Google Firebase. The data storage and management programs are written in Python language instead of C because complex algorithms are easier to be developed in Python using Python optimization and developed mathematical libraries. The application of Raspberry Pi as intermediate station of data acquisition module has enabled easier data communication with EMS module in later stage. For instance, the RS-232 protocol can easily be modified to TX and Rx serial communication.

The communication between the Raspberry Pi data acquisition module and Raspberry Pi EMS module is made wireless to avoid long table connection between the two modules. It is noted that the data acquisition unit should be placed in a location closer to the sensors (close to external environment) whereas the EMS module can be placed closer to the HESS of the standalone PV system. An ad-hoc network is used to perform wireless data transfer between the two modules. A wireless ad-hoc network is an Independent Basic Service (IBSS) which consists of local wireless devices (nodes) discovering each other and forming a network so that each can forward data to other nodes. Access point such as router is not required at all to manage the communication.

A great advantage of this method is that there is no need for internet service since internet service may not be available in certain rural areas. Therefore, the chance of the proposed system setup to be adopted in an area beyond the reach of internet connectivity is greatly improved. Should any troubleshooting be required during the maintenance of the system, the process is greatly simplified as any computer can gain access to the ad-hoc network with approved credential without the need of physical disassembling the data acquisition module beforehand. Via this ad-hoc network, these Raspberry Pi can exchange data via SSH connection anytime. Thus, the Raspberry Pi EMS module can perform a regular routine to read the csv file stored in the Raspberry Pi data acquisition module.

Both DC-DC converters in Figure 7-12 are connected to the Raspberry Pis via simple USB TX and Rx serial communication. The main microcontrollers in both DC-DC converters are Arduino Uno boards. As so, the DC-DC converters can receive instructions or data from Raspberry Pis that they are connected to in real time.

References

[1] S. K. Kollimalla, M. K. Mishra, and N. L. Narasamma, “Design and analysis of novel control strategy for battery and supercapacitor storage system,” *IEEE Trans Sustain Energy*, vol. 5, no. 4, pp. 1137–1144, 2014, doi: 10.1109/TSTE.2014.2336896.

[2] N. R. Tummuru, M. K. Mishra, and S. Srinivas, “Dynamic Energy Management of Renewable Grid Integrated Hybrid Energy Storage System,” *IEEE Transactions on Industrial Electronics*, vol. 62, no. 12, pp. 7728–7737, 2015, doi: 10.1109/TIE.2015.2455063.

[3] C. Xiang, Y. Wang, S. Hu, and W. Wang, “A new topology and control strategy for a hybrid battery-ultracapacitor energy storage system,” *Energies (Basel)*, vol. 7, no. 5, pp. 2874–2896, 2014, doi: 10.3390/en7052874.

[4] G. Wang, M. Ciobotaru, and V. G. Agelidis, “Power Smoothing of Large Solar PV Plant Using Hybrid Energy Storage,” vol. 5, no. 3, pp. 834–842, 2014.

[5] S. K. Kollimalla and M. K. Mishra, “Coordinated Control and Energy Management of Hybrid Energy Storage System in PV System,” pp. 363–368, 2014.

[6] H. S. Khaldi and A. C. Ammari, “Design and Comparison of two DC / DC Converter Topologies Interfacing a Hybrid Energy Storage System to the DC Bus,” *International Conference on Control, Engineering & Information Technology (CEIT’14)*, pp. 88–94, 2014.

[7] J. Li *et al.*, “Design and advanced control strategies of a hybrid energy storage system for the grid integration of wind power generations,” *IET Renewable Power Generation*, vol. 9, no. 2, pp. 89–98, 2015, doi: 10.1049/iet-rpg.2013.0340.

[8] T. Alnejaili, S. Drid, D. Mehdi, L. Chrifi-Alaoui, R. Belarbi, and A. Hamdouni, “Dynamic control and advanced load management of a stand-alone hybrid renewable power system for remote housing,” *Energy Convers Manag*, vol. 105, pp. 377–392, 2015, doi: 10.1016/j.enconman.2015.07.080.

[9] C. Lee Wai, Y. W. Wong, R. K. Rajkumar, R. K. Rajkumar, and D. Isa, “Hybrid energy storage systems and control strategies for stand-alone renewable energy power systems,” *Renewable and Sustainable Energy Reviews*, vol. 66, pp. 174–189, 2016, doi: 10.1016/j.rser.2016.07.059.

[10] L. W. Chong, Y. W. Wong, R. K. Rajkumar, and D. Isa, “An optimal control strategy for standalone PV system with Battery-Supercapacitor Hybrid Energy Storage System,” *J Power Sources*, vol. 331, pp. 553–565, 2016, doi: 10.1016/j.jpowsour.2016.09.061.

[11] L. W. Chong, Y. W. Wong, R. K. Rajkumar, and D. Isa, “An adaptive learning control strategy for standalone PV system with battery-supercapacitor hybrid energy storage system,” *J Power Sources*, vol. 394, no. February, pp. 35–49, 2018, doi: 10.1016/j.jpowsour.2018.05.041.

[12] S. K. Kollimalla, M. K. Mishra, and N. L. Narasamma, “Design and analysis of novel control strategy for battery and supercapacitor storage system,” *IEEE Trans Sustain Energy*, vol. 5, no. 4, pp. 1137–1144, 2014, doi: 10.1109/TSTE.2014.2336896.

[13] S. K. Kollimalla and M. K. Mishra, “Coordinated Control and Energy Management of Hybrid Energy Storage System in PV System,” pp. 363–368, 2014.

[14] R. Tariq *et al.*, “Artificial intelligence assisted technoeconomic optimization scenarios of hybrid energy systems for water management of an isolated community,” *Sustainable Energy Technologies and Assessments*, vol. 48, no. August, 2021, doi: 10.1016/j.seta.2021.101561.

[15] N. R. Tummuru, M. K. Mishra, and S. Srinivas, “Dynamic Energy Management of Renewable Grid Integrated Hybrid Energy Storage System,” *IEEE Transactions on Industrial Electronics*, vol. 62, no. 12, pp. 7728–7737, 2015, doi: 10.1109/TIE.2015.2455063.

[16] G. Wang, M. Ciobotaru, and V. G. Agelidis, “Power Smoothing of Large Solar PV Plant Using Hybrid Energy Storage,” vol. 5, no. 3, pp. 834–842, 2014.

[17] H. S. Khaldi and A. C. Ammari, “Design and Comparison of two DC / DC Converter Topologies Interfacing a Hybrid Energy Storage System to the DC Bus,” *International Conference on Control, Engineering & Information Technology (CEIT’14)*, pp. 88–94, 2014.

[18] R. A. Dougal, S. Member, S. Liu, and R. E. White, “Power and Life Extension of Battery – Ultracapacitor Hybrids,” vol. 25, no. 1, pp. 120–131, 2002.

[19] C. Xiang, Y. Wang, S. Hu, and W. Wang, “A new topology and control strategy for a hybrid battery-ultracapacitor energy storage system,” *Energies (Basel)*, vol. 7, no. 5, pp. 2874–2896, 2014, doi: 10.3390/en7052874.

[20] A. C. Baisden, S. Member, A. Emadi, and S. Member, “ADVISOR-Based Model of a Battery and an Ultra-Capacitor Energy Source for Hybrid Electric Vehicles,” vol. 53, no. 1, pp. 199–205, 2004.

[21] A. M. Gee, F. V. P. Robinson, and R. W. Dunn, “Analysis of Battery Lifetime Extension in a Small-Scale Wind-Energy System Using Supercapacitors,” vol. 28, no. 1, pp. 24–33, 2013.

[22] S. Y. Kan, M. Verwaal, and H. Broekhuizen, “The use of battery – capacitor combinations in photovoltaic powered products,” vol. 162, pp. 971–974, 2006, doi: 10.1016/j.jpowsour.2005.07.001.

[23] Y. Zhang, A. Lundblad, P. E. Campana, and J. Yan, “Comparative Study of Battery Storage and Hydrogen Storage to Increase Photovoltaic Self-sufficiency in a Residential Building of Sweden,” *Energy Procedia*, vol. 103, pp. 268–273, 2016, doi: 10.1016/j.egypro.2016.11.284.

[24] T. Bocklisch, M. Böttiger, and M. Paulitschke, “Multi-storage hybrid system approach and experimental investigations,” *Energy Procedia*, vol. 46, pp. 186–193, 2014, doi: 10.1016/j.egypro.2014.01.172.

[25] Z. Cabrane, M. Ouassaid, and M. Maaroufi, “Analysis and evaluation of battery-supercapacitor hybrid energy storage system for photovoltaic installation,” *Int J Hydrogen Energy*, vol. 41, no. 45, pp. 20897–20907, 2016, doi: 10.1016/j.ijhydene.2016.06.141.

[26] T. Ma, H. Yang, and L. Lu, “Development of hybrid battery-supercapacitor energy storage for remote area renewable energy systems,” *Appl Energy*, vol. 153, pp. 56–62, 2015, doi: 10.1016/j.apenergy.2014.12.008.

[27] T. Alnejaili, S. Drid, D. Mehdi, L. Chrifi-Alaoui, R. Belarbi, and A. Hamdouni, “Dynamic control and advanced load management of a stand-alone hybrid renewable power system for remote housing,” *Energy Convers Manag*, vol. 105, pp. 377–392, 2015, doi: 10.1016/j.enconman.2015.07.080.

[28] H. Musbah, H. H. Aly, and T. A. Little, “Energy management of hybrid energy system sources based on machine learning classification algorithms,” *Electric Power Systems Research*, vol. 199, no. June, p. 107436, 2021, doi: 10.1016/j.epsr.2021.107436.

[29] C. Lee Wai, Y. W. Wong, R. K. Rajkumar, R. K. Rajkumar, and D. Isa, “Hybrid energy storage systems and control strategies for stand-alone renewable energy power systems,” *Renewable and Sustainable Energy Reviews*, vol. 66, pp. 174–189, 2016, doi: 10.1016/j.rser.2016.07.059.

[30] C. Zhao, P. B. Andersen, C. Træholt, and S. Hashemi, “Grid-connected battery energy storage system: a review on application and integration,” *Renewable and Sustainable Energy Reviews*, vol. 182. Elsevier Ltd, Aug. 01, 2023. doi: 10.1016/j.rser.2023.113400.

[31] S. Basnet, K. Deschinkel, L. Le Moyne, and M. Cécile Péra, “A review on recent standalone and grid integrated hybrid renewable energy systems: System optimization and energy management strategies,” *Renewable Energy Focus*, vol. 46. Elsevier Ltd, pp. 103–125, Sep. 01, 2023. doi: 10.1016/j.ref.2023.06.001.

[32] F. Garcia-Torres, L. Valverde, and C. Bordons, “Optimal Load Sharing of Hydrogen-Based Microgrids with Hybrid Storage Using Model Predictive Control,” *IEEE Transactions on Industrial Electronics*, vol. PP, no. 99, p. 1, 2016, doi: 10.1109/TIE.2016.2547870.

[33] P. Boza and T. Evgeniou, “Artificial intelligence to support the integration of variable renewable energy sources to the power system,” *Appl Energy*, vol. 290, no. October 2020, p. 116754, 2021, doi: 10.1016/j.apenergy.2021.116754.

[34] S. K. Jha, J. Bilalovic, A. Jha, N. Patel, and H. Zhang, “Renewable energy: Present research and future scope of Artificial Intelligence,” *Renewable and Sustainable Energy Reviews*, vol. 77, no. May 2016, pp. 297–317, 2017, doi: 10.1016/j.rser.2017.04.018.

[35] J. F. Toubeau *et al.*, “Machine learning-assisted outage planning for maintenance activities in power systems with renewables,” *Energy*, vol. 238, 2022, doi: 10.1016/j.energy.2021.121993.

[36] J. Aguilar, A. Garces-Jimenez, M. D. R-Moreno, and R. García, “A systematic literature review on the use of artificial intelligence in energy self-management in smart buildings,” *Renewable and Sustainable Energy Reviews*, vol. 151, no. August, p. 111530, 2021, doi: 10.1016/j.rser.2021.111530.

[37] D. Tayal, “Achieving high renewable energy penetration in Western Australia using data digitisation and machine learning,” *Renewable and Sustainable Energy Reviews*, vol. 80, no. January, pp. 1537–1543, 2017, doi: 10.1016/j.rser.2017.07.040.

[38] L. Ramos, M. Colnago, and W. Casaca, “Data-driven analysis and machine learning for energy prediction in distributed photovoltaic generation plants: A case study in Queensland, Australia,” *Energy Reports*, vol. 8, pp. 745–751, 2022, doi: 10.1016/j.egyr.2021.11.123.

[39] Y. Zhou, Y. Liu, D. Wang, X. Liu, and Y. Wang, “A review on global solar radiation prediction with machine learning models in a comprehensive perspective,” *Energy Convers Manag*, vol. 235, no. 13, p. 113960, 2021, doi: 10.1016/j.enconman.2021.113960.

[40] S. S. Haykin, *Neural Networks and Learning Machines*, 3rd Editio. Pearson Prenctice Hall, 2009. doi: 10987654321.

[41] A. Mellit and A. Massi, "A 24-h forecast of solar irradiance using artificial neural network : Application for performance prediction of a grid-connected PV plant at Trieste , Italy," *Solar Energy*, vol. 84, no. 5, pp. 807–821, 2010, doi: 10.1016/j.solener.2010.02.006.

[42] H. Yu, D. Tarsitano, X. Hu, and F. Cheli, "Real time energy management strategy for a fast charging electric urban bus powered by hybrid energy storage system," *Energy*, vol. 112, pp. 322–331, 2016, doi: 10.1016/j.energy.2016.06.084.

[43] S. Berrazouane and K. Mohammedi, "Parameter optimization via cuckoo optimization algorithm of fuzzy controller for energy management of a hybrid power system," *Energy Convers Manag*, vol. 78, pp. 652–660, 2014, doi: 10.1016/j.enconman.2013.11.018.

[44] T. Vigneysh and N. Kumarappan, "Autonomous operation and control of photovoltaic/solid oxide fuel cell/battery energy storage based microgrid using fuzzy logic controller," *Int J Hydrogen Energy*, vol. 41, no. 3, pp. 1877–1891, 2016, doi: 10.1016/j.ijhydene.2015.11.022.

[45] M. H. Athari and M. M. Ardehali, "Operational performance of energy storage as function of electricity prices for on-grid hybrid renewable energy system by optimized fuzzy logic controller," *Renew Energy*, vol. 85, pp. 890–902, 2016, doi: 10.1016/j.renene.2015.07.055.

[46] A. Derrouazin, M. Aillerie, N. Mekkakia-Maaza, and J. P. Charles, "Multi input-output fuzzy logic smart controller for a residential hybrid solar-wind-storage energy system," *Energy Convers Manag*, vol. 148, pp. 238–250, 2017, doi: 10.1016/j.enconman.2017.05.046.

[47] S. Lekhchine, T. Bahi, I. Abadlia, and H. Bouzeria, "PV-battery energy storage system operating of asynchronous motor driven by using fuzzy sliding mode control," *Int J Hydrogen Energy*, vol. 42, no. 13, pp. 8756–8764, 2017, doi: 10.1016/j.ijhydene.2016.05.298.

[48] E. Kamal, L. Adouane, A. Aitouche, and W. Mohammed, "Robust Power Management Control for Stand-Alone Hybrid Power Generation System," *J Phys Conf Ser*, vol. 783, no. 1, p. 012035, Jan. 2017, doi: 10.1088/1742-6596/783/1/012035.

[49] I. Abadlia, T. Bahi, and H. Bouzeria, "Energy management strategy based on fuzzy logic for compound RES/ESS used in stand-alone application," *Int J Hydrogen Energy*, vol. 41, no. 38, pp. 16705–16717, 2016, doi: 10.1016/j.ijhydene.2016.07.120.

[50] P. García, J. P. Torreglosa, L. M. Fernández, and F. Jurado, "Optimal energy management system for stand-alone wind turbine/photovoltaic/ hydrogen/battery hybrid system with supervisory control based on fuzzy logic," *Int J Hydrogen Energy*, vol. 38, no. 33, pp. 14146–14158, 2013, doi: 10.1016/j.ijhydene.2013.08.106.

[51] H. Zhang, A. Davigny, F. Colas, Y. Poste, and B. Robyns, "Fuzzy logic based energy management strategy for commercial buildings integrating photovoltaic and storage systems," *Energy Build*, vol. 54, pp. 196–206, 2012, doi: 10.1016/j.enbuild.2012.07.022.

[52] M. Tiar, A. Betka, S. Drid, S. Abdeddaim, M. Becherif, and A. Tabandjat, "Optimal energy control of a PV-fuel cell hybrid system," *Int J Hydrogen Energy*, vol. 42, no. 2, pp. 1456–1465, 2017, doi: 10.1016/j.ijhydene.2016.06.113.

[53] Z. Roumila, D. Rekioua, and T. Rekioua, "Energy management based fuzzy logic controller of hybrid system wind/photovoltaic/diesel with storage battery," *Int J Hydrogen Energy*, vol. 42, no. 30, pp. 19525–19535, 2017, doi: 10.1016/j.ijhydene.2017.06.006.

[54] Z. Cabrane, M. Ouassaid, and M. Maaroufi, “Battery and supercapacitor for photovoltaic energy storage: a fuzzy logic management,” *IET Renewable Power Generation*, vol. 11, no. 8, pp. 1157–1165, 2017, doi: 10.1049/iet-rpg.2016.0455.

[55] M. Higuita Cano, K. Agbossou, S. Kelouwani, and Y. Dubé, “Experimental evaluation of a power management system for a hybrid renewable energy system with hydrogen production,” *Renew Energy*, vol. 113, pp. 1086–1098, 2017, doi: 10.1016/j.renene.2017.06.066.

[56] A. Tabanjat, M. Becherif, D. Hissel, and H. S. Ramadan, “Energy management hypothesis for hybrid power system of H 2 /WT/PV/GMT via AI techniques,” *Int J Hydrogen Energy*, pp. 1–15, Jul. 2017, doi: 10.1016/j.ijhydene.2017.06.085.

[57] Y. Liu and G. K. Venayagamoorthy, *An Intelligent Energy Management System for a Photovoltaic-Battery System*, vol. 45, no. 21. IFAC, 2012. doi: 10.3182/20120902-4-FR-2032.00022.

[58] S. Safari, M. M. Ardehali, and M. J. Sirizi, “Particle swarm optimization based fuzzy logic controller for autonomous green power energy system with hydrogen storage,” *Energy Convers Manag*, vol. 65, pp. 41–49, 2013, doi: 10.1016/j.enconman.2012.08.012.

[59] L. W. Chong, Y. W. Wong, R. K. Rajkumar, and D. Isa, “An optimal control strategy for standalone PV system with Battery- Supercapacitor Hybrid Energy Storage System,” *J Power Sources*, vol. 331, pp. 553–565, 2016, doi: 10.1016/j.jpowsour.2016.09.061.

[60] E. De Santis, A. Rizzi, and A. Sadeghian, “Hierarchical genetic optimization of a fuzzy logic system for energy flows management in microgrids,” *Applied Soft Computing Journal*, vol. 60, pp. 135–149, 2017, doi: 10.1016/j.asoc.2017.05.059.

[61] S. Abedi, A. Alimardani, G. B. Gharehpetian, G. H. Riahy, and S. H. Hosseinian, “A comprehensive method for optimal power management and design of hybrid RES-based autonomous energy systems,” *Renewable and Sustainable Energy Reviews*, vol. 16, no. 3, pp. 1577–1587, 2012, doi: 10.1016/j.rser.2011.11.030.

[62] D. Nauck, “What are Neuro-Fuzzy Systems?,” Neural Network and Fuzzy Systems. Accessed: Feb. 02, 2018. [Online]. Available: http://fuzzy.cs.ovgu.de/nfdef.html

[63] J. S. R. Jang, “ANFIS: Adaptive-Network-Based Fuzzy Inference System,” *IEEE Trans Syst Man Cybern*, vol. 23, no. 3, pp. 665–685, 1993, doi: 10.1109/21.256541.

[64] N. Mahmud, A. Zahedi, and A. Mahmud, “A Cooperative Operation of Novel PV Inverter Control Scheme and Storage Energy Management System Based on ANFIS for Voltage Regulation of Grid-Tied PV System,” *IEEE Trans Industr Inform*, vol. 13, no. 5, pp. 2657–2668, 2017, doi: 10.1109/TII.2017.2651111.

[65] P. García, C. A. García, L. M. Fernández, F. Llorens, and F. Jurado, “ANFIS-Based control of a grid-connected hybrid system integrating renewable energies, hydrogen and batteries,” *IEEE Trans Industr Inform*, vol. 10, no. 2, pp. 1107–1117, 2014, doi: 10.1109/TII.2013.2290069.

[66] T. Bogaraj and J. Kanakaraj, “A Novel Energy Management Scheme using ANFIS for Independent Microgrid,” vol. 6, no. 3, 2016.

[67] R. YUMURTACI, “Role of Energy Management in Hybrid Renewable Energy Systems: Case Study Based Analysis Considering Varying Seasonal Conditions,” *Turkish Journal of Electrical Engineering & Computer Sciences*, pp. 1077–1091, 2013, doi: 10.3906/elk-1112-85.

[68] M. C. C. Di Piazza, G. La Tona, M. Luna, and A. Di Piazza, “A two-stage Energy Management System for smart buildings reducing the impact of demand uncertainty,” *Energy Build*, vol. 139, pp. 1–9, 2017, doi: 10.1016/j.enbuild.2017.01.003.

[69] B. Yuce, Y. Rezgui, and M. Mourshed, “ANN-GA smart appliance scheduling for optimised energy management in the domestic sector,” *Energy Build*, vol. 111, pp. 311–325, 2016, doi: 10.1016/j.enbuild.2015.11.017.

[70] P. Chaudhary and M. Rizwan, “Energy management supporting high penetration of solar photovoltaic generation for smart grid using solar forecasts and pumped hydro storage system,” *Renew Energy*, vol. 118, pp. 928–946, 2018, doi: 10.1016/j.renene.2017.10.113.

[71] C. H. Huang, “Modified neural network for dynamic control and operation of a hybrid generation systems,” *Journal of Applied Research and Technology*, vol. 12, no. 6, pp. 1154–1164, 2014, doi: 10.1016/S1665-6423(14)71674-8.

[72] J. Djuris, S. Ibric, and Z. Djuric, “Neural computing in pharmaceutical products and process development,” in *Computer-Aided Applications in Pharmaceutical Technology*, Elsevier, 2013, pp. 91–175. doi: 10.1533/9781908818324.91.

[73] G. Capizzi, G. Lo Sciuto, C. Napoli, and E. Tramontana, “An advanced neural network based solution to enforce dispatch continuity in smart grids,” *Applied Soft Computing Journal*, vol. 62, pp. 768–775, 2018, doi: 10.1016/j.asoc.2017.08.057.

[74] F. Bonanno, G. Capizzi, G. Lo Sciuto, C. Napoli, G. Pappalardo, and E. Tramontana, “A novel cloud-distributed toolbox for optimal energy dispatch management from renewables in IGSs by using WRNN predictors and GPU parallel solutions,” *2014 International Symposium on Power Electronics, Electrical Drives, Automation and Motion, SPEEDAM 2014*, pp. 1077–1084, 2014, doi: 10.1109/SPEEDAM.2014.6872127.

[75] K. Roy, K. Krishna Mandal, A. Chandra Mandal, and S. Narayan Patra, “Analysis of energy management in micro grid – A hybrid BFOA and ANN approach,” *Renewable and Sustainable Energy Reviews*, vol. 82, no. November 2016, pp. 4296–4308, 2018, doi: 10.1016/j.rser.2017.07.037.

[76] S. R. Gunn, “Support Vector Machines for classification and regression,” *Technical Report of SVM*, 1998, doi: 10.1039/B918972F.

[77] M. Abedi, G. H. Norouzi, and A. Bahroudi, “Support vector machine for multi-classification of mineral prospectivity areas,” *Comput Geosci*, vol. 46, pp. 272–283, 2012, doi: 10.1016/j.cageo.2011.12.014.

[78] A. S. Ahmad *et al.*, “A review on applications of ANN and SVM for building electrical energy consumption forecasting,” *Renewable and Sustainable Energy Reviews*, vol. 33, pp. 102–109, 2014, doi: 10.1016/j.rser.2014.01.069.

[79] P. V. D and S. K. Kottayil, “Energy-Aware Intelligent Controller for Dynamic Energy Management on Smart Microgrid,” *Power and Energy Systems: Towards Sustainable Energy*, no. Pestse 2014, 2014.

[80] M. Rambabu, G. V. Nagesh Kumar, and S. Siva Nagaraju, “Energy management of micro grid using support vector machine (SVM) model,” *IIOAB J*, vol. 7, no. 11Specialissue, pp. 116–132, 2016.

[81] Y. Y. Chia, L. H. Lee, N. Shafiabady, and D. Isa, “A load predictive energy management system for supercapacitor-battery hybrid energy storage system in solar application using the Support Vector Machine,” *Appl Energy*, vol. 137, pp. 588–602, 2015, doi: 10.1016/j.apenergy.2014.09.026.

[82] K. Huang, X. Wang, and L. Wang, “Optimal energy management of grid-connected photovoltaic micro-grid,” *2015 IEEE International Conference on Cyber Technology in Automation, Control, and Intelligent Systems (CYBER)*, pp. 234–239, 2015, doi: 10.1109/CYBER.2015.7287941.

[83] S. Paudel, P. H. Nguyen, W. L. Kling, M. Elmitri, B. Lacarrière, and O. Le Corre, “Support Vector Machine in Prediction of Building Energy Demand Using Pseudo Dynamic Approach,” 2015, [Online]. Available: http://arxiv.org/abs/1507.05019

[84] T. Kohonen, “The self-organizing map,” *Neurocomputing*, vol. 21, pp. 1–6, 1998, Accessed: Feb. 21, 2018. [Online]. Available: https://ac.els-cdn.com/S0925231298000307/1-s2.0-S0925231298000307-main.pdf?_tid=3902c12c-16d1-11e8-9efe-00000aab0f27&acdnat=1519195029_43b926f17b978da2e98a144b5ae5cc1a

[85] J. Llanos, D. Sáez, R. Palma-Behnke, A. Núñez, and G. Jiménez-Estévez, “Load profile generator and load forecasting for a renewable based microgrid using Self Organizing Maps and neural networks,” *Proceedings of the International Joint Conference on Neural Networks*, pp. 10–15, 2012, doi: 10.1109/IJCNN.2012.6252648.

[86] L. Hernández, C. Baladrón, J. M. Aguiar, B. Carro, A. Sánchez-Esguevillas, and J. Lloret, “Artificial neural networks for short-term load forecasting in microgrids environment,” *Energy*, vol. 75, pp. 252–264, 2014, doi: 10.1016/j.energy.2014.07.065.

[87] J. Llanos *et al.*, “Load estimation for microgrid planning based on a self-organizing map methodology,” *Applied Soft Computing Journal*, vol. 53, pp. 323–335, 2017, doi: 10.1016/j.asoc.2016.12.054.

[88] P. Vora and B. Oza, “A Survey on K-mean Clustering and Particle Swarm Optimization,” *International Journal of Science and Modern Engineering*, vol. 1, no. 3, 2013, Accessed: Feb. 21, 2018. [Online]. Available: http://citeseerx.ist.psu.edu/viewdoc/download?doi=10.1.1.679.2229&rep=rep1&type=pdf

[89] S. D. Chavan and N. P. Adgokar, “An Overview on Particle Swarm Optimization: Basic Concepts and Modified Variants,” *International Journal of Science and Research (IJSR) ISSN (Online Index Copernicus Value Impact Factor*, vol. 14, no. 5, pp. 2319–7064, 2013.

[90] Z. Michalewicz, R. Hinterding, and M. Michalewicz, “Evolutionary Algorithms,” pp. XII, 287, 1997, doi: 10.1007/978-3-662-44874-8.

[91] J. Carr, “An Introduction to Genetic Algorithms,” *Whitman College Mathematics Department*, pp. 1–40, 2014, doi: 10.1016/S0898-1221(96)90227-8.

[92] J. McCall, “Genetic algorithms for modelling and optimisation,” *J Comput Appl Math*, vol. 184, no. 1, pp. 205–222, 2005, doi: 10.1016/j.cam.2004.07.034.

[93] M. Mitchell, “An Introduction to Genetic Algorithms (Complex Adaptive Systems),” *The MIT Press*, p. 221, 1998, doi: 10.1016/S0898-1221(96)90227-8.

[94] R. Gholami, M. Shahabi, and M. R. Haghifam, “An efficient optimal capacitor allocation in DG embedded distribution networks with islanding operation capability of micro-grid using a new genetic based algorithm,” *International Journal of Electrical Power and Energy Systems*, vol. 71, pp. 335–343, 2015, doi: 10.1016/j.ijepes.2015.03.005.

[95] S. U. Agamah and L. Ekonomou, “Energy storage system scheduling for peak demand reduction using evolutionary combinatorial optimisation,” *Sustainable Energy Technologies and Assessments*, vol. 23, no. August, pp. 73–82, 2017, doi: 10.1016/j.seta.2017.08.003.

[96] Y.-Y. Hong and P.-S. Yo, “Novel Genetic Algorithm-Based Energy Management in a Factory Power System Considering Uncertain Photovoltaic Energies,” *Applied Sciences*, vol. 7, no. 5, p. 438, 2017, doi: 10.3390/app7050438.

[97] M. Elsied, A. Oukaour, T. Youssef, H. Gualous, and O. Mohammed, “An advanced real time energy management system for microgrids,” *Energy*, vol. 114, pp. 742–752, 2016, doi: 10.1016/j.energy.2016.08.048.

[98] S. Ali and D.-H. Kim, “Optimized Power Control Methodology Using Genetic Algorithm,” *Wirel Pers Commun*, vol. 83, no. 1, pp. 493–505, 2015, doi: 10.1007/s11277-015-2405-3.

[99] M. H. Moradi, M. Abedini, and S. M. Hosseinian, “Optimal operation of autonomous microgrid using HS-GA,” *International Journal of Electrical Power and Energy Systems*, vol. 77, pp. 210–220, 2016, doi: 10.1016/j.ijepes.2015.11.043.

[100] D. Merkle and M. Middendorf, “SWARM INTELLIGENCE,” *Science (1979)*, p. Chapter 14, 2001, [Online]. Available: http://link.springer.com/chapter/10.1007/978-1-4614-6940-7_8

[101] R. Poli, J. Kennedy, and T. Blackwell, “Particle swarm optimization,” *Swarm Intelligence*, vol. 1, no. 1, pp. 33–57, 2007, doi: 10.1007/s11721-007-0002-0.

[102] P. García-Triviño, L. M. Fernández-Ramírez, A. J. Gil-Mena, F. Llorens-Iborra, C. A. García-Vázquez, and F. Jurado, “Optimized operation combining costs, efficiency and lifetime of a hybrid renewable energy system with energy storage by battery and hydrogen in grid-connected applications,” *Int J Hydrogen Energy*, vol. 41, no. 48, pp. 23132–23144, 2016, doi: 10.1016/j.ijhydene.2016.09.140.

[103] M. Abdoos and M. Ghazvini, “Multi-objective particle swarm optimization of component size and long-term operation of hybrid energy systems under multiple uncertainties,” vol. 015902, 2018.

[104] T. Niknam, F. Golestaneh, and M. Shafiei, “Probabilistic energy management of a renewable microgrid with hydrogen storage using self-adaptive charge search algorithm,” *Energy*, vol. 49, no. 1, pp. 252–267, 2013, doi: 10.1016/j.energy.2012.09.055.

[105] C. Keles, B. B. Alagoz, and A. Kaygusuz, “Multi-Source Energy Mixing for Renewable Energy Microgrids by Particle Swarm Multi-Source Energy Mixing for Renewable Energy Microgrids by Particle Swarm Optimization,” no. September, pp. 2–6, 2017.

[106] Y. S. Cheng, M. T. Chuang, Y. H. Liu, S. C. Wang, and Z. Z. Yang, “A particle swarm optimization based power dispatch algorithm with roulette wheel re-distribution mechanism for equality constraint,” *Renew Energy*, vol. 88, pp. 58–72, 2016, doi: 10.1016/j.renene.2015.11.023.

[107] L. Ju, H. Li, J. Zhao, K. Chen, Q. Tan, and Z. Tan, “Multi-objective stochastic scheduling optimization model for connecting a virtual power plant to wind-photovoltaic-electric vehicles considering uncertainties and demand response,” *Energy Convers Manag*, vol. 128, pp. 160–177, 2016, doi: 10.1016/j.enconman.2016.09.072.

[108] M. Abedini, M. H. Moradi, and S. M. Hosseinian, “Optimal management of microgrids including renewable energy scources using GPSO-GM algorithm,” *Renew Energy*, vol. 90, pp. 430–439, 2016, doi: 10.1016/j.renene.2016.01.014.

[109] A. Baziar and A. Kavousi-Fard, “Considering uncertainty in the optimal energy management of renewable micro-grids including storage devices,” *Renew Energy*, vol. 59, pp. 158–166, 2013, doi: 10.1016/j.renene.2013.03.026.

[110] N. Bigdeli, “Optimal management of hybrid PV/fuel cell/battery power system: A comparison of optimal hybrid approaches,” *Renewable and Sustainable Energy Reviews*, vol. 42, pp. 377–393, 2015, doi: 10.1016/j.rser.2014.10.032.

[111] P. García-Triviño, F. Llorens-Iborra, C. A. García-Vázquez, A. J. Gil-Mena, L. M. Fernández-Ramírez, and F. Jurado, “Long-term optimization based on PSO of a grid-connected renewable energy/battery/hydrogen hybrid system,” *Int J Hydrogen Energy*, vol. 39, no. 21, pp. 10805–10816, 2014, doi: 10.1016/j.ijhydene.2014.05.064.

[112] M. Dorigo, M. Birattari, and T. Stutzle, “Ant colony optimization,” *IEEE Comput Intell Mag*, vol. 1, no. 4, pp. 28–39, 2006, doi: 10.1109/MCI.2006.329691.

[113] M. Marzband, E. Yousefnejad, A. Sumper, and J. L. Domínguez-García, “Real time experimental implementation of optimum energy management system in standalone Microgrid by using multi-layer ant colony optimization,” *International Journal of Electrical Power and Energy Systems*, vol. 75, pp. 265–274, 2016, doi: 10.1016/j.ijepes.2015.09.010.

[114] N. K. Jhankal and D. Adhyaru, “Bacterial foraging optimization algorithm: A derivative free technique,” *2011 Nirma University International Conference on Engineering: Current Trends in Technology, NUiCONE 2011 - Conference Proceedings*, pp. 8–10, 2011, doi: 10.1109/NUiConE.2011.6153240.

[115] S. Das, A. Biswas, S. Dasgupta, and A. Abraham, “Bacterial Foraging Optimization Algorithm : Theoretical Foundations , Analysis , and Applications,” *Foundations of Computational Intelligence Volume 3*, vol. 3, pp. 23–55, 2009, doi: 10.1007/978-3-642-01085-9_2.

[116] S. Sadeghiram, “Bacterial foraging optimisation algorithm, particle swarm optimisation and genetic algorithm: A comparative study,” *International Journal of Bio-Inspired Computation*, vol. 10, no. 4, 2017, doi: 10.1504/IJBIC.2017.087923.

[117] M. Shehab, A. T. Khader, and M. A. Al-Betar, “A survey on applications and variants of the cuckoo search algorithm,” *Applied Soft Computing Journal*, vol. 61, pp. 1041–1059, 2017, doi: 10.1016/j.asoc.2017.02.034.

[118] A. S. Joshi, O. Kulkarni, G. M. Kakandikar, and V. M. Nandedkar, “Cuckoo Search Optimization-A Review,” *Mater Today Proc*, vol. 4, no. 8, pp. 7262–7269, 2017, doi: 10.1016/j.matpr.2017.07.055.

[119] X. S. Yang and S. Deb, "Cuckoo search via Levy flights," *2009 World Congress on Nature and Biologically Inspired Computing, NABIC 2009 - Proceedings*, pp. 210–214, 2009, doi: 10.1109/NABIC.2009.5393690.

[120] S. Das and P. N. Suganthan, "Differential evolution: A survey of the state-of-the-art," *IEEE Transactions on Evolutionary Computation*, vol. 15, no. 1, pp. 4–31, 2011, doi: 10.1109/TEVC.2010.2059031.

[121] D. Zaharie, "Differential evolution: From theoretical analysis to practical insights," *Mendel*, vol. 1, 2012.

[122] A. D. Lilla, M. A. Khan, and P. Barendse, "Comparison of Differential Evolution and Genetic Algorithm in the design of permanent magnet Generators," *Industrial Technology (ICIT), 2013 IEEE International Conference on*, pp. 266–271, 2013, doi: 10.1109/ICIT.2013.6505683.

[123] J. Zhang, Y. Wu, Y. Guo, B. Wang, H. Wang, and H. Liu, "A hybrid harmony search algorithm with differential evolution for day-ahead scheduling problem of a microgrid with consideration of power flow constraints," *Appl Energy*, vol. 183, pp. 791–804, 2016, doi: 10.1016/j.apenergy.2016.09.035.

[124] R. Mallol-Poyato, S. Jiménez-Fernández, P. Díaz-Villar, and S. Salcedo-Sanz, "Joint optimization of a Microgrid's structure design and its operation using a two-steps evolutionary algorithm," *Energy*, vol. 94, pp. 775–785, 2016, doi: 10.1016/j.energy.2015.11.030.

[125] R. Mallol-Poyato, S. Jimenez-Fernandez, L. Cornejo-Bueno, P. Diaz-Villar, and S. Salcedo-Sanz, "Nested evolutionary algorithms for joint structure design and operation of micro-grids under variable electricity prices scenarios," *INISTA 2015 - 2015 International Symposium on Innovations in Intelligent SysTems and Applications, Proceedings*, 2015, doi: 10.1109/INISTA.2015.7276735.

[126] S. Ikeda and R. Ooka, "A new optimization strategy for the operating schedule of energy systems under uncertainty of renewable energy sources and demand changes," *Energy Build*, vol. 125, pp. 75–85, 2016, doi: 10.1016/j.enbuild.2016.04.080.

[127] R. Mallol-Poyato, S. Salcedo-Sanz, S. Jiménez-Fernández, and P. Díaz-Villar, "Optimal discharge scheduling of energy storage systems in MicroGrids based on hyper-heuristics," *Renew Energy*, vol. 83, pp. 13–24, 2015, doi: 10.1016/j.renene.2015.04.009.

[128] A. Bouchachia, B. Gabrys, and Z. Sahel, "Overview of Some Incremental Learning Algorithms," in *2007 IEEE International Fuzzy Systems Conference*, 2007, pp. 1–6. doi: 10.1109/FUZZY.2007.4295640.

[129] E. D. Michie, D. J. Spiegelhalter, and C. C. Taylor, "Machine Learning , Neural and Statistical Classification," 1994.

[130] S. Furao and O. Hasegawa, "An incremental network for on-line unsupervised classification and topology learning," *Neural Networks*, vol. 19, no. 1, pp. 90–106, 2006, doi: 10.1016/j.neunet.2005.04.006.

[131] S. Furao, T. Ogura, and O. Hasegawa, "An enhanced self-organizing incremental neural network for online unsupervised learning," *Neural Networks*, vol. 20, no. 8, pp. 893–903, 2007, doi: 10.1016/j.neunet.2007.07.008.

[132] L. W. Chong, Y. W. Wong, R. K. Rajkumar, and D. Isa, “Modelling and Simulation of Standalone PV Systems with Battery- supercapacitor Hybrid Energy Storage System for a Rural Household,” *Energy Procedia*, vol. 107, no. September 2016, pp. 232–236, 2017, doi: 10.1016/j.egypro.2016.12.135.

[133] G. Reikard and C. Hansen, “Forecasting solar irradiance at short horizons : Frequency and time domain models,” *Renew Energy*, vol. 135, pp. 1270–1290, 2019, doi: 10.1016/j.renene.2018.08.081.

[134] A. N. Abdalla *et al.*, “Integration of energy storage system and renewable energy sources based on artificial intelligence: An overview,” *J Energy Storage*, vol. 40, no. June, p. 102811, 2021, doi: 10.1016/j.est.2021.102811.

[135] J. Ascencio-Vásquez, J. Bevc, K. Reba, K. Brecl, M. Jankovec, and M. Topič, “Advanced PV performance modelling based on different levels of irradiance data accuracy,” *Energies (Basel)*, vol. 13, no. 9, pp. 1–12, 2020, doi: 10.3390/en13092166.

[136] M. Ghayekhloo, M. Ghofrani, M. B. Menhaj, and R. Azimi, “A novel clustering approach for short-term solar radiation forecasting,” *Solar Energy*, vol. 122, pp. 1371–1383, 2015, doi: 10.1016/j.solener.2015.10.053.

[137] H. Musbah, G. Ali, H. H. Aly, and T. A. Little, “Energy management using multi-criteria decision making and machine learning classification algorithms for intelligent system,” *Electric Power Systems Research*, vol. 203, no. June 2021, p. 107645, 2022, doi: 10.1016/j.epsr.2021.107645.

[138] S. D. Miller, M. A. Rogers, J. M. Haynes, M. Sengupta, and A. K. Heidinger, “Short-term solar irradiance forecasting via satellite/model coupling,” *Solar Energy*, vol. 168, no. October 2017, pp. 102–117, 2018, doi: 10.1016/j.solener.2017.11.049.

[139] R. H. Inman, H. T. C. Pedro, and C. F. M. Coimbra, “Solar forecasting methods for renewable energy integration,” *Prog Energy Combust Sci*, vol. 39, no. 6, pp. 535–576, Dec. 2013, doi: 10.1016/j.pecs.2013.06.002.

[140] A. Hammer, D. Heinemann, and B. Luckehe, “Short-term forecasting of solar radiation : A statistical approach using satellite data,” *Solar Energy*, vol. 67, no. 1992, pp. 139–150, 2000.

[141] M. Caldas, “Very short-term solar irradiance forecast using all-sky imaging and real-time irradiance measurements,” *Renew Energy*, vol. 143, pp. 1643–1658, 2019, doi: 10.1016/j.renene.2019.05.069.

[142] C. Demircan, H. C. Bayrakçı, and A. Keçebaş, “Machine learning-based improvement of empiric models for an accurate estimating process of global solar radiation,” *Sustainable Energy Technologies and Assessments*, vol. 37, no. November 2019, 2020, doi: 10.1016/j.seta.2019.100574.

[143] R. Blaga, A. Sabadus, N. Stefu, C. Dughir, M. Paulescu, and V. Badescu, “A current perspective on the accuracy of incoming solar energy forecasting,” *Prog Energy Combust Sci*, vol. 70, pp. 119–144, 2019, doi: 10.1016/j.pecs.2018.10.003.

[144] M. S. Ibrahim, W. Dong, and Q. Yang, “Machine learning driven smart electric power systems: Current trends and new perspectives,” *Appl Energy*, vol. 272, no. June, p. 115237, 2020, doi: 10.1016/j.apenergy.2020.115237.

[145] M. Paulescu and E. Paulescu, “Short-term forecasting of solar irradiance,” *Renew Energy*, vol. 143, pp. 985–994, 2019, doi: 10.1016/j.renene.2019.05.075.

[146] A. Khosravi, R. O. Nunes, M. E. H. Assad, and L. Machado, “Comparison of artificial intelligence methods in estimation of daily global solar radiation,” *J Clean Prod*, vol. 194, pp. 342–358, 2018, doi: 10.1016/j.jclepro.2018.05.147.

[147] R. Medar, A. B. Angadi, P. Y. Niranjan, and P. Tamase, “Comparative study of different weather forecasting models,” in *2017 International Conference on Energy, Communication, Data Analytics and Soft Computing, ICECDS 2017*, IEEE, 2018, pp. 1604–1609. doi: 10.1109/ICECDS.2017.8389719.

[148] N. Zougagh, A. Charkaoui, and A. Echchatbi, “Artificial intelligence hybrid models for improving forecasting accuracy,” *Procedia Comput Sci*, vol. 184, pp. 817–822, 2021, doi: 10.1016/j.procs.2021.04.013.

[149] S. E. Haupt *et al.*, “Combining Artificial Intelligence with Physics-Based Energy Forecasting,” 2020.

[150] M. Lachmann, J. Maldonado, W. Bergmann, F. Jung, M. Weber, and C. Büskens, “Self-learning data-based models as basis of a universally applicable energy management system,” *Energies (Basel)*, vol. 13, no. 8, pp. 1–42, 2020, doi: 10.3390/en13082084.

[151] Y. Ren, P. N. Suganthan, and N. Srikanth, “Ensemble methods for wind and solar power forecasting - A state-of-the-art review,” *Renewable and Sustainable Energy Reviews*, vol. 50, pp. 82–91, 2015, doi: 10.1016/j.rser.2015.04.081.

[152] Y. Gala, Á. Fernández, J. Díaz, and J. R. Dorronsoro, “Hybrid machine learning forecasting of solar radiation values,” *Neurocomputing*, vol. 176, pp. 48–59, 2016, doi: 10.1016/j.neucom.2015.02.078.

[153] J. Jiang, L. Yu, X. Zhang, X. Ding, and C. Wu, “EV-Based reconfigurable smart grid management using support vector regression learning technique machine learning,” *Sustain Cities Soc*, vol. 76, no. August 2021, p. 103477, 2022, doi: 10.1016/j.scs.2021.103477.

[154] A. Fouilloy *et al.*, “Solar irradiation prediction with machine learning: Forecasting models selection method depending on weather variability,” *Energy*, vol. 165, pp. 620–629, 2018, doi: 10.1016/j.energy.2018.09.116.

[155] L. Benali, G. Notton, A. Fouilloy, C. Voyant, and R. Dizene, “Solar radiation forecasting using artificial neural network and random forest methods: Application to normal beam, horizontal diffuse and global components,” *Renew Energy*, vol. 132, pp. 871–884, 2019, doi: 10.1016/j.renene.2018.08.044.

[156] E. Akarslan and F. O. Hocaoglu, “A novel method based on similarity for hourly solar irradiance forecasting,” *Renew Energy*, vol. 112, pp. 337–346, 2017, doi: 10.1016/j.renene.2017.05.058.

[157] E. Akarslan, F. O. Hocaoglu, and R. Edizkan, “Novel short term solar irradiance forecasting models,” *Renew Energy*, vol. 123, pp. 58–66, 2018, doi: 10.1016/j.renene.2018.02.048.

[158] A. P. Grantham, P. J. Pudney, L. A. Ward, M. Belusko, and J. W. Boland, “Generating synthetic five-minute solar irradiance values from hourly observations,” *Solar Energy*, vol. 147, pp. 209–221, 2017, doi: 10.1016/j.solener.2017.03.026.

[159] H. Bouzgou and C. A. Gueymard, “Fast short-term global solar irradiance forecasting with wrapper mutual information,” *Renew Energy*, vol. 133, pp. 1055–1065, 2019, doi: 10.1016/j.renene.2018.10.096.

[160] A. Khosravi, R. N. N. Koury, L. Machado, and J. J. G. Pabon, “Prediction of hourly solar radiation in Abu Musa Island using machine learning algorithms,” *J Clean Prod*, vol. 176, pp. 63–75, 2018, doi: 10.1016/j.jclepro.2017.12.065.

[161] T. R. Ayodele, A. S. O. Ogunjuyigbe, A. Amedu, and J. L. Munda, “Prediction of global solar irradiation using hybridized k-means and support vector regression algorithms,” *Renewable Energy Focus*, vol. 29, no. June, pp. 78–93, 2019, doi: 10.1016/j.ref.2019.03.003.

[162] A. Takilalte, S. Harrouni, and B. P. El Alia, “Daily Direct Normal Irradiance Forecasting by Support Vector Regression Case Study : in Ghardaia- Algeria,” in *2019 International Conference on Advanced Electrical Engineering (ICAEE)*, IEEE, 2019, pp. 1–6.

[163] M. Marzouq, Z. Bounoua, H. El Fadili, A. Mechaqrane, K. Zenkouar, and Z. Lakhliai, “New daily global solar irradiation estimation model based on automatic selection of input parameters using evolutionary artificial neural networks,” *J Clean Prod*, vol. 209, pp. 1105–1118, 2019, doi: 10.1016/j.jclepro.2018.10.254.

[164] J. M. Bright, C. J. Smith, P. G. Taylor, and R. Crook, “Stochastic generation of synthetic minutely irradiance time series derived from mean hourly weather observation data,” *Solar Energy*, vol. 115, pp. 229–242, 2015, doi: 10.1016/j.solener.2015.02.032.

[165] A. Alfadda, S. Rahman, and M. Pipattanasomporn, “Solar irradiance forecast using aerosols measurements: A data driven approach,” *Solar Energy*, vol. 170, no. June, pp. 924–939, 2018, doi: 10.1016/j.solener.2018.05.089.

[166] O. El Alani, “Short term solar irradiance forecasting using artificial neural network for a semi-arid climate in Morocco,” in *2019 International Conference on Wireless Networks and Mobile Communications (WINCOM)*, IEEE, 2019, pp. 1–7.

[167] M. Lotfi, M. Javadi, G. J. Osório, C. Monteiro, and J. P. S. Catalão, “A Novel Ensemble Algorithm for Solar Power Forecasting Based on Kernel Density Estimation,” *Energies (Basel)*, vol. 13, no. 1, p. 216, Jan. 2020, doi: 10.3390/en13010216.

[168] G. Shi and S. Eftekharnejad, “Data-Driven Solar Generation Forecast Considering Temporal Characteristics of Data,” in *2020 IEEE Texas Power and Energy Conference (TPEC)*, IEEE, Feb. 2020, pp. 1–6. doi: 10.1109/TPEC48276.2020.9042521.

[169] G. Bianchini, D. Pepe, and A. Vicino, “Estimation of photovoltaic generation forecasting models using limited information,” *Automatica*, vol. 113, p. 108688, Mar. 2020, doi: 10.1016/j.automatica.2019.108688.

[170] P. Mpfumali, C. Sigauke, A. Bere, and S. Mulaudzi, “Day ahead hourly global horizontal irradiance forecasting—application to South African data,” *Energies (Basel)*, vol. 12, no. 18, pp. 1–28, 2019, doi: 10.3390/en12183569.

[171] T. A. Fathima, V. Nedumpozhimana, Y. H. Lee, S. Winkler, and S. Dev, “Predicting Solar Irradiance in Singapore,” in *Proc. Progress In Electromagnetics Research Symposium (PIERS)*, Dec. 2019, pp. 3–6. [Online]. Available: http://arxiv.org/abs/1912.07187

[172] C. Huang, L. Wang, and L. L. Lai, “Data-Driven Short-Term Solar Irradiance Forecasting Based on Information of Neighboring Sites,” *IEEE Transactions on Industrial Electronics*, vol. 66, no. 12, pp. 9918–9927, Dec. 2019, doi: 10.1109/TIE.2018.2856199.

[173] J. Wojtkiewicz, M. Hosseini, R. Gottumukkala, and T. L. Chambers, “Hour-Ahead Solar Irradiance Forecasting Using Multivariate Gated Recurrent Units,” *Energies (Basel)*, vol. 12, no. 21, p. 4055, Oct. 2019, doi: 10.3390/en12214055.

[174] M. Alhussein, S. I. Haider, and K. Aurangzeb, “Microgrid-Level Energy Management Approach Based on Short-Term Forecasting of Wind Speed and Solar Irradiance,” *Energies (Basel)*, vol. 12, no. 8, p. 1487, Apr. 2019, doi: 10.3390/en12081487.

[175] X. Huang *et al.*, “Hybrid deep neural model for hourly solar irradiance forecasting,” *Renew Energy*, vol. 171, pp. 1041–1060, 2021, doi: 10.1016/j.renene.2021.02.161.

[176] X. Wang, Y. Sun, D. Luo, and J. Peng, “Comparative study of machine learning approaches for predicting short-term photovoltaic power output based on weather type classification,” *Energy*, vol. 240, p. 122733, 2022, doi: 10.1016/j.energy.2021.122733.

[177] W. Wang, Z. Zhen, K. Li, K. Lv, and F. Wang, “An Ultra-short-term Forecasting Model for High-resolution Solar Irradiance Based on SOM and Deep Learning Algorithm,” in *2019 IEEE Sustainable Power and Energy Conference (iSPEC)*, IEEE, Nov. 2019, pp. 1090–1095. doi: 10.1109/iSPEC48194.2019.8974983.

[178] R. Manuel and G. De Castro, “Solar Irradiance Forecast Using Artificial Intelligence Techniques,” Instituto Superior Tecnico Lisboa, Lisboa, Portugal, 2016.

[179] E. Soares, P. Costa, B. Costa, and D. Leite, “Ensemble of evolving data clouds and fuzzy models for weather time series prediction,” *Applied Soft Computing Journal*, vol. 64, pp. 445–453, 2018, doi: 10.1016/j.asoc.2017.12.032.

[180] T. Mozer, “Embedded AI is here,” Embedded Computing Design. Accessed: Jul. 09, 2018. [Online]. Available: http://www.embedded-computing.com/embedded-computing-design/embedded-ai-is-here

[181] X. Fan, “Real-Time Embedded Systems | SciTech Connect,” SciTech Connect. Accessed: Jul. 09, 2018. [Online]. Available: http://scitechconnect.elsevier.com/real-time-embedded-systems/

[182] M. Versace, “Does Artificial Intelligence Require Specialized Processors? - The New Stack,” The NewStack. Accessed: Jul. 10, 2018. [Online]. Available: https://thenewstack.io/ai-hardware-software-dilemma/

[183] K. Z. Haigh, A. M. Mackay, M. R. Cook, and L. G. Lin, “Machine Learning for Embedded Systems : A Case Study,” *BBN Technologies*, 2015, [Online]. Available: http://www.cs.cmu.edu/~khaigh/papers/2015-HaighTechReport-Embedded.pdf

[184] P. Stavroulakis, S. Chen, C. Delorme, P. Bointon, G. Tzimiropoulos, and R. Leach, “Rapid tracking of extrinsic projector parameters in fringe projection using machine learning,” *Opt Lasers Eng*, vol. 114, no. August 2018, pp. 7–14, 2019, doi: 10.1016/j.optlaseng.2018.08.018.

[185] S. Oniga and J. Suto, “Activity recognition in adaptive assistive systems using artificial neural networks,” *Elektronika ir Elektrotechnika*, vol. 22, no. 1, pp. 68–72, 2016, doi: 10.5755/j01.eee.22.1.14112.

[186] M. Sajjad *et al.*, “Raspberry Pi assisted face recognition framework for enhanced law-enforcement services in smart cities,” *Future Generation Computer Systems*, 2017, doi: 10.1016/j.future.2017.11.013.

[187] M. Al Qurishee, “Low-cost deep learning UAV and Raspberry Pi solution to real time pavement condition assessment”.

[188] B. A. D. J. C. K. Basnayake, Y. W. R. Amarasinghe, R. A. Attalage, T. D. I. Udayanga, and A. G. B. P. Jayasekara, “Artificial Intelligence Based Smart Building Automation Controller for Energy Efficiency Improvements in Existing Buildings,” *International Journal of Advanced Information Science and Technology*, vol. 2319, no. 40, pp. 150–156, 2015, doi: 10.15693/ijaist/2015.v4i8.85-91.

[189] R. J. Hyndman and A. B. Koehler, “Another look at measures of forecast accuracy,” *Int J Forecast*, vol. 22, no. 4, pp. 679–688, 2006, doi: 10.1016/j.ijforecast.2006.03.001.

[190] B. K. Puah *et al.*, “A regression unsupervised incremental learning algorithm for solar irradiance prediction,” *Renew Energy*, vol. 164, pp. 908–925, 2021, doi: 10.1016/j.renene.2020.09.080.

[191] Y. Riffonneau, S. Bacha, F. Barruel, and S. Ploix, “Optimal power flow management for grid connected PV systems with batteries,” *IEEE Trans Sustain Energy*, vol. 2, no. 3, pp. 309–320, Jul. 2011, doi: 10.1109/TSTE.2011.2114901.

[192] TNB, “ELECTRICITY SUPPLY APPLICATION HANDBOOK,” 2022.

[193] M. Fadaeenejad, M. A. M. Radzi, M. Z. A. Abkadir, and H. Hizam, “Assessment of hybrid renewable power sources for rural electrification in Malaysia,” *Renewable and Sustainable Energy Reviews*, vol. 30, pp. 299–305, 2014, doi: 10.1016/j.rser.2013.10.003.

[194] D. Hao *et al.*, “Solar energy harvesting technologies for PV self-powered applications: A comprehensive review,” *Renew Energy*, vol. 188, pp. 678–697, 2022, doi: 10.1016/j.renene.2022.02.066.

[195] A. Zain-Ahmed, K. Sopian, Z. Zainol Abidin, and M. Y. H. Othman, “The availability of daylight from tropical skies—a case study of Malaysia,” *Renew Energy*, vol. 25, no. 1, pp. 21–30, 2002, doi: 10.1016/S0960-1481(00)00209-3.

[196] M. Kasemann, L. M. Reindl, and K. Rühle, “C8.3 - Photovoltaic Energy Harvesting under Low Lighting Conditions,” pp. 483–485, 2020, doi: 10.5162/sensor2013/c8.3.

[197] POWERTHRU, “LEAD ACID BATTERY working-LIFETIME STUDY.” Accessed: Aug. 20, 2022. [Online]. Available: http://www.power-thru.com/documents/The%20Truth%20About%20Batteries%20-%20POWERTHRU%20White%20Paper.pdf